UNIVERSITY OF BIRMINGHAM

Development of a Biorelevant Dynamic Model of Human Proximal Colon:

a Tool for Designing Colon – Specific Drug Delivery Systems

by

Konstantinos Stamatopoulos

A thesis submitted to

The University of Birmingham

for the degree of

DOCTOR OF PHILOSOPHY

School of Chemical Engineering

The University of Birmingham

December 2016

Abstract

A novel Dynamic Colon Model (DCM) that represents the anatomy and physiology of the human proximal colon was developed. Analysis of the hydrodynamics was performed using Positron Emission Particle Tracking (PEPT) system and Positron Emission Tomography (PET). The pressures generated by the wall motion of the DCM tube compared with the available published *in vivo* data. The hydrodynamics in USP 2 dissolution apparatus were also assessed using Particle Image Velocimetry (PIV) and Planar Induced Fluorescence (PLIF). Areal distribution and individual striation methods showed high mixedness level close to tip.

PEPT experiments were performed using particles of different buoyancy. Use of different particles gave different results in terms of velocities and residence times within the DCM tube.

PET images showed that antegrade propagating waves of amplitude lower than the minimum threshold used *in vivo* studies were associated with flow episodes. In addition, flow episodes can occur which are not related to the wall motion.

Dissolution profiles of theophylline, a high water soluble drug, released from a hydrophilic matrix obtained at viscous shear thinning media, mimicking the dewatering process in the human colon.

The novel DCM provides a realistic colonic environment, enabling biorelevant *in vitro* assessment of the *in vivo* performance of dosage forms.

“To my family, to my friends, to my comrades of the Communist Party of Greece (KKE)”

Acknowledgements

First, I would like to thank my supervisors Prof. Mark Simmons and Dr. Hannah Batchelor for their guidance, fruitful discussions, suggestions and academic mentorship throughout my studies. In addition to my personal passion for research, their support and friendship helped me stay motivated and keep on top of things. It would be unforgivable, if I wouldn't say anything about Mrs Lynn Draper for all the administrative assistance and her kindness.

Many thanks to the following people for their technical assistance: Mr. Steve Brookes, manager of Physics' workshop, and the rest technical staff for their excellent and professional work. Without their help, the development of the novel Colon model would be impossible. In addition, I would like to thank Mr. Andrew Tanner from Biosciences' workshop and his patient to try to covert my crazy ideas to reality. Many thanks go to EPSRC for funding my research.

Thanks are due to my colleague Dr. Federico Alberini for his contribution to this research project with sharing his ideas and introducing me to the "magic" world of Matlab. Many thanks go to all my colleagues in Chem Eng who helped in any way to my research work.

Many thanks to my friend Alvaro Gil-Garcia for sharing with me some carefree moments during jogging along Birmingham canals and his truly friendship.

I'm grateful to my wife Vasiliki, who came so unexpectedly to my life, giving me the most valuable gift, a family. Thanks to her selfless help, I had a daily life which allowed me to be focused on my work, making possible to finalise my writing up.

I'm also grateful to Dr. Evangelos Katsoyannos, Dr. Archontoula Chatzilazarou and Dr. Spyros J. Konteles who are my friends, my colleagues, my mentors, my family and who have contributed to my personal and professional development.

Last but not least, I would like to thank my mother and my sister, since without their support, I wouldn't be able to finish my under- and postgraduate studies in order to be qualified for a doctoral research.

Table of Contents

List of Tables

List of Figures

Abbreviations

CD	Crohn's disease
DCM	Dynamic Colon Model
DGM	Dynamic Gastric model
GI	gastrointestinal tract
IBD	Inflammatory bowel diseases
MR	modified-release
PEPT	Positron Emission Particle Tracking
PET	Positron Emission Tomography
PIV	Particle Image Velocimetry
PLIF	Planar Laser Induced Fluorescence
TIM-1	TNO (gastro-) Intestinal Models
TIM-2	TNO Colon Model
UC	ulcerative colitis
USP	United States Pharmacopeia

1 Introduction

1.1 Overview

Inflammatory bowel diseases (IBD), including Crohn's disease (CD) and ulcerative colitis (UC), are long-term (i.e. chronic) conditions resulting in inflammation of the gastrointestinal tract with unknown aetiology (Burisch et al., 2013). The terminal ileum and the colon are the main regions of the gastrointestinal tract (GI) affected by CD and UC. Typical symptoms are abdominal pain, diarrhoea, tiredness, feeling generally unwell or feverish, mouth ulcers, loss of appetite, weight loss and anaemia. In Europe it has been estimated that approximately 2.5–3 million people are affected by IBD, with the treatment costs for the healthcare systems 4.6–5.6 billion Euros/year (Burisch et al., 2013). The corresponding estimated number of affected people in the United Kingdom is approximately 620000 (Molodecky et al., 2012). Due to the increasing number of people suffering from IBD (Kaplan, 2015), a lot of effort has been exerted to effectively deliver drugs for the local treatment of the inflamed colon (Amidon et al., 2015a) as well as for systemic treatment.

Most of the drugs are administrated orally and hence, the drug should pass through the upper GI tract before reaching the colon. To improve the local and systemic drug delivery via the complex GI tract environment, several modified-release (MR) colon specific drug delivery systems have been developed. Upon ingestion, the formulation enters a highly dynamic environment in which disintegration, dissolution and absorption/local action occurs. This complex *in vivo* process is usually evaluated *in vitro* using pharmacopoeia disintegration and dissolution tests. Predictive dissolution methods can contribute to a reduction in the number of costly *in vivo* studies required during the design, development and evaluation of these formulations.

It has been realised that both physicochemical characteristics of the gastrointestinal fluids as well as the hydrodynamics need to be reproduced in order to make a powerful *in vitro* model to predict *in vivo* performance (Garbacz et al., 2008, Garbacz and Klein, 2012, Fotaki et al.,

2009a). Existing compendial dissolution methods oversimplify the complex and dynamic environment of the human colon (Spratt et al., 2005) with the convention being the use of the USP dissolution Testing Apparatus 2 (USP 2) by the pharmaceutical industry (Zuleger et al., 2002, Mitchell et al., 1993). This apparatus presents some drawbacks (Kostewicz et al., 2014) and numerous published works have indicated that there is high variability in dissolution profiles using USP 2 (Costa and Lobo, 2001, Kukura et al., 2003b, Bai et al., 2011, Qureshi and Shabnam, 2001a).

Recently, the small volume USP 2 apparatus has gained popularity due to the reduced mass of material required, analytical methodology and discriminatory power of conventional apparatus (Klein and Shah, 2008a). However, there is still a need to analyze the hydrodynamics since the miniaturised systems do not exactly reflect the conditions of the standard USP2 paddle system (Klein and Shah, 2008a), nor the conditions in the GI tract. In addition, the effect of changing and increasing viscosity of the fluids, due to the dewatering process which takes place in human colon, may increase the uncertainty and the variability of the results from the dissolution test.

Understanding the hydrodynamics inside the USP 2 apparatus does not in itself explain how a dosage form will perform within the environment of the GI tract. Thus, in addition to the application of the biorelevant media in dissolution methods (Schellekens et al., 2007, Jantratid et al., 2009), attempts have been made to improve the bio-relevance of the hydrodynamic and mechanical conditions (Klancar et al., 2013, Thuenemann et al., 2015). The most advanced models currently available such as the TNO TIM-1 (Minekus, 2015), TIM-2 (Venema, 2015) and IFR Dynamic Gastric model (DGM) (Thuenemann et al., 2015), aim to simulate the GI environment under well controlled conditions and have progressed dissolution science, yet they are not considered to be the final solution to the problem (McAllister, 2010). Some of the major drawbacks of TIM-2 are the cost, complexity of the technique and lengthy equipment setup time resulting in a limited amount of data which can be obtained in a reasonable time

period. Furthermore, the TIM-2 is not physiologically representative, with a different length, volume and mixing process when compared with the human colon (Blanquet et al., 2001a).

Thus, the development of more realistic biorelevant *in vitro* models is an ongoing research topic with significant potential for the improvement of colon- targeted dosage forms.

Many modified release (MR) dosage forms have been designed to release the active compound within the human proximal colon. This particular section of the human colon has been targeted due to higher water availability for drug and nutrients absorption. Thus, there is a need to analyse the hydrodynamics of this region of the human colon and understand their effects on the performance of solid drug products.

Physiologically realistic *in vitro* models should reproduce the widely accepted "law of the intestine" which states that the propulsion of the bolus occurrs due to the combined ascending excitatory (muscle contraction) coupled with the forward descending inhibition (muscle relaxation). In addition, presence of taenia coli (i.e. the thickest layer of the longitudinal muscle) and semilunar folds, which form the characteristic pockets in the colon called haustra, play a major role in regulation of transit through the colon (Langer and Takács, 2004). There is limited data in the literature which investigates the relationships between wall motion and movements of the contents in human proximal colon (Cook et al., 2000, Dinning et al., 2008). Monitoring techniques used to obtain human colon motility such as manometry and scintigraphy have some technical limitations. As a further consequency, contradictory results have been obtained among *in vivo* studies with regards to the association between wall motion and flow episodes. These limitations are due to the sensitivity of the manometry which is affected by the diameter of the proximal colon (>0.056 m) (Von Der Ohe et al., 1994), and the viscosity of the contents (Proano et al., 1990). *In vitro* studies assessing the performance of manometry have been conducted in fully filled tubes (Arkwright et al., 2013), despite previous *in vivo* studies showing that the volume in the colon varies from 10 – 125 mL which does not reflect a fully filled tube (Sutton, 2009, Schiller et al., 2005). Thus, the interpretation of the

manometry measurements should be performed in a representative system that reflects the volume of the fluids in the (partly-filled) human proximal colon and the diameter of the tube.

Furthermore, there is no information about how the degree and rate of occlusion of the human proximal colon wall will affect the interpretation of manometry in combination with the volume and the viscosity of the fluids. Thus, the current reliance on manometry to characterize wall motion and correlate it with flow episodes could limit and/or mislead the interpretation of the results.

Scintigraphy has been utilized to visualize *in vivo* flow episodes in human colon, however, without linkage to changes in human colon diameter. Hence, a more systematic analysis of the motility in human proximal colon has still to be reported to investigate how viscosity and volume of fluids will affect the interpretation of manometry as well as the propulsion and mixing of the colonic contents. However, this is difficult to perform *in vivo* in a controllable way, due to the high variability between subjects. Thus, the development of a biorelevant *in vitro* model offers advantages to investigate the interplay of those parameters (i.e viscosity, volume, wall motion etc.) on fluid mixing and transit. To ensure that the *in vitro* model provides a realistic environment, the anatomy of the proximal colon should be reproduced as much accurately as possible. This model enables assessment of the performance of dosage forms within a realistic colonic environment.

Positron Emission Tomography (PET) is used in this project, as an alternative to scintigraphy flow visualization technique, to understand how motility pattern, viscosity and volume of the fluids affect the mixing process and the propulsion of the contents in the *in vitro* model.

The pressure forces generated from the wall motion are recorded and compared with *in vivo* data obtained from literature using manometry which is a common clinical method to investigate abnormalities in the human colon motor.

Positron Emission Particle Tracking (PEPT) system is used as an alternative method to magnetic pill tracking systems which has been used to monitor colonic movements in healthy subjects and determine velocities and displacements of the contents upon wall motion.

Particle Image Velocimetry (PIV) as well as Planar Laser Induced Fluorescence (PLIF) have extensively been used to assess fluid flow and mixing performance of stirred tanks as well as USP 2 dissolution apparatus.

1.2 Thesis Aims & Objectives

The aim of this thesis is to understand the impact of the hydrodynamics in the human proximal colon, in particular relating the motility of the colon wall and the viscosity of the fluids to the performance of MR dosage forms, mixing processes and underlying fluid hydrodynamics. The development of a biorelevant engineering model which can reproduce the complex environment of the human colon to a greater level compared to existing models is the driving force for the current project. As further consequence, the model will be used to assess the dissolution profile of high water soluble drug released from hydrophilic matrices. Thus, the main objectives of the current project in order to achieve these goals are as follows:

- To develop a biorelevant *in vitro* model of human proximal colon which reproduces the main features of the organ in terms of anatomy and motility patterns.
- Understand motility, flow and mixing in the human proximal colon using the *in vitro* model under predetermined conditions in terms of motility pattern, volume and viscosity of fluids.
- To investigate how viscosity of the fluids and wall motion will affect the dissolution profile and the distribution of high water soluble drug released from a hydrophilic matric.

Comparison of the dissolution of a drug in the *in vitro* model with the compendial mini volume USP 2 dissolution apparatus was also performed.

1.3 Thesis Breakdown

This thesis is structured in the following manner: Chapter II presents a literature review which discusses the viability of the human colon as a site for drug delivery describing its environment

in terms of anatomy, physiology, motility and physicochemical properties of the contents. Subsequently, available colonic-targeted drug delivery systems are presented alongside the key parameters affecting their performance. Then, the chapter focuses on the current status in the dissolution science, describing the existing compendial dissolution apparatus used to assess the performance of the dosage forms and moving towards the advanced dynamic apparatus. Finally, a brief description of the associated experimental techniques and analysis methods used in the work presented in this thesis is included.

Based on the conclusions drawn from this review, characterisation of the mini vessel USP 2 dissolution apparatus used to assess the performance of the MR dosage forms is described. Chapter III discusses the impact of media viscosity on dissolution of a highly water soluble drug within a USP 2 mini vessel dissolution apparatus using an optical Planar Induced Fluorescence (PLIF) method and is published in part in Stamatopoulos et al. 2015. Chapter IV builds on this work, focussing on the mixing performance of small volume USP 2 apparatus in shear thinning media and is published in part in Stamatopoulos et al. 2016a.

The next three results chapters focus on the development of an artificial Dynamic Colon Model (DCM) as an alternative to compendial dissolution apparatus, providing a more representative colonic environment to assess the performance of the MR dosage form used previously in the mini volume USP 2 dissolution experiments. The analysis of the data from the DCM is divided into three parts: Chapter V discusses the development, design and fabrication of DCM to simulate colon motility. The effect of wall motion, viscosity and volume of the fluids on the performance of the manometry was investigated whereas Positron Emission Tomography (PET) was used to visualize the fluid flow.

Langer et al., (2004) examined the anatomical significance of the presence of taenia, haustra and semilunar folds on the effective propulsion of contents in human colon. Their project describes the design of a 2D and 3D model of the haustrum and semilunar folds using isolated specimens of human colon, along with anonymized MRI images of human GI tract provided by Heartlands Hospital in Birmingham. Sadahiro et al., (1992) reported the average values of

length and diameter of the human proximal colon which were used to inform the design of the *in vitro* model. A modified version of the apparatus used by Arkwright et al. (2013) was developed to assess the effect of viscosity and volume of the fluid as well as the degree and occlusion rate of the wall on the performance of the manometry. Dinning et al. (2014) provided a detailed analysis on the pressure amplitudes and frequency of the motility events in the human proximal colon using advanced high-resolution fiber-optic manometry. This work was utilized along with Dinning et al. (2008) to reproduce the main motility pattern occurred in the proximal colon and the pressure amplitudes obtained *in vitro*, compared with the available data in literature. Flow episodes upon predetermined wall motion of the *in vitro* model, monitored with using Positron Emission Tomography (PET), were compared mainly with Cook et al. (2000) and Dinning (2008) as both studies deal with the relationships of pressure events and movements of contents.

Finally, dissolution test was conducted with using the *in vitro* model and the results were compared with the USP 2 mini volume dissolution apparatus. The current compedial apparatus was chosen since the volume of 100 mL were within the range of the volume of the colonic fluids in the caecum – ascending region.

Chapter VI discusses how the interpretation of the mixing and fluid flow were affected by the interplay between predetermined conditions (i.e. wall motion, viscosity, volume of fluids) and the properties of the radioactive particle used to track the movements of the contents in the partially filled DCM using Positron Emission Particle Tracking (PEPT). Chapter VII discusses the dissolution profile of theophylline modified release tablets, within the DCM and is published in part in Stamatopoulos et al. (2016b). In this Chapter a comparison of dissolution within DCM and mini volume UPS 2 apparatus is also presented.

Finally, Chapter VIII presents an overall conclusion of the research within this thesis, highlighting the importance of the work conducted and the limitations of the results. This chapter also suggests potential topics for future research to improve *in vitro* models of human GI tract.

The results chapters' structure reflects the required format of the journals where the chapters submitted.

1.4 Publications arising from this thesis

- Stamatopoulos et al., (2015). **Understanding the impact of media viscosity on dissolution of a highly water soluble drug within a USP 2 mini vessel dissolution apparatus using an optical planar induced fluorescence (PLIF) method.** International Journal of Pharmaceutics (495) 362-73.

- Stamatopoulos et al., (2016). **Use of PLIF to assess the mixing performance of small volume USP 2 apparatus in shear thinning media.** Chemical Engineering Science (145) 1-9.

- Stamatopoulos et al., (2016). **Dissolution profile of theophylline modified release tablets, using a biorelevant Dynamic Colon Model (DCM).** European Journal of Pharmaceutics and Biopharmaceutics (108) 9-17.

- Alexiadis et al., (2017). **Using discrete multi-physics for detailed exploration of hydrodynamics in an in vitro colon system.** Computers in Biology and Medicine. (81) 188–198.

- Stamatopoulos et al., (2016, for submission). **Development of an artificial Dynamic Colon Model (DCM): a tool for analysing motility and mixing in the human proximal colon.**

- Stamatopoulos et al., (2016, for submission). **Understanding flow and mixing process in proximal human colon, using a novel Dynamic Colon Model.**

1.5 Conference presentations arising from this thesis

- Stamatopoulos et al., (2016) “Analysing mixing process in human proximal colon by Positron Emission Particle Tracking System (PEPT) using an in vitro Dynamic Colon Model (DCM)” **in Mixing XXV. June 26 - July 1, Quebec City, Canada**
- Stamatopoulos et al., (2016) “Insight to human colon motility by Positron Emission Particle Tracking System (PEPT) using an in vitro Dynamic Colon Model (DCM)” **in 10th World Meeting on Pharmaceutics, Biopharmaceutics and Pharmaceutical Technology 4-7 April, 2016 Glasgow, UK.**
- Stamatopoulos et al., (2016) “A novel biorelevant dynamic colon model (DCM) for analyzing colon motility and fluid movements using Positron Emission Particle Tracking System (PEPT) and Positron Emission Tomography (PET)” **in Association of Coloproctology of Great Britain & Ireland 2016 Annual Meeting.**
- Stamatopoulos et al., (2014) “A dynamic engineering model of human colon: a tool for designing colon-specific drug delivery systems” **in 3rd Galenus Workshop, Predictive Dissolution Testing – News and Views July 02 – 04, Greifswald**
- Stamatopoulos et al., (2014) “A dynamic engineering model of human colon: a tool for designing colon-specific drug delivery systems” **in 9th September UK PharmSci, The Science of Medicines, UK (Invited Oral presentation selected from abstract).**

Abbreviations

API	Active Pharmaceutical Ingredient
CCD	Charged Coupled Device
GI	Gastrointestinal
HAPCs	High Amplitude Propagating Contractions
IA	Interrogation Area
ICCs	Interstitial Cells of Cajal
LAPCs	Low Amplitude Propagating Contractions
PEG	Polyethylene Glycol
PEPT	Positron Emission Particle Tracking
PIV	Particle Image Velocimetry
PLIF	Planar Laser Induced Fluorescence
PS	Propagating Sequences
RPMs	Radio – opaque Markers
TIM-1	TNO (gastro-) Intestinal Models
TIM-2	TNO Colon simulator
TNO	Nederlandse Organisatie voor Toegepast
USP	United States Pharmacopeia

2 Literature Review

2.1 Drug delivery to the colon

Millions of people suffer from bowel diseases such as ulcerative colitis, cirrhosis disease, amoebiasis, and cancer with thousands of new cases diagnosed annually (Yang et al., 2002). Hence, effective local delivery of drug substances for the treatment of these disorders is of high value (Khan et al., 1999). The colon has been considered an attractive region for systemic delivery of proteins and peptides due to less diversity, and intensity of digestive enzymes (Prasanth et al., 2012), as well as low proteolytic enzyme activities compare to the upper GI tract (Yang et al., 2002). Furthermore, the higher responsiveness to absorption enhancers (e.g. chitosan) (Sinha et al., 2007) and the much longer transit times compared to the upper Gastrointestinal (GI) tract (Sinha and Kumria, 2003), is advantageous on the improvement of the bioavailability of certain drug substances. Localised delivery allows topical treatment for inflammatory bowel disease.

The oral route, for drug administration, is the most convenient method to deliver drugs for local and systemic treatment (Prasad, 2011). Due to the distal location of colon, a delivery system should prevent the drug release during its passage through the upper GI tract (Johnson and Gee, 1981). Thus, different approaches have been used to develop delivery systems triggered by the local environment of human colon. These systems could be categorized as follow: pH dependent, time controlled release, microbial triggered, pressure and osmotic controlled (Prasanth et al., 2012).

Because of the high variability in the conditions prevailing in the GI tract, typically, a single-unit system fails to effectively deliver drugs into the colon (Das et al., 2010). Thus, multiparticulate delivery systems (i.e. the drug is hosted in independent subunits) have gained increased importance since they depend less on gastric emptying and hence on inter- and intra-subject GI transit time variability (Dey et al., 2008).

The transit time of a modified dosage form through the GI tract differs significantly with the highest variability being observed in the human colon; although the residence times in the small intestine are fairly constant (between 3 - 4 h) (Asghar and Chandran, 2006), in the human colon have been reported to be as high as 33 h in men and 47 h in women (Hinton et al., 1969). However, there are large inconsistencies in the literature concerning transit times since many factors such as bowel diseases (e.g. diarrhoea, constipation and ulcerative colitis), diet, fasted or fed state, and age alter the transit times resulting in a wide range of 25 h - 160 h (Cummings et al., 1992). Rapid transit, as in case of diarrhoea (Manfred R. von der Ohe, 1993) reduces the residence time for the dosage form before its elimination via defecation, whilst prolonged colonic residence, as in constipation, may result in overexposure of drug (Washington et al., 2000).

As moving towards the distal colon, the dewatering and hence the solidification of faecal matter results in an increase in the viscosity of the colonic fluids (Washington et al., 2002). As a further consequence, the diffusivity of the drug is decreased in the colonic fluid.

Thus the ascending colon is considered a more favourable site for drug delivery (Erik, 2010). In this region the colonic luminal material is sufficiently fluid for the dissolution of the drug, the surface area is somewhat larger and the bacterial activity is higher (Cummings et al., 1992, Yang, 2008). After the mid-transverse colon, the absorption of even the most water-soluble drugs is reduced, due to the very low water content of luminal fluids (Washington et al., 2002).

Unlike the upper GI tract (i.e. stomach and small intestine), the colonic environment possesses diverse and abundant microflora (Cox et al., 1982) with some bacterial species to have found exclusively in colon (Cox et al., 1983; Schiller et al., 2005; Washington et al., 2002). The energy supply for the vast microflora in the colon comes from the fermentation of the undigested residues of small intestinal fluids (Cox et al., 1982). The indigestible portion of food, which reaches the colon, includes di-, tri-polysaccharides, mucopolysaccharides, etc. (Rubinstein, 1990). These substances interact with bacteria to produce a variety of reductive and hydrolytic enzymes. The presence of this diverse class of digestive enzymes has led to

the development of various systems for drug delivery to this part of the GI tract. Prodrugs (V. R. Sinha & Kumria, 2001a) and systems based upon biodegradable polymers are two typical classes of colonic microbial triggered delivery systems (Kukura, Arratia, Szalai, & Muzzio, 2003; V. R. Sinha & Kumria, 2001b).

Another challenge in effectively delivering drugs to the colon is the impact of bowel disorders on the physicochemical characteristics of the lumen (Vertzoni et al., 2010) as well as on the delivery system (Kong & Singh, 2008). The physiological pH of the colon in healthy humans varies between 5.5–7.8 (Washington et al., 2002). However, in patients with ulcerative colitis, the colonic pH can be from 5.0–7.0, whereas, in other subjects may be very low: 2.3, 2.9 and 3.4 (Fallingborg, Christensen, Jacobsen, & Rasmussen, 1993). Furthermore, the lumen pH changes according to the status of the subject (i.e. fasted or fed state) (Diakidou et al., 2009).

The colonic absorption of drugs may differ significantly from the upper GI tract due to several physiological, physicochemical, and biopharmaceutical factors (Thombre, 2005). However, solubility and permeability are in general the most important parameters affecting drug absorption regardless of the region of the GI tract (Baxter et al., 2005). The solubility and rate of dissolution of a drug can be evaluated *in vitro* with a dissolution test. As explained later in more detail (see section 2.5), the concept behind the use of dissolution test for predicting the *in vivo* performance is to assess the rate of solubilisation of a drug as it must first be dissolved in the aqueous phase of the GI contents before it can be absorbed (Jantratid et al., 2009). In modified release dosage forms the dissolution test may give a measure of the extent and the rate of the drug released. However, the drug release profile is affected by several factors such as properties of the active ingredient, formulation design and manufacturing process as well as the chemical and mechanical environment of the test method. Great care must be taken in the evaluation of these factors concerning their contribution and impact on the drug release to develop meaningful dissolution test methods. Nevertheless, studies have shown that the *in vitro* solubility (i.e. dissolution) profile of a drug is not always proportional to its *in vivo*

performance (Ahmed & Ayres, 2011) but depends on the dissolution method and the physicochemical properties of the drug.

As mentioned before, bowel disorders alter the colonic environment in terms of transit times, pH, and water content. Higher absorption rates are anticipated for drugs during long transit times because of an increased contact of lumen contents with the colonic wall. However, Hebden et al., 1999, showed that accelerated transit and increased stool water content, enhances drug absorption whilst slow transit and decreased stool water content, tends to diminish drug absorption (Wang, 2009). Consequently, there is a need to clarify the impact not only of these two variables (Klein & Shah, 2008) but also all those parameters (i.e. motility, pH etc.) which determine the colonic environment.

2.1.1 *Drug absorption by the human colon*

Several barriers limit drug absorption from the colon. Figure 2.2 shows a schematic representation of the factors that affect drug bioavailability. In the lumen itself, the drug can interact with the dietary components resulting in specific and non-specific binding with dietary components. For example, lectins may interact with sugar residues on the protein of a glycoprotein drug molecule whereas non-selective interaction may occur between indigestive foodstuffs like alginates and waxes and the drug compound (Prasad, 2011). Pro-drugs released by the microflora in the colonic lumen could also lead to specific and non-specific binding events. The present of reactive groups, such as free sulfhydryls, in the drug molecule might promote drug-binding interactions with the colonic bacteria (Mrsny, 1992). Moreover, the drug molecules remaining in the lumen, face the increase in bacterial content during their passage from the proximal to the distal colon (Rangachari, 1990) which could further compromise drug bioavailability.

The rate of the drug absorption for weak acid or basic drugs will be controlled by the pH of absorptive site as well as the partition coefficient. That means that, the pH of the microclimate

at the mucosal surface, and not the pH of the lumen, will determine the dissociation of the drug and hence its absorption rate (Washington et al., 2002).

The dewatering of the faeces within the colon leads to inadequate mixing in the bulk phase and hence less access to the mucosal surface. In addition, the reduction in the water content has also impact on drug dissolution and hence on drug bioavailability. Furthermore, the contact of the drug with the mucosa can be inhibited by the presence of gas in the colon.

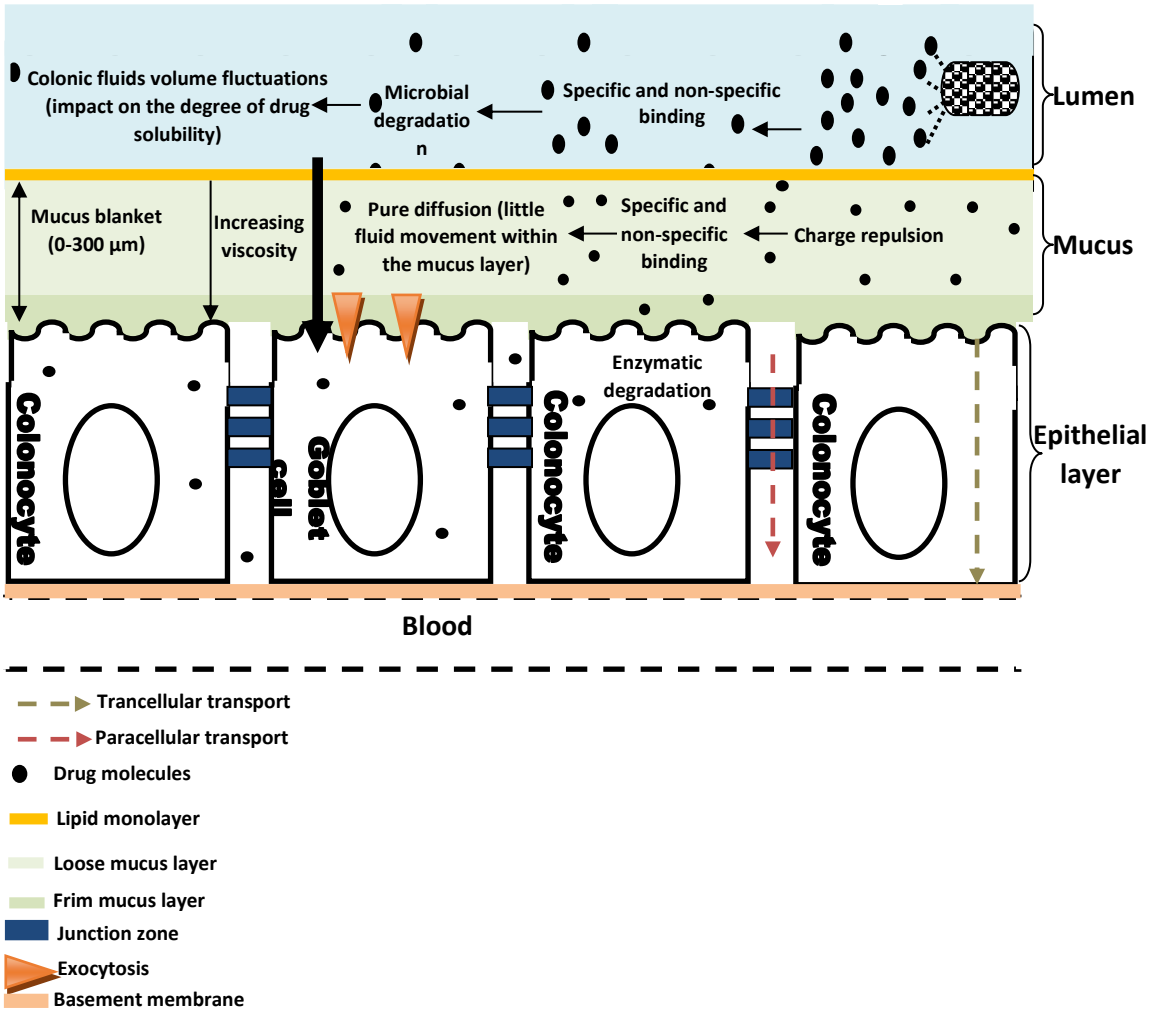

Figure 2.1. Drug absorption pathway with uptake barriers found within lumen, mucus and epithelial layer.

It has been suggested that some gel-forming polysaccharide gums increase the thickness of the unstirred water layer (Johnson & Gee, 1981). Moreover, dietary fibres such as pectin and chitosan have cation-exchange properties which may bind drug molecules. These physical factors will all act to slow drug absorption in the colon, with increasing effect as water is removed and the transport properties of the faecal mass are reduced.

2.2 Physiology of human colon

The gastrointestinal (GI) tract is composed by the oesophagus, stomach, small intestine and the colon as the final organ. The other physiological terms used for the colon such as large intestine and bowel will be used interchangeably in the present text.

The human colon (Figure 2.2) is the last site of absorption for digestive residues. It is comprised of the caecum as well as ascending, transverse, descending, sigmoid colon and rectum. The ascending and transverse regions form the main parts of the proximal, or right colon, whereas the distal, or left, is composed of the descending and sigmoid regions. At the end of the ascending colon there is a sharp bend known as hepatic, or right, flexure before the continuation of the colon towards the transverse region. Thereafter, there is another bend known as splenic, or left, flexure located at the end of the transverse segment and the beginning of the descending colon, as indicated in Figure 2.2.

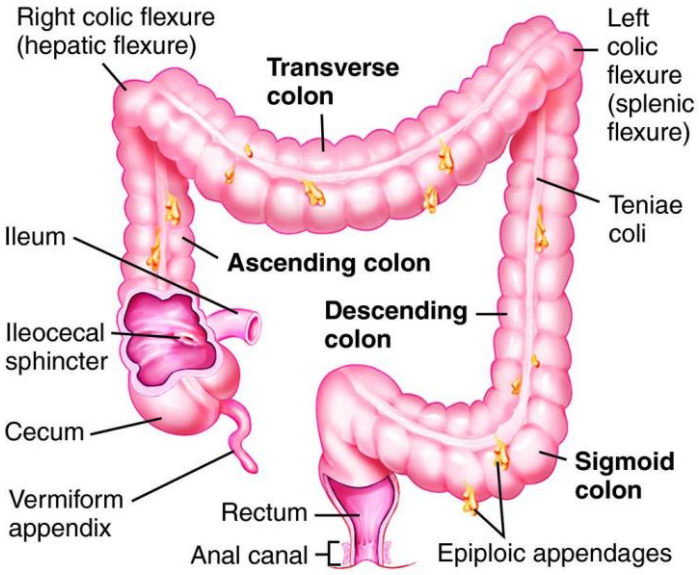

Figure 2.2.Human colon anatomy (Mosby's Medical Dictionary, 8th Edition)

The large intestine is a continuous non-perfectly cylindrical tube approximately 1.29 ±0.16 m in length, although, there are various gender and age differences (Sadahiro et al., 1992). Regarding the diameter, it starts with a value of around 8.5 cm at the caecum and ends up to 2.5 cm at the sigmoid colon (Washington et al., 2000).

The undigested food from small intestine flows to the caecum which is regulated by the ileocecal valve. The caecum and ascending colon seems to have as a main functions the reception of the ileum contents as well as the storage, mixing and absorption of the colonic contents (Cook et al., 2000, Hiroz et al., 2009). The ascending colon is on average 0.16 m in length (Sadahiro et al., 1992), appearing between the ileocaecal valve and the hepatic flexure. Thereafter is the transverse colon, which is approximately 0.42 m in length (Sadahiro et al., 1992). This is the largest region of the colon with the most motility (Davidson et al., 2011). After the transverse colon is the splenic flexure which ends up to descending colon. The descending colon is longer (0.20 m) than the ascending because of the higher position of the splenic flexure in the body, (Sadahiro et al., 1992; Washington et al., 2000). The current region (i.e. descending) serves as a conduit between the storage (i.e. transverse colon) and excretory

areas (i.e. sigmoid colon) (Hiroz et al., 2009). The sigmoid colon, so called `S-shaped' colon, is approximately 0.40 m in length and 0.033 m in diameter (Sadahiro et al., 1992), and it begins at the pelvic brim as a continuation of the descending colon.

The main digestive functions of the colon include: absorption of water, electrolytes and nutrients from partially digested food (Szmulowicz and Hull, 2011); fermentation (proximal colon) of non-digestible carbohydrates (e.g. dietary fibre) from small intestinal enzymes; conversion of vitamin K1 to K2 by colonic microflora (Conly et al., 1994), and distal propulsion of contents as well as storage of faecal matter until defecation. As will be discussed in more detail later, there are differences between the colonic regions in terms of motility, absorption etc. For example the blood supply of the proximal and distal colon is different (Picon et al., 1992), whereas, the right colon (i.e. caecum, ascending, hepatic flexure and mid-transverse) absorbs more water and electrolytes than the left (Sandle, 1998).

The colon wall consists of two layers of smooth muscle. The circular oriented muscle is in the interior of the colon wall whereas the outer layer is oriented perpendicular to the circular muscle and runs longitudinally along the colon tube. On the longitudinal muscular layer there are three strips so called taeniae coli (Langer and Takács, 2004).

Haustra (i.e. small pouches) are formed throughout the colon because taeniae are shorter than the true length of the organ (Kelvin and Gardiner, 1987) causing sacculation of the colon, resulting in its segmented appearance (see Figure 2.3). The folds between the haustra are known as semilunar folds and contain all layers of the colonic wall. The semilunar folds are formed due to “anchoring” of circular muscles on taeniae (Langer and Takács, 2004). The haustra within the proximal colon are fixed anatomical structures because of the fusion between the taeniae and the underlying circular muscle, whereas, in the distal colon they are formed by a combination of contraction, relaxation or passive extension of circular and longitudinal muscles (Langer & Takács, 2004).

Moving towards the interior of the colon wall there is a connective tissue called submucosa which is located between the circular muscle layer and mucosa (Figure 2.2). The mucus membrane is a moist tissue which covers the most of the organs surfaces and cavities of the human body such as the intestines, lungs and nose (Edsman and Hagerstrom, 2005).

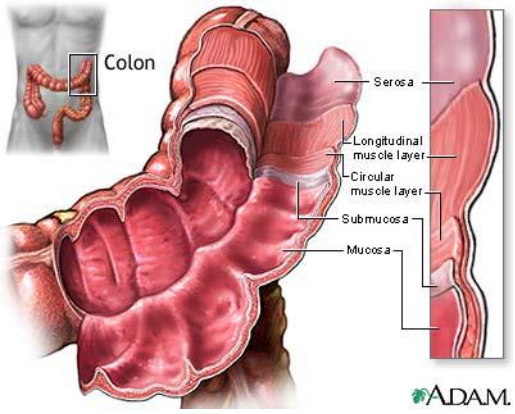

Figure 2.3.Anatomy of human colon wall (www.umm.edu)

The colonic mucosa contains enterocytes, as well as goblet and enteroendocrine cells (Varum et al., 2008); enterocytes are responsible for absorption, goblet cells secrete mucus and enteroendocrine cells produce hormones.

The function of mucus in the GI tract is to lubricate the surface of the organs for minimizing the frictional forces during the peristaltic transport of the contents (Lai et al., 2009) while allowing rapid entry and exit of nutrients and waste (Florey, 1955). In the colon, mucus protects the epithelial cells from the hosting bacteria.

2.3 Human colon motility

The human colon performs several different functions, including storing, mixing and propulsion of the colonic fluids (Scott, 2003), essential for the optimal absorption of water, electrolytes and bacterial metabolites (Cook et al., 2000). The diverse functions of the colon require a complex motor activity to slowly propel the contents for maximal absorption whilst avoiding over-solidification of the faeces (Sarna and Shi, 2006).

Animal studies using isolated sections of intestine (Crema et al., 1970, D'Antona et al., 2001, Dinning et al., 2011, Dinning et al., 2012, Costa et al., 2013a, Costa et al., 2015) and advances

in monitoring techniques, like high resolution video imaging (Costa et al., 2013c) as well as high resolution manometry (Dinning et al., 2013, Corsetti et al., 2016), have provided improved understanding of colonic motility. These studies are highly valuable since most of the motility patterns that occur in animal intestine are found also in the human colon (Spencer et al., 2016).

2.3.1 Mechanisms controlling colon motility

Motility refers to the temporal and spatial coordinated contractions and relaxations of the longitudinal and circular muscle cells (Spencer et al., 2016). The movements of the colonic muscle are controlled by the interplay of two main fundamental mechanisms. The first one, so called 'myogenic' activity is generated by networks of pacemaker interstitial cells of Cajal (ICCs) (Sanders et al., 2014) which are responsible for spreading this activity to smooth colonic muscle cells (Liu et al., 2012). This type of contractile activity causes slow rhythmic contractile patterns (Mañé et al., 2015). However, the myogenic activity is not enough to effectively propel the contents and therefore an additional activity is required (Spencer et al., 2016). The second mechanism, so called neurogenic activity, involves polarized reflexes, activated by distension of the colonic fluids (Spencer et al., 2012), and cyclical colonic migrating motor complex. These two neural pathways are involved in the propulsion of the contents (Dinning et al., 2012).

Distended contents trigger enteric ascending excitatory (i.e. contraction of circular muscle) and descending inhibitory (i.e. relaxation of the circular muscle) neural pathways (Dinning et al., 2014b); this is referred in literature as 'law of the intestine' (Sinnott et al., 2012). It has been proposed that this simultaneous contraction/relaxation is controlled by a so called 'neuromechanical loop' (Costa et al., 2013b). This is a feedback mechanism which adapts the colon motility accordingly to the redistribution of the contents after the contraction and relaxation of the circular muscle (Figure 2.4; reproduced from Costa et al., 2015). The redistribution of the contents depends on their consistency (e.g. viscosity), ranging from liquid to solid pellets formed during the dewatering process. Moreover, there is a relationship

between the surface area occupied by the semi-solid material and the speed of the propulsion, reflecting the number of the mechano-sensitive neurons activated by the bolus (Costa et al., 2015).

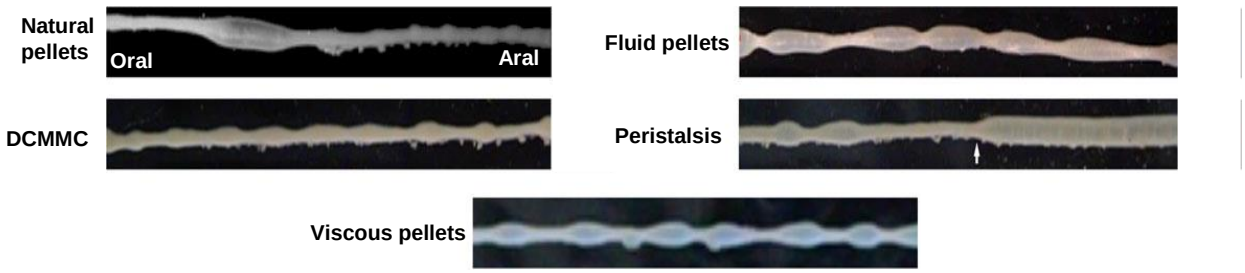

Figure 2.4. Propulsion patterns with respect to the consistency of the luminal contents in guinea-pig colon; DCMMC: distal colonic migrating motor complexes (Figure reproduced from Costa et al., 2015 with permission).

2.3.2 Motility patterns in human colon

The best described motility patterns in human colon are the so called 'mass movements' of the contents. These movements are associated with strong contractions of the circular muscle which extensively propagate along the colon (Figure 2.5). This motility pattern is frequently referred as high amplitude (>100 mmHg) propagating contractions (Dinning et al., 2010) (HAPCs) or sequences (Dinning et al., 2014a), occurring 3 – 24 times per day. They often predominate after morning waking (Bampton et al., 2001), however, can also appear shortly after a high calorie meal (Bassotti et al., 1993, Bassotti et al., 1995). Previous *in vivo* studies have shown that HAPCs are absent in an empty 'prepared' colon, suggesting that, as with the neurogenic peristaltic contractions observed in animals, luminal distention is required to evoke HAPCs (Spencer et al., 2016). For instance, undigested starch in the colon can increase the incidence of HAPCs (Jouët et al., 2011). However, HAPCs can also be triggered by chemical stimuli such as bisacodyl, chenodeoxycholic acid, and short-chain fatty acids (Kamm et al., 1992, Cook et al., 2000, Bampton et al., 2001) which acts by triggering the mucosal afferent neurons (Dinning et al., 2014a). In addition, the fact that HAPCs appear after a meal (Bassotti

and Gaburri, 1988, Bampton et al., 2001, Dinning et al., 2010), suggests that enteric neurons are modulated by extrinsic neural inputs.

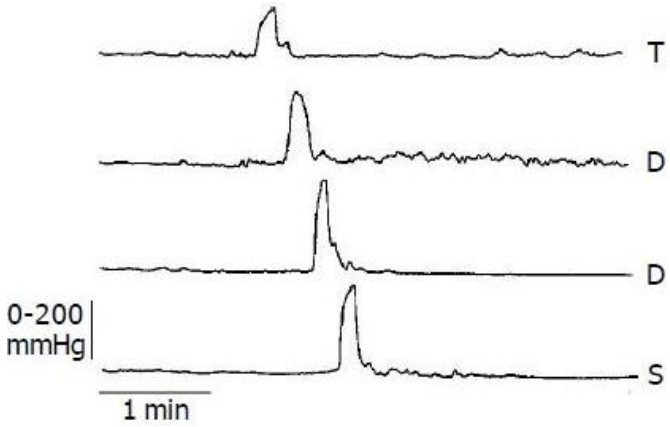

Figure 2.5. Manometric tracing of a high amplitude propagating contraction (HAPC) using low-resolution manometry (recording points are 12 cm apart) placed from the distal transverse (T) to the proximal sigmoid colon (S); distending colon (D). Figure reproduced from Bassotti et al. 2005.

For several decades, it was widely accepted that between HAPCs, the main motility pattern in healthy human colon was the so called, segmental, non-propagating, contractile activity (Narducci et al., 1987, Bampton et al., 2001, Rao et al., 2001, Gabrio Bassotti, 2005). Thus, based on the previous *in vivo* studies, using low-resolution manometry (i.e. sensors spaced ≥7 cm), the human colon motility was categorized between the propagating activity, including low amplitude propagating contractions (LAPCs) and HAPCs, and non-propagating (i.e. segmental) (Bassotti et al., 1995). The segmental activity could be appeared either as irregular *'bursts'* with some to be *'rhythmic'* or *'arrhythmic'*, or as isolated, sporadic event (Scott, 2003). The rhythmic frequency of the segmental contractile activity is mostly comprised in the range 2 – 8 min^{-1} (Rao et al., 2001), and it is mainly observed in the distal (descending and sigmoid colon) (Bassotti et al., 1990). However, other studies showed that these motility patterns sporadically appeared in other regions of the colon (Bampton et al., 2001) and they can travel orally or aborally (Rao and Welcher, 1996).

In recent years, high resolution manometry (sensor spacing 1 cm) revealed that half of all propagating motor patterns are either missed or incorrectly classified as sporadic and/or *'burst'* events (Dinning et al., 2013, Dinning et al., 2014a). These small amplitude intermediate rhythmic frequency cyclic contractions (2 – 8 min^{-1}), labelled in earlier studies as *'burst'*, non – propagating events, were shown to be propagating motility patterns (Dinning et al., 2013). This contractile activity predominates between HAPCs and occurs in all regions of the colon but prevails in distal colon, sigmoid and rectum, suggesting that they occur to maintain continence and control defecation (Dinning et al., 2014a). Figure 2.6 (reproduced from Dinning et al. 2013) shows the difference between manometric tracing graph obtained with using low- and high-resolution manometry, demonstrating how large (i.e. 10 cm) and small (i.e. 1 cm) spacing of the sensors affect the interpretation of manometric measurements. For example, the short extend retrograde propagating contractions appeared in high resolution manometry (Figure 2.6a, inside the blue boxes), they would be labelled as segmental, non-propagating, isolated contractile activity (Figure 2.6b) if low resolution manometry had used. On the other hand, the same retrograde propagating contractions (or sequences) (Figure 2.6c) would be labelled as low amplitude aborally propagating contractions in low resolution manometric graph (Figure 2.6d). Furthermore, the manometric graphs show that there are also regional differences with regards to the motility patterns that predominate. For instance, high resolution manometry showed that extended or short propagating contractions originated from the ascending colon, whereas most of the short – extended retrograde propagating contractions appeared in the sigmoid colon.

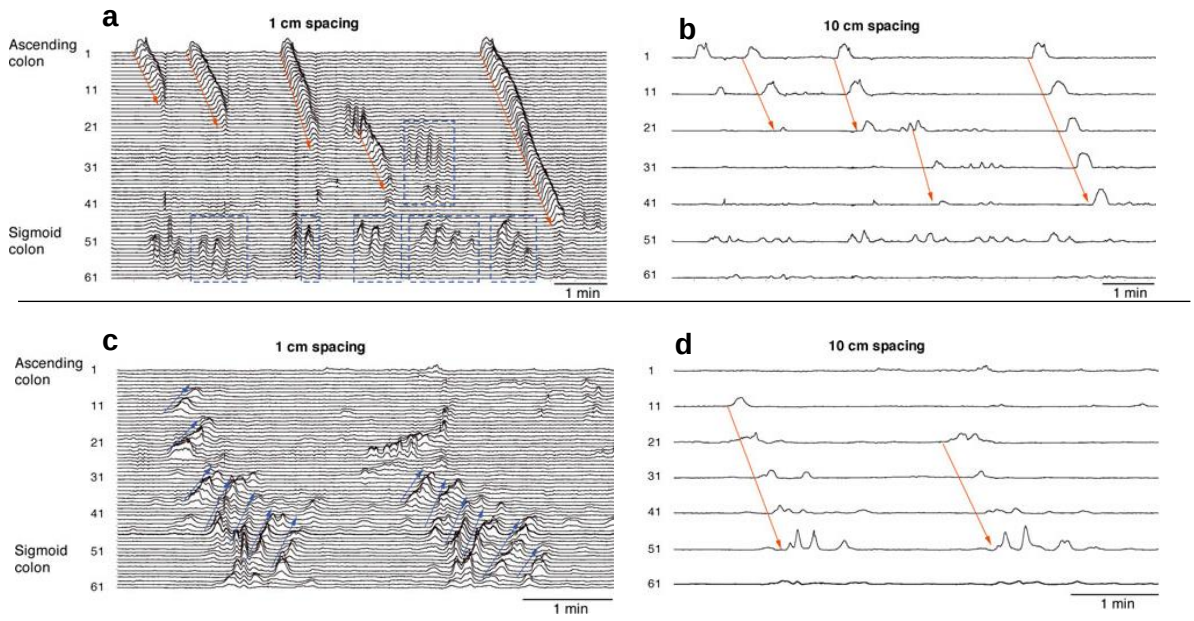

Figure 2.6. Representative section of colonic manometry displayed with 10 cm and 1 cm spacing. Several antegrade (red arrows) and retrograde (blue arrows) propagating sequences could be detected using 1 cm spacing (Figure reproduced from Dinning et al. 2013 with permission).

High resolution manometry has also highlighted three other propagating sequences (Figure 2.7) in human colon (Dinning et al., 2014a): (i) cyclic propagating motility (or motor) pattern (ii) short single motility patterns which are isolated patterns that propagate antegradely or retrogradely and occur in the proximal and distal colon, (iii) long single motility patterns propagate along the colon at longer distances compared to myogenic cyclic contractions, with velocity 0.018 ±0.012 m s^{-1}; this motility pattern originates form the proximal colon to the mid – descending colon, and (iv) retrograde slow propagating motility patterns travel at low velocity (0.005 m s^{-1}) over long distances (>0.4 m).

Retrograde cyclic propagating motility pattern predominates in sigmoid colon (Figure 2.7B) and it has been suggested that the prominence of this motor pattern is to help to retard flow (Dinning et al., 2014a). However, retrograde flow can also occur within the proximal colon

where a magnetic pill, used to track colon motility, was observed to slowly move in a retrograde direction from transverse to ascending colon over several hours (Hiroz et al., 2009).

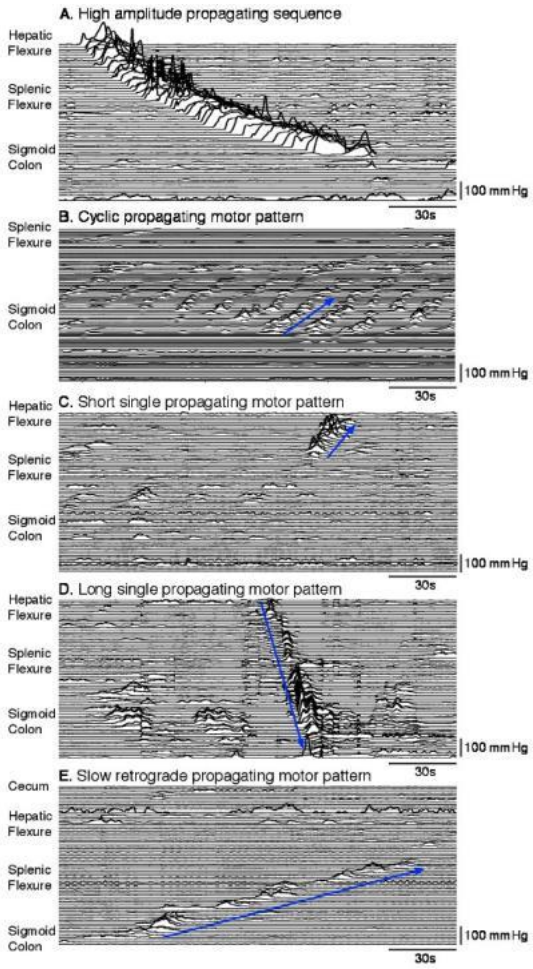

Figure 2.7. High resolution manometry recordings from healthy human colon (Figure reproduced from Dinning et al. 2014 with permission).

Very recently, another motility pattern, termed pan-colonic pressurizations, has been detected and is associated with the relaxation of the internal anal sphincter (Corsetti et al., 2016). Pressures recorded simultaneously along the entire length of the human colon (Figure 2.8) with amplitude of 15 ±3 mm Hg and 24 ±4 s duration. Pan-colonic pressurizations are increased significantly during a meal, however, decreased afterward. These simultaneous pressures are correlated with farting (Corsetti et al., 2016).

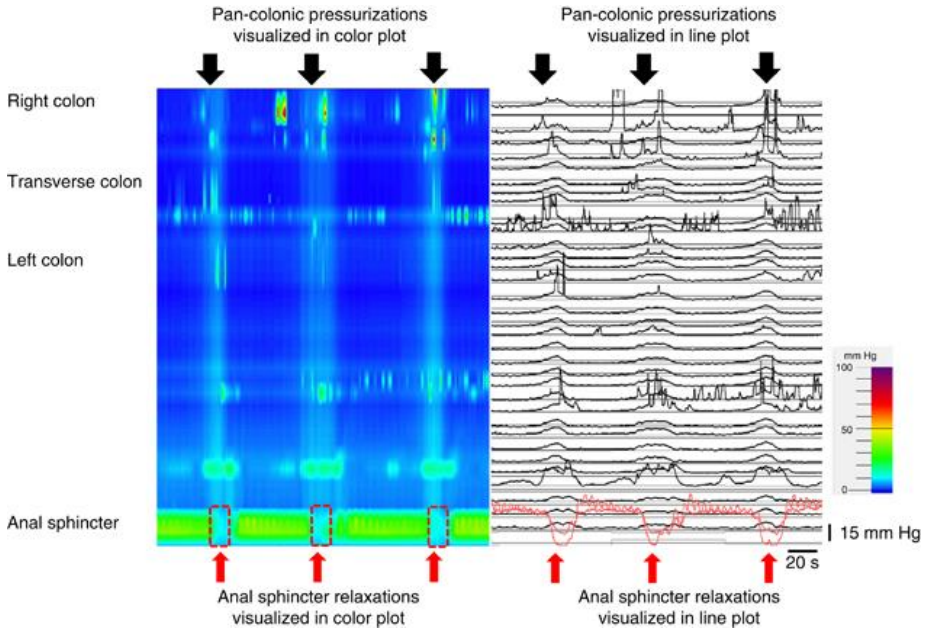

Figure 2.8. Repeated pan-colonic pressurizations associated with anal sphincter relaxation (Figure reproduced from Corsetti et al. 2016 with permission)

2.3.3 Relationships between propagating sequences and propulsion of the contents

Several *in vitro* studies have shown that propagating sequences (PS) or pressure waves are important determinants to the propulsion and the defecation of the colon contents (Moreno-Osset et al., 1989, Bazzocchi et al., 1991, Reddy et al., 1991, Herbst et al., 1997, Cook et al., 2000). Alterations to PS, are linked to abnormalities of the colon motility (Bassotti and Gaburri, 1988, Bassotti et al., 1992, Rao et al., 2004, Dinning et al., 2004); Table 2.1 shows the relationship between different colonic disorders and alterations in the contractile activity of the human colon. However, there is a lack of understanding between the different motility patterns of the human colon and their association with the propulsion of the contents (Cook et al., 2000). This is because on the one hand, manometry failed to adequately describe the colon wall motion (Dinning et al., 2008) and on the other hand scintigraphy, used to visualise flow episodes in human colon, can be limited from the low frame rate (Reddy et al., 1991, Bazzocchi et al., 1991) and the pure visual analysis of isotope flow (Cook et al., 2000).

Improvements made on these two techniques (i.e. use of manometry with closely spaced sensors combined with higher frame rate scintigraphy), revealed the propulsion nature of most of propagating sequences (Dinning et al., 2008); the authors found that 93% of the antegrade PS recorded in proximal colon were associated with flow episodes. However, the authors also showed that over the half of flow episodes occurred in the absence of PS and their association with fluid motion was significantly reduced in the ascending colon. A possible explanation, given by the authors, was that apart from the tone of colon wall (Moreno-Osset et al., 1989) and the viscosity of the contents (Proano et al., 1990), contributing to the propulsion of the fluids, it is likely that a proportion of the motility patterns will be missed due to reduced sensitivity of the manometry within gut regions of diameter exceeding 0.056 m (Von Der Ohe et al., 1994), as in case of the caecum – ascending region.

Arkwright et al. (2013) evaluated the performance of the manometry in an *in vitro* apparatus used to simulate non – occluding (i.e. no physical contact of the manometric catheter with the colon wall) oscillation of a flexible wall. The authors found that the manometry detected non – occluding events and that the interpretation of the results was affected by the viscosity of the luminal contents and the occlusion rate. However, the authors did not reproduce the complete environment of the caecum – ascending colon since the tube was fully filled with medium. However, the caecum – ascending region is partially and not uniformly field with fluids, with fluid present in pockets (Schiller et al., 2005). Furthermore, the authors did not examine whether the manometry could differentiate changes in the degree of luminal occlusion for non – occluding events, since the greater the occlusion degree the more volume of fluids will be expelled from the contracting point.

Thus, it remains to be answered how the volume of the fluids will affect the performance of manometry and how this will reflect the association of the pressure waves with the propulsion of the contents within the colon. In addition, manometry failed to differentiate intraluminal pressures from pressure forces generated by the wall motion (Sinnott et al., 2015). Thus, care should be taken when *in vivo* pressure values used in *in vitro* dissolution testing machines for

the evaluation of the performance of the dosage forms. This is because the pressure forces might not reflect how extensively and intensively the fluid are propelled and mixed.

Table 2.1. Effect of colon diseases, fasted and fed state on transit times, pH as well as colon motility

		Type of propagate sequence	
Disorders	**Transit times**	**HAPCs**	**Segmentation/other ante- retrograde short extended propagating motor patterns**
Diarrhoea	6 times faster (Manfred R. von der Ohe, 1993)	Increased (Bharucha, 2012)	Reduced (Bharucha, 2012)
Constipation	Increased (Rao et al., 2009)	Decreased (Asghar and Chandran, 2006, Dinning et al., 2010)	Increased (Asghar and Chandran, 2006, Dinning et al., 2010)
Ulcerative colitis	Varied (Fallingborg et al., 1993)	Increased (Fallingborg et al., 1993, Bassotti et al., 2004)	Decreased (Bassotti et al., 2014) even after meal (Reddy et al., 1991)

2.3.4 Other non – invasive methods to monitor human colon motility and transit times

Scintigraphy and radio – opaque markers (RPMs) are common methods used to estimate transit times in human colon (Kim and Rhee, 2012). In particular, RPMs are plastic beads ingested in a capsule containing 20 – 50 markers. There are two methods followed to assess the transit times in human colon. In the single capsule technique, one capsule is ingested followed by several abdominal X-rays images captured every 24 h until the complete defecation of the markers (Southwell et al., 2009). However, this incurs high exposure to radiation for the patients and is time consuming. In the multiple-marker technique, a capsule

is ingested on 3 consecutive days and X-rays images are captured at 4th and 7th day, or only at 7th day (Kim and Rhee, 2012).

Scintigraphy, besides the technical limitations of the technique, gives information about the movements of the physiological meal (Maqbool et al., 2009), whereas radio – opaque markers (RPMs) doesn't (Kim and Rhee, 2012) but mainly the overall transit.

Wireless capsule (Saad and Hasler, 2011) and magnetic pill tracking system (Hiroz et al., 2009) have been introduced as alternative non – invasive monitor techniques of the human colon motility and transit. Wireless capsule has shown good correlation with scintigraphy isotope distribution within the human colon at a given time (Deiteren et al., 2010) (Maqbool et al., 2009) and radio – opaque markers (Rao et al., 2009). Pressure amplitudes measured with wireless pill are in a good agreement with manometry (Brun et al., 2012), however, a wireless pill with only one pressure sensor is not able to show the propagation of the different motility patterns (Tran et al., 2012). In addition, wireless pill behaves as a free-floating body (Farmer et al., 2013) making its motion (i.e. speed, location, orientation) unpredictable (Koulaouzidis et al., 2015). Several studies have been conducted using the so called SmartPill®, to monitor transit times, pH and pressure amplitudes at fed and fasted state (Schneider et al., 2016) as well as at different disease states (Saad, 2016); revealing the high variability in pressures during gastric emptying process e.g. before and after administration of high-caloric, high-fat (964 kcal) FDA standard breakfast (Koziolek et al., 2015).

Magnetic pill tracking system was used by Stathopoulos et al. (2005) and Hiroz et al. (2009) to monitor human digestive motility. In both studies rhythmic 'to and fro' motion of the magnetic pill within the caecum – ascending region was observed, resulting in slow and small net forward propulsion (0.026 m h^{-1}). In addition, the authors observed retrograde displacements of the pill, suggesting that this motion contributes to intraluminal mixing. Hiroz et al. (2009) reported that the pill followed the flow motion, however, the much lighter radiopaque markers were found to overtake the much heavier magnetic pill. The current magnetic tracking system needs further validation with simultaneous use of manometry (Stathopoulos et al., 2005) and

also comparison of the results with scintigraphy. Nevertheless, the current technique is the only non – invasive method giving some information about *in vivo* velocities and residence times of the colonic fluids characterized by a dense tablet. However, the properties of the tablet (e.g. relaxation time and buoyancy) need also to be taken into consideration for proper fluid flow characterization.

2.4 Colon specific drug delivery systems

In this section, a brief description of the available colon specific drug delivery systems is presented.

As described above, human colon is a dynamically changing environment in terms of contractility, transit times, microflora, volume and viscosity of the fluids. These conditions can change under normal or disease state but also due to diet. For instance, patients with ulcerative colitis have shorter average transit times (~24 h) compared to healthy subjects (~52 h) (Amidon et al., 2015a). The pH in caecum - right colon was found to vary in the range of 5.7 – 6.8 in healthy subjects, 2.3 – 7.2 in patients with ulcerative colitis and 5.3 – 7.2 in patients with Crohn's disease (Nugent et al., 2001); the range in pH values is based on the data reported from different studies and summarised by Nugent et al. (2001). The pH can be influenced by a diet rich in carbohydrates where upon fermentation short fatty acids are formed (Macfarlane et al., 1992), resulting in increased caecal acidity (Nugent et al., 2001).

Oral route is the most convenient way to administer drugs in humans. As mentioned above, colon is a favourable site for local and systemic treatment. Thus, a dosage form needs to survive its passage via the stomach and small intestine to reach the human colon. Then, within the colon, the dosage form should release the active pharmaceutical ingredient (API) in a controlled way.

Factors that influence the delivery and the bioavailability of the drug includes the physicochemical properties of the API, the dose and the excipients used in formulations

(Amidon et al., 2015a). However, due to low amount (1 – 14 mL (Schiller et al., 2005)) of colonic fluids, the dose (Amidon et al., 2015a) and the solubility (Wang and Flanagan, 2009) are critical factors affecting the dissolution and hence bioavailability of the API. Additionally, the presence of numerous enzymes produced by the hosted colonic microflora may metabolize drugs, forming pharmacologically active, inactive, or sometimes even toxic metabolites (Kang et al., 2012).

Different strategies have been developed to deliver APIs to the human colon: pH dependent, time dependent, prodrugs, bioadhesive systems, microbiologically triggered systems including also polysaccharide-based delivery system, pulsatile delivery, pressure and osmotic controlled systems.

pH dependent: The main principle of this formulation is the delayed release of the API by protecting it from the low gastric pH with using a polymer which is soluble in more basic pH (Chourasia and Jain, 2003). However, the solubility of these polymers rises as the pH increases. Hence, drug release might be prevented in the proximal small intestine but it may be dissolved in lower small intestine. In addition, lag time in the ileocecal junction zone and rapid transit via ascending colon can also cause poor site-selectivity. Poly-methacrylate based polymers such as Eudragit® L and Eudragit® S have unique pH at which they dissolve. Blends of these two polymers have been used in combination to effectively deliver drugs to the human colon (Khan et al., 2000). Additionally, relative thick coatings of these polymers have been used in pulsatile systems to prolong their dissolution, resulting in extending the drug release (Maroni et al., 2013).

Time dependent: This type of formulation has been designed to release the drug in the colon after a specified amount of time. It is assumed that transit times (3 – 4 h) in the small intestine is relatively constant (Alvarez-Fuentes et al., 2004) and can be used as a specific time window before reaching the colon. However, gastric emptying is not constant between individuals and can fluctuate based on food intake (Fukui et al., 2000). In addition, as mentioned above, transit times are influenced from several disorders associated with colon. Different layers of enteric-

coated polymer and hydrophilic polymers have been combined for sustainable delivery to the colon (Gazzaniga et al., 1994). Specific technologies have been developed and scaled to commercial dosage forms. In particular, TIMERx® technology, which is based on slowly eroding matrix, consists of two polysaccharides, namely, xanthan gum and locust bean gum. These two polysaccharides work synergistically forming a tight gel structure upon hydration, which retards water penetration into the dosage form, hence, controls the release of the active ingredient. Slofedipine XL (nifedipine) and Cystrin CR (oxybutynin) are based on this technology and are marketed in Europe.

Prodrugs: Inactive derivatives of APIs where the active drug is released after enzymatic hydrolysis. Azo conjugates are the most researched groups utilized to form an inactive derivative of APIs either by linking the drug to e.g. sulfate group (Kim et al., 2012) or to a carrier such as pectin, cyclodextrin, glucuronide, dextran, and amino acids (Amidon et al., 2015a). All these bonds are broken down by colonic microflora (Chourasia and Jain, 2003). Olsalazine is a characteristic commercially prodrug, under the brand DIPENTUM, of mesalazine a compound with anti-inflammatory activity in ulcerative colitis.

Bioadhesive systems: There are two terms used separately to identify whether the drug carrier adhesives to a biological tissue or to the mucus layer on the surface of a tissue. Thus, bioadhesion referred to the first case and mucoadhesion to the second one (Shaikh et al., 2011). This type of formulation was developed to increase the residence time of the active drug and improve bioavailability (Peppas et al., 2009). Some polymers with bio--mucoadhesion properties used in this type of formulation are chitosan, polyethylene glycol, hydroxyethyl cellulose, polyacrylic acid and polyvinyl alcohol (Shaikh et al., 2011). Rice starch has been also utilized to deliver metronidazole to the colon (Ahmad et al., 2012). The bioadhesive properties can be influenced by the hydrophilicity of the polymer, the pH, the concentration of the carrier, molecular weight, and cross-linking (Jiménez-castellanos et al., 1993). Furthermore, enhancement of the bioadhesive properties of the carrier might be

achieved with using polymers, e.g. carbomers, capable to reach the firmly adherent mucus layer due to the polymer chain diffusion (Varum et al., 2011).

Microbial triggered systems: The colon contains numerous species of anaerobic bacteria (clostridia, enterococci, eubacteria etc.) which produce several enzymes like azoreductase, nitroreductase, glucuronidase and xylosidase to ferment polymers which have not been digested from the upper GI tract (Rubinstein, 1990). Thus, colon specific systems can be developed by using polymers which degrade by these enzymes found only in colon. Acetyl derivative of guar gum (Roos et al., 2008), inulin azo hydrogels and many other modified polymers have been developed and summarized by Sinha and Kumria (2003). Furthermore, polysaccharides naturally presented in plants (e.g. pectin), algal (e.g., alginates), or microbial (e.g., dextran) origin have been used for colon targeting (Kosaraju , 2005). Other types of polysaccharides are cyclodextrins which are cyclic oligosaccharides break into small saccharides by *Bacteroides* (Sinha and Kumria, 2001).

Pressure controlled systems: Intraluminal pressures are higher in colon due to the present of a more viscous chyme formed during dewatering process. Thus, capsules can be developed to deliver drugs based on luminal pressure (Takaya et al., 1998, Wilde et al., 2014a, Wilde et al., 2014b).

Osmotic controlled systems: This type of system is regulated by the osmotic pressure of the chyme. The capsule consists from hard gelatin which dissolved in the pH of the small intestine. Inside the capsule there are 5 – 6 units coated with enteric polymer. A commercially available technology, so called DUROS®, consists of a cylindrical within there is a semipermeable membrane which comprises an osmotic push compartment and a drug compartment. As the water enters the push compartment swells pushing out the drug through an orifice. The flow rate of the drug depends on the rate that water enters the unit. A lag time between enteric coating dissolution and the drug's release prevents from premature release of the drug in small intestine (Philip and Pathak, 2006). Polysaccharides such as pectin, chitosan, chondroitin sulfate, galactomannan, and amylose are some of which have been used to deliver drug to

the colon because they can be degraded from the colonic microflora and their derivatives are harmless to the organisms (Philip and Philip, 2010).

Pulsatile delivery: this type of formulation utilizes the timed – released systems with pH – dependent properties to achieve colon – targeted delivery. The pulsincap system is a characteristic example of a formulation combines both these techniques (Krögel and Bodmeier, 1998). The current system consists of a water insoluble capsule containing the drug, a hydrogel which seals the open part of the capsule and then a water-soluble cap covers the hydrogel. Then the whole capsule is coated with an acid insoluble film coating to prevent premature release of the drug in stomach. When the coating film starts to dissolve in the small intestine, the water enters the capsule causing swelling of the hydrogel. The progressively swelling of the hydrogel allows for a lag time before the drug is released. The lag time depends on the concentration of the hydrogel used (Sindhu Abraham, 2007). However, as mentioned above, transit times as well as pH values varied between individuals and under different disease states. In addition, pulsatile delivery systems have some limitations such as low drug loading capacity and incomplete release of drug as well as multiple manufacturing steps (Jain et al., 2011). Furthermore, releasing the active compound in the colonic lumen, may lead to degradation of the drug from the microflora (e.g. proteins and peptides for colon cancer) and hence to ineffective local treatment. Considering these factors, pulsatile systems might need further improvements to reliably and consistently delivery drugs to the colon.

2.5 Dissolution testing of the oral solid dosage forms

The concept behind dissolution testing is that the API should be first dissolved into the bulk solution before it can be absorbed by the human body. The dissolution of an API consists of two steps. The first one is the formation of solvated molecules of the drug upon contact with the solvent and the second is the mass transport of the drug molecules from the solid – liquid interface to the bulk solution (Wang and Flanagan, 2009).

Overall the release of the drug from the dosage form is affected by the properties of the API (e.g. pKa, solubility), manufacturing process, formulation design, the chemical and the mechanical (e.g. agitation speed) conditions of the test method selected to monitor drug release.

A dissolution method can be used during the development process of a formulation as well as for quality control to monitor batch-to-batch consistency. However, the complexity of the dissolution method, in terms of media composition and reproduction of the hydrodynamics take place in GI tract, is often increased when an *in vivo – in vitro* correlation needs to be developed. This is especially important for the new developed APIs which tend to be less water soluble and more sensitive to the lumenal environment (Reppas et al., 2014).

2.5.1 Compendial dissolution methods

USP I (basket) and II (paddle) (Figure 2.9) are the main apparatuses used for dissolution testing of oral dosage forms (Long and Chen, 2009). However, there are also so called dynamic dissolution apparatus which introduce hydrodynamic or mechanical aspects of the human GI tract; these types of dissolution apparatus will be further discuss in the following sections.

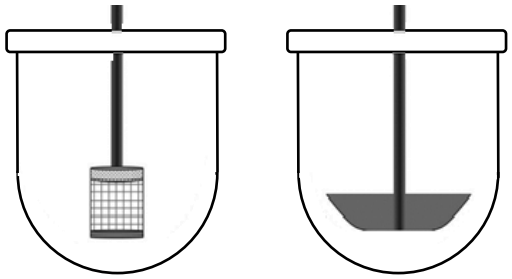

Figure 2.9. Schematic representation of the USP I (basket) and II (paddle) dissolution apparatuses

The choice of dissolution apparatus, between USP 1 and 2, to be used depends on which type of formulation need to be tested (Kostewicz et al., 2014). For instance, capsules float and hence a sinker is normally used to keep it at the bottom of the USP 2 apparatus, alternatively

a USP 1 might be more suitable. On the other hand, both apparatus can be used for tablets. However, when the release characteristics need to be tested for enteric coated products, USP 1 is more suitable when a full change of the medium, i.e. from gastric to intestinal fluid, is required as the basket can be transferred easily (Kostewicz et al., 2014).

The limitations of using USP 1/2 have been presented extensively in literature (Gray et al., 2009, McAllister, 2010, Kostewicz et al., 2014) with respect to their relevance to the human GI tract environment in terms of volume and hydrodynamics. For instance, hydrodynamics in USP 2 are problematic not only because they are far from the *in vivo* conditions but also because they are highly inhomogeneous (D'Arcy et al., 2005, Baxter et al., 2005a, Bai et al., 2007), causing variation in the dissolution data. In addition, based on the density, shape, size and location of the dosage within the USP 2 vessel, different dissolution results may be obtained (Kostewicz et al., 2014). Another issue with USP 2 is the coning effect appeared below the shaft and close to the bottom of the vessel forming a stagnant zone. Increase of the agitation speed as well as replacing the round bottom vessel with so-called peak vessel have been examined (Mirza et al., 2005) as alternative strategies to avoid coning.

The media volumes which are normally used in USP 1/2 range from 500 to 1000 mL. These volumes are used to ensure sink conditions during the quality control of the formulation in order to examine if the drug will be completely released from the dosage form. Volumes of 1L or even higher are likely to be reached in stomach at fed state. However, in case where the product should be administered in fasted state with a glass of water, gastric volumes might not exceed 250 mL (Schiller et al., 2005) and thus the volumes used in the dissolution methods do not reflect the *in vivo* conditions. Nevertheless, sink conditions for BCS (Biopharmaceutics Classification System) class 1 (high solubility, high permeability) and 3 (high solubility, low permeability) drugs prevail even at low volumes, whereas the use of high volumes can lead to overestimation of the dissolution of poorly water soluble drugs in the stomach.

With regards to the intestinal environment, sink conditions may be created with the removal of the drug from the lumen by uptake across the gut wall (Kostewicz et al., 2014). Thus, in this

case the permeability of the drug might determine whether it is appropriate to generate sink conditions.

When small volume is more appropriate for the formulation under test, mini volume USP 2 dissolution apparatus is useful to simulate conditions in stomach and intestine in the fasted state. However, the hydrodynamics in small version of the USP 2 do not reflect those in the 1 L vessel (Klein and Shah, 2008b). In addition, there is no harmonization on the design and dimensions among the manufacturers. Thus, it is important to assess the mixing conditions within the mini volume USP 2 used.

Apart from USP 1 and 2, other compendial dissolution apparatuses have been used such as USP 3 (reciprocating cylinder) and 4 (Flow-through cell). In USP 3 there is hydrodynamic dead zone as in the case of USP 1 and 2; provided that the dosage form remains in the reciprocating basket as well as there is no undissolved material at the bottom of the vessel Kostewicz et al. (2014). Previous study showed that, although the in vitro hydrodynamics affected the release rate of the drug from hydrophilic matrix, USP 1, 2, 3 and 4 showed to be equal to predict the *in vivo* profile in average basis Fotaki et al. (2009b). However, USP 3 and 4 is more suitable when the dosage form should be exposed to different media.

However, other dynamic models of the upper GI tract have been developed such as the dynamic gastric model (Thuenemann et al., 2015), the artificial stomach duodenal model (Castela-Papin et al., 1999, Carino et al., 2006) and TNO TIM-1 (Minekus, 2015) to overcome the limitations of the compendial dissolution apparatus.

2.5.2 In vitro models of human colon

In this section a brief description of the existing *in vitro* models of the human colon is presented.

2.5.2.1 Three-Stage Compound Continuous Culture System

Macfarlane et al. 1998 developed a fermentation system (Figure 2.11) to mainly study the differences in physiology and ecology of human colon microflora between proximal (i.e. cecum

– ascending – hepatic flexure - mid transverse) and distal (mid transverse – splenic flexure – descending) colon. The first vessel was used to simulate the physicochemical environment of the proximal using medium of pH 5.5 that was fed with fresh culture medium rich in carbohydrates. The other two vessels were operated at higher pH, 6.2 and 6.8 respectively, with the contents of the first vessel feeding the second and subsequently from the second to the third. The results showed that the current system can maintain stable and diverse populations of faecal microflora for an extended period. However, some of the main drawbacks of this fermentation system are that it does not reproduce intestinal secretion, absorption of the fermentation products and that oversimplifies the hydrodynamics of the human colon by using a simple magnetic stirrer.

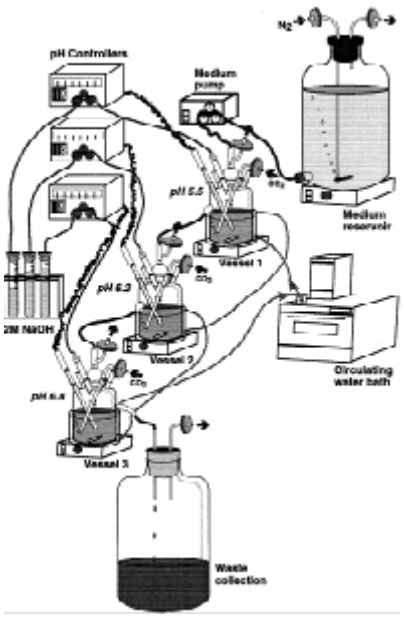

Figure 2.10. Three-stage compound continuous culture system developed by Macfarlane et al. 1998 (Figure reproduced from Macfarlane et al. 1998 with permission).

2.5.2.2 Three-stage tubular engineering model of human colon

The three-stage tubular model (Figure 2.12), developed by Spratt et al. 2005, was an improved version of the three-chemostat gut model system described above. In this model the water and the fermentation products (principally short chain fatty acids) were removed using a tubular semipermeable 1000 Dalton molecular weight cut-off cellulose membrane surrounded by a shell. The media was pumped inside the membrane using a peristaltic pump whereas outside the membrane an aqueous solution of PEG3350 (polyethylene glycol), including also salts acids and bases, was flowing. Thus, the osmotic pressure was the primary driving force for the flux of water and the fermentation metabolites across the membrane.

The issue with this system, as also with the previous one, is that both were designed to assess the fermentation process in the human colon and not the hydrodynamics. The flow inside the three-stage tubular model is induced by a peristaltic pump and not from the oscillations of the membrane wall as in the human colon. Thus, the current system does not facilitate understanding the relationships between wall motion and movements of the colon contents. In addition, the fluid flow inside an oscillating collapsible tube is more complicated compared to dispersed plug flow model used to describe flow motion and mixing in the tubular system. For instance, during the peristaltic motion of the human colon wall, pressure gradients occur between the relaxing point and the contracting point of the colon wall whereas vortex rings appeared within the relaxing point (Sinnott et al., 2012). These vortex rings are important for mixing and transport and they have previously been observed in peristaltic flow models using prescribed wall motion (Connington et al., 2009).

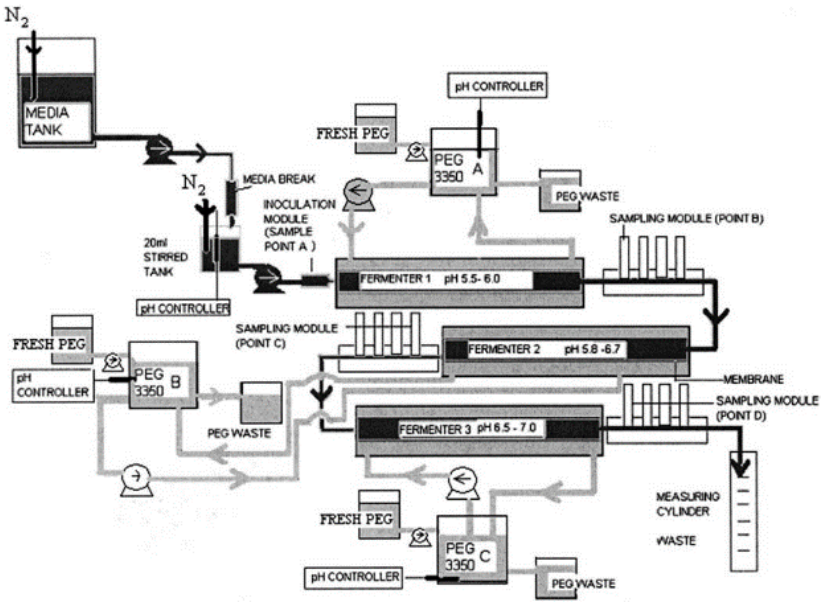

Figure 2.11.Schematic representation of the three – stage engineering model of human colon (figure reproduced from Spratt et al. 2005 with permission)

2.5.2.3 TNO TIM-2 colon simulator

The most advanced commercialized *in vitro* model of the human colon is the TIM-2 (Figure 2.14) developed by Nederlandse Organisatie voor Toegepast (TNO) Nutrition and Food Research Institute (Zeist, The Netherlands). It is a multicompartmental, dynamic, computer controlled simulator of the human colon (Venema, 2015). Unlike the previous models, the mixing of the contents is performed by changes of the water pressure, causing contraction and relaxation of a membrane installed inside a glassy shell. The removal of the fermentation products is performed using hollow semipermeable fibres whereas pH is controlled with secretion of NaOH and the temperature is kept constant with the circulation of water inside the glassy shell.

Despite the fact that the TIM-2 model reproduces the colonic environment in a more advanced and reproducible way compared to the previous models, it is still not considered to be fully representative of the human colon (McAllister, 2010). In addition, TIM-2 system is not representative of the environment of human colon in terms of design, dimensions and volume (Blanquet et al., 2001b).

Based on our knowledge there is lack of information with regards to the following issues:

- Analysis of the hydrodynamics inside the TIM-2 system and how the viscosity changes, upon water removal from the dialysis system, will affect the mixing performance of the system.
- Measurements of the pressure forces generated from the oscillations of the flexible membrane in TIM-2. Although, in TIM-1 system pressures have been measured with using wireless smart pill (Minekus, 2015), it is questionable if the TNO system reproduces the physical mixing of the contents, since the wireless pill does not show the propagation of the different motility patterns (Tran et al., 2012).
- Most of the studies using TNO TIM-1 and TIM-2 system do not give any information about the frequency of the contractions of the membrane but mainly the residence times in each compartment (Larsson et al., 1997, Krul et al., 2000, Souliman et al., 2006, Souliman et al., 2007, Dickinson et al., 2012, Verwei et al., 2016). The only exception found to be in the works of Brouwers et al. 2011 and Hens et al. 2014 in which the frequency of the peristaltic contractions in TIM-1 was 3 min^{-1} and 6 min^{-1}, respectively. However, no corresponding information was found for TIM-2.
- The surface area of the dialysis hollow fibres in which the contents are exposed. The absorptive surface area of the human colon is 0.2 m^2 (Sandle, 1998) and as mentioned above, the colonic fluids are not uniformly distributed and hence exposed along the surface area of the colon wall. However, the dialysis system used the TIM-2 seems to be completely immersed in the fluids (Figure 2.12b).

Furthermore, based on the design of the TIM-2, the distribution of the fluids is not representative of the human colon in which the fluid contents appear as pockets (Schiller et al., 2005). Beside the improvements that TIM-2 brought into the dissolution science, the question how the physiology, the motility and the volume of the contents in the human proximal colon will affect the hydrodynamics and hence the fluid flow, mixing and subsequently the performance of the dosage forms, remains to be answered.

a b

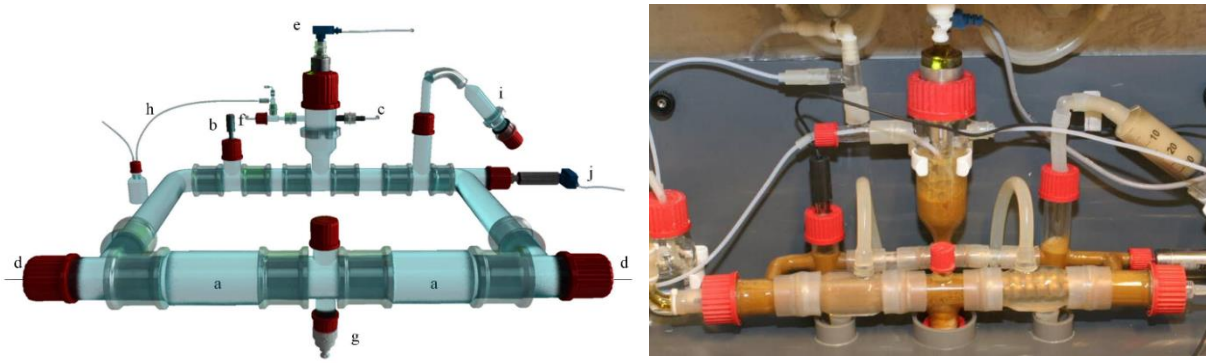

Figure 2.12. a) Schematic representation of TIM-2 colon simulator. a) peristaltic compartments with hollow dialysis membrane installed inside the tube, b) pH sensor, c) NaOH secretion, d) dialysate system, e) level sensor, f) gaseous N2 inlet, g) sampling port, h) gas outlet, i) feeding syringe of the TIM-1 contents, j) temperature sensor. Figure reproduced from Aguirre et al. 2014; b) TIM-2 in operation.

2.6 Techniques to assess mixing and visualize fluid flow

2.6.1 Particle Image Velocimetry (PIV)

PIV is a non-invasive laser optical technique, allowing for 2-D velocity vector mapping of a flow field (Figure 2.13). The current technique is based on tracking seeded particles in transparent fluid by sequential illumination using a pulsing thin plane of laser light. The position of the illuminated particles (either by scattered laser light or emitted fluorescent light) are captured by a digital camera so called Charged Coupled Device (CCD); a very small time difference between the images facilitated by a frame-straddling camera enables the shift in position of the particles between frames to be correlated. CCD is an electronic sensor converting photons (light) to electric charges with a typical size of 10 x10 μm^2.

Cross-correlation of pairs of images enables the velocity vector field for the measured area to be obtained (Figure 2.14). Each frame is sub-divided into a grid with each square being termed the interrogation area (IA). The size of this area can range from 8 × 8 to 128 × 128

pixels, with 64 × 64 pixels being a common choice based upon optimal displacement of the particles (¼ of the interrogation area) and the camera resolution. The vector displacement for the two images is determined by cross – correlation of each interrogation area. Then, the degree of the correlation between the two interrogation areas of the two frames is determined statistically with the highest value in the correlation plane being used to obtain the particle displacement. The procedure is repeated until to build the completely 2D velocity vector map.

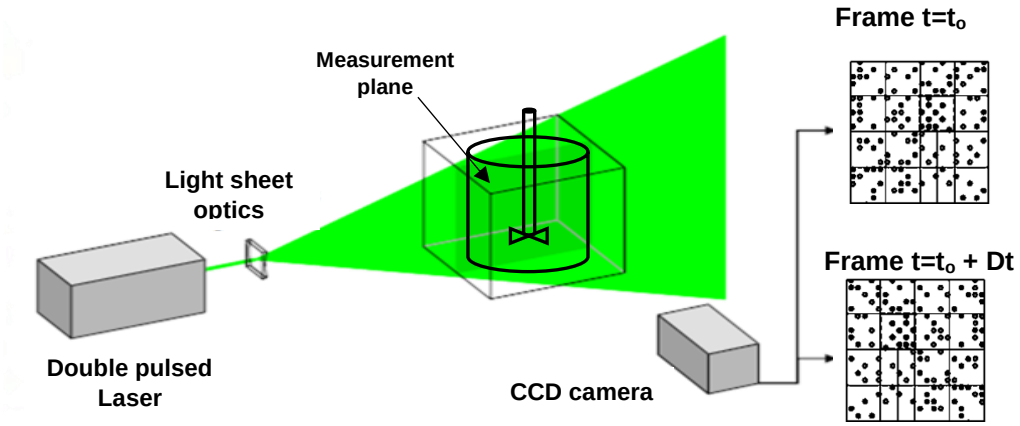

Figure 2.13.Schematic representation of the Particle Image Velocimetry experimental set up.

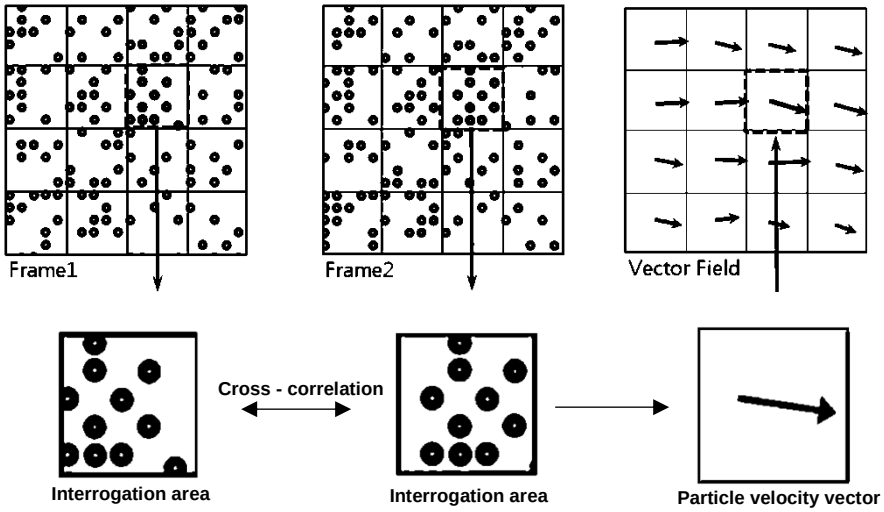

Figure 2.14.Image interrogation process

The resolution of the PIV depends on the camera implemented, the magnification and the seeding particle size used. The current technique has been used to assess the hydrodynamics in standard (Kukura et al., 2003b, Kukura et al., 2004, Baxter et al., 2005a) and mini volume (Stamatopoulos et al., 2015, Wang and Armenante, 2016) USP 2 dissolution apparatus.

2.6.2 Planar Laser Induced Fluorescence (PLIF)

Planar laser induced fluorescence is a powerful optical technique widely used to visualize flow patterns in transparent fluids and may be considered as a variant of PIV, using similar equipment. In principle, PLIF is based on the utilization of a chemical substance which become fluorescent when excited by a light source of specific wavelength. Thus, a map of the concentration gradients can be obtained as a function of time at the illuminated plane of the fluid flow. This can be done by converting fluorescence intensities to dye concentration by using images of the illuminated plane of the flow field captured by CCD camera at predetermined time intervals. Rhodamine-B (Miller et al., 2007), -MT (Kukura et al., 2004) and -6G (Stamatopoulos et al., 2016a) are some fluorescent dyes used in PLIF applications. This technique has previously been used to assess the mixing performance of standard (1 L) USP 2 dissolution apparatus (Baxter et al., 2005a). Examples of images of standard USP 2 apparatus captured using the PLIF technique are presented in Figure 2.15.

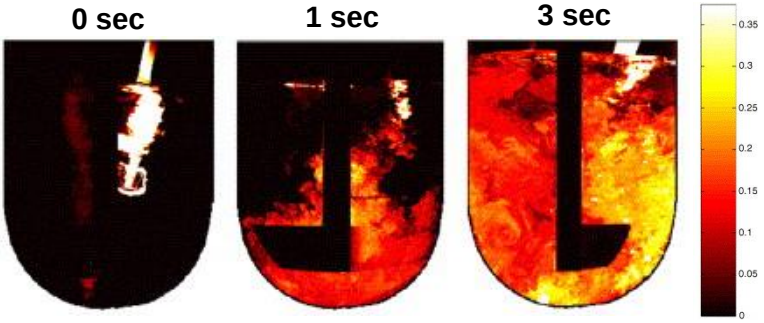

Figure 2.15. PLIF images of standard USP 2 captured at predetermined time intervals (Figure reproduced from Dave et al. 2007 with permission). The images illustrate the mixing pattern of rhodamine-B solution after rapid addition to the main fluid (i.e. water)

2.6.3 Positron Emission Particle tracking (PEPT) system

Positron emission particle tracking enables to detect the motion of a labelled tracer particle with using a positron camera and a location algorithm for computing the time-space location of the tracer (Guida et al., 2009). The particle is labelled with a positron-emitting nuclide normally ^{18}F with half-time 110 min, however, other radio isotopes like ^{61}Cu (half-time 3.3 h) have also been used (Parker et al., 1997). The positron emitted by the labelled tracer particle annihilates with an electron, emitting a pair of almost exactly back-to-back (i.e. collinear) 511 keV γ-rays (Figure 2.16). The two γ-rays are detected simultaneously from the two positron camera heads working in coincidence (Parker and Fan, 2008). Each head of the two positron cameras contains a rectangular sodium iodide crystal optically connected to a group of photomultiplier tubes. When the γ-rays pair emitted after positron annihilation, produce two coincident scintillations in the crystals and the corresponding photomultipliers provide positional signals and the 2D centroids are determined by the associated software.

Different strategies have been used to develop particle tracers form various materials (Parker and Fan, 2008). Initially ^{18}F radioisotope is produced in the cyclotron of the University of Birmingham with bombarding pure water of solid material with 33MeV ^{3}He beam based on the following reaction

$$^{16}O(^{3}He,p)^{18}F \text{ and } ^{16}O(^{3}He,p)^{18}Ne \rightarrow ^{18}F$$

The ^{18}F can be added to a particle via surface absorption or ion-exchange. In this study, strong-base anion exchange resin was used which are quaternary ammonium derivative provided in chloride form. However, the affinity of ^{18}F to the functional group of the resin $R–CH_2N(CH_3)_3^+$ or $R–CH_2N(CH_3)_2(CH_2CH_2OH)^+$, where R is the organic backbone, is lower compared to Cl^-. Thus, the resin should first be converted to fluoride form or hydroxide form before use. To convert the chloride form of the resin to fluoride one, the resin slurry is eluted with 1 M KF solution. After the procedure, the F^- ions can exchange with ^{18}F. For water application, the resin should be coated with lacquer, otherwise, the radioactivity will leak into

the fluid. Furthermore, painting can be applied to make neutrally buoyant particles. The affinity of the ^{18}F is stronger with using strong-base resin as this type of resin is less affected by hydroxide ions formed upon interaction with water.

PEPT can be utilized to analyse the flow field in non-transparent fluids and in apparatuses with complex geometries, since no light scattering phenomena exist in this technique as occurred in PIV and PLIF when a thin laser plane hits a curved and/or opaque surface. The intrinsic spatial resolution of the positron camera used in the PEPT experiments is 6 mm. The accuracy of the tracer location is given by Equation 2.1.

$$\frac{W}{\sqrt{fN}} \tag{2.1}$$

where W is the spatial resolution of the camera and N is the number of the events detected during the location intervals and f the fraction of these events used for the determination of the location. Thus, using PEPT, the location of the particle tracer can be detected with high spatial resolution several tens to hundreds times per second based on the velocity of the tracer. For example a tracer travelling with high velocity 1 m s^{-1} can be located within 500 μm 250 times per second and with slow moving within 100 μm 50 times per second (Parker et al., 2002).

In previous years, PEPT have found numerous applications in solid–liquid suspension (Guida et al., 2009), multiphase systems (Pianko-Oprych et al., 2009), static mixers (Mihailova et al., 2015) and many others summarized by Parker and Fan (2008). In this study PEPT will be implemented as an alternative technique to the magnetic pill tracking system used in vivo studies.

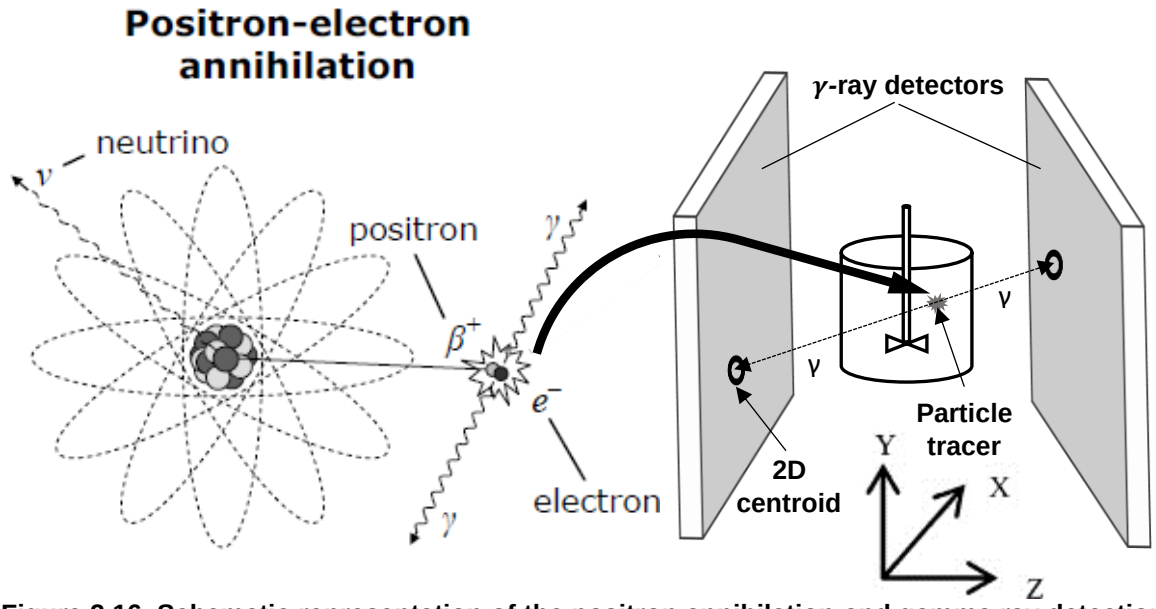

Figure 2.16. Schematic representation of the positron annihilation and gamma ray detection by positron camera

2.7 Conclusions

The human proximal colon is considered a favourable site to deliver drugs for systemic and local treatments. As the oral route is the most common way to administer drugs a dosage form will face a dynamic-complex environment during its passage through the GI tract. It has been realized that hydrodynamics and physicochemical composition of the human chyme should be reproduced to adequately assess the *in vivo* performance of the dosage forms.

Mixing, propulsion, storage, dewatering, secretion, microflora hosting take place in the human colon. Complex muscle contractions are required to facilitate these functions of the human colon. Manometry and scintigraphy are used to monitor the colon motility patterns and movements of the contents *in vivo*. However, these methods have some technical limitations making the association between wall motion and flow episodes a difficult task. In addition, the human colon environment is dynamically changing as a function of time, making it very complex to examine the interplay between the different parameters (i.e. viscosity) involved in the hydrodynamics which take place in the human colon. Thus, an *in vitro* model, which

reproduces the main features of the colon anatomy and motility, may give insights of the colonic environment in which the dosage forms will be exposed.

Compendial dissolution methods such as USP 2 dissolution apparatus, are widely used to assess the *in vivo* performance of the dosage form as well as batch-to-batch consistency. However, the current dissolution apparatuses oversimplify the environment of the human GI tract whereas the most advanced GI simulators like the TNO TIM-2 are not biorelevant in terms of human physiology and motility.

This literature review has justified the aim of this study to develop an *in vitro* model of human proximal colon to examine how the physiology, motility and the viscosity of the fluid will affect the hydrodynamics in the human colon. In addition, characterization of the dissolution profile of a dosage form will also be performed. As described in the later chapters a modified release hydrophilic matrix containing theophylline, a high water soluble drug, was chosen as a case study to evaluate the effect of the wall motion and the viscosity of the fluids on the dissolution profile of the tested drug. Theophylline was chosen to avoid the solubility to be the limiting factor that would make the evaluation more complicated. However, comparison of the proposed model with the compendial dissolution apparatuses should be performed. Mini volume (100 mL) UPS 2 was chosen, since its volume is closer to the volumes appeared in the human proximal colon and our model. In addition, since dewatering process takes place in the human colon, the effect of the viscosity on the dissolution profile of theophylline as well as on the mixing performance of the mini volume USP 2 should be also examined.

The remainder of this thesis consists of the results Chapters, starting with the characterization of the mini volume USP 2 apparatus in Chapters III and IV and then the development and characterization of the proposed *in vitro* model of the human colon in Chapters V, VI and VII.

Nomenclature

k_S	Metzner-Otto constant
$\underline{\underline{C}}$	concentration matrix
$\underline{\underline{A}}$	matrix of constant vales
$\underline{\underline{G}}$	matrix of averaged Grayscale values
$\underline{\underline{B}}$	matrix of intercept values for the linear regression
$\bar{t}_i$	central point of the observed time interval
ΔM_i	differential amount of drug dissolved
D	impeller diameter (m)
f_2	Similarity factor
k	proportionality constant related to the structural and geometrical properties of the matrix
m	Diffusional exponent
M_t/M_∞	fraction of drug released at time t
n	power law exponent
N	rotational speed (rps)
n_p	number of time points
Re	Reynolds number
R_t	Dissolution (%) for drug formulation at time t
T_t	Dissolution (%) for dye formulation at time t

Greek symbols

$\dot{\gamma}$	Shear rate (s^{-1})
μ_A	Apparent viscosity (mPa s)
p	Density (kg m^{-3})
τ	Shear stress (Pa)
τ_γ	Yield stress (Pa)

Abbreviations

ANOVA	Analysis of Variance
C.V	Coefficient of Variance
CCD	Charged Coupled Device
CFD	Computational Fluid Dynamics
GI	Gastrointestinal
HCl	Hydrochloric acid
MDT	Mean Dissolution Time
NaCMC	Sodium carboxymethylcellulose
PIV	Particle Image Velocimetry
PLIF	Planar Laser Induced Fluorescence
PLIF	Planar Induced Fluorecence
RH-6G	Rhodamine-6G
SP	Sampling Point
THE	Theophylline
USP	United States Pharmacopeia

3 Understanding the impact of media viscosity on dissolution of a highly water soluble drug within a USP 2 mini vessel dissolution apparatus using an optical Planar Induced Fluorescence (PLIF) method[1]

Abstract

In this study, planar induced fluorescence (PLIF) was used for the first time to evaluate variability in drug dissolution data using Rhodamine-6G doped tablets within small volume USP 2 apparatus. The results were compared with tablets containing theophylline (THE) drug via conventional dissolution analysis. The impact of hydrodynamics, sampling point, dissolution media viscosity and pH were investigated to note effects on release of these two actives from the hydrophilic matrix tablets. As expected mixing performance was poor with complex and reduced velocities at the bottom of the vessel close to the tablet surface; this mixing became even worse as the viscosity of the fluid increased. The sampling point for dissolution affected the results due to in-homogenous mixing within the vessel; this effect was exacerbated with higher viscosity dissolution fluids. The dissolution profiles of RH-6G measured via PLIF and THE measured using UV analysis were not statistically different demonstrating that RH-6G is an appropriate probe to mimic the release profile of a highly soluble drug. A linear correlation was accomplished between the release data of the drug and the dye (R^2>0.9).

The dissolution profile of the dye, obtained with the analysis of the PLIF images, can be used to evaluate how the viscosity and the mixing performance of USP 2 mini vessel affect the interpretation of the dissolution data of a drug.

[1] This chapter has been published in part in Stamatopoulos, K., Batchelor, H. K., Alberini, F., Ramsay, J. & Simmons, M. J. H. (2015). *International Journal of Pharmaceutics*, 495, 362-373. doi: 10.1016/j.ijpharm.2015.09.002

3.1 Introduction

A drug delivery system that provides a constant rate of release over the required time interval offers many benefits in treatment. Zero-order release provides a constant release rate and no time lag or burst effect over a prolonged time period (Amidon et al., 2015b). Hence, much research effort has been invested in development of zero-order oral drug delivery systems i.e. time independent release kinetics (Klein and Shah, 2008a). The use of hydrophilic matrices has become very popular in solid oral dosage forms (Qureshi and Shabnam, 2001b); a sustained release matrix tablet consists of the active ingredient(s) with either single or multiple gel forming agents which retard the release of the drug (Baxter et al., 2005a). In the case of highly water-soluble drugs (Maderuelo, Zarzuelo, & Lanao, 2011), swelling-controlled oral drug delivery systems have so far shown the most promise.

The mechanisms by which drugs are released from a hydrophilic matrix upon hydration involve: a) the entry of the solvent into the matrix, b) a progressive change in the matrix from a glassy to a rubbery state resulting in swelling, c) dissolution of the drug molecules, d) diffusion of the drug through the gel layer and e) release of the drug in the solution (Kukura et al., 2003a). In the final stage, there are two phenomena which both contribute to the overall release rate of the incorporated drug: release from low viscosity gels occurs by erosion of the gel layer; whilst for high viscosity gels, the release is by diffusion of the active agent through a stable gel with limited polymer dissolution. The transition between the two mechanisms results in diffusion kinetics lying between the square root time dependence of Fickian diffusion (Jantratid et al., 2009) and zero-order or ‘case II’ diffusion (Moroni and Ghebre-Sellassie, 1995). Often, both phenomena occur simultaneously due to diffusion and the relaxation of the polymer (Zuleger and Lippold, 2001).

Orally administered dosage forms, usually tablets, are the most convenient way for delivering drugs to patients. Upon ingestion, the tablets enter a highly dynamic environment in which disintegration, dissolution and absorption occur. This complex *in vivo* process is usually evaluated *in vitro* using disintegration and dissolution tests. In the case of hydrophilic matrices,

the timescale for gel formation and the resistance of the gel layer to physiological shear stress, experienced during their passage through the gastrointestinal (GI) tract, are essential parameters that control the drug dissolution characteristics (Garbacz et al., 2009).

Recently, the small volume USP 2 apparatus has gained popularity due to the reduced mass of material requried, analytical methodology and discriminatory power of conventional apparatus. Furthermore, small volume apparatus may be beneficial in the development of biorelevant methods, particularly for paediatric populations.

Officially introduced almost 4 decades ago, the conventional (1L) USP dissolution Testing Apparatus 2 (USP 2) is the most commonly used equipment in the pharmaceutical industry (Zuleger et al., 2002, Mitchell et al., 1993). However, this apparatus presents some drawbacks (Kostewicz et al., 2014). Numerous published works have indicated that there is high variability in dissolution profiles using USP 2 (Costa and Lobo, 2001, Kukura et al., 2003b, Bai et al., 2011, Qureshi and Shabnam, 2001a).

Some studies (Zuleger et al., 2002, Bai et al., 2011, Cox et al., 1982) have shown that the fluid flow in USP 2 is highly heterogeneous. The shear distribution is non-uniform (Cox et al., 1982), whereas, the velocity vectors are highly dependent on the location within the vessel, especially at the bottom of the vessel where the tablet is located during dissolution testing (Zuleger et al., 2002). These complex hydrodynamics can contribute to the poor reproducibility, as can the tablet position in the vessel. The small volume USP 2 apparatus is a miniaturised version of the conventional apparatus, however, there is still a need to analyze the hydrodynamics since the miniaturised systems do not exactly reflect the conditions of the standard paddle system (Klein and Shah, 2008b), nor the conditions in the GI tract.

The effect of viscosity on the dissolution test may increase the uncertainty and the variability of the results, since, the hydrodynamics of the USP 2 apparatus will be more complicated. In addition, other variables, like sampling cannula position, especially sampling depth, and inconsistencies in the technique of the analysts performing the test can affect dissolution rate

and reproducibility (Cox et al., 1983). Previous works (Parojcic et al., 2008, Radwan et al., 2012) testing different dosage forms in viscous media do not give any information about the sampling cannula position or possible changes in hydrodynamics (e.g. shear rates and/or velocities) or mixing patterns.

Planar Induced Fluorecence (PLIF) has been widely used as a non-intrusive visualization technique for the evaluation of mixing systems (van Cruyningen et al., 1990, Law and Wang, 2000, Bruchhausen et al., 2005). Furthermore, Particle Image Velocimetry (PIV) combined with Computational Fluid Dynamics (CFD) have been used to characterize the flow pattern in conventional (1 L) USP 2 apparatus dissolution vessel (Kukura et al., 2003b, Bai et al., 2011), revealing the non-uniform velocity field and thus an uneven distribution shear rates.

These visualization techniques have mainly been used either by injecting a fluorescent dye in the USP 2 vessel, at different injection points, for characterising mixing patterns in simple buffer solution (Cox et al., 1982, Bai et al., 2011) or by using nondisintegrating salicylic acid tablets containing phenolphthalein as an indicator agent for investigating the effect of tablets movements at the bottom of the vessel on drug dissolution profiles (Bai et al., 2011, Baxter et al., 2005b). In addition, visualization studies were performed by blending salicylic acid with phenolphthalein as a first step in affirming the fluid flow patterns in USP 1 and 2 (Bampton and Dinning, 2013), demonstrated previously using laser Doppler anemometry (Bocanegra et al., 1990).

Kukura et al. (2003, 2004) performed PLIF experiments in conventional (1 L) USP 2 dissolution apparatus under laminar and turbulent conditions. Under laminar flow (Re=150) non-uniform mixing with segregation zones were observed due to the failure of dye to reach the upper regions of the dissolution vessel. In case of turbulent flow (Re=5000) the authors could not find a significant difference in dissolution profiles of the targeted drug at the different sampling points, although, large fluctuations of the mixing patterns were observed with time. This contradiction might be due to the fact that the PLIF method is capable of capturing local time-dependent mixing conditions in the USP 2 apparatus which are not observable with the

conventional sampling technique. Furthemore, Kukura et al. (2003, 2004) did not repeat the experiment for low Re numbers and compare the PLIF results with those from dissolution experiments.

It is important to understand whether variability in dissolution is due to the manufacturing process of the dosage form, leading to a burst effect from sustained release formulations, especially when highly water soluble drugs are presented in high amounts (Cox et al., 1983); or due to the dissolution testing method, e.g. physicochemical properties of the media (e.g. viscosity) with direct effect on hydrodynamics of the USP 2 dissolution apparatus.

Whilst PLIF and other visualisation techniques such as PIV have been used to previously evaluate the drawbacks of the USP 2 dissolution apparatus (Kukura et al., 2003b, Bai et al., 2011), they do not allow any direct or indirect correlation with the dissolution profile of the active compound, since the form of PLIF used involved injecting fluorescent dye at different points inside the USP 2 vessel, rather than dye release from a tablet. Due to the complexity of the hydrodynamics and mixing intensity in the vessel, a PLIF method which incorporates a fluorescent dye into a hydrophilic matrix (which can mimic the dissolution profile of a highly water soluble drug) and then tracks the release through the vessel over time overcomes these limitations.

Thus, in this chapter, PLIF has been utilized as a non-intrusive method for visualizing the mixing patterns and quantifying the local concentrations of RH-6G, released from a hydrophilic matrix that also contained the targeted drug. Thus, indirect evaluation of the impact of the hydrodynamics, viscosity and sampling point on the dissolution of the drug has been performed. A correlation of the dissolution experiments of the RH-6G using PLIF with those of the targeted drug using the conventional analytical technique is presented. This work, coupled with the texture analysis of the hydrophilic matrix, gives an overview of the critical parameters affecting the interpretation of the dissolution results. Theophylline (THE) was selected as a well-known, highly soluble drug where extensive *in vitro* dissolution data from hydrophilic matrices is readily available. As mentioned above, the USP 2 small volume (100 mL)

dissolution apparatus was chosen as an alternative to the standard paddle set up, as this apparatus has not previously been investigated.

3.2 Materials and methods

3.2.1 Materials

Sodium carboxymethylcellulose of 90000 ($NaCMC_{90000}$) and 700000 ($NaCMC_{700000}$) molecular weight was purchased from Sigma (St., Louis, USA). Theophylline anhydrous and potato starch were bought from Acros Organics (Loughborough, UK). Sodium hydroxide, Rhodamine-6G, hydrochloric acid (1M), silicone dioxide and potassium hydrogen (KH_2PO_4)- and dihydrogen phosphate (K_2HPO_4) were purchased from Sigma (St., Louis, USA).

3.2.2 Fluids and fluid properties

$NaCMC_{700000}$ was selected as a chemically inert, water-soluble polymer which can mimic the shear thinning rheology of the chyme. $NaCMC_{700000}$ buffered solutions of 0.25, 0.5 and 0.75% (w/w) were prepared using 0.05M phosphate buffer pH 7.4 (KH_2PO_4/K_2HPO_4). This pH value was selected as a representative pH for the large intestine. All the tested fluids were deaerated using an ultrasound bath before conducting dissolution and PLIF experiments.

The rheology of the NaCMC solutions was measured using a Discovery Hybrid Rheometer (TA Instruments – a division of Waters Ltd.) coupled with a 40mm diameter, 4° cone and plate geometry. The temperature was controlled to 37 ^{o}C using an in-built Peltier plate (at the same temperature as the USP 2 experiments). The rheology was obtained by performing a shear ramp over a range of shear rate from 0.1-1000 s^{-1}. The data was found to fit the Herschel-Bulkley model.

$$\tau = \tau_Y + K\dot{\gamma}^n \quad (3.1)$$

Where τ is the shear stress (Pa), τ_Y is the yield stress (Pa) $\dot{\gamma}$ is the shear rate (s^{-1}), *K* is the consistency index and *n* is the power law exponent. The apparent viscosity, μ_A, can be thus determined by evaluating $\tau / \dot{\gamma}$ at a given value of shear rate. The rheological properties of the experimental fluids are presented in Table 3.1.

3.2.3 Tablet preparation

A 500 mg tablet was prepared according to the following composition: 50% THE, 44.1% $NaCMC_{90000}$, 4.9% potato starch and 1% silicone dioxide. From practical point of view, $NaCMC_{90000}$ was chosen as the rate controlling polymer, since there is an extensive experience in Pharmacy department of the University of Birmingham of using the current polymer to prepare a compressed hydrophilic tablet. The powders were sieved and mixed for 10 min then placed into a single die tableting machine (Kilian, Coln, D) fitted with flat-faced 9.8 mm punches and instrumented with piezoelectric load washer (Kistler,Winterthur, CH) to enable compression force measurements. To investigate the effect of the compression load and compression time on dissolution profile of drug from the tablet, a load pressure range of 980.6 – 1961.2 bars for 20 and 40 seconds was applied. The cylindrical tablets had a final weight of 500 ±25 mg. The same method was followed for the tablets used in PLIF experiments containing 0.02% RH-6G. Figure 3.1a shows pictures of the different tablets used in dissolution, PIV and PLIF experiments. For the PIV experiments, a piece of acrylic cut to match the dimensions of the tablet was used to enable monitoring of the flow above the surface of the tablet.

3.2.4 Experimental Apparatus: USP 2 mini paddle

A schematic of the USP 2 mini paddle dissolution apparatus (Dissolution Tester 6000, Antech, UK) is shown in Figure 3.1b. The volume of media used in all experiments was 100

mL and the paddle rotational speed was fixed at 50 rpm. The same apparatus was used for (i) dissolution (ii) PLIF and (iii) PIV studies. All the experiments were performed at 37 ^{o}C. The flow regime in the vessel was determined by calculation of the Reynolds number

$$\mathrm{Re} = \frac{\rho N D^2}{\mu_A} \tag{3.2}$$

Where ρ is the fluid density (kg m^{-3}), N is the rotational speed (rps), D is the impeller diameter (m). The apparent viscosity, μ_A (mPa s) was estimated using the Metzner-Otto method (Metzner and Otto, 1957) which assumes the shear rate in the vessel is proportional to the impeller speed, thus

$$\mu_A = \frac{\tau_Y}{k_S N} + K\left(k_S N\right)^{n-1} \tag{3.3}$$

The value of Metzner-Otto constant, k_S, in the above expression was 10 (Edwards et al., 1992). Here, is the proportionality between the average shear rate in the mini vessel and the impeller rotational speed. The calculated values of Re are given in Table 3.1.

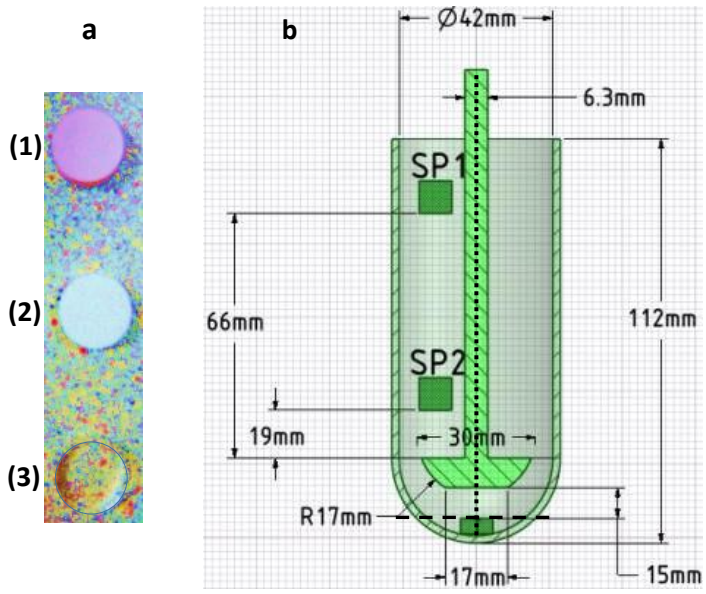

Figure 3.1. a) The three tablets used in: (1) PLIF (containing RH-6G), (2) dissolution tests and (3) PIV experiments (acrylic); b) Dimensions of the USP II mini vessel used in dissolution, PIV, PLIF

experiments indicating the two sampling areas (SP1 and SP2) as well as the horizontal (- - - -) and vertical plane (·····) that laser cut the vessel in PIV experiments.

3.2.5 Dissolution experiments

Dissolution tests (six replicates) were performed in 0.1N HCl solution (gastric conditions) and in 0.05M phosphate buffer solution (pH 7.4 ±0.2) assuming fasted conditions in large intestine, although, pH drops to an average value of 6.0 in fed state (Diakidou et al., 2009). The dissolution tests for the viscous media were conducted only at pH 7.4; assuming that viscosity increases as the dewatering of the chyme takes place in large intestine. Two sampling positions were selected (Figure 3.1b), denoted SP1 and SP2, located at a distance of 66 mm and 20 mm from the paddle blade, respectively. Samples of 1 mL volume were withdrawn at predetermined time intervals (5, 10, 15, 30, 60, 120, 240, 480, 560 min and the last one after completing 21 h dissolution testing). The volume of the medium removed at each time point was replaced with fresh media. Each sample was filtered using a 0.4 μm PTFE filter (Palma et al., 1981) and appropriately diluted prior to quantitative analysis in order to be within the linear region of the calibration curve (Eq. 3.4). Quantitative analysis of theophylline was undertaken using a UV spectrophotometer (Jenway Genova Plus) at 270 nm.

A calibration curve was obtained by plotting the absorbance of the theophylline at 270 nm versus the concentration (mg L^{-1}). For this purpose standard solutions of theophylline were prepared at several concentration intervals (2, 5, 10, 20, 40 mg L^{-1}); there was no impact of pH of the media on the dissolution curve of theophylline.

$$y = 0.0575x - 0.0024 \quad (R^2 = 0.9987) \tag{3.4}$$

The dissolution data obtained as a function of time were fitted to the following equation (Eq. 3.5) which is widely used to describe the drug release behaviour from hydrophilic polymeric matrices (Conti et al., 2007b, Korsmeyer et al., 1983).

$$\frac{M_t}{M_\infty} = kt^m \tag{3.5}$$

where M_t/M_∞ is the fraction of drug released at time t, k is the proportionality constant related to the structural and geometrical properties of the matrix, and m is the diffusional exponent indicative of the drug release mechanism. The exponent, m, is strongly dependent upon relaxation rate at the swelling front and the polymer swelling characters. As this equation is valid only for the early stages (< 70 %) of drug release, it was only fitted to values of M_t/M_∞ < 0.7.

3.2.6 PIV and PLIF studies

Both PIV and PLIF studies were carried out using a TSI PIV system comprised of a 532 nm Nd-YAG laser (Litron NanoPIV) pulsing at 7.4 Hz, and a single TSI Powerview 4MP (2048 × 2048 pixels) 12 bit frame-straddling CCD camera, both controlled using a synchronizer (TSI 610035) attached to a personal computer equipped with TSI Insight 4G software. The spatial resolution of the measurements was 10 μm pixel^{-1}. The small volume USP 2 vessel was placed in a glass box filled with water which served the dual purpose of eliminating refractive index issues due to vessel curvature and also in enabling temperature to be kept constant at 37^{o}C by circulating the fluid in the box through a water bath using a peristaltic pump. The laser sheet was aligned vertically, passing across the diameter of the vessel, i.e. aligned with the impeller shaft along the vessel axis.

PIV experiments were carried out by seeding the fluid with 10 *μm* silver coated particles (Dantec Inc, DU) which possess a sufficiently small relaxation time to be able to follow the fluid streamlines (Gabriele et al., 2009). 500 image pairs were recorded for each experiment and the average flow fields obtained using the TSI Insight and Tecplot Focus 2013 software (Tecplot Inc., USA).

For the PLIF experiments, a cut-off filter at 545 nm was fitted to the CCD camera to eliminate reflected laser light and to capture only the fluorescent light emitted by the RH-6G (λ_{em} = 560 nm). The system was calibrated for each solution used at fixed laser power by filling the USP 2 100 mL (small volume) vessel with well mixed solutions at concentrations ranging 0 – 1.0 mg L^{-1}; in steps of 0.1 mg L^{-1}. 50 images were captured at each concentration to enable the variation of laser power upon the resultant grayscale values in the image to be obtained. The relative standard deviation in values was consistently less than 3.6% and therefore not significant. A mask was set as shown in Figure 3.2a to consider only half of the illuminated tank, up to the vessel axis (the remainder being in shadow due to impingement of the laser sheet on the impeller shaft). The calibration was developed by taking the average grayscale values over the 50 images, then on a pixel by pixel basis and performing a linear regression over two concentration ranges from 0 – 0.6 mg L^{-1} and 0.6 – 1.0 mg L^{-1}, respectively. This was due to quenching phenomena which occurred for RH-6G concentrations > 0.6 mg L^{-1}. The amount of RH-6G in the tablet was chosen such that the final concentration in the dissolution vessel was 1 mg L^{-1} ensuring all values were below the saturation signal of the CCD camera used in PLIF experiments. In addition, 1 mg L^{-1} was also the proper amount for the establishment of sink conditions. The analysis was carried out using MATLAB (Matlab 7.6.0 R2008a) to produce calibration matrix.

$$\underline{\underline{C}} = \underline{\underline{A}}\underline{\underline{G}} + \underline{\underline{B}} \tag{3.6}$$

Where $\underline{\underline{C}}$ is the concentration matrix, $\underline{\underline{A}}$ is the matrix of constant vales, $\underline{\underline{G}}$ is the matrix of averaged Grayscale values and $\underline{\underline{B}}$ is the matrix of intercept values for the linear regression. The regression was carried out using a standard least-squares method.

The PLIF measurements were conducted by addition of the RH-6G tablet into the bottom of the vessel, and following the same dissolution protocol (section 3.2.5). 10 images were recorded at each predetermined time interval. Following post-processing using the calibration

matrix, two interrogation regions were selected matching the sampling points used in the dissolution experiments (SP1 and SP2). Assuming that during the sampling process in dissolution experiments, the cannula might draw material from a wider area (Figure 3.2b), three different sampling point areas were considered of 100 × 124, 182 × 218 and 211 × 304 pixels respectively (Figure 3.2c). Average values of concentration as a function of time and as a function of the two sampling areas (SP1 and SP2) were thus obtained to enable direct comparison with the theophylline dissolution tests described in section 3.2.5.

3.2.7 Gel layer strength and thickness measurements

Tablets with and without RH-6G were placed in two solutions with different values of pH (1.0 and 7.4), and the impeller speed and the operation temperature were set as described in section 3.2.4. In order to avoid deformation during the analysis, one planar base of the tablets was stuck to a metal flat base. The swollen tablets were removed from the dissolution apparatus after 1.0, 2.0 and 5.5 h for texture analysis. The strength and thickness of the gel layer, during swelling process, was tested in triplicate using a Texture Analyzer (TA.XT2, Stable Micro System, Goldalming, UK), which provided force-time curves recorded during the penetration process. The penetration of a flat-tipped round steel probe (4 mm diameter and 30 mm length) into swollen matrices was determined at a constant speed of 0.1 mm s^{-1}, under increasing load. Data collection and analyses were performed by a computer equipped with Texture Expert® software. A predetermined maximum penetration of 3 mm was established in order to prevent the contact of the probe with the glassy core.

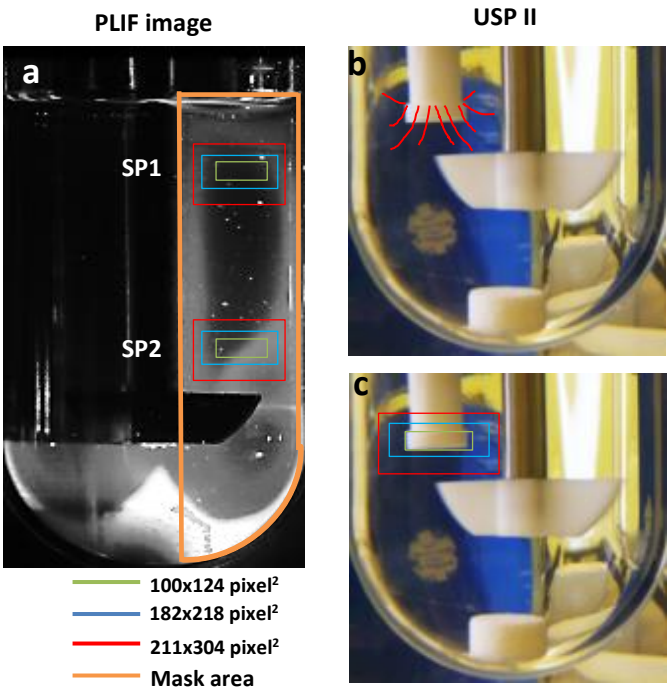

Figure 3.2. a) Schematic representation of the sampling point and size selected within the mask area of PLIF images corresponding to the cannula position in USP 2 mini vessel dissolution apparatus; b) Red streamlines illustrate the pumped material by the cannula around its filter diameter and c) the corresponding theoretical sampling area selected for processing PLIF images.

3.2.8 Statistical analysis

Comparison of the dissolution profiles of THE and RH-6G was conducted using model-dependent and model-independent methods. Differences between the two sampling points for both dissolution tests (i.e. conventional USP 2 and PLIF) as well as the size of the sampling area in PLIF images, were tested for significance using Analysis of Variance (ANOVA) with a value of $p<0.05$. The release rate mechanism in the simple buffer at both pH used (i.e. 1.0 and 7.4) was determined using Korsmeyer-Peppas fitting model as described in Eq. 3.5. The similarity between dissolution curves of THE and RH-6G, obtained in different viscous media,

was tested by the f_2-statistic (Eq. (3.7)) where f_2 value between 50 and 100 suggests that two dissolution profiles are similar (Radwan et al., 2012).

$$f_2 = 50 * log\left[\frac{100}{1 + \sqrt{\frac{\sum_{t=1}^{t=n}(R_t - T_t)^2}{n_p}}}\right] \tag{3.7}$$

R_t = Dissolution (%) for drug formulation at time t

T_t = Dissolution (%) for dye formulation at time t

n_p = number of time points

The concentration values of RH-6G were normalized (% release) before calculating the similarity factor. In addition, mean dissolution time (MDT) was calculated as model-independent parameter describing kinetics of drug and dye dissolution under various viscous media (Eq. (3.8)).

$$MDT = \frac{\sum_i \bar{t}\ \Delta M_i}{\sum_i \Delta M_i} \tag{3.8}$$

where: $\bar{t}_i$ is the central point of the observed time interval and ΔM_i is the differential amount of drug dissolved.

Finally, linear regression of the dissolution data of THE and the RH-6G obtained under the experimental conditions was performed.

3.3 Results

3.3.1 Effect of compression load and time on dissolution profile of theophylline

When manufacturing hydrophilic matrices by direct compression, it is very important to take into consideration the load of the compression process (Kukura et al., 2003a), since variations in the compression force can affect subsequent drug release when a low viscosity grade polymer is used (Garbacz et al., 2008). The dissolution data of THE obtained at compression pressures of 980.6 bar and 1961.2 bar respectively, showed no influence of compression time on the release of the THE. These results are consistent with works from other authors working on hydrophilic matrices who found either a very slight reduction in drug release (Fotaki et al., 2009b) or no significant effect (McConnell et al., 2008, Dinning et al., 1999, Quigley et al., 1984). Thus, for the following THE and RH-6G dissolution tests, compression pressures and time were fixed at 980.6 bar and 20 s respectively.

3.3.2 Particle Image Velocimetry (PIV)

The rheological properties of the fluids used in this study are presented in Table 3.1.

Table 3.1. Rheological characteristics of the dissolution media employed

	ρ (kg m^{-3})	τ_Y (Pa)	μ_A (mPa s)	K ***(mPa s^n)***	n	k	m	Re	Regime
"Simple" buffer	1000.10		1		1		1	1503.0	
0.25% NaCMC (w/w)	1017.60	0.03	13.34	0.04	0.87	0.044	0.58	114.6	Transitional
0.50% NaCMC (w/w)	1020.40	0.18	98.11	0.2	0.74	0.229	0.72	17.6	
0.75% NaCMC (w/w)	1024.50	0.76	575.60	0.83	0.6	0.830	0.85	2.6	Laminar

ρ: density (kg m^{-3}), τ_Y: yield stress (Pa), μ_A: apparent viscosity (mPa s), K: consistency index (mPa s^n), n: power law exponent, k: proportionality constant related to the structural and geometrical properties of the matrix, Re: Reynolds number and m is the diffusional exponent indicative of the drug release mechanism

Figure 3.3 shows the time average velocity fields (m s^{-1}) measured by PIV experiments in water and three different viscous NaCMC media. In all experimental fluids the maximum time average velocity was 10% (0.008 m s^{-1}) of the paddle speed (0.08 m s^{-1}). Each subfigure shows the spatial distribution of the time average velocity in the vertical plane of the impeller (top) and in the transverse cross section of the mini vessel at the top surface of the tablet (bottom). Based on the calculated Reynolds numbers (Table 3.1) the results span both transitional ('simple' buffer, 0.25% and 0.50% NaCMC w/w) and laminar (0.75% NaCMC w/w) regimes. In case of the viscous media, the most intense motion takes place mainly around the impeller, whereas away from the impeller blades the flow slows and becomes almost stagnant. In the vertical, two circulation zones were observed with clockwise (below the blade) counter-clockwise (above the blade) flowing pattern. As the viscosity is increased the circulation loop becomes smaller with reduced velocities in the most viscous medium (i.e. 0.75% NaCMC w/w) shown in Figure 3.3d. However, relatively high velocities were observed close to blade and the shaft corner and below the blade compared to the flow away from this area. In the 'simple' buffer (water), another loop was detected at the top of the vessel where the sampler was located (sampling point 1; SP1) forming a second mixing area. This was not observed in the viscous media. The velocity vectors indicate, except for the 0.25% NaCMC (w/w), that there was a downward flow starting from the top region of the vessel to the blade. In contrast, for the 0.25% NaCMC (w/w) (Figure 3.3b), an upward flow pattern was observed close to the wall which extended from the tip to the top region of the vessel. In addition, the velocities vectors showed that the flow, outside the circulation zone and parallel to the blade, had a direction from the shaft to the wall encountering the upward flow pattern coming from the tip. This flow pattern differs from 0.5% and 0.75% NaCMC (w/w), possible due to fluid motion generated by the shaft rotation. The effect of the shaft rotation seems to be inefficient in order to generate fluid motion in the more viscous media; i.e. 0.5% and 0.75% NaCMC (w/w).

The flow fields in the transverse sections in Figure 3.3 (bottom) illustrate the presence of a circular low velocity region located at the vessel axis above the tablet surface. The maximum velocity was 3.75% (0.003 m s^{-1}) of the paddle speed, although, in 0.75% NaCMC was below

0.0024 m s^{-1} (<3%). This region is extended from the tablet surface to the lowest point of the shaft and is critical to the performance of the dissolution test (Kostewicz et al., 2014), since it defines the shear forces applied on the surface of the hydrophilic matrix and hence the erosion of the gel layer. Therefore, the drug release will be strongly influenced by the hydrodynamics in this region. This region increases in size, becoming larger than the tablet diameter, as the viscosity increases. These observations are in accordance with the previous studies illustrating the poor mixing performance of USP 2 dissolution apparatus and the complex and reduced velocities within the bottom area in which where the tablet is placed (Zuleger et al., 2002, Bai et al., 2011, Baxter et al., 2005b, Cox et al., 1982).

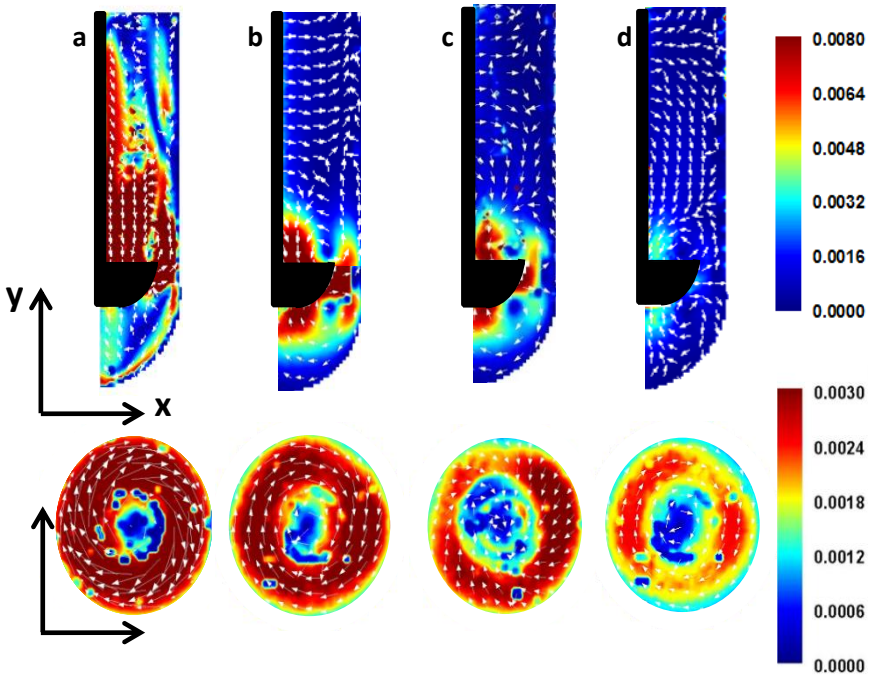

Figure 3.3. Time average velocity fields measurements in vertical USP II mini vessel (top) and horizontal section (bottom) above the tablet surface for: a) "simple buffer" $(Re = 1503.0)$**, b) 0.25% NaCMC (w/w)** $(Re = 114.64)$**, c) 0.5% NaCMC (w/w)** $(Re = 17.63)$ **and d) 0.75% NaCMC (w/w)** $(Re = 2.67)$ **NaCMC (w/w). The units of velocity magnitude are m s^{-1}. Impeller speed: 0.785 m s^{-1} and operation temperature 37 ºC.**

It has been shown that due to this inadequate agitation at the bottom of the vessel causes accumulation of particles, a phenomenon so called coning (Higuchi et al., 2014). Parameters such as the particle size, the particle density, the fluid viscosity, the fluid density, the apparatus configurations and the agitation strength are involved on the occurrence of coning phenomena.

3.3.3 Drug and RH-6G dissolution and release kinetics

Figure 3.4 shows the effect of the sampling point and the size of the sampling area on the dissolution profile of RH-6G obtained from the PLIF and comparison with the profile of theophylline (released %). The results showed for SP2 that the average concentration values of the RH-6G (mgL^{-1}), were not statistically different ($p>0.05$) between each of the three different sample sizes (100×124, 182×218, 211×304; $pixel^2$) for all the experimental fluids. However, in case of 0.25%, 0.5% NaCMC (w/w), the average value of dye concentration was found to decrease as the size of the sampling area was increased for the SP1. This was due to the fact that in the large sampling size more low concentration values were included from the dead zones resulting in a decrease of the average value. Nevertheless, the standard deviations bars are overlapped implying no statistically significant difference.

In addition, as the sampling size and the viscosity of the fluid were increased, the coefficient of variation (C.V) ((σ/μ) *100; standard deviation σ, mean μ) also increased. The C.V for the simple buffer lay between 5 – 10% for SP2 as the sampling area increases from 100*x*124 to 211*x*304 $pixel^2$. Higher values of C.V were observed (22 – 29%) for the corresponding results at SP1. The viscosity of the fluid had a significant impact on the concentration variability of RH-6G within the selected sampling area and especially in SP1. In case of 0.25% NaCMC (w/w), C.V values ranged 32.6 – 52.6% and 7.2 – 26.5% for SP1 and SP2, respectively. Even higher C.V values were observed in 0.5% NaCMC (w/w). In particular, C.V values for SP1 and SP2 were 44.6 – 46.6% and 39.2 – 41% respectively, whereas in 0.75% NaCMC (w/w), were 37.2 – 45.8% (SP1) and 38.4 – 42% (SP2).

Furthermore, a faster release profile was obtained for both compounds based on SP2 data, compare to the corresponding SP1 one.

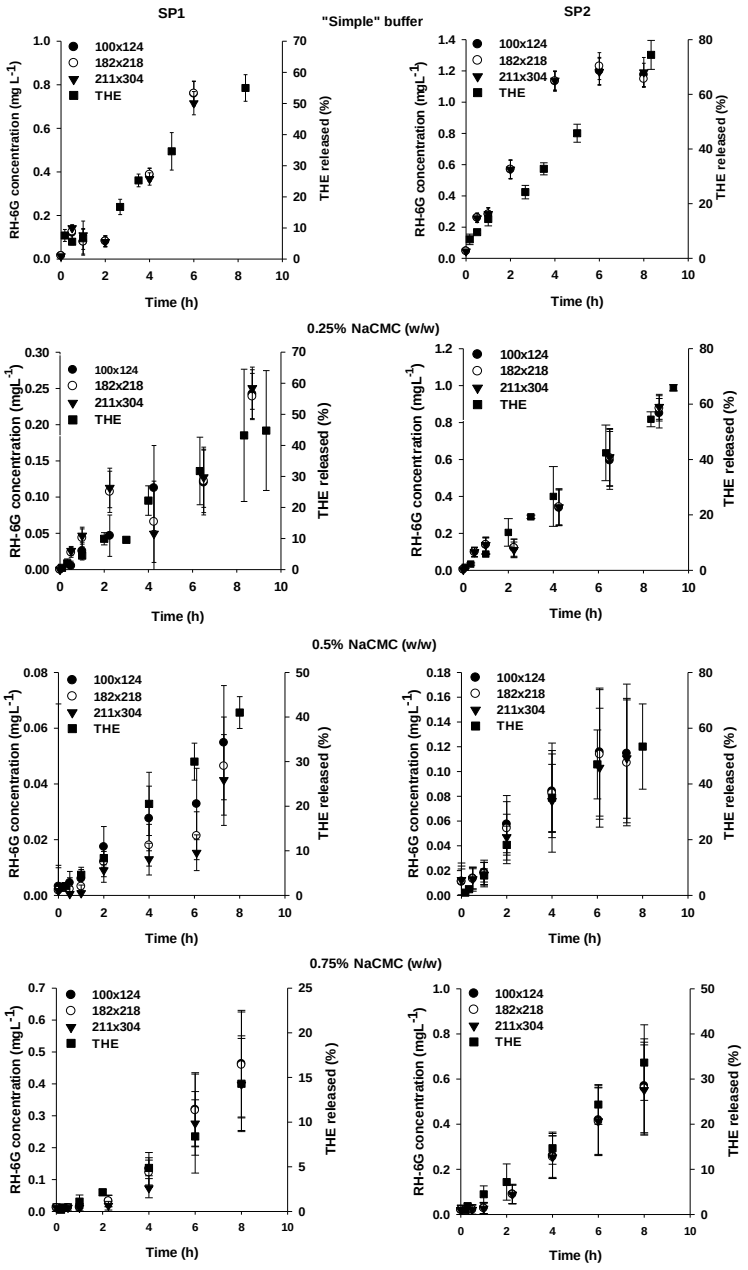

Figure 3.4. Effect of size of the sampling area on the interpretation of the dissolution data of RH-6G obtained from PLIF images and comparison with theophylline (THE) release profile obtained at sampling point 1 (SP1) and sampling point 2 (SP2) in different viscous media. The legend entries refer to sample size (● 100x124, ○ 182x218 and ▼ 211x304) for the RH-6G profile and the release profile (■) of theophylline (THE). Standard deviation bars for RH-6G (n=10) and THE (n=6).

Table 3.2 presents the local colour scaled concentration values of RH-6G throughout the mini vessel as a function of dissolution time, under different experimental fluids. The main observations are that: a) the concentration of the dye was always higher around the blade, in contrast to the upper region, explaining the faster release rate observed based on SP2 compare to SP1 (Figure 3.4), b) as the viscosity is increased dead zones and high fluctuations in the distribution of the dye was occurred, revealing the high C.V values obtained in viscous media, c) in the most viscous media (i.e. 0.50% and 0.75%) the dye accumulates at the bottom of the vessel before it reaches the upper region of the vessel. These results can explain the high standard deviation observed in theophylline release data and the dissimilarities in the dissolution profiles between SP1 and SP2.

Comparison of RH-6G and THE dissolution profile was not possible with using the similarity factor (f_2) (Table 3.3) for those cases where C.V was >10%. Nevertheless, the standard deviation bars of THE data points and those of RH-6G (Figure 3.4) overlapped; implying that from statistical point of view there was no a significant difference. Failure of obtaining $f_2 > 50$, in case of pH 1.0 for SP2, might be also due to burst release upon hydration of the tablet in 0.1N HCl solution. Similar effects were noted by (Conti et al., 2007a). In this case, the gel hydration rate is slower and the dye molecules present at the surface of the tablet can dissolve and pass into the fluid; the solubility of RH-6G is 20 mg mL^{-1} @ 23 ^{o}C compared to THE which is 8.3 mg mL^{-1}. However, sink conditions, defined as having a volume of medium at least three times the volume required to form a saturated solution of drug substance, are present in both cases which ensures that the dissolution test reflects the properties of the dosage form and not the drug substance (Convention, 2009). However, the rate of RH-6G dissolution may be faster than that for THE due to this difference in solubility values. This can lead to a fast saturation of the area around the blade (SP2 position) resulting in an intense fluorescence causing high grayscale values reflecting high release rates. As the dye reaches the upper region the concentration is decreased resulting in more normal values and better fitting with theophylline. Furthermore, particle size differences and the distribution of the particles of the

RH-6G and THE within the tablet may also affect the release rate of the dye, leading to dissimilarities between the dissolution profile of the drug and the dye.

Table 3.2. Distribution of the RH-6G (average concentration (mg L^{-1})) throughout the USP 2 mini vessel in different viscous media.

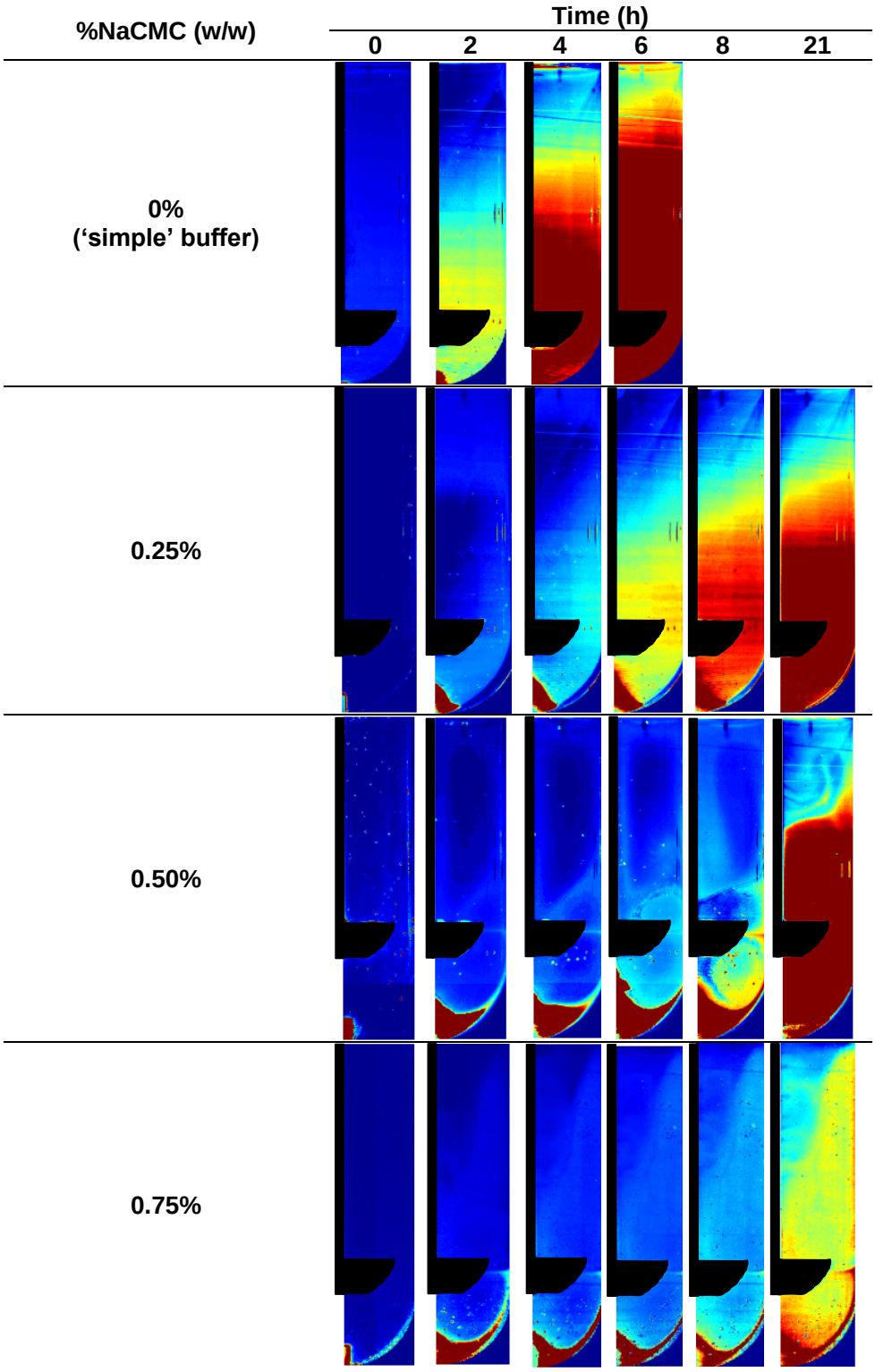

An additional outcome is that in 'simple' buffer the dissolution profiles of THE obtained from the two sampling points were similar (f_2>50), but that was not the case in viscous media demonstrating the effect of viscosity on dissolution.

Furthermore, the values of *m* exponent (Table 3.3) showed that: a) the sampling point can alter the *m* values, b) the mechanism characterizing the release was the same for both compounds, since it was within the range of 0.5 – 0.89 (pH 1.0) and above one for pH 7.4. This implies that at pH 1.0, diffusion of the compound and polymer chain relaxation (anomalous non-Fickian) mainly affect the release of the compounds whereas at pH 7.4, high *m* values (>1) are typical for hydrophilic matrices, in which high release rate occurs due to high solubility of the polymer (i.e. NaCMC) at this pH, leading to gel erosion. This is further evidence that PLIF data can also describe the release mechanism of a highly water soluble drug from a hydrophilic matrix.

The effect of media viscosity on the mean dissolution time (MDT) is presented in Table 3.3. The results showed that as the viscosity increases the MDT also increases. The value of MDT between the two techniques (i.e. USP and PLIF) was not statistically significant (*p*>0.05) at each experimental condition.

Table 3.3.Comparison of the release kinetic mechanism of theophylline and Rhodamine-6G from hydrophilic matrix under different experimental fluids, using model-dependent and – independent parameters.

	'Simple buffer'				%NaCMC (w/w)[a]					
	pH 1.0		pH 7.4		0.25		0.50		0.75	
	USP	PLIF	USP	PLIF	USP	PLIF	USP	PLIF	USP	PLIF
f_2	- SP2=35.9		- SP2=55.2		- SP2=51.9		-		-	
	51.0[b]	32.7[b]	52.6[b]	30.9[b]	46.8[b]	30.8[b]	-	-	-	-
MDT[c]	3.82	3.90	3.12	2.97	4.13	4.20	4.41	4.30	4.94	4.77
m[d]	0.75 – 0.82	0.57 – 0.61	1.46 – 1.52	1.24 – 1.33						
R^2	0.985	0.993	0.992	0.941						

[a] 0.05M phosphate buffer (pH 7.4); [b] f_2 values obtained by comparing SP1 and SP2 dissolution data of theophylline and RH-6G separately; [c] Mean dissolution time (MDT); [d] the lowest values were obtained from fitting the dissolution data of sampling point 1 (SP1) whereas the highest values are for the sampling point 2 (SP2)

A linear correlation between THE and RH-6G release data was achieved for SP2 (Figure 3.5). It was found that the average concentration of the drug obtained from conventional technique was in good correlation with the mean concentration of the dye for the same time intervals. The correlation plots were characterized by the coefficient of correlation values 0.908, 0.919, 0.988 and 0.991 for the 'simple buffer' (pH 7.4), 0.25%, 0.5% and 0.75% NaCMC (w/w), respectively.

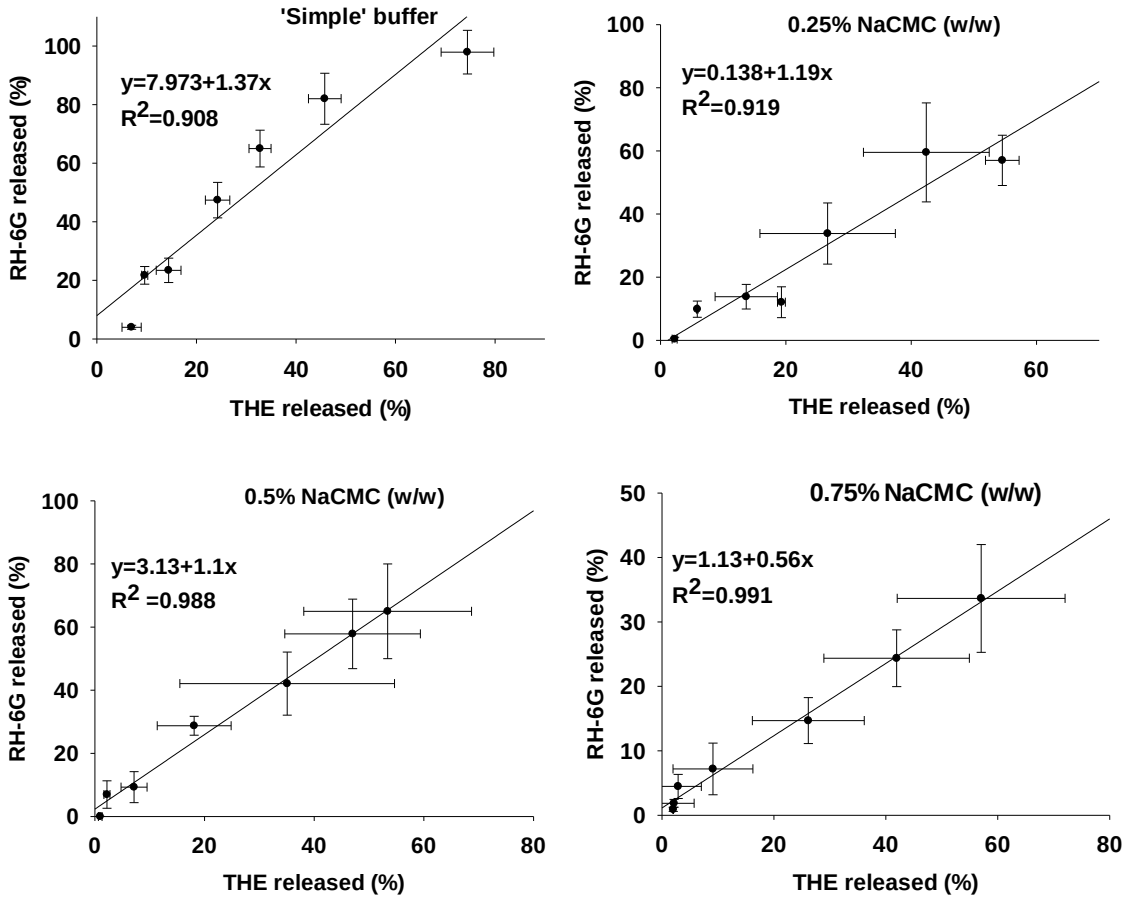

Figure 3.5. Correlation between theophylline (THE) and rhodamine-6G (RH-6G) release data for SP2; (a) water, (b) 0.25%, (c) 0.50% and (d) 0.75% NaCMC (w/w); Standard deviation bars (±SD, n=6).

3.3.4 Gel layer strength measurements

Previously researchers have carried out compression analysis experiments on hydrophilic matrices (Conti et al., 2007b, Ochoa et al., 2005, Qureshi and Shabnam, 2001b, Yang et al., 1998) in order to make a correlation between the thickness and the strength of the tablet gel layer with the dissolution profiles of matrix tablet. Compression experiments performed in this work gave information about: 1) the gel layer strength (Figure 3.6a), which is the measurement of the slope of the texture analysis curves (force vs probe penetration distance), 2) gel layer thickness (Figure 3.6b) of NaCMC matrix at the two pH values under which the dissolution experiments were conducted and 3) the corresponding dissolution profile of THE (Figure 3.6c). The gel strength of the hydrophilic matrix was stronger at pH 1.0 compared to the strength obtained at pH 7.4. In contrast the gel layer thickness was bigger at pH 7.4 compared to pH 1.0. This explains why the release rate of THE at pH 7.4 was higher (Figure 3.6c) compared to pH 1.0. The hydration of the hydrophilic matrix was faster at pH 7.4 which is indicated by a significant increase of gel layer thickness of about 4 times within 5.5 hours compared to 2.5 times in case of pH 1.0. As a further consequence of fast hydration, the concentration of the polymer (i.e. NaCMC) within the gel layer is decreased leading to lower gel strength (Zuleger et al., 2002). It has been reported that the drug release is increased as the gel thickness increases and the slope of force-penetration curve decreases (Ochoa et al., 2005). At pH 1.0 NaCMC is not soluble which may affect the hydration and subsequently the dissolution of the drug in the gel layer. In addition, the insufficient hydration at pH 1.0 results in the formation of a stronger gel layer (50 – 10 g s^{-1}) at pH 1.0 compared to pH 7.4 (19 – 4 g s^{-1}). This implies that the drug release mechanism is mainly due to the diffusion through the thick gel layer and no due to the erosion; since the erosion of the gel layer requires sufficient hydration of the polymer chains in order to reach the disentanglement concentration where the macromolecules begin to detach from the swollen matrix (Zuleger et al., 2002). The same conclusion has been made with regard to the release mechanism of THE at pH 1.0 by the release kinetics analysis based on *m* exponent values obtained after fitting the dissolution data using Korsmeyer-Peppas model. However, it has to be pointed out that other factors such as

high loadings (e.g. 50%) of water soluble drugs as well as hydrophilic additives (i.e. potato starch which is used in this study) may also have an impact on swelling behaviour and gel layer texture properties (Mitchell et al., 1993, Zuleger et al., 2002) and hence on drug release. Nevertheless, the high drug loading in the current dosage form might also alter the release rate due to the increased porosity which leads to a fast release rate (Maderuelo et al., 2011) and which is not linked to the lower hydration at pH 1.0 compared to pH 7.4. Furthermore, burst release can occur at pH 1.0 since the gel hydration rate is slower and the drug molecules present at the surface of the dosage form can easily dissolve and pass into the medium (Conti et al., 2007a). Hence, these additional factors might explain why there was no a difference between the release profile of THE at two pH values (Figure 3.6c) especially at the first two hours whilst the differences in gel thickness and strength were remarkable. Finally, there was no effect on the gel layer thickness and gel strength with the addition of RH-6 G in dosage form.

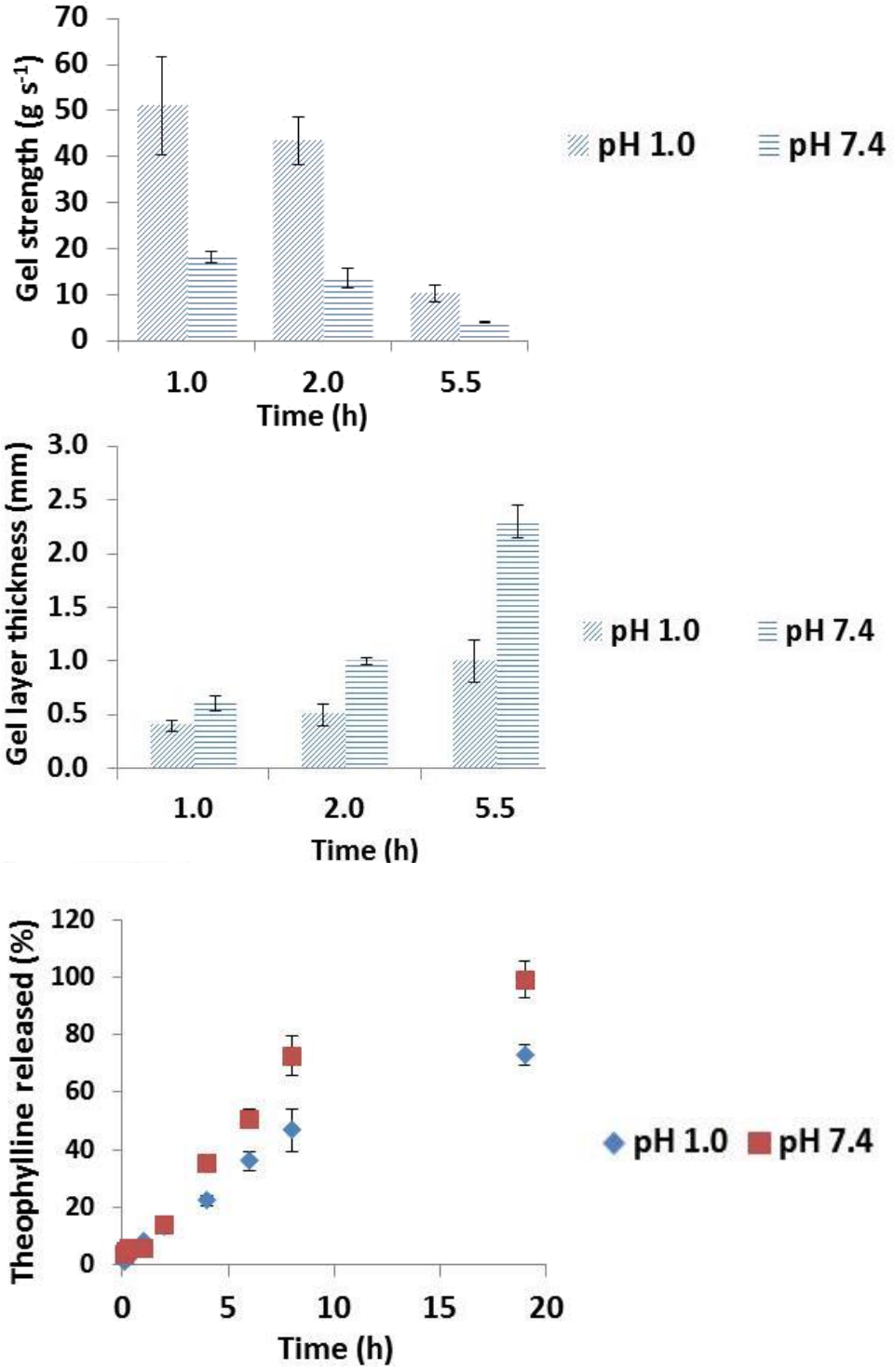

Figure 3.6. Effect of pH on the gel layer strength (a) and thickness (b) as well as on the dissolution profile of THE (c). Standard deviation bars for gel strength and thickness (n=6) and for dissolution profile of THE (n=6).

3.4 Conclusions

In this chapter, the dissolution profile of a fluorescent dye Rhodamine 6G (RH-6G) released from a hydrophilic matrix tablet has been determined in a USP 2 mini vessel using PLIF. The profiles determined have been compared with results obtained using theophylline (THE), a highly soluble drug.

The dissolution profiles of both RH-6G and THE were found to be statistically similar: a highly linear correlation was determined between the release data of the drug and the dye (R^2>0.9). Thus, RH-6G is an appropriate probe to mimic the release profile of a highly soluble drug.

Using viscous media, segregated zones were identified in the vessel, where high amounts of dye accumulated on the bottom of the vessel. This is due to highly inhomogeneous mixing intensities across the vessel resulting in non-uniform distribution of the dye. Analysis of PLIF images using MATLAB showed that for a given time, the concentration of RH-6G around the impeller was always higher in all experimental fluids compared to the upper region of the USP 2 mini vessel. This time delay for the released dye-drug to reach the upper zone of the dissolution apparatus leads to different release rates when different sampling points are used for generating the dissolution profile of the targeted drug.

The proof of concept that the dissolution profile of the fluorescent dye matches that of a common drug allows prediction of the performance of the dissolution test and thus guidelines in terms of sampling point and possible variance of the drug dissolution data obtained. The PLIF images showed better uniformity of the dye distribution above the blade and close to the wall. Thus, based on this analysis, positioning the cannula within this zone could minimize the variance of the dissolution data. Nevertheless, due to the design of the USP 2 there will be always limitations on the mixing performance and hence on the reproducibility of the dissolution data. These are critical and important results for practitioners using the device.

In this chapter the decision based on where the sample probe should be positioned relies on observing the PLIF image instead of a systemic quantitative analysis. Furthermore, the dissolution profile of the drug as well as the fluorescence dye was assessed mainly around

the most common locations that the sampling probe is normally positioned. However, since the dye matches the release profile of the drug, this allows further assessment of the distribution of the active compound throughout the mini vessel. Thus, in the following chapter the analysis of the distribution of the drug is performed with the combination of the coefficient of variation, allowing assessing the range of drug concentrations, and the areal distribution method as well as individual striation methods, providing information for the local distribution of the drug concentration. Areal distribution method and individual striation method have been used in the past to assess the mixing performance in stirred tanks. These methods will allow evaluating the mixedness level and its percentage distribution throughout the vessel. Thus, indicating the location in which the highest mixing level occurred, to determine the best position to place the sampling probe, providing the lowest variability of the dissolution experiments.

Nomenclature

k_S	Metzner-Otto constant
$\underline{\underline{C}}$	concentration matrix
$\underline{\underline{a}}$	matrix of constant vales
$\underline{\underline{G}}$	matrix of averaged Grayscale values
$\underline{\underline{b}}$	matrix of intercept values for the linear regression
μ_A	apparent viscosity
C_i	fully mixed concentration
D	impeller diameter (m)
G_i	Level of mixedness
$\bar{G}_i$	mean value of grayscale in the experimental image
K	Consistency index
n	power law exponent
N	rotational speed (rps)
N_p	total number of the pixels in the region of interest
Re	Reynolds number

Greek symbols

$\dot{\gamma}$	Shear rate (s^{-1})
μ_A	Apparent viscosity (mPa s)
p	Density (kg m^{-3})
τ	Shear stress (Pa)
τ_γ	Yield stress (Pa)

Abbreviations

ANOVA	Analysis of Variance
API	Active Pharmaceutical Ingredient
C.V	Coefficient of Variance
CCD	Charged Coupled Device
CD	Crohn's Disease
CFD	Computational Fluid Dynamics
DCM	Dynamic Colon Model
HCl	Hydrochloric acid
NaCMC	Sodium carboxymethylcellulose
PLIF	Planar Induced Fluorecence
RH-6G	Rhodamine-6G
RSD	Relative Standard Deviation
THE	Theophylline
USP	United States Pharmacopeia

4 Use of PLIF to assess the mixing performance of small volume USP 2 apparatus in shear thinning media[2]

Abstract

Planar Laser Induced Fluorescence (PLIF) was used to assess mixing in small volume USP 2 dissolution apparatus for a range of viscous fluids which mimic gastrointestinal media, especially in the fed state. The release into the media from a specially prepared tablet containing Rhodamine 6G dye was tracked in time and the areal distribution method developed by Alberini et al. (2014a) was implemented to characterise the mixing performance. The distributions of the individual striations for selected mixing levels were also presented. These findings illustrate the poor mixing performance of the apparatus resulting in high variance of the dissolution data when working with viscous media. Analysis of data using coefficient of variance (C.V) gives misleading results for the mixing performance of the small volume USP 2 dissolution apparatus. The results showed that the best mixing was mainly located above the blade and close to the wall, i.e. in the region where intensive motion takes place. This work presents important guidelines and precautions for choosing the proper sampling point for a wide range of liquid viscosities to minimize the variability of the dissolution data.

[2] Stamatopoulos, K., Alberini, F., Batchelor, H. & Simmons, M. J. H. 2016. Chemical Engineering Science, 145, 1-9.

4.1 Introduction

The USP 2 dissolution apparatus, which is an agitated mixing device, is the most commonly used piece of equipment for *in vitro* evaluation of solid oral dosage forms. However, several reports have suggested considerable variability, unpredictability and randomness in dissolution profiles obtained from it (Cox et al., 1982, Cox et al., 1983, Qureshi and Shabnam, 2001b), even when calibrator tablets are used (Kukura et al., 2003a, Baxter et al., 2005a).

In the pharmaceutical industry, accurate prediction of the *in vivo* biopharmaceutical performance of oral drug formulations is critical to product and process development. As a part of a general drive to develop predictive *in vitro* models, biorelevant media have been proposed and have evolved over the last decade as a tool for *in vitro* biorelevant dissolution tests (Jantratid et al., 2009). The usefulness of the biorelevant dissolution test is that both media composition and hydrodynamics are taken into consideration. This is essential to provide a baseline for drug and dosage-form performance as well as determining possible food effects on the dissolution and bioavailability of orally dosage forms (Qingxi Wang, 2009).

Studies have shown that food viscosity is one of the physiological parameters that can affect oral drug absorption (Levy and Jusko, 1965, Radwan et al., 2012). To examine this, several authors have conducted drug dissolution and disintegration experiments, which under viscous conditions showed reduced dissolution and disintegration rates (Parojcic et al., 2008, Radwan et al., 2012).

Nevertheless, introducing viscosity into the dissolution test may increase the uncertainty and the variability of the results, since the hydrodynamics of the USP 2 apparatus will change as the flow enters the laminar and transitional regimes, where mixing performance is known to worsen with increasing viscosity.

The characterization of the mixing performance of conventional stirred tanks (as used in the chemical industries) using visualization techniques such as Planar Laser Induced Fluorescence (PLIF), has been extensively investigated under different conditions and using

viscous fluids (Hu et al., 2010, Cheng et al., 2015, Zhang et al., 2013, Busciglio et al., 2014). Using this non-intrusive method, qualitative and quantitative evaluation of the mixing performance is possible by tracking the motion of a fluorescent tracer injected into the fluid. Thus, the uniformity of the distribution of the fluorescent dye depends upon the mixing performance of the system.

As mentioned in the previous chapter, several studies have used PLIF (Baxter et al., 2005a; Kukura et al., 2004) and PIV combined with Computational Fluid Dynamics (CFD) (Baxter et al., 2005a; Kukura et al., 2003) to characterize the mixing performance and the velocity field in conventional (1 L) USP 2 apparatus dissolution vessel. Whilst these studies are valuable for highlighting the drawbacks of the USP 2 dissolution apparatus, they do not allow any direct or indirect correlation with the dissolution profile of an active compound. The concern is that they use a method, i.e. PLIF capable of capturing local time-dependent mixing conditions in the USP 2 and yet use a conventional sampling technique for generating dissolution profiles of the targeted drug. Indeed, Kukura et al. (2003, 2004) could not find a significant difference in dissolution profiles of the targeted drug at the different sampling points, although, large fluctuations of the mixing patterns were observed with time (Kukura et al., 2003a, Kukura et al., 2004). Previous works (Parojcic et al., 2008; Radwan et al., 2012) testing different dosage forms in viscous media did not give any information as to the position of the sample tube to generate the dissolution profile of the tested drug or possible changes in hydrodynamics (e.g. shear rates and/or velocities) or mixing patterns. Thus, there is a need for a study that uses PLIF data generated by capturing images of a fluorescent dye released from compressed tablets, which mimics the release mechanism of the targeted drug. A study which includes sampling location is essential to provide data relevant to the conventional drug dissolution experiments.

It has been recognised that the choice of method or algorithm used to evaluate the mixing performance is of critical importance and that a simple numerical measure based on concentration variance or scale of segregation (Danckwerts, 1952) (obtained after image

analysis of the fluid flow) cannot describe the complexity of a flow pattern within a mixer (Alberini et al., 2014a).

Regarding the mixing performance in the USP 2 apparatus, the release of drug and/or dye from a tablet into a viscous medium could reflect a case where a second element is introduced into the fluid and, therefore, segregation area and concentration variance should both be considered. This multi-dimensional analysis of mixing is the basis of the so called areal distribution method (Alberini et al., 2014b). This method was developed to analyse the blending of two fluid components with different apparent viscosities under laminar mixing in a static mixer in which viscous filaments are formed.

Similarly, Stamatopoulos et al. (2015) using the small volume USP 2 apparatus showed that filaments of highly concentrated RH-6G were formed when dye is released in a controlled manner from a tablet. They showed also dramatic differences in flow regime as a function of viscosity from PIV measurements (Figure 4.1).

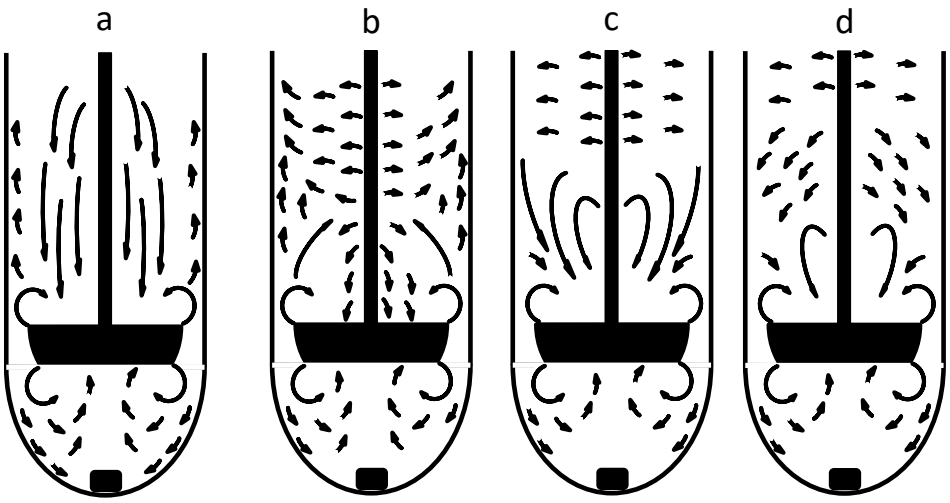

Figure 4.1. Schematic representation of the experimental fluid flow patterns within USP2 mini vessel based upon PIV analysis conducted by Stamatopoulos et al. (2015); a) "simple" buffer, b) 0.25% NaCMC, c) 0.50% NaCMC and d) 0.75% NaCMC.

Assessing the distribution of the released drug molecules in a viscous media is very important for the performance of the dissolution method. For example, drawing a sample from a “dead zone” may lead to inconsistent dissolution data. This is due to the fact that drug molecules from highly concentrated areas could enter low concentration regions due to flow generated locally by the pumping tube. Thus, whilst C.V enables the range of concentrations to be assessed, it does not consider the local distribution of the dye concentration; the areal distribution method and individual striation methods use both which is a clear advantage.

In this paper, dissolution experiments using a RH-6G blended tablet were carried out using the small volume USP 2 apparatus. The distribution of the released RH-6G dye within the small vessel was determined by capturing PLIF images at several time intervals; reflecting the typical sampling process to generate the dissolution profile of the targeted drug. The mixing performance was evaluated in different viscous fluids using C.V, the areal distribution and individual striation methods. This paper examines the effect of the viscosity on the mixing performance of the small volume USP 2 apparatus giving valuable guidelines and precautions for choosing the proper sampling point for a wide range of viscosities to minimize as much as possible the variability of the dissolution data.

4.2 Materials and Methods

4.2.1 Materials

Sodium carboxymethylcellulose of 90000 ($NaCMC_{90000}$) and 700000 ($NaCMC_{700000}$) molecular weight were purchased from Sigma (St., Louis, USA). Theophylline anhydrous (THE) and potato starch were bought from Acros Organics (Loughborough, UK). Sodium hydroxide, Rhodamine-6G, hydrochloric acid (1M), silicon dioxide and potassium hydrogen (KH_2PO_4)- and dihydrogen phosphate (K_2HPO_4) were purchased from Sigma (St. Louis, USA).

4.2.2 Fluids and fluid properties

$NaCMC_{700000}$ was selected as a water-soluble polymer with shear thinning rheology to mimic the shear thinning nature of the chyme (Kong and Singh, 2008). $NaCMC_{700000}$ buffered solutions of 0.25, 0.5 and 0.75% (w/w) were prepared using 0.05M phosphate buffer pH 7.4 (KH_2PO_4/K_2HPO_4). A pH of 7.4 was selected as a representative pH value for the large intestine. All the tested fluids were deaerated using an ultrasound bath before conducting PLIF experiments.

The rheology of the NaCMC solutions was measured using a Discovery Hybrid Rheometer (TA Instruments – a division of Waters Ltd.) coupled with a 40 mm diameter, 4° cone and plate geometry. The temperature was set to 37 ^oC using an in-built Peltier plate (set at the same temperature as the USP 2 experiments). The rheology was obtained by performing a shear ramp over a range of shear rates from 0.1-1000 s^{-1} and the data were found to fit the Herschel-Bulkley model.

$$\tau = \tau_Y + K\dot{\gamma}^n \quad (4.1)$$

Where τ is the shear stress (Pa), τ_Y is the yield stress (Pa) $\dot{\gamma}$ is the shear rate (s^{-1}), *K* is the consistency index and *n* is the power law exponent. The apparent viscosity, μ_A, can be thus determined by evaluating $\tau / \dot{\gamma}$ at a given value of shear rate. The rheological properties of the experimental fluids are presented in Table 3.1 in section 3.3.2, Chapter 3.

4.2.3 Tablet preparation

A 500 mg tablet was prepared according to the following composition: 50% THE, 44.1% $NaCMC_{90000}$, 4.9% potato starch, 1% silicone dioxide and 0.02% RH-6G. The powders were sieved, mixed for 10 min and compressed at fixed pressure of 980.6 bar using a single die tableting machine (Kilian, Coln, D) fitted with flat-faced 9.8 mm punches (Kistler,Winterthur, CH). The cylindrical tablets had a final weight of 500±25 mg.

4.2.4 Experimental Apparatus: USP 2 mini paddle

A schematic of the small volume USP 2 dissolution apparatus (Dissolution Tester 6000, Antech, UK) used in PLIF experiments is shown in Figure 4.2. USP 2 consists of an unbaffled cylindrical and hemispherical bottomed vessel, with an internal diameter of 42 mm. The agitation system consists of a 2-paddle impeller mounted on a shaft with a diameter of 6.3 mm, the length of the top edge of the blade is 30 mm whereas the length of the bottom edge of the blade is 17 mm. The distance from the bottom of the impeller to the bottom of the vessel was 20 mm. The volume of media was 100 mL and the paddle rotational speed was fixed at 50 rpm. All the experiments were performed at 37°C. The flow regime in the vessel was determined by calculation of the Reynolds number

$$\mathrm{Re} = \frac{\rho N D^2}{\mu_A} \tag{4.2}$$

Where ρ is the fluid density (kg m^{-3}), N is the rotational speed (rps), D is the impeller diameter (m). The apparent viscosity, μ_A, was estimated using the Metzner-Otto method (Metzner and Otto, 1957) which assumes the shear rate in the vessel is proportional to the impeller speed, thus for a Herschel-Bulkley fluid:

$$\mu_A = \frac{\tau_Y}{k_S N} + K\left(k_S N\right)^{n-1} \tag{4.3}$$

The value of Metzner-Otto constant, k_S, in the above expression was 10 (Edwards et al., 1992). Here, k_S is the proportionality between the average shear rate in the mini vessel and the impeller rotational speed. The calculated values of Re are given in Table 4.1.

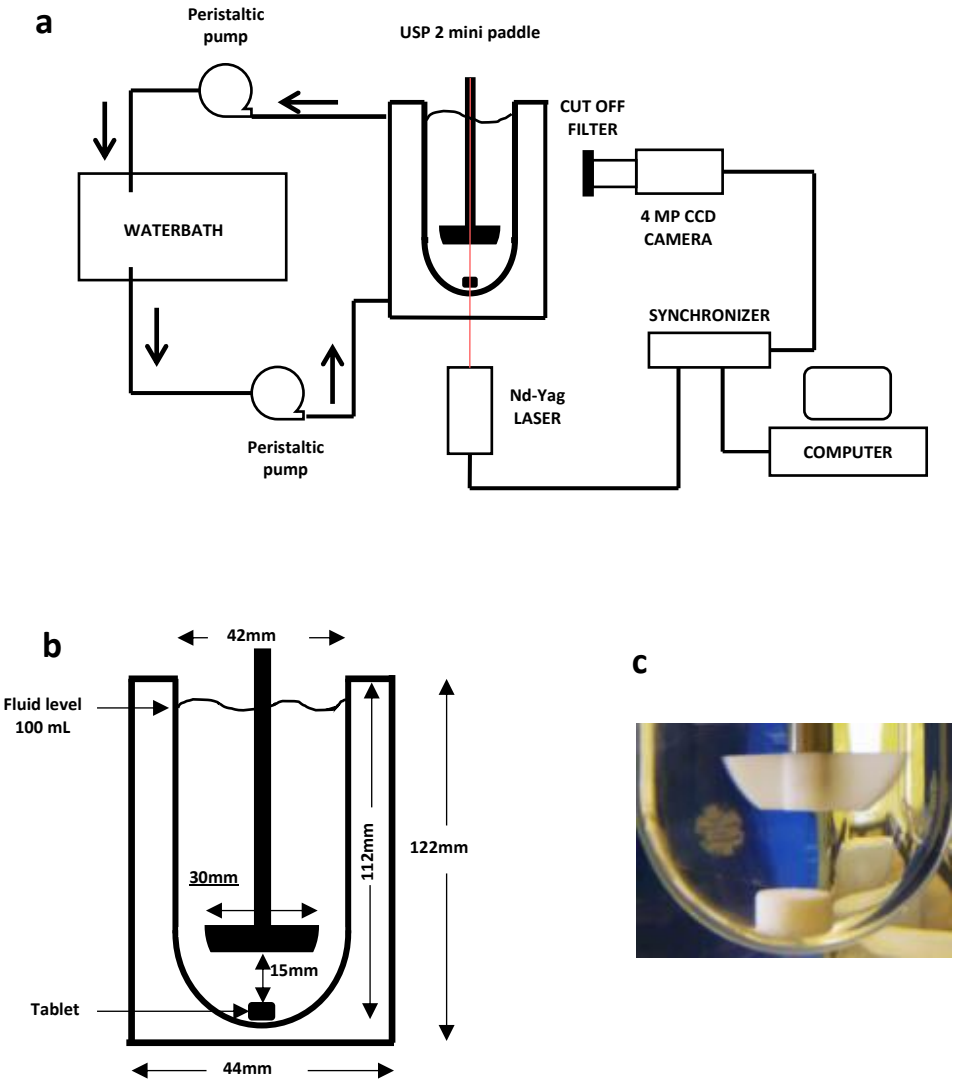

Figure 4.2. a) Overall schematic diagram of the PLIF experimental setup; b) dimensions of the small vessel USP 2; c) photo of an USP apparatus 2-bladed impeller used in dissolution experiments.

4.2.5 Analysis of PLIF images

The 2-D PLIF measurements were performed using a TSI PIV system comprised of a 532 nm Nd-YAG laser (Litron NanoPIV) pulsing at 7.4 Hz, and a single TSI Powerview 4MP (2048 × 2048 pixels) 12 bit frame-straddling CCD camera, both controlled using a synchronizer (TSI 610035) attached to a personal computer equipped with TSI Insight 4G software. The spatial

resolution of the measurements was 10 μm pixel^{-1}. The small volume USP 2 vessel was placed in an acrylic box filled with distilled water in order to eliminate refractive index issues due to vessel curvature as well as keeping a constant temperature of 37^{o}C by circulating the fluid in the box through a water bath using a peristaltic pump. The laser sheet was aligned vertically, passing across the diameter of the vessel, i.e. aligned with the impeller shaft along the vessel axis.

A cut-off filter at 545 nm was fitted to the CCD camera to eliminate reflected laser light and to capture only the fluorescent light emitted by the RH-6G (λ = 560 nm). The system was calibrated for each solution used at fixed laser power by filling the USP 2 mini vessel with well mixed solutions at concentrations ranging 0 – 1.0 mg L^{-1}; in steps of 0.1 mg L^{-1}. Potential variation in the laser power was assessed by capturing 50 images for each standard RH-6G solution; values of the relative standard deviation (RSD%) were consistently less than 3.6% and therefore not significant. The region of interest of the illuminated tank is the area where the sampling tube (cannula) is normally inserted as shown in Figure 4.3a; the remainder being in shadow due to impingement of the laser sheet on the impeller shaft. Pixel by pixel calibration was developed by taking the average grayscale values over the 50 images. Subsequently, a linear regression over concentration range was performed. The amount of RH-6G incorporated in the tablet was carefully chosen in order the final concentration of the fluorescent dye in the mini vessel to be a maximum of 1 mg L^{-1}. Thus all the grayscale values were within the range of the calibration and below the saturation signal of the CCD camera. The analysis was carried out using MATLAB (Matlab 7.6.0 R2008a) to produce a calibration matrix.

$$\underline{\underline{C}} = \underline{\underline{a}}\underline{\underline{G}} + \underline{\underline{b}} \tag{4}$$

Where $\underline{\underline{C}}$ is the concentration matrix, $\underline{\underline{a}}$ is the matrix of constant values, $\underline{\underline{G}}$ is the matrix of averaged Grayscale values and $\underline{\underline{b}}$ is the matrix of intercept values for the linear regression. The regression was carried out using a standard least-squares method.

The PLIF measurements were conducted by addition of the RH-6G tablet into the bottom of the mini vessel. Dissolution tests (six replicates) were performed in 0.1N HCl solution (gastric conditions) and in 0.05M phosphate buffer solution (pH 7.4) mimicking the fasted state conditions in large intestine. The dissolution tests for the viscous media were conducted only at pH 7.4; assuming dewatering of the chyme in large intestine resulting in an increase in viscosity. 10 images were recorded at each predetermined time interval: 0.17 h, 1.0 h, 2.0 h, 6.5 h and finally 20 h.

4.2.6 Areal distribution method

A typical raw image obtained from PLIF performed using viscous media is shown in Fi

gure 4.3a. An asymmetric distribution of the fluorescent dye within the USP 2 mini vessel is observable, forming striations with different concentrations of the RH-6G fluorescent dye. The mean value of grayscale in the experimental image ($\bar{G}$) was determined for each time interval at which the PLIF image has been captured. This is based on the fact that only a fraction of the RH-6G dye has been released from the tablet at any given time during the imaging process. Thus, in the current work, $\bar{G}_i$ is the mean value of grayscale in the experimental image corresponds to the fully mixed concentration (C_i) at time *i*. Here, the fully mixed concentration C_i replaces C_∞ used in Alberini et al. (Alberini et al., 2014b), in the areal distribution method (assuming no further release of RH-6G occurs from time *i* until the time necessary for full homogenisation to occur).

The experimentally determined $\bar{G}_i$ were used to calculate grayscale values corresponding to a given level of mixedness. Then G_i is defined as a percentage of this fully mixed value $\bar{G}_i$. Giving an example, G_i% mixing will correspond to grayscale values of either $G_{i-} = [1-(1-G_i)]\ \bar{G}_i$ or $G_{i+} = [1-(1+G_i)]\ \bar{G}_i$. Thus for 80% mixing, $G_{i-} = 0.80\bar{G}_i$ and $G_{i+} = 1.2\bar{G}_i$.

Using MATLAB (2008a) and the freeware image analysis tool Image J, the pixels in the image are identified which correspond to $G_{i-} < \bar{G}_i < G_{i+}$, thus corresponding to a mixing intensity of $> G_i$%.

4.2.7 Individual striation method

The work individual striation method was implemented to illustrate indirectly how the mixing performance of USP 2 mini vessel, and therefore the distribution of the dye in the viscous media, affects the reproducibility and hence the variability of the dissolution data of the targeted drug (Alberini et al. 2015b). Thus, identification of individual striations within different ranges of G_i was performed. The individual striations were determined using a MATLAB script which utilizes both the MATLAB image processing toolbox and the DIPimage toolbox developed by the Quantitative Imaging Group at TU Delft (http://www.diplib.org). The image analysis scripts used in this work are available by contacting the corresponding author.

Firstly the image is imported in MATLAB and a rectangular mask is created to identify the region of interest; as shown in Figure 4.3a. The area within the mask was chosen since this region is where the cannula is normally placed. Using the value of $\bar{G}_i$, the levels of mixing intensity, G_i, per pixel, are determined as previously (section 4.2.5). Then the ranges of G_i are defined and for each range, two images are created by MATLAB where only the striations in the range of interest are shown: the first shows all the striations in the range of G_{i-} and the second shows all the striations for G_{i+}. An example of this procedure is shown in Figure 4.3b.

The fraction of RH-6G released at time *i* was determined by normalizing $\bar{G}_i$ values with the G_∞ obtained after the complete release of RH-6G from the tablet; i.e. based on the final PLIF image captured after 22 h dissolution testing and the complete disintegration of the tablet.

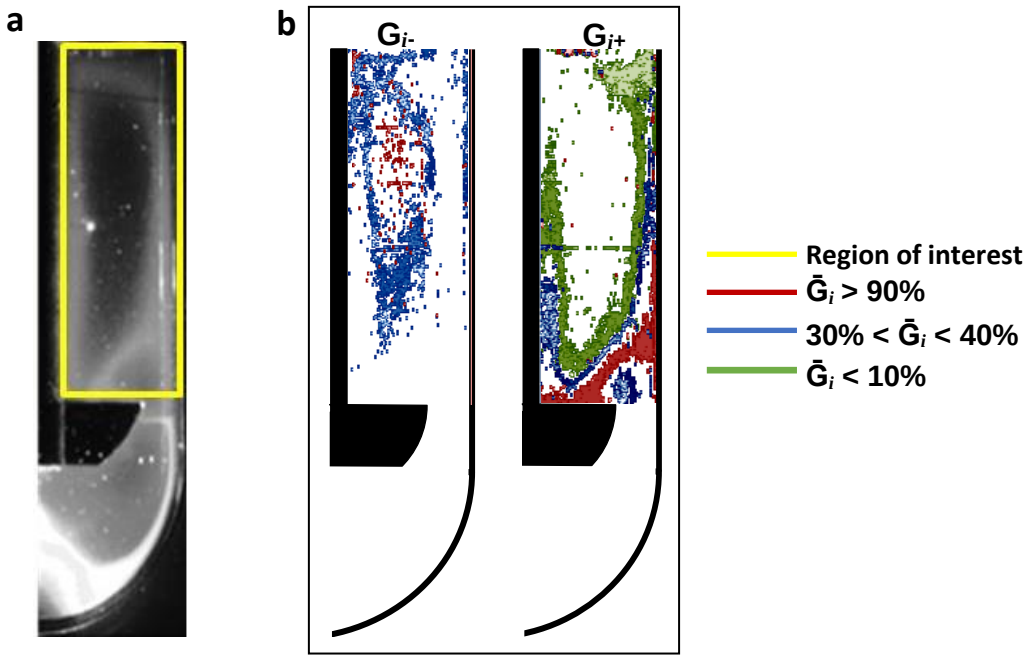

Figure 4.3. Development of areal analysis method: a) raw images with region of interest (yellow line); b) example of image processing for the 0.5% NaCMC (w/w) with the upper (G_{i-}) and lower (G_{i+}) limits of the individual striations: G_i>90% (red labeled pixels), 30%< G_i <40% (blue labeled pixels) and G_i<10% (green labeled pixels).

4.2.8 Coefficient of variation

The C.V was determined using Equation (4.5). N_p is the total number of the pixels in the region of interest, C_i the concentration in each pixel which is proportional to the grayscale value and $\bar{C}$ corresponds to the (C_i) and hence to the $\bar{G}$i.

$$C.V = \frac{\sigma}{\bar{C}} = \frac{1}{N_p}\sum_i^{N_p}\frac{\sqrt{(C_i-\bar{C})^2}}{\bar{C}} \quad (4.5)$$

4.3 Results and Discussion

4.3.1 Images obtained from PLIF technique

Figure 4.4 shows raw PLIF images captured at predetermined time intervals for each viscous medium. When the viscosity of the medium is increased, different patterns of striations are formed. The dye is concentrated in thin striations, for example in the 0.5% NaCMC (w/w) fluid throughout the dissolution experiment, or in a single thick striation forming a large arc as in the case of the 0.25% NaCMC (w/w) fluid; this striation disappears 2.0 h into the dissolution test.

PIV analysis in the USP 2 mini vessel carried out previously by Stamatopoulos et al., (2015), showed that high velocities occurred mainly around the impeller and along the shaft. The non-uniform mixing results in large gradients of the shear rates in USP 2 vessel (Baxter et al., 2005a). As the NaCMC concentration increases, the shear thinning nature of the fluid increases. This implies that in regions where high velocities and thus high velocity gradients occur, the fluid moves significantly whereas in dead zones the fluid will be stagnant. The shear thinning nature of the fluid within the regions of high shear rates will increase leading to inequalities of the viscosity profile throughout the vessel. As a further consequence, striations will form of different size and shape affecting the mixing performance in viscous media.

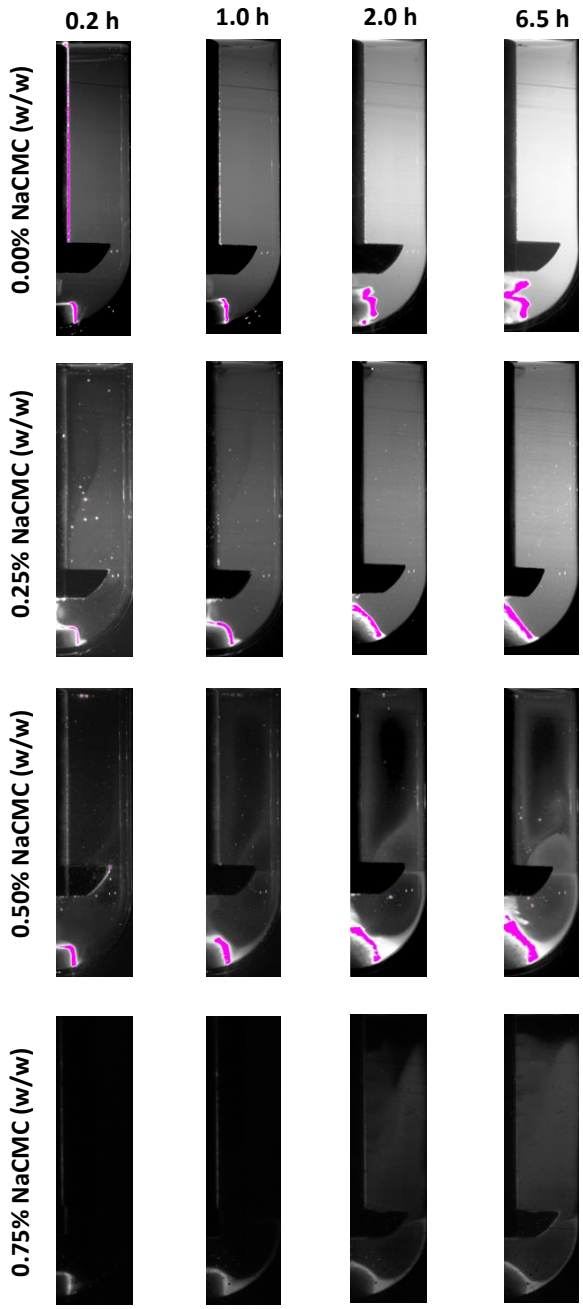

Figure 4.4. PLIF images captured at predetermined time interval for water at pH 7.4 (a) and 1.2 (b), whereas (c) 0.25%, (d) 0.5% and (e) 0.75% NaCMC (w/w) buffered (pH 7.4) solution.

Examining the PLIF images it seems that the distribution of the dye in USP 2 mini vessel becomes quite uniform in water and in 0.25% NaCMC, especially after 2 h. Although, the difference between grayscale values throughout the USP 2 decreases drastically with time,

without image analysis it is impossible to evaluate the mixing performance by eye in the ostensibly uniformly distributed dye in these two media. This is also necessary for the 0.75% NaCMC fluid in which the homogeneity of the dye appears on first glance to be greater than for the 0.5% NaCMC (w/w) fluid.

4.3.2 Areal distribution method

Figure 4.5 shows the distribution of area fraction as a function of level of mixedness, G_i, from the areal distribution method for different viscous media at each predetermined time interval. The level of mixedness was determined for the corresponding normalized fraction ($\bar{G}_i/G_\infty$) of RH-6G released at time *i*.

The poor mixing performance of USP 2 mini vessel is revealed from multiple levels of mixedness for each dissolved fraction. In particular, comparing the PLIF images of “simple” buffer with the corresponding results from the areal distribution analysis (Figure 4.5a), an ostensibly homogeneous distribution of dye would be expected to giving few different levels of mixedness and the area fraction with G > 90% to be predominant. This is of importance when the dissolution profiles of a drug released from different dosage forms are compared. This is possible only if the standard deviation of the dissolution data of each formulation is ≤10%. Relatively similar patterns of areal fractions as a function of levels of mixedness were also observed in 0.25% NaCMC (w/w) (Figure 4.5b). This spread of the different levels of mixedness becomes even worse in viscous media and in particular for the 0.5% NaCMC medium (Figure 4.5c). The areal distribution method reveals here why it was so challenging to compare the dissolution data of the drug and the fluorescence dye as mentioned in Stamatopoulos et al. (2015). Moreover, it is also problematic that in 0.75% NaCMC (w/w) medium (Figure 4.5d) the areal fraction is mainly < 30%; within the region where normally the sampling probe is located. This means that the dissolution profile generated under these experimental conditions underestimates the actual release rate of the dye due to the poor mixing performance; this will increase also the variance of the dissolution data.

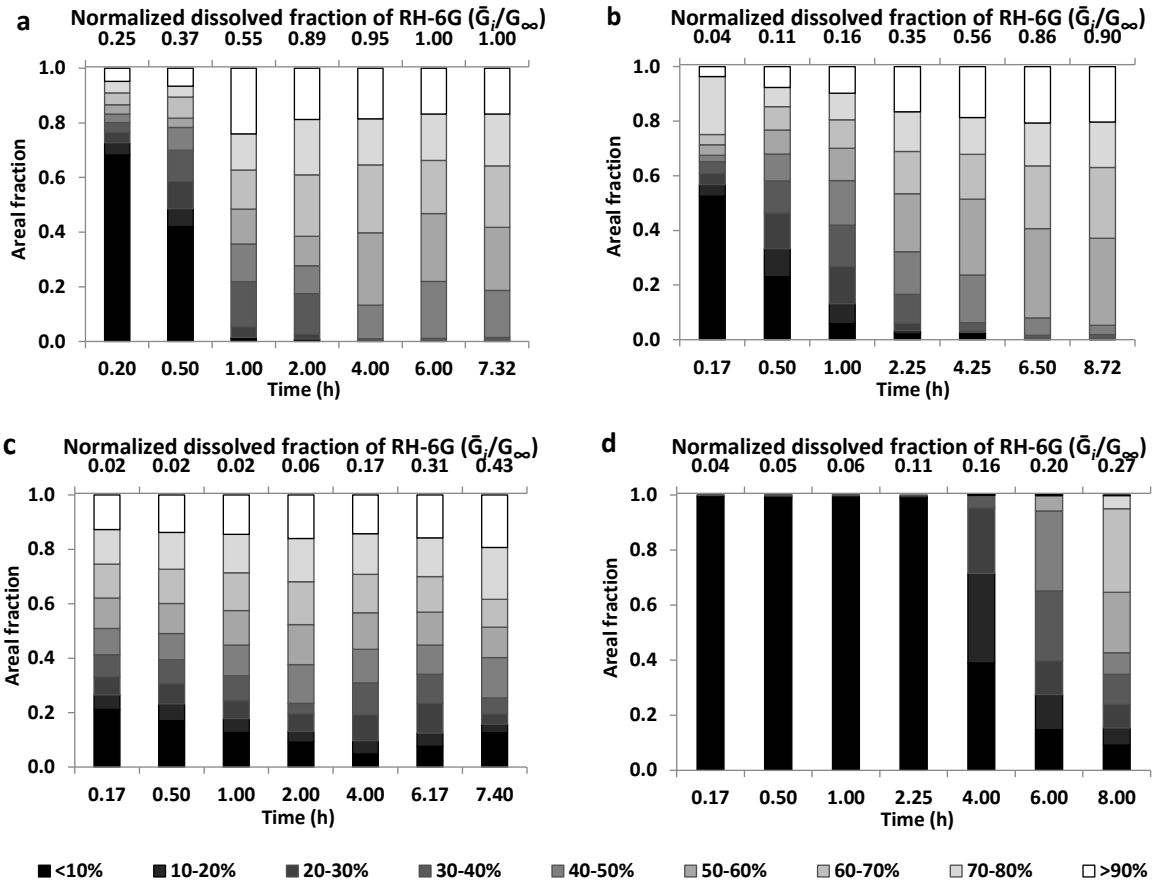

Figure 4.5. Bar graph showing discrete areal intensity distributions in viscous media: (a) "simple buffer"; (b) 0.25% NaCMC (w/w); (c) 0.50% NaCMC (w/w); (d) 0.75% NaCMC (w/w).

As expected, the rate of release of RH-6G from the tablet decreases as the viscosity is increased. This is showed in Figure 4.6a by plotting the normalized dissolved fraction of RH-6G ($\bar{G}_i/G_\infty$) vs. time. Moreover, the fraction of G_i> 70% increases and reaches a plateau in "simple" buffer after 2 h whereas the corresponding time for 0.25% NaCMC (w/w), 0.5% NaCMC (w/w) and 0.75% NaCMC (w/w) were 6.0, 7.4 and 8.0 h, respectively (Figure 4.6b).

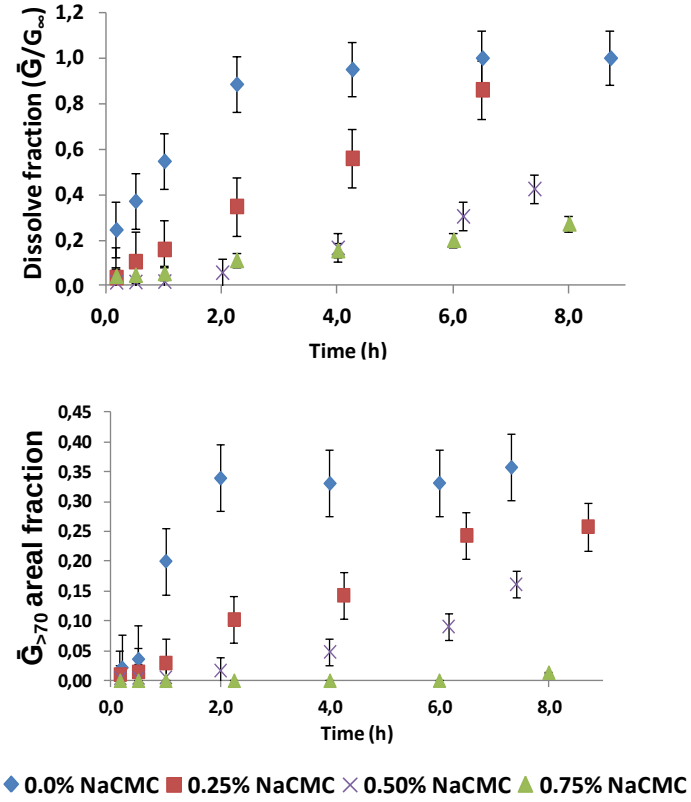

Figure 4.6. Evaluation of mixing performance of USP 2 small volume dissolution apparatus. (a) rate of the normalized dissolved fraction of RH-6G ($\bar{G}_i/G_\infty$) released from the tablet and (b) mixing intensity G_i> 70% as a function of time in different viscous media

Furthermore, the RG-6G is released faster, as the Fig. 4.6 showed, compared to theophylline (refer to Fig. 3.4). Beside the dissimilarities on the release rates between RH-6G and theophylline, a high linear correlation was obtained (refer Fig. 3.5).

4.3.3 Individual striation method

The different striations detected by the MATLAB script are identified with different colours. Due to the high number of area fractions used in areal distribution method (as shown in Figure 4.5), overlapping of the colored striations occurred making difficult to distinguish the individual striations. Thus, to show the location and the size of the striations for the corresponding area fractions throughout the USP 2 mini vessel, fixed ranges of area fraction were chosen. Images of the striations detected by the individual striation method are shown for G<10%, 30%<G<40%, 70%<G<80% and G>90% in Figure 4.7. The sub-figures for G_{i-} and G_{i+} show

the different striations for the lower and upper limits of the selected ranges of level of mixedness, G_i, as described in §4.5.2.

The shape and the size of the striations change as a function of time and hence as function of the released fraction of RH-6G dye, as well as the viscosity of the fluid. Large striations for the upper limit of the selected ranges were observed close to the wall and above the blade, where the mixing is more intense. In “simple” buffer and for the upper limit of the selected ranges, homogeneous zones above the blade were observed, starting from the highest level of mixedness G_i>90% (above the blade), and continuing with 70%<G_i<80%, 30%<G_i<40% and G_i<10% moving upwards. In addition, the striations in “simple” buffer are more concentrated, occupying small area compared to the striations of the same ranges in the viscous media which are wider and extended from the blade to the top of the mini vessel. With regards to the lower limit of the selected ranges (G_{i-}), striations were detected at the middle of the distance between the blade and the top of the mini vessel for the first 0.17 h of the dissolution experiment in “simple” buffer. At 1 h and 2 h a small striation was detected in the top region of the vessel but not at 6.5 h.

In 0.5% NaCMC (w/w), at 0.17 h, the identified regions of G_{i+} are shown to be extended from the blade to the top of the mini vessel along the wall whereas the regions of G_{i-} are located on the opposite side along the shaft; forming almost a mirror image. This pattern is changed at 2.0 and 6.5 h, where a loop around the region of interest is formed. The lower limits of 70%<G_i<80% and 30%<G_i<40% are located inside the core of the loop whereas the corresponding upper limit of 30%<G_i<40% is outside and around the striation of G_i<10%. Regarding the upper limits of G_i>90% and 70%<G_i<80%, these striations are located around the circulation zone close to the tip.

In 0.75% NaCMC (w/w) and for 0.17 – 1.0 h, striations for the 30%<G_i<40% and 70%<G_i<80% are extended throughout the region of interest whereas a thin line of the G_i>90% fraction extends from the blade to the top of the mini vessel and along the shaft. However, at 2.0 h, the striation of G_i>90% is limited: a region of G_{i+} > 90% is located at the connection point

of the shaft and the blade whereas G_{i-} is located at the top. The same flow behavior is also observed for the corresponding upper limit of the other two fractions $30\%<G_i<40\%$ and $70\%<G_i<80\%$.

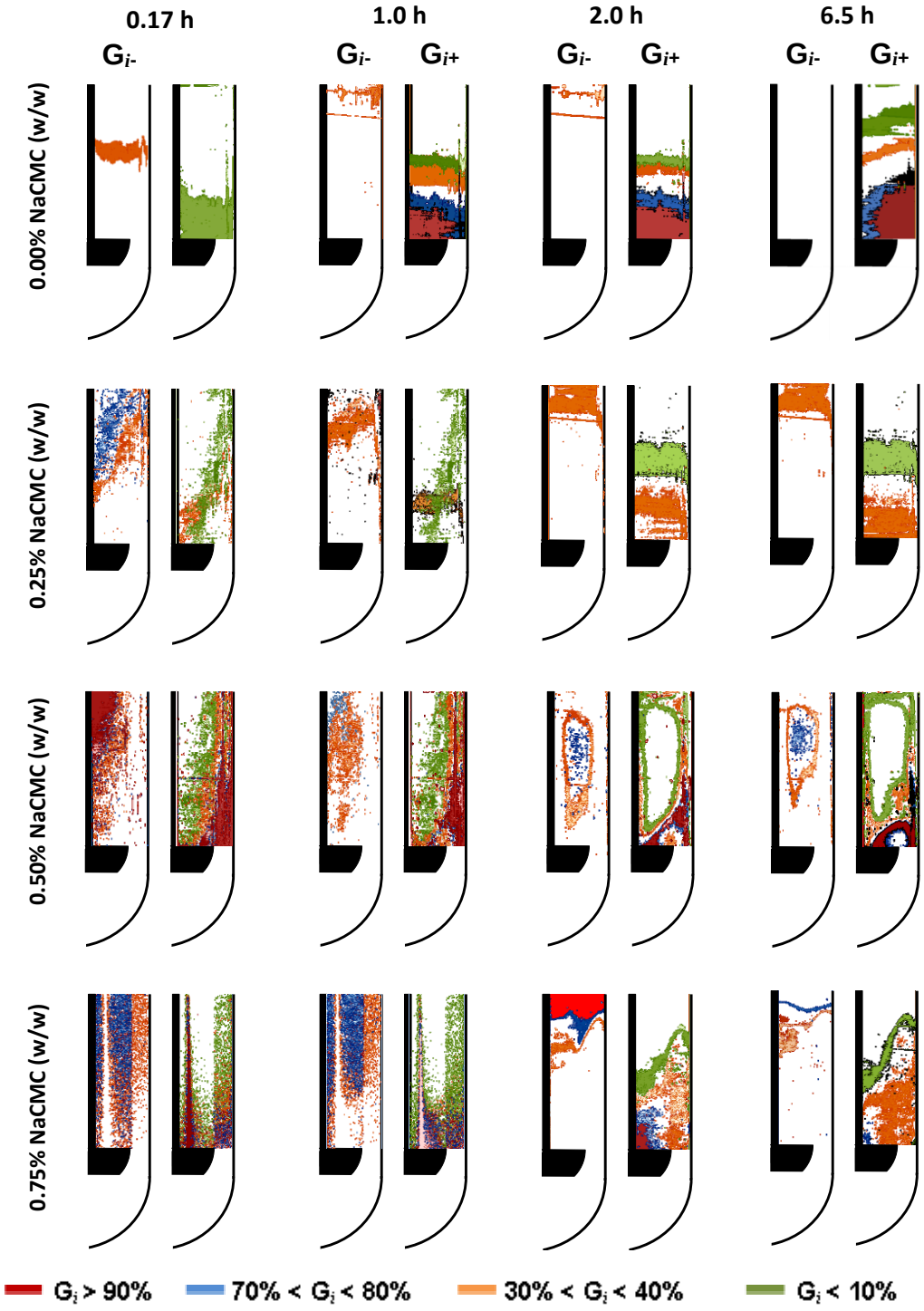

Figure 4.7. Illustration of striations detected using the individual striation method for selected ranges of level of mixedness, G_i, for (a) "simple buffer"; (b) 0.25% NaCMC (w/w); (c) 0.50% NaCMC (w/w); (d) 0.75% NaCMC (w/w).

The results presented in Chapter 3 and 4 are in a good agreement with the recently published work by Wang and Armenante (2016) using computational fluid dynamics (CFD) to characterize the flow field in mini USP 2 apparatus; Chapter 3 has been cited by Wang and Armenante (2016). The authors observed similar results in terms of vertical upper and lower recirculation loops above and below the impeller. In addition, a low recirculation zone was observed in the lower part of the vessel. Furthermore, the radial and axial velocities below the impeller are very small especially in the zone below the paddle, where tablet dissolution occurs. Furthermore, high velocities were observed close to the tip, as it has also been observed in our experiments, explaining why high level of mixedness was observed within this region.

4.3.4 Coefficient of variation

The mixing performance of small volume USP 2 was also evaluated by calculation of C.V as a function of dissolution time in different viscous media (Figure 4.8). As expected, the mixing performance reduces as the viscosity increases. Unlike the areal distribution method, the C.V parameter describes a statistical level of mixing across the whole measurement region. Thus the detail is lost. Characteristic examples are shown for the “simple” buffer, 0.50% NaCMC (w/w) and 0.75% NaCMC (w/w). In the first case a sharp decrease of C.V from 1.0 to 0.4 was observed between 0.2 and 0.5 h dissolution time; implying a 60% mixedness level. However, the areal distribution method showed that the 60-70% fraction consists only the 7% measured area at 0.5 h whereas the fraction <10% is 38% of the area (Figure 4.5a) – thus a large unmixed area. In the second case, the C.V analysis shows better mixing performance in 0.75% NaCMC (w/w) throughout the dissolution experiment compared with the 0.50% NaCMC (w/w) medium. Nevertheless, areal distribution method showed clearly that the mixing efficiency is inadequate in the most viscous media, where even after 2.25 h the mixedness fraction of <10% is predominant. Thus, use of C.V alone may be misleading.

These findings show that individual striation method coupled with areal distribution method is very promising not only to evaluate the mixing performance of small volume USP 2

apparatus and therefore its impact on the reproducibility of the dissolution data, but also to determine the location of the different mixedness levels in the dissolution vessel, via the local distribution of the concentration. This is not possible by consideration of the C.V of the dissolution data alone.

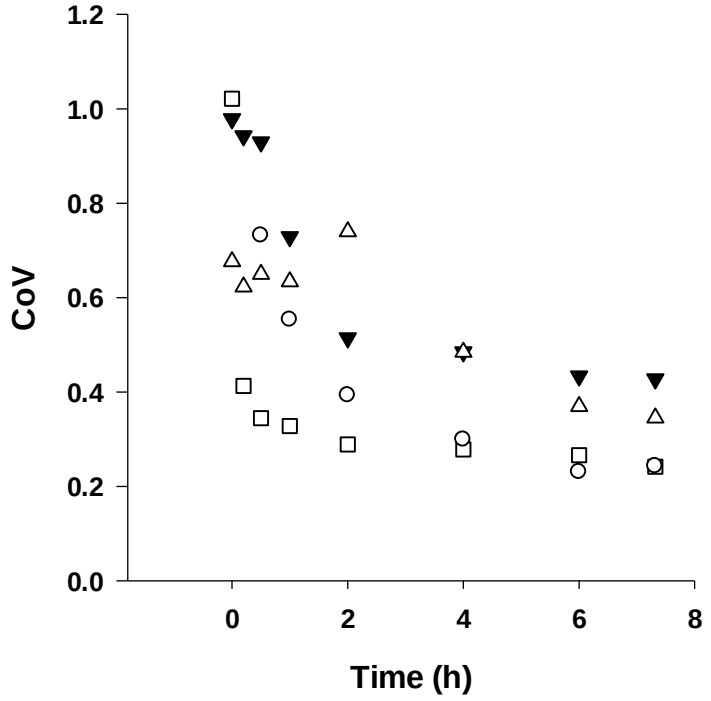

Figure 4.8. Time evolution of the coefficient of variation (C.V) as a function of viscosity; (▫) "simple" buffer, (○) 0.25% NaCMC (w/w), (▼) 0.50% NaCMC (w/w) and (△) 0.75% NaCMC (w/w).

4.4 Conclusions

The mixing performance of small volume USP 2 apparatus has been determined in shear thinning media from the distribution of a fluorescent dye released from hydrophilic matrix which mimics the dissolution profile of a targeted drug (Stamatopoulos et al., 2015). The areal distribution method presented by Alberini et al. (2014a), in combination with the individual striation method by Alberini et al. (2014b) was used to provide an improved and more detailed measure of the mixing performance according to the level of mixedness, G_i. This is advantageous to determine which region within the USP 2 mini vessel shows the highest

mixing level; something very important in terms of choice of sampling point. Thus, might be possible to minimize the variance of the dissolution data as well as to know in advance the degree of the variability of the data obtained from the selected region. Analysis of data using C.V alone can give misleading results.

Overall, for all measured fluid media, the highest mixedness level is mainly located above the blade and close to the wall, i.e. the region where intensive mixing takes place; therefore, the recommendation is that the sample tube (cannula) should be placed in this region.

With Chapter 3 and the Chapter 4, an extensive characterization of the mixing performance of the mini volume USP 2 dissolution apparatus was performed. The dissolution profile of a highly water soluble drug released from a hydrophilic matrix was obtained under increasing viscosity of the media used. The mini volume USP 2 dissolution apparatus has chosen because the volume of the media (i.e. 100 mL) is more relevant to the contents in the human proximal colon; i.e. 10 – 125 mL (Schiller et al., 2005). Thus, the work conducted in these forms the basis for the comparison of the USP 2 with the biorelevant Dynamic Colon Model (DCM) basis presented in the following chapters.

Greek symbols

$\dot{\gamma}$	Shear rate (s^{-1})
μ_A	Apparent viscosity (mPa s)

Abbreviations

DCM	Dynamic Colon Model
NaCMC	Sodium carboxymethylcellulose
PEPT	Positron Emission Particle Tracking
PET	Positron Emission Tomography
PSs	Propagating Sequences
fps	frames per second

5 Development of an artificial Dynamic Colon Model (DCM): understanding relationships between wall motion, manometric measurements and fluid motility

Abstract

Understanding motility and flow episodes in the colon is complex and correlations between manometry and scintigraphy are not simple. A biorelevant Dynamic Colon Model (DCM) was designed and used to better understand the relationship between manometric measurements and flow episodes under typical colonic conditions.

The sensitivity of the manometric data generated was assessed as a function of degree of luminal occlusion, occlusion rate, fluid apparent viscosity and level of fill. Positron Emission Tomography (PET) was used to visualize the fluid flow under fixed conditions.

The position of the catheter, the occlusion rate of the flexible wall, the viscosity and the fluid volume affected the manometric measurements. The manometry failed to differentiate changes for degree of luminal occlusion < 80% and for low apparent viscosities. Pressure >2 mmHg, characterized in *in vivo* studies as propagating sequences (PSs), measured in fully filled apparatus in viscous media. However, in half-full, the same wall motion gave measured amplitudes < 2 mmHg; despite PET images revealing these waves are highly associated with fluid motion.

The criteria, on which pressure waves should be counted as PSs and associated with flow episodes *in vivo*, should be reconsidered. The interpretation of the manometry results can potential contributes on management strategies, both diagnostic and therapeutic, in the human proximal colon. Furthermore, the results showed that the in vivo manometric data do not reflect entirely the environment of GI tract and it should carefully be used in so called dynamic in vitro models.

5.1 Introduction

Propulsion of the colonic contents involves synchronized contractions and relaxations of the smooth circular muscle layer along the colon (Sinnott et al., 2015). The strength of these contractions is normally measured with using manometry via insertion of a catheter (Sinnott et al., 2015) and any variations of the amplitude and frequency are associated with abnormalities in colon motility (Dinning and Di Lorenzo, 2011). On the other hand, scintigraphy has been used to visualize the movements of the contents inside the colon (Hammer et al., 1997).

In previous *in vivo* studies, manometry and scintigraphy have been combined and relationships between wall motion and fluid flow have been evaluated (Bassotti et al., 1993, Cook et al., 2000, Dinning et al., 2008). However, these *in vivo* studies have presented contradictory information regarding the association or correlation between flow episodes and contractile activity. This was found to be due to technical limitations of the manometry since its sensitivity is decreased when the gut diameter is ≥0.05 m as in the proximal colon (Dinning et al., 2014a). Early scintigraphy work was limited by relatively slow frame capture rates (Hammer et al., 1997, Dinning et al., 2008). Technical advances have improved the performance of these techniques, helping to reveal that both, low amplitude propagating sequences (2 – 5 mmHg) and high amplitude motility events can be associated with flow episodes (Dinning et al., 2014a).

However, other factors such as fluid apparent viscosity and the 50% reflux (i.e. backflow) of the bolus will also affect the movements of the contents (Proano et al., 1990), making the *in vivo* investigation of these relationships a difficult task. To overcome these difficulties, previous measurements have been made on an isolated rabbit distal colon (Costa et al., 2013b), combining simultaneous manometry and visualization of spatiotemporal variations in wall diameter. These *ex vivo* studies have given valuable information about the neurogenic and myogenic actives of the smooth muscle and how they are related with the intraluminal pressures and movements of the bolus. However, the diameter of the rabbit distal colon is

smaller (≈0.01 m) compared to human proximal colon (≥0.05 m) (Sadahiro et al., 1992). In addition, the manometry was performed when the isolated rabbit colon was full of fluid, which is not representative of the *in vivo* conditions in the human proximal colon. In particular, the volume of the colonic fluids in an adult varies between 10 – 125 mL (Sutton, 2009) and the fluid is not uniformly distributed (Schiller et al., 2005, Mudie et al., 2014). In addition, the volumes of the colonic fluids have been found to be 22.3 ±7.7 mL and 29.9 ±10.8 mL in the fasted and in the fed state, respectively (Diakidou et al., 2009).

Arkwright et al. (2013) performed manometry in an artificial latex based tube and in an isolated rabbit colon segment. Although, the authors revealed the dependency of the amplitude of the pressure on the viscosity, again the tube was fully-filled with viscous media. Thus, the performance of manometry in a diameter based on the human proximal colon as well as in a partially filled tube remains to be investigated. It is necessary to determine how these parameters will affect the performance of the manometry, since this technique fails to differentiate intraluminal pressures from the forces applied on the catheter, from the colonic wall motion (Sinnott et al., 2015).

To be able to correctly interpret manometry it would be advantageous to have a suitable biomechanical model mimicking the contraction/relaxation mechanism for the propulsion of a bolus within the colon. Thus, in this study an *in vitro* model of the human proximal colon, the dynamic colon model (DCM), focused mainly on the caecum – ascending region was designed and constructed. The model reproduces the main features of the proximal colon anatomy in terms of the formation of the characteristic pockets, the haustra. Manometry was performed under predetermined conditions in terms of viscosity, motility pattern, volume of fluids, and occlusion degree and rate of the flexible wall. In addition, Positron Emission Tomography (PET) was used as alternative to scintigraphy to visualize the fluid flow under the same conditions. Thus, relationships between wall motion and movements of the contents were evaluated in a representative model of the human colon.

5.2 Materials and methods

5.2.1 Materials

Sodium carboxymethylcellulose (NaCMC) of 700000 molecular weight was purchased from Sigma (St., Louis, USA). Polycraft T – 15 RTV translucent silicone rubber was purchased from MB Fibreglass (Newtownabbey, UK). The radioactive solution of radionuclide ^{18}F used in PET experiments was provided from the School of Physics and Astronomy at the University of Birmingham, UK.

5.3 Development of the Dynamic Colon Model (DCM)

A biomechanical engineering model of the adult human proximal colon was modelled based on physiology observed in anonymised abdominal MRI images provided by the Radiology Department of Birmingham Heartlands Hospital, UK. The images show the transverse views of the caecum – ascending colon (Fig. 5.1a). In addition, coronal planes give information about the width and the number of the haustra, along the length of the caecum – ascending (C-A) region as well as the width of the thickest part of the longitudinal muscular layer (taenia coli).

5.3.1 Mimicking the human proximal colon anatomy

The MRI images (Figure 5.1a) were utilised to gain information about the architecture of the proximal colon as well as some basic dimensions of the haustra. Examining the MRI images, demonstrated that the number of the haustra along C-A region was not constant and their width was not uniform. However, to simplify the design of the model, the number and the width of the haustra were fixed based on average values. Figure 5.1b shows the reconstructed 2D model of the haustra design based on the MRI images with physiological ranges of anatomical parameters obtained from the literature. The width of the haustra was 0.02 m whereas the

thickness of the semilunar folds and taenia coli was 0.2 mm and 5 mm, respectively (Langer and Takács, 2004). Figure 5.1c shows the proposed 3D model of the haustra based upon which an acrylic mould was manufactured to fabricate the DCM tube.

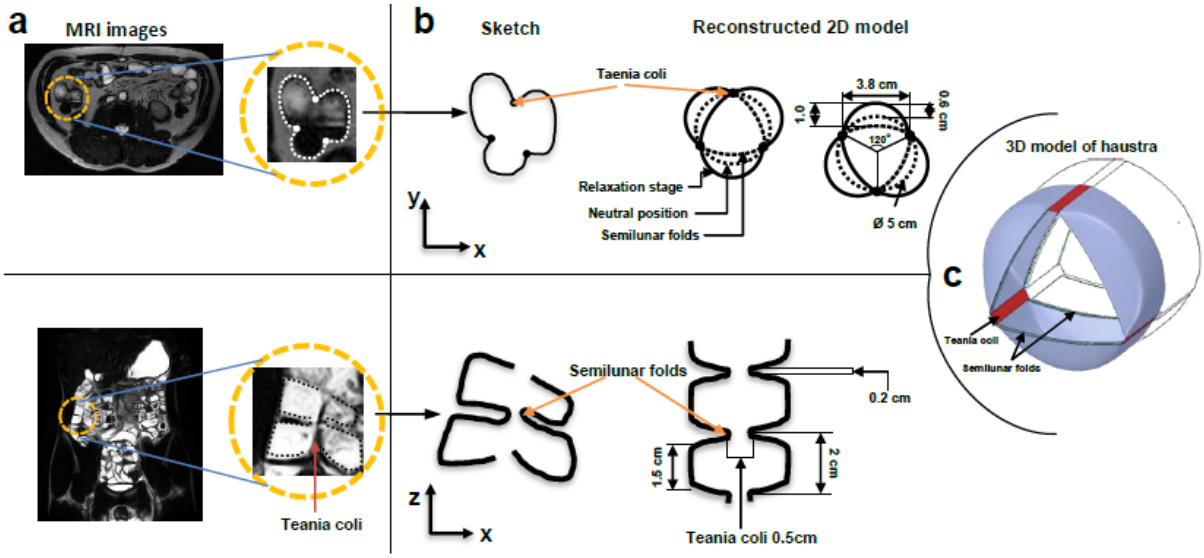

Figure 5.1. a) Transverse and coronal MRI images of the human caecum – ascending colon; b) Haustra geometry model; c) 3D model of the haustra.

5.3.2 Prototyping

Figure 5.2 shows the process followed to develop a prototype prior to the fabrication of the DCM tube. As shown in the 3D model of the haustra (Figure 5.1c) there are three pockets in a triangular configuration whereas the thickest layer of the longitudinal muscle located at the "contact" point of the pockets. Based on this design a prototype consisting of three acrylic pieces was developed in order to reproduce the configuration of the haustra. The two edges of each acrylic piece represent the semilunar folds whereas the cavity between the two edges represent the haustrum (Figure 5.2a). A sheet of rubber silicone attached on each acrylic piece to mimic the contractions of the smooth muscle (Figure 5.2b). The assembled acrylic pieces formed a single segment (Figure 5.2c) and connected to a syringe using a quick fit connector (Figure 5.2d). Deflation and inflation of the three membranes performed with pushing and pulling the syringe using water as incompressible hydraulic liquid. Different strategies were

followed in order to sufficiently attach the membrane to the acrylic segment (Figure 5.2e – h) to avoid leakage of the water and increase the robustness of the system. The most efficient method was chosen and used to fabricate the DCM tube described in the following section.

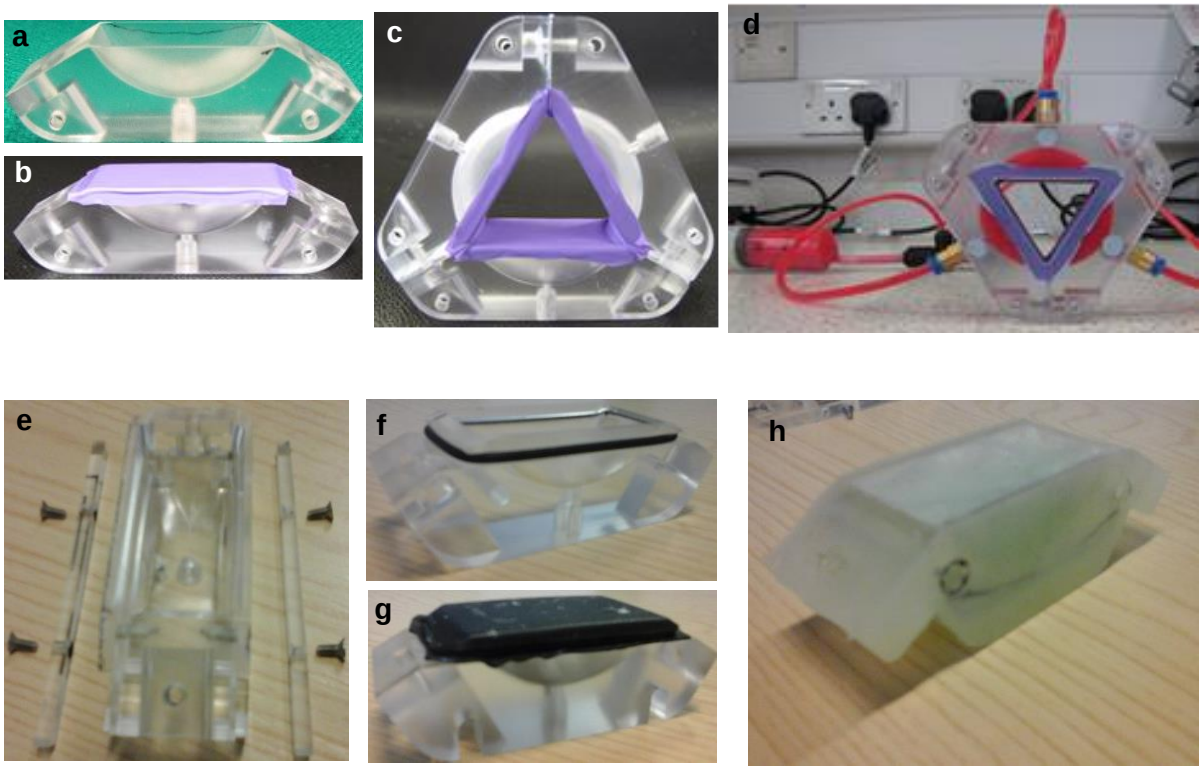

Figure 5.2. Prototype development process. a) acrylic piece representing a haustrum; b) a silicone rubber membrane attached to the acrylic piece using blu-tack; c) assembly of the three acrylic pieces in triangular configuration with the silicone rubber membrane attached; e) use of two side acrylic bars to screw and hold the membrane tightly to the acrylic piece; f) machining a groove around the cavity and use an O-ring rubber to hold the membrane; g) silicone rubber attached to the acrylic piece using the O-ring rubber and h) acrylic piece covered with liquid silicone solidified after curing process. The membrane formed with filling the cavity of the acrylic piece with wax which removed after curing the silicone.

5.3.3 Fabrication process of the DCM tube

Figure 5.3 shows the fabrication process of the *in vitro* model. An acrylic segment which reproduces the shape of a haustrum was manufactured (Figure 5.3a). Then, three replicas of this segment were manufactured and filled with wax (Figure 5.3b). The segments were placed in a mould with a triangular shaped acrylic piece being positioned at the centre (Figure 5.3c). Thus, a gap of 0.4 mm was formed between the segments and the central acrylic piece, serving to form a thin silicone layer for the flexible membrane. The gap between the edges of the segments was 0.005 m to form a thick silicone layer which represents the taenia coli. Then, the mould was filled with deaerated liquid silicone rubber (Figure 5.3d) and cured for 6 h, at ambient temperature; the time to cure the silicone was based on manufacturer guidelines.

Subsequently, the wax was removed by placing the cured silicone unit in a hot water bath (90 ^{o}C). Wax residues were removed using mineral oil, next the silicone washed thoroughly with soap and then with distilled water; Figure 5.3e shows the fabricated unit with quick fit connectors assembled. Ten replicas were fabricated and assembled to form the DCM tube (Figure 5.4).

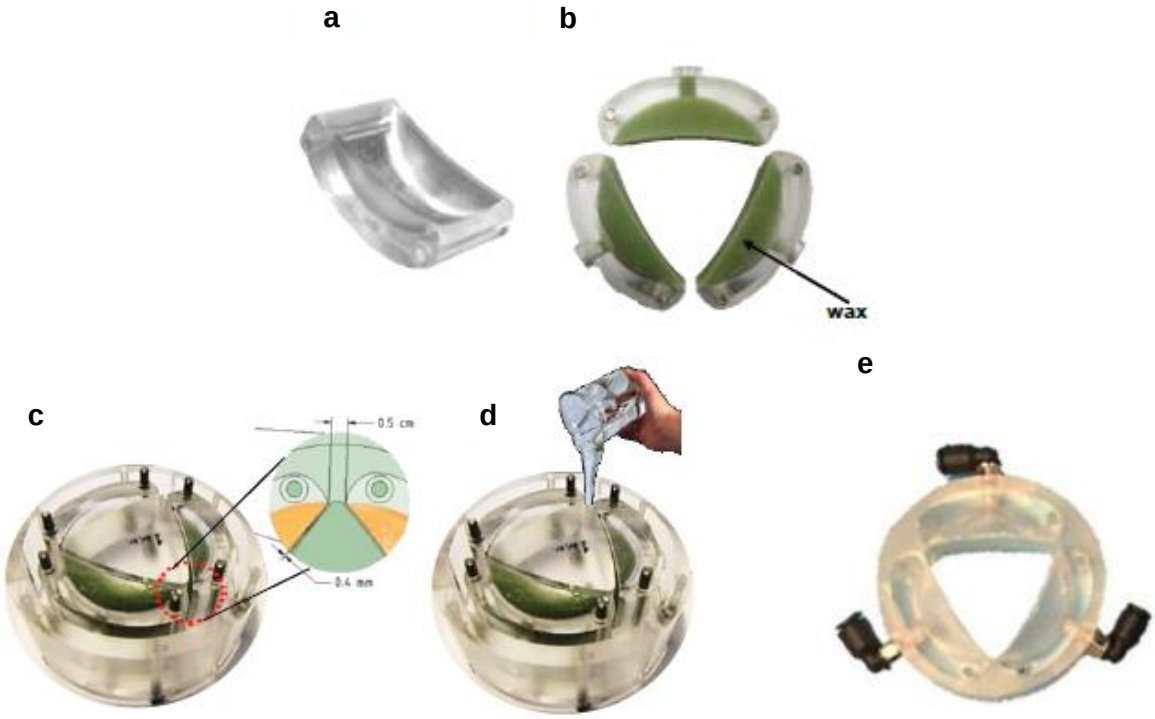

Figure 5.3. Fabrication process of the silicon unit of the *in vitro* model; a) acrylic segment manufactured to reproduce the geometry of the haustrum; b) acrylic segments filled with wax;

c) configuration of the mold used to fabricate the unit; d) filling the mold with deaerated liquid silicon rubber and d) fabricated silicon unit with quick fit connectors.

The total length of the tube was 0.20 m and the internal total volume was 290 mL which is within the range of published *in vivo* data; average length of caecum-ascending colon was found to be 0.195 m (Sadahiro et al., 1992) and the volume was within the range 76 – 390 mL (Pritchard et al., 2014). A 3D printed rigid siphon was placed at the end of the biomechanical model which was used to keep the fluids inside the DCM tube during the motion of the flexible membrane.

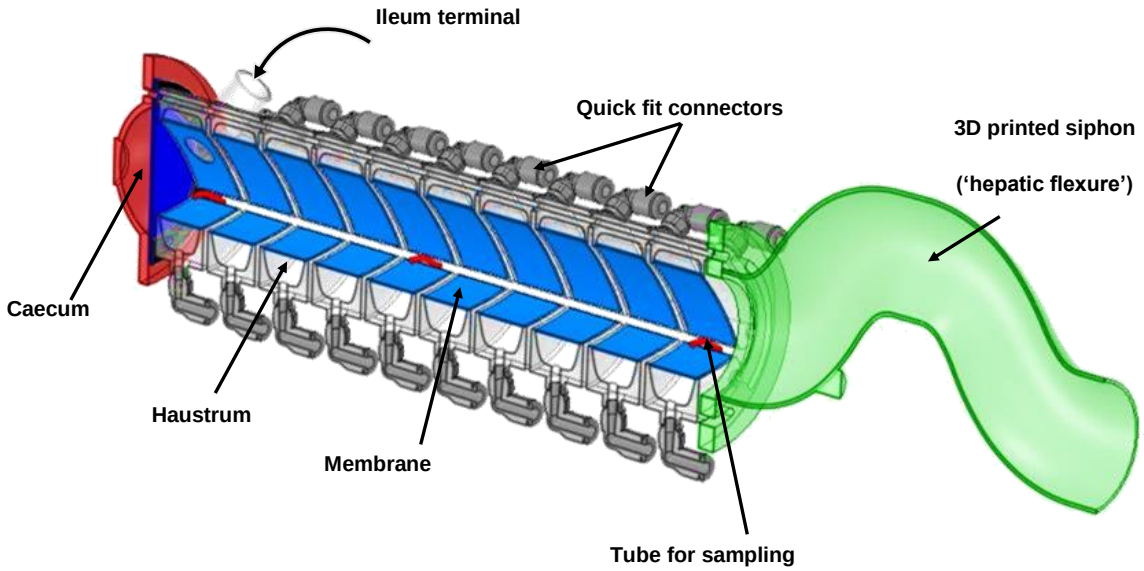

Figure 5.4. 3D model of the biomechanical Dynamic Colon Model of human proximal colon with main focus on caecum – ascending region.

5.3.4 Measuring pressure amplitudes inside a single unit using a solid – state catheter

To reproduce the physical amplitudes that occur in the proximal colon, the relationship between the membrane motion and the pressure forces generated inside the cavity of a single unit of the DCM tube were established.

A computer – controlled hydraulic system was developed in order to synchronize the motion of the membranes in each unit and reproduce the motility patterns reported *in vivo* within the human proximal colon using manometry (Dinning et al., 2014a). Each unit was connected to a syringe which used to inflate and deflate the membrane; water was used as incompressible fluid for the hydraulic system.

Initially, the hydraulic system was calibrated by developing a correlation between syringe displacements and membrane movements. A camera was used to capture images of the cross section of the DCM unit at 50 frames per second (fps). The images were used to determine the occlusion degree (i.e. reduction of the diameter of the DCM unit) and the occlusion rate (i.e. velocity) of the membrane with respect to different travel distance (0.005, 0.010, 0.015, 0.020, 0.025, 0.035, 0.040, 0.042 and 0.045 m) and travel speeds (0.001, 0.002, 0.005 and 0.008 m s^{-1}) of the syringe. The syringe movements were controlled with stepper motor being driven by Nanopro software (Nanotec Electronic GmbH & Co. KG, Germany).

After calibration of a single configuration (i.e. stepper motor – syringe – DCM unit), ten replicas were assembled into a framework manufactured by the Physics workshop at the University of Birmingham (Figure 5.5). The motors were connected in parallel using a controller (SMCI12, Nanotec Electronic GmbH & Co. KG, Germany) for each motor. The software used to control the hydraulic system was developed by the Biosciences workshop at the University of Birmingham; Figure 5.6 shows the interface of the software used.

Then, manometric measurements were performed by placing a solid state catheter manufactured by Unisensor (Unisensor AG, Attikon, CH-8544, Switzerland) inside the cavity of the unit. The catheter was 2.6 mm in diameter and contained 1 pressure sensing element. The pressure forces generated by the oscillations of the membrane were measured using a modified version (Figure 5.7) of the apparatus used by Arkwright et al. (Arkwright et al., 2013).

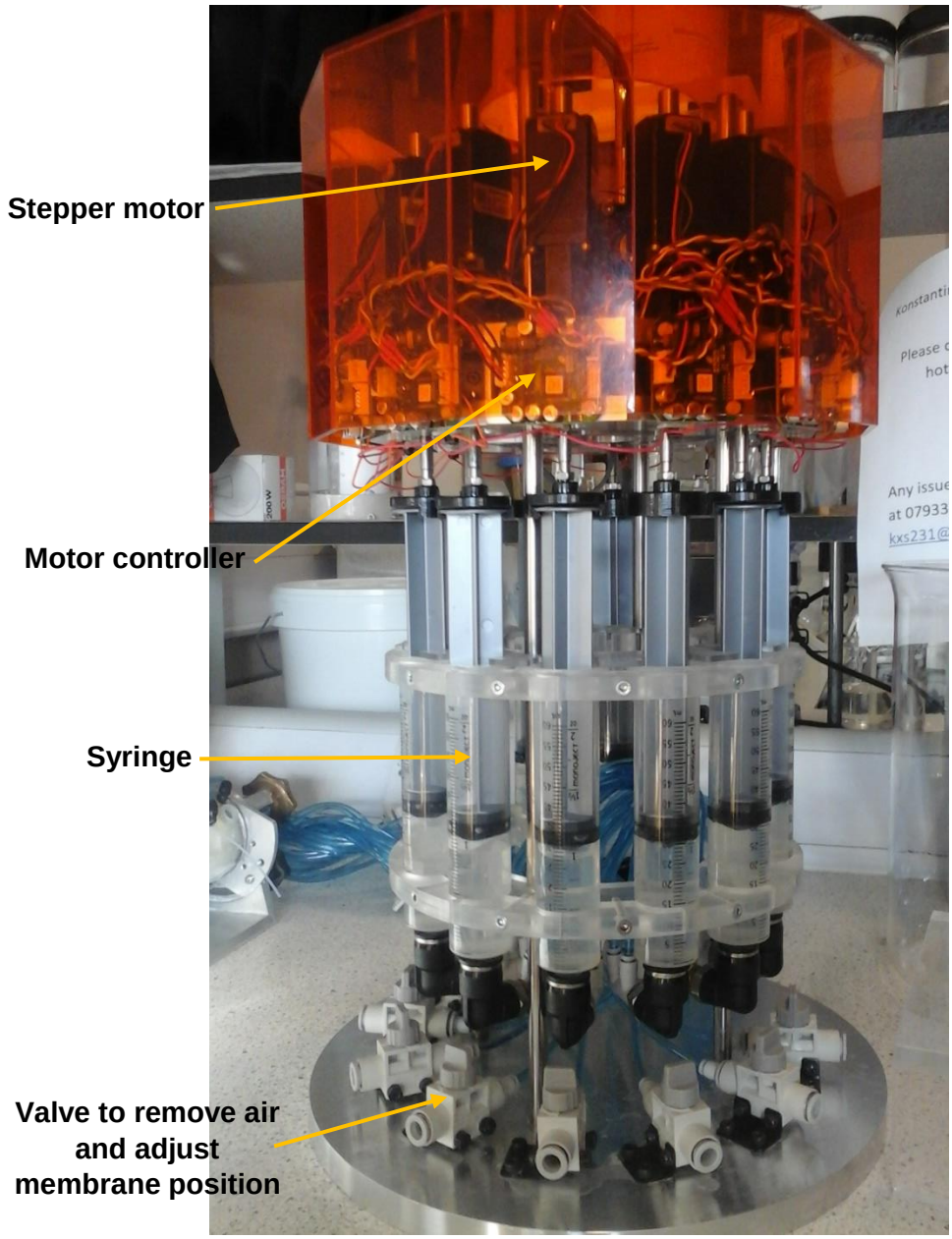

Figure 5.5. Complete configuration of the computer – controlled hydraulic system used to control the motion of the membrane of the Dynamic Colon Model (DCM).

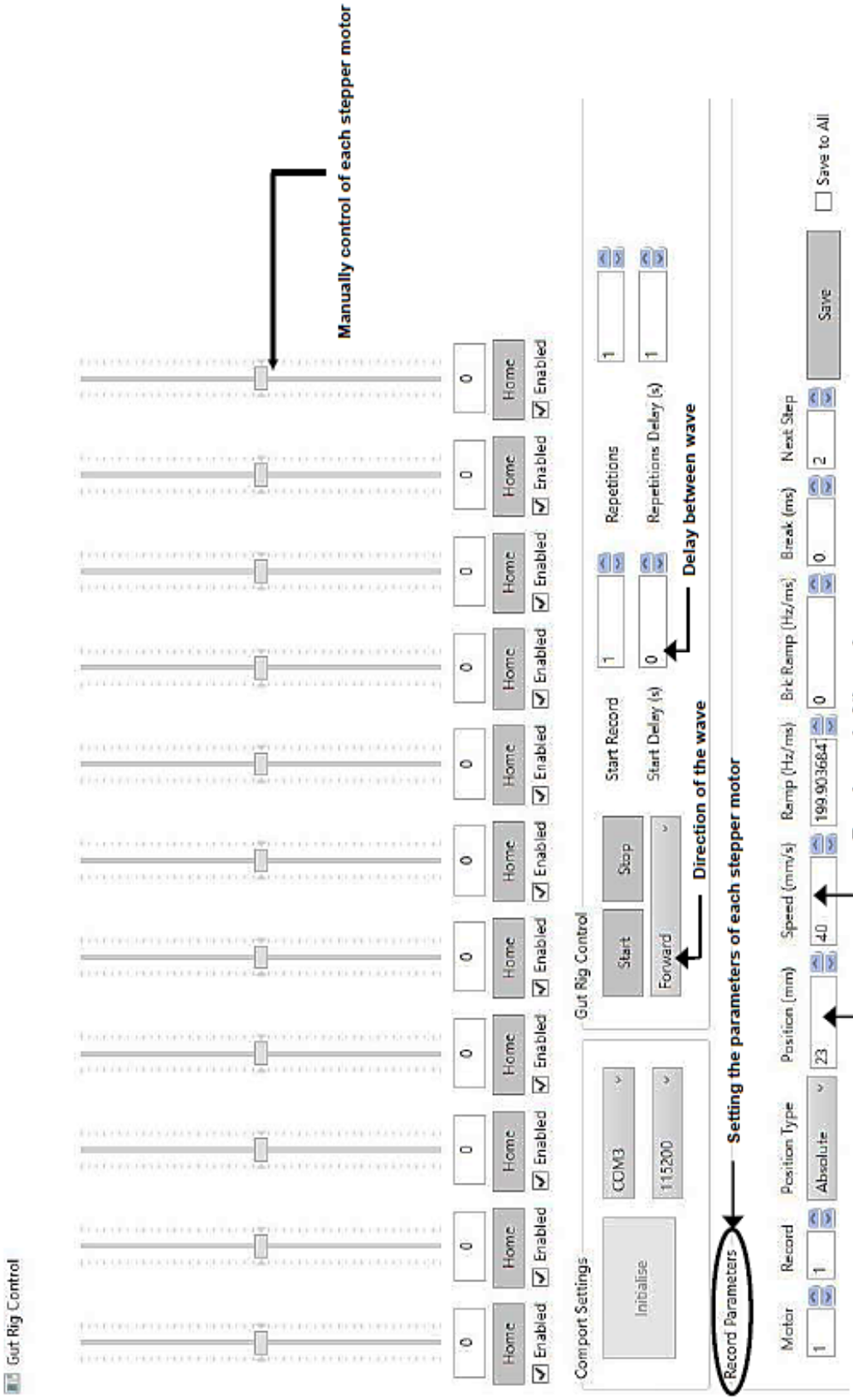

Figure 5.6. Interface of the software used to control and synchronize the stepper motors of the hydraulic system.

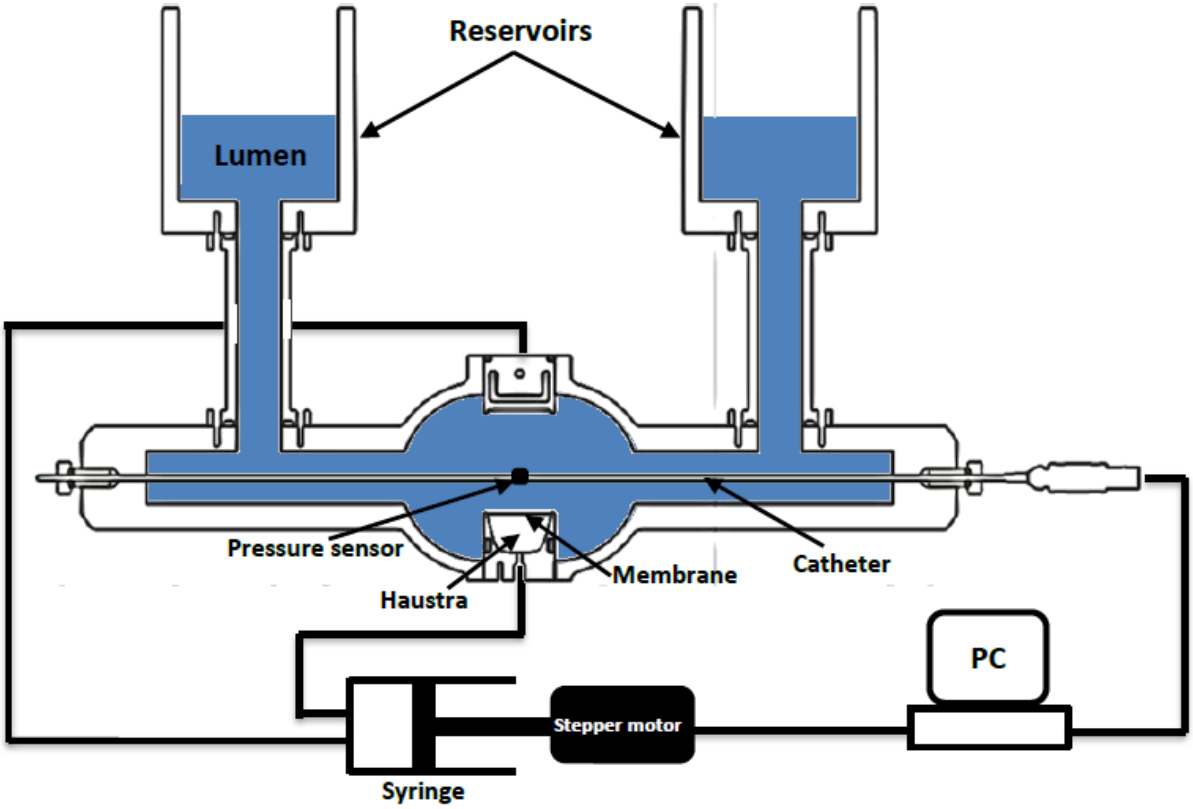

Figure 5.7. Schematic representation of the device used to generate movement of the flexible wall of a single unit of DCM tube. A syringe, controlled by a stepper motor, is used to inflate and deflate the membrane results in reductions in diameter. Thus, the membrane of the segment moves inward toward the manometric catheter, in a controlled rate producing pressure signals. The segment is filled with a solution of known $NaCMC_{(MW:700000)}$ concentration (w/w) (blue), from the two reservoirs.

After filling the apparatus with fluid, the catheter was autozero-ed to subtract the initial pressure signal output of the catheter due to the hydrostatic pressure. Small changes of the hydrostatic pressure were observed due to the fluctuations of the lumen height caused by inflation and deflation of the membrane. However, these changes were of 0.01 mmHg magnitude and therefore their effect on the interpretation of the results was negligible. Since the interpretation of the manometric data was affected by the apparent viscosity of the fluids (Arkwright et al., 2013), the signal output of the catheter was recorded in different

concentrations of NaCMC aqueous solutions (0.25, 0.50, 0.62, 0.75 and 1.00%, (w/w)); the apparent viscosities (obtained at shear rate of 10 s^{-1}) of the fluids are presented in Table 5.1.

Table 5.1. Rheological properties of the fluids used in manometry and PET experiments

%NaCMC (w/w)	μ_A (m Pa s)	ρ (kg m^{-3})
0.25	8	1017.60
0.50	106	1020.40
0.62	123	1021.23
0.75	200	1024.50
1.00	525	1031.80

5.3.5 Positron Emission Tomography (PET) to visualise fluid motion within the DCM

Positron Emission Tomography was utilised to assess the propulsive and non-propulsive events within the DCM tube under predetermined motility patterns. In addition, relationships between wall motion and propulsion of contents were examined. Details of the PET system can be found in Broadbent et al. (1993). A half prefilled DCM tube (i.e. 100 mL of fluid) was placed between the two detectors of the DAC Forte PET scanner and 1 mL of radiolabelled water was injected in the first segment through a hole of 0.1 m Ø, which represents the human terminal ileum.

Previous *in vivo* studies showed that the main motility pattern in human proximal colon is comprised of antegrade propagating pressure waves of low amplitude (Dinning et al., 2014a). Thus, the motility pattern of the DCM tube was set up to produce an antegrade propagating wave of 0.02 m s^{-1} speed and 0.2 m travel distance; i.e. the total length of the DCM tube. The speed is within the range of velocities of cyclic propagating pressure waves which is the main motility type reported in the colon of healthy humans based on manometric measurements (Dinning et al., 2014a). In addition, this value is within the range of the velocities (0.002 –

0.012 m s^{-1}) of the pressure waves considered as PSs (Dinning et al., 2008). PET images were recorded at 1s/frame and synchronized with the membrane motion.

Fig 5.8a shows the inflation (i.e. contraction) and deflation (i.e. relaxation) profile of the membrane of each individual segment and the corresponding pressure amplitude measured with using solid-state catheter (Fig 4b), whereas Fig 4c shows the overall profile of the CPPW. To reproduce the intestine law (i.e. contraction of the first segment with the simultaneous relaxation of the proximal segment), the profile of the wave of the DCM wall was setup as follows: 1) the membrane of the first segment was inflated (i.e. contraction; ascending excitatory) whereas in the second was deflated (i.e. relaxation; descending inhibition) at the same speed 0.0016 m s^{-1}. 2) When the first segment reaches the maximum degree of luminal occlusion (i.e. 40%), it stays at this position for 1 s before going back to its neutral position with a speed of 0.0035 m s^{-1}; the slower speed was used to mimic the viscoelastic properties of the colon wall.

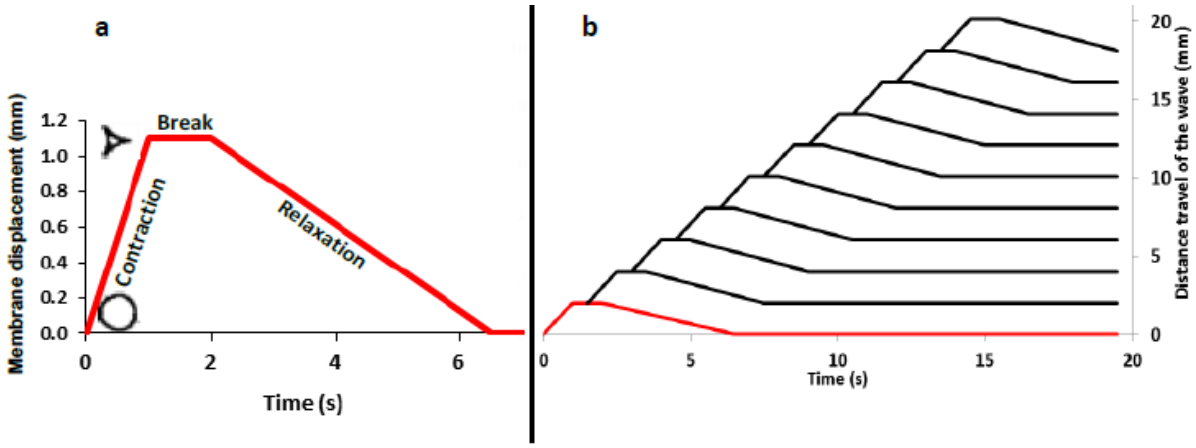

Figure 5.8. a) Profile of contraction-break-relaxation cycle of each DCM unit, b) the overall cyclic propagating pressure wave (CPPW) traveling along the DCM tube.

In addition, keeping the segment at the contraction stage for 1 s prevents back flow as shown in Fig. 5.9. The timings of the motion of each segment were aligned so that the motion within the DCM was representative of that within the human colon and minimised backflow within the DCM.

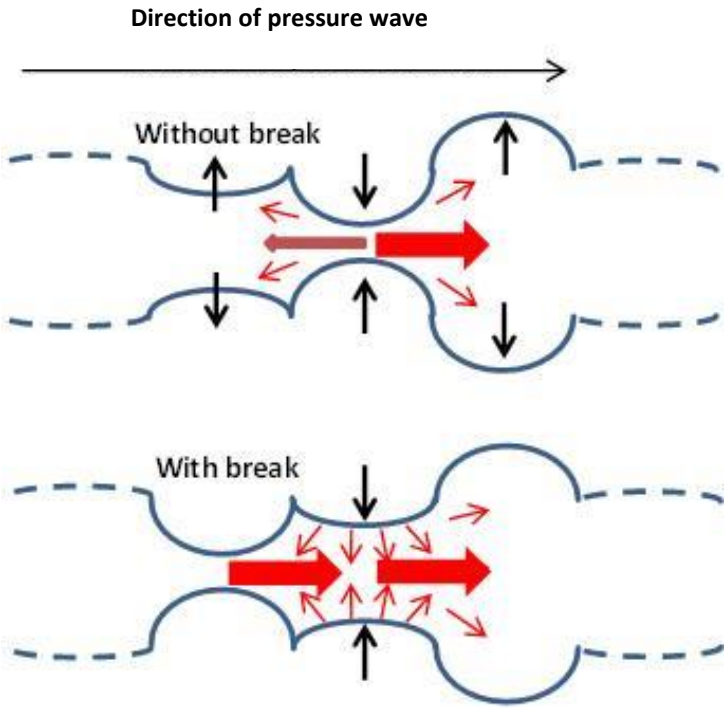

Figure 5.9. Forward fluid motion is induced by introducing a standing period (break) at the contraction stage of the starting segment.

5.4 Results and Discussion

Different methods were tested (§ 5.3.2) to develop the haustra prior to the fabrication and the further calibration of the DCM system. The challenge was how to effectively attach the membrane to the acrylic without tearing the membrane and with no leakage of the hydraulic liquid (i.e. water) during oscillations of the membrane. In addition, the fabrication process should be easy, fast and robustness to efficiently produce several haustra (Fig. 5.3 e). The issue with the blu-tack was that there was no a permanent and good isolation, whereas it was not the proper method to produce several units for the DCM tube. With regards to the use of side bars (Fig. 5.2 e), the problem here was that the membrane could easily be torn at the edges of the groove when tightening the bar with the screws on the main acrylic body. The following approach was to use a rubber O-ring to hold the membrane tightly to the acrylic piece (Fig. 5.2 f – g). With this method, the membrane could easily be attached and without having

issues of tearing the membrane. However, when assembling the three haustrum, leakage of the hydraulic liquid was occurring regardless of how tightly the acrylic bodies were attached to each other. That was due to the unequal pressure around the groove and the folds of the membrane that occurred after assembling the three haustra. The final and most successful method was to cover the whole acrylic body with liquid silicone. However, the main challenge here was how a thin layer would be created above the cavity of the acrylic body. The solution was to fill the cavity with wax, and after curing the silicone, wax was melted with using heat to leave a thin layer of silicone. After this stage, the fabrication process of a single unit consisted from three haustrum (Fig. 5.3) was developed (§ 5.3.3).

5.4.1 Calibration of the hydraulic system

Calibration of the hydraulic system was performed to correlate the occlusion degrees and rates of the membrane with the syringe travel distances and speeds. Figure 5.10 shows an example of how the membrane oscillates under different travel speeds of the syringe; Figure 5.10a and Figure 5.10b refer to 1 mm s^{-1} and 2 mm s^{-1} travel speed of the syringe, respectively. The distance covered, for a certain syringe's displacement (i.e. 10 mm), was determined by measuring the difference between the lowest points of the membrane observed in the images (Figure 5.10c; white dot) captured at the initial and final position of the syringe. The results showed good reproducibility with constant peak height and width, revealing the accuracy and stability of the hydraulic system operated at different speeds. Figure 5.11a shows the second order polynomial relationships between the membrane oscillation rate and syringe travel speeds. The results showed that the membrane covers a certain distance at twice the syringe travel speed for velocities < 2 mm s^{-1} whereas for syringe travel speeds between 5 – 8 mm s^{-1} the corresponding membrane velocities were 7.8 – 9.8 mm s^{-1}. Since water, used as hydraulic incompressible fluid, there should be an absolute correspondence between the syringe and the membrane movements. These dissimilarities probably should be due to the elasticity of the silicone rubber used and its relaxation relative to the speed of fill. Due to viscoelastic properties, the silicone rubber behaves as rigid material at high strain rate (i.e.

high syringe speeds) and thus the relaxation of the membrane is smaller relative to the syringe speed. On the other hand, the relaxation of the membrane is much faster at low strain rate; i.e. syringe speeds. Figure 5.11b shows the linear relationship between syringe and membrane displacements as well as the corresponding percentage of the diameter decrease at given membrane covered distance.

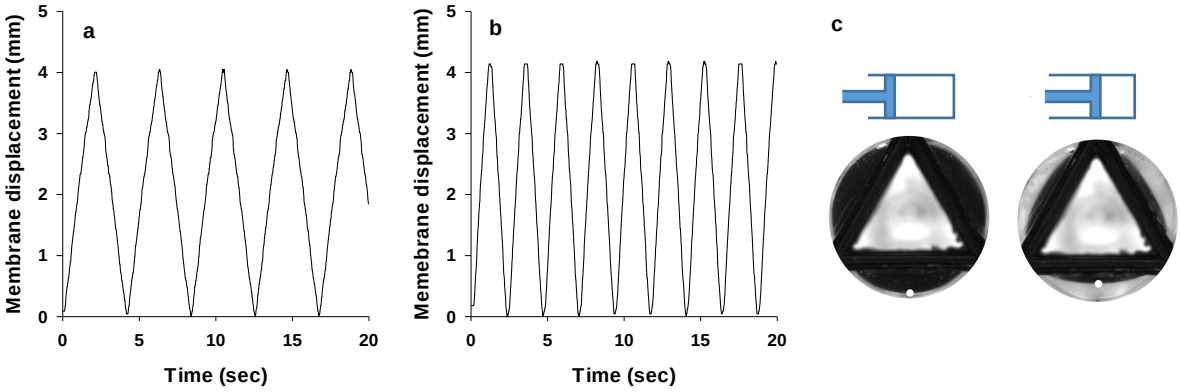

Figure 5.10. Curves of membrane oscillations obtained at (a) 1mm s^{-1} and (b) 2 mm s^{-1} syringe travel speeds for fixed travel distance (10 mm). The white dot on the cross section image of the DCM unit shows the reference point used to measure the travel distance of the membrane; a camera used at 50 fps to capture images of the cross section of the DCM unit during membrane's oscillations.

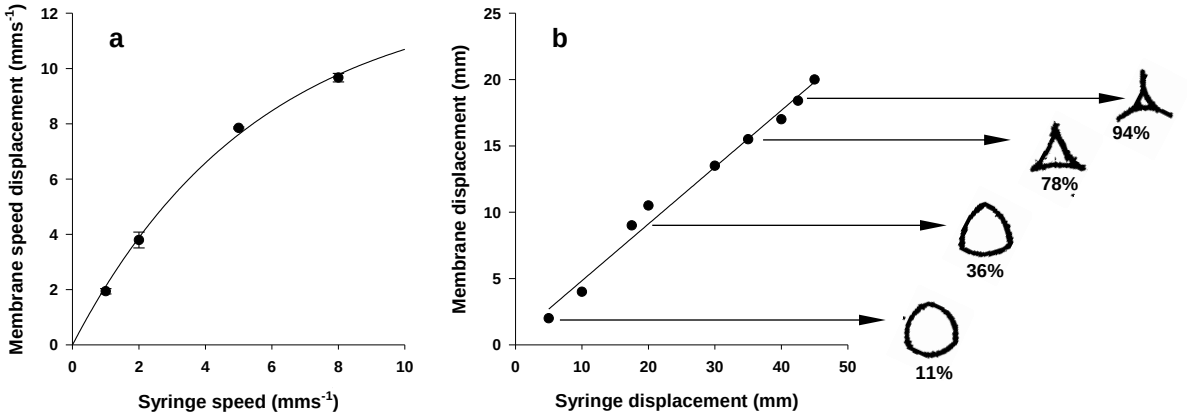

Figure 5.11. Calibration of the hydraulic system; a) plot of syringe speeds (mm s^{-1}) and the corresponding membrane speed displacement (mm s^{-1}); b) plot of syringe displacements (mm) and the corresponding membrane displacement (mm), indicating also the % reduction of the cross-section area of the DCM unit. Standard deviation bars for the membrane travel speed (n = 3).

5.4.2 Effect of membrane oscillations and viscosity of the fluid on manometry measurements

Figure 5.12 shows the measured amplitudes of the pressure forces generated from the membrane oscillations under different displacements, velocities and fluid viscosities. The results showed that the dominant parameters affecting the measured pressure amplitudes are the occlusion rate and the fluid viscosity; the occlusion degree has only a weak effect. For a given apparent viscosity (e.g. 525 mPa s for 1% NaCMC, w/w) the amplitude of the measured pressure increased from 2.2 to 5.7 mmHg for an increase in the occlusion rate from 4.3 to 9.8 mm s^{-1}, regardless of the occlusion degree. For the low viscosity fluid (i.e. water, 1 mPa s) the amplitude of the measured pressure was the same regardless of the occlusion degree and displacement velocity (i.e. from 1.8 to 2 mmHg) for apparent viscosities ≤ 106 mPa s (i.e. NaCMC concentrations ≤ 0.5% (w/w). When the NaCMC concentration was between 0.62 – 1% (w/w), which corresponds to apparent viscosities between 132 – 525 mPa s, a noticeable increase of the amplitude was observed. A plateau after the peak was observed for membrane

displacements >4 mm and low occlusion rates (i.e. 4.3 mm s^{-1}) when the membrane was traveling back to the initial position. This plateau was less significant at low viscosities and higher displacement velocities.

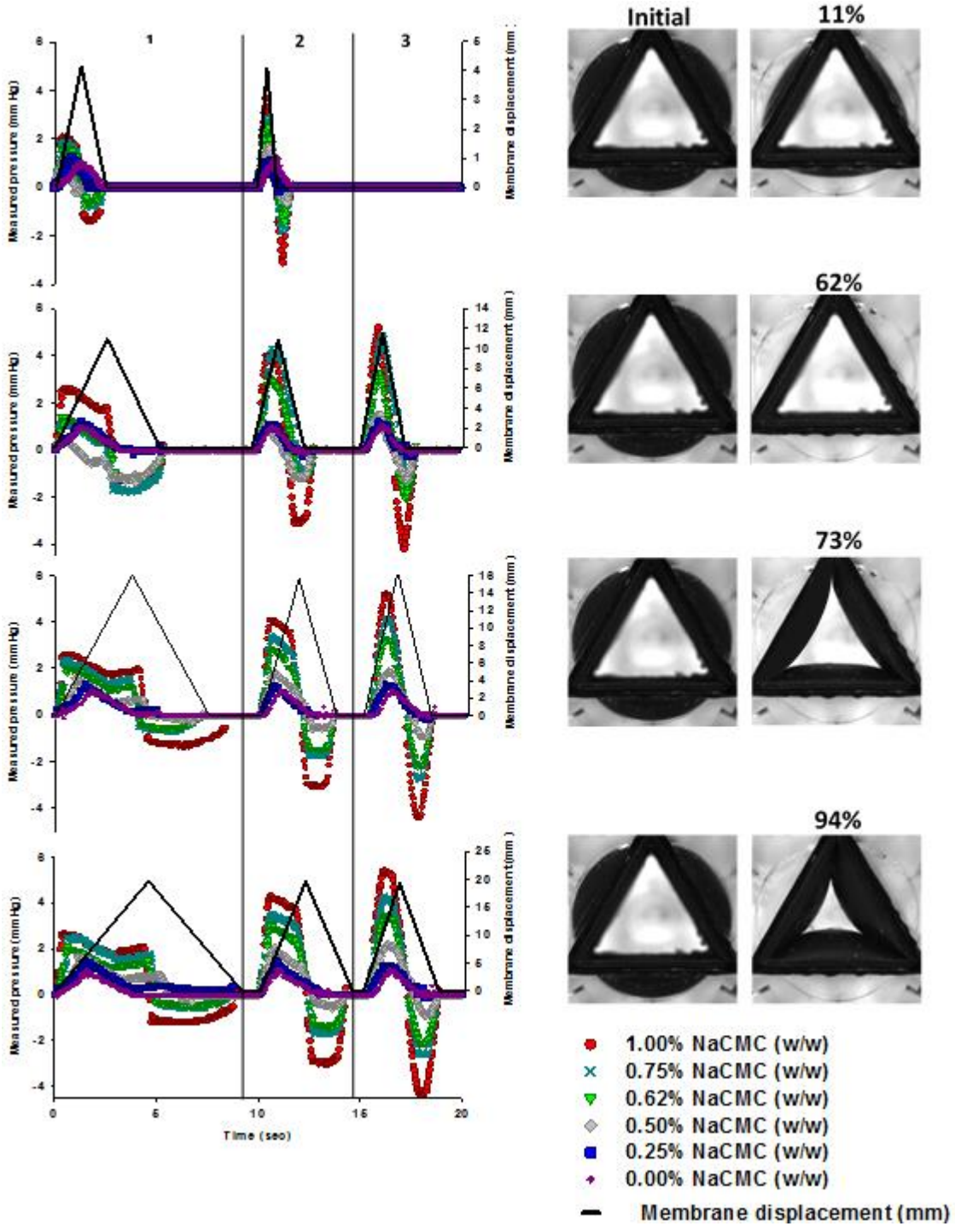

Figure 5.12. Measured pressures in different NaCMC concentrations (w/w), membrane displacements (a = 4 mm; b = 12 mm; c = 16 mm; d = 18 mm) and membrane occlusion rates (1: 4.3 mm s^{-1}; 2: 8.5 mm s^{-1}; 3: 9.8 mm s^{-1}).

High amplitudes of 120 mmHg magnitude were obtained only when the occlusion degree was 98% (almost complete constriction of the diameter of the DCM unit) where the membrane touched and partially squeezed the pressure sensor of the catheter (Figure 5.13). In this case the pressure amplitude was the same regardless of the viscosity and the occlusion rate of the membrane.

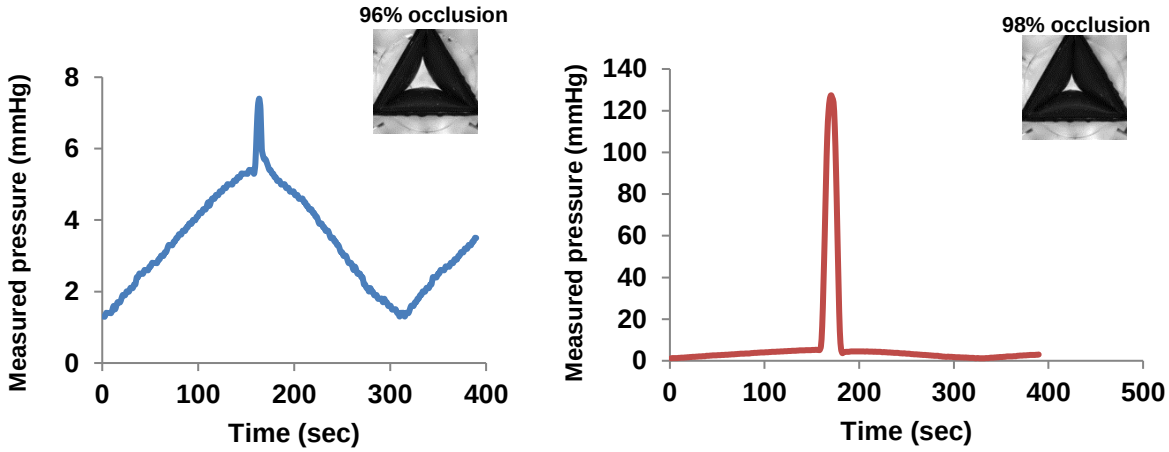

Figure 5.13. Measured pressures obtained at different occlusion degrees of the membrane in full filled apparatus and pressure sensor positioned at the centre of the DCM unit. At 96% occlusion, the pressure is rising gradually before a sharp peak appeared due to physical contact of the membrane with the sensor. In case of 98% occlusion a slight increase in the pressure was observed before a sharp increase occurred due to physical contact and squeeze of the sensor, reaching amplitude of ≈130 mmHg. The travel speed of the membrane was 2 mm s^{-1}.

The results showed that the manometry failed to capture all the oscillations of the membrane. The manometry will show similar pressure amplitudes for a given viscosity and occlusion rate regardless of the degree of luminal occlusion (Figure 5.14). This means that for the same measured pressure, different volume of fluids will be propelled, since the higher the occlusion degree the higher the volume expelled during the contraction of the wall. It is likely that one of

the parameters that probably would affect the correlation between the amplitude and the fluid flow is that the manometry fails to differentiate the different occlusion degrees of the membrane.

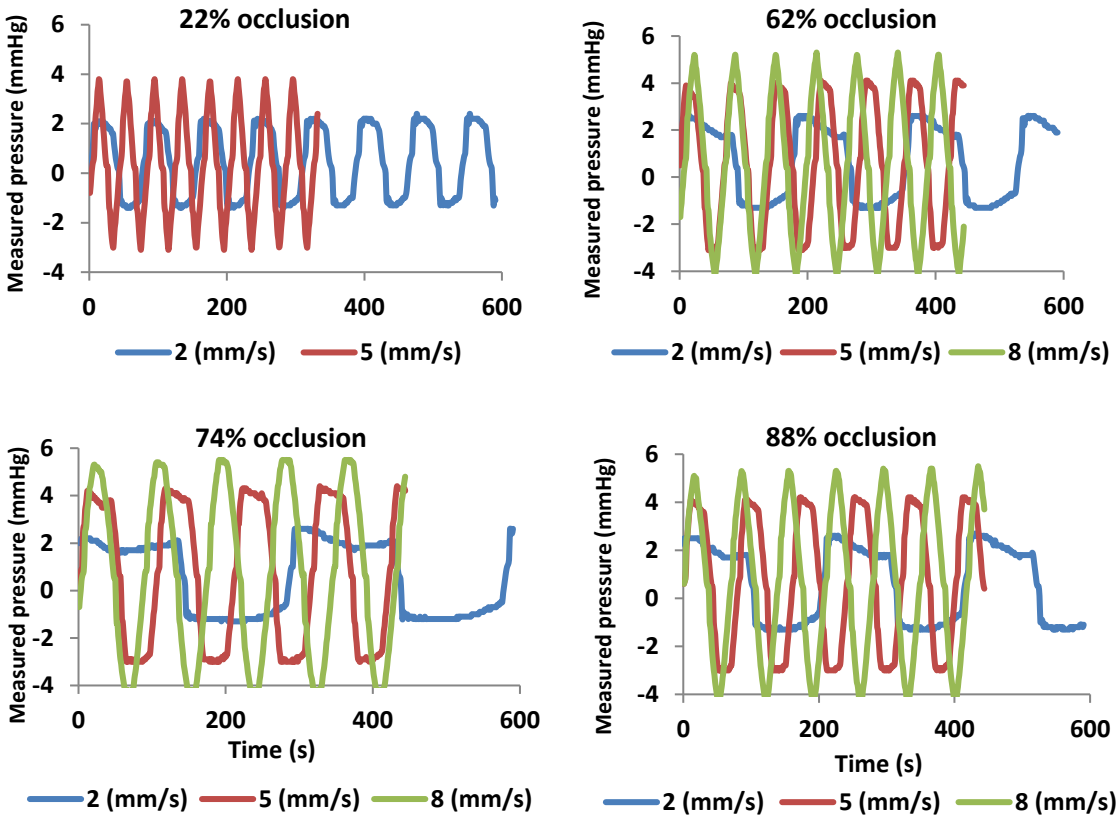

Figure 5.14. Measured pressures obtained at different occlusion rates and degrees in full filled apparatus and pressure sensor positioned at the centre of the DCM unit. Only the occlusion rate affects the interpretation of the manometry whereas the method failed to differentiate the different occlusion degree. Positive values correspond to inward occlusion of the membrane whereas negative values obtained when the membrane returned to its initial position.

However, it was only possible to distinguish between the different occlusions degree at low occlusion rates, achieved due to the plateau, appearing for occlusion degrees between 62 – 88%.

In previous studies, manometry missed the vast majority of the motility events in the proximal colon (Von Der Ohe et al., 1994). This is because the diameter in this region is ≥ 0.05 m, which

affects the sensitivity of the technique (Dinning et al., 2008). In addition, the colon is only partially filled with fluids (Sutton, 2009) which, as the results showed, further decreases the performance of the method. However, it should be noted that gas production upon fermentation has not been reproduced in the *in vitro* model and this is likely to also affect the interpretation of the manometric results.

Beside this limitation, our results agree with von der Ohe et al. (1994); revealing the limitations of manometry. Furthermore, the study by Arkwright et al. (2013) concluded that the viscosity affects the manometry measurements and that this technique can monitor non – occluding events (i.e. physical contact and/or squeezing of the pressure sensor). However, Arkwright et al. (2013) did perform experiments in fully-filled apparatus and at fixed occlusion degree.

It must also be noted that in Arkwright et al. (2013) study the catheter was positioned exactly at the centre of the tube under slight tension to be exactly at the centre of the tube. In our study, there were two configurations. In the first one the catheter was placed in the same way as in Arkwright et al. (2013) study and in the other was not under tension, allowing the catheter to naturally settle representative of *in vivo* studies. Further experiments with half-filled apparatus and the catheter positioned at the centre of the tube (i.e. under tension and no physical contact with the membrane) the pressure was 1.0 ±0.2 mmHg independent of the degree of luminal occlusion, occlusion rate and the viscosity of the fluid. The pressure was raised only when the membrane touched and squeezed the catheter. In the case where the catheter was settled, the measured pressure was unchanged (i.e. 1.1 mmHg) for occlusion degrees ≤88% (Figure 5.15); a sharp increase was observed only when the membrane touched and squeezed the sensor.

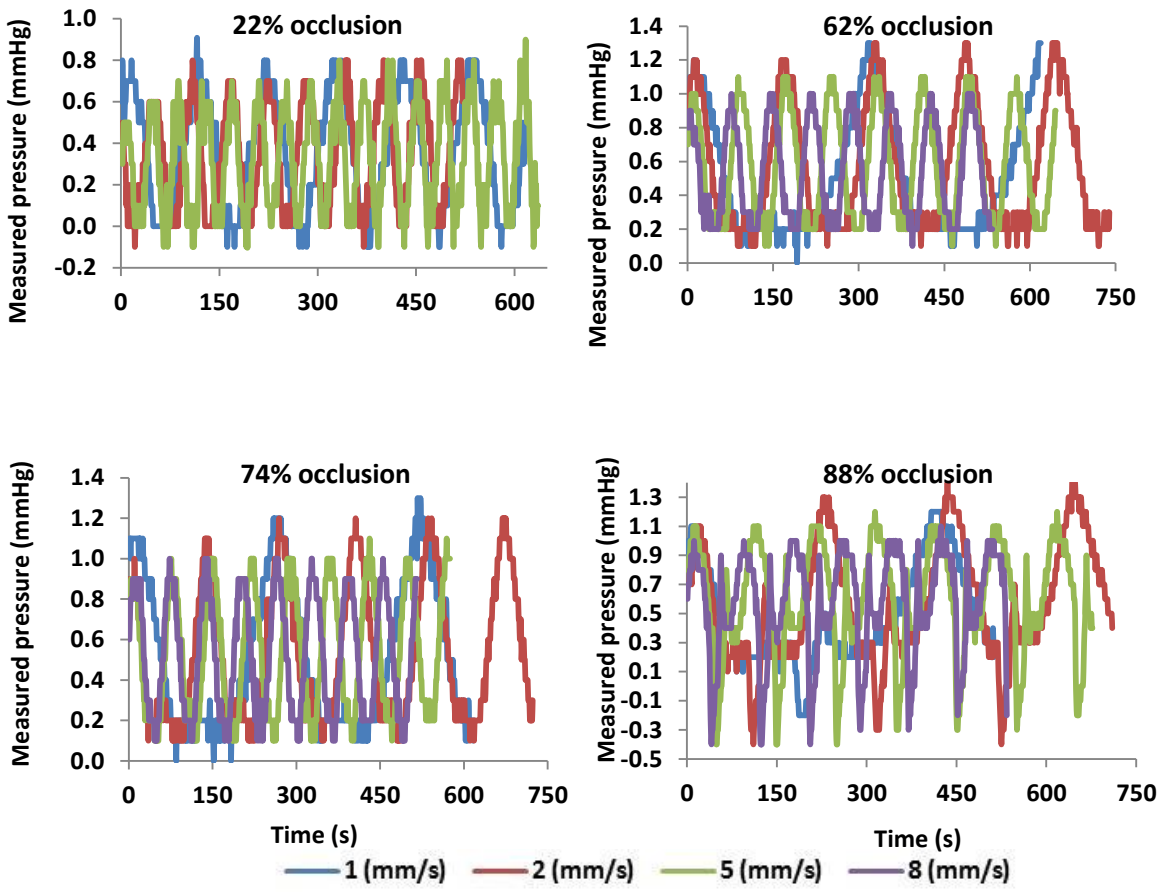

Figure 5.15. Measured pressures at different occlusion rates and occlusion degrees of the membrane in half-filled apparatus and catheter located at the bottom of the DCM unit. The experiments were performed with using 0.75% NaCMC (w/w). When the apparatus is half filled and the occlusion is <94% the amplitude of the pressure is relatively unaffected from the occlusion rate and occlusion degree. Similar results were obtained in the less viscous media.

In viscous fluids, a second peak was observed in the manometry graphs for occlusion degrees ≥75% (Figure 5.16). This peak appeared before a sharp increase in the pressure amplitude, caused from the physical contact of the membrane with the catheter. It seems that in the partially filled apparatus, the viscosity will first cause a small increase of the pressure (i.e. 2 ±0.3 mmHg) and then a further increase will depend on the degree of the luminal occlusion. Hence, the volume of the fluids also affects the manometry measurements. As the occlusion rate was increasing, the amplitude of the first peak was decreasing and for 80%

occlusion, the measured pressure amplitude of the first peak was decreased from 1.8 ±0.1 mmHg to 0.7 ±0.1 mmHg when the occlusion rates increased between 2 – 8 mm s^{-1}. It was noted, in the low – to – medium viscosity media (i.e. 0 – 0.5% NaCMC w/w), that at high occlusion rates the expulsion of the fluid was faster during the contraction of the membrane. Thus, the catheter was not sufficiently submersed in the fluid, decreasing further the sensitivity of the manometry. In contrast, the occlusion rate did not affect the results in high viscosity media. For the most viscous media (i.e. 0.75 and 1.00% NaCMC w/w), the fluid behaved like solid body over the short timescales of the wall motion (insufficient time for appreciable level change due to fluid flow) raising the level of the medium accordingly to the membrane displacement thus, in this case the catheter was sufficiently submersed.

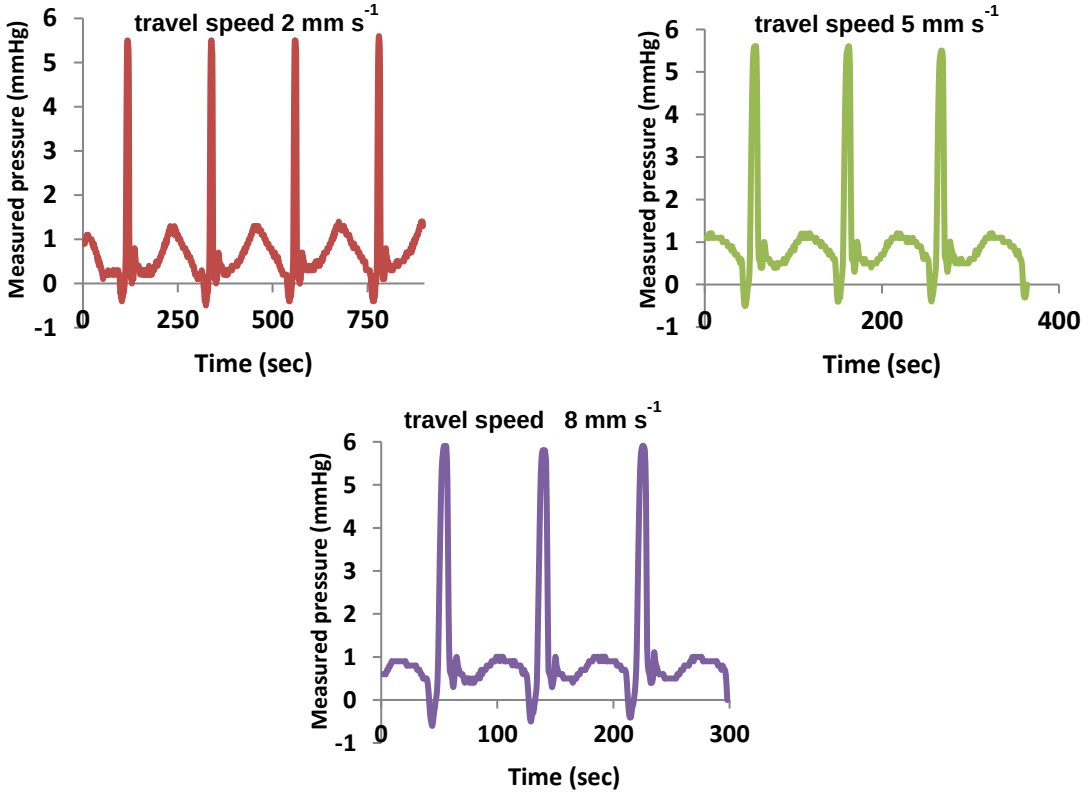

Figure 5.16. Measured pressures obtained at 94% occlusion degree of the membrane in half filled apparatus and with catheter being positioned at the bottom of the DCM unit. The catheter freely moved in this configuration. The first peak (a) in the manometry graphs appeared due to the pressure applied on the sensor from the fluid (apparent viscosity 525 mPa s; 0.75% NaCMC w/w). The second peak (b) appeared due to the physical contact of the sensor with the membrane.

A recently published work by Schneider et al. (2016), showed the high variability of the pressures occurred in human colon at fed and fasted state. The authors used a wireless SmartPill® enabling to monitor simultaneously the pH, temperature, pressure and transit times in human GI tract. The highest pressure monitored in the colon was 105 ±56 mmHg and 123 ±21 mmHg in fasting and fed state respectively. Our experiments showed, but also manometric measurements (refer to Chapter 1 & 2), that that high pressures mainly occurred when strong contractions of the smooth muscle (in our case complete occlusion of the membrane of the DCM) take place; normally during peristaltic motion (i.e. mass movements). However, SmartPill® will be also suffer from the technical limitations similar to the manometry. Thus, to fully characterize the hydrodynamics in human GI tract, different monitoring techniques should be combined, if possible simultaneously, enabling to establish relationship between pressures and flow episodes (i.e. mixing). Furthermore, as it will be discussed in the following Chapter, the properties of the SmartPill®, or any particle tracer used to monitor the motility, in terms of density, buoyancy, relaxation times, should be carefully addressed, to ensure that the particle will adequate follow the motion and the transit of the chyme.

5.4.3 Positron Emission Tomography

Relationships between membrane motion and fluid flow were investigated, performing positron emission tomography in different viscous media. Unlike the dynamically changing colonic environment, the conditions were fixed in this *in vitro* study to understand, the interplay between the wall motion, fluid flow, viscosity etc.

Figure 5.17, Figure 5.18 and Figure 5.19 show the time series of PET images of single antegrade CPPW in 0.25, 0.50 and 0.75% NaCMC (w/w), respectively. Furthermore, the relaxation, neutral and contraction stage of the flexible wall of the DCM is also presented. It should be noted that the image capture rate in PET was much higher (i.e. one fps) compared to *in vivo* studies (one frame per 10 s; Dinning et al. 2008). This allowed a more detailed temporal analysis of the flow episodes as a function of the wall motion. The results showed

that at low viscosity (Figure 5.17) the movement of the fluid followed the motion of the wall for the first 3 seconds after which the fluid flows back while the wave was travelling towards the end of the tube. This occurred because the level of the fluid was raised close to the wall of the rigid siphon without passing over it, resulting in a strong backflow due to gravity and relaxation of the wall back to neutral; leading to poor overall propulsion of the contents. This backflow effect was less significant in the more viscous media. Figure 5.18 shows a portion of the radioactive tracer to cover a longer distance (see frame at 7 s) before it moved back. In contrast, in the most viscous fluid (Figure 5.19) the radioactive tracer travelled across the entire length of the tube before flowed back, ending at the middle of the tube. In addition, PET images showed that the DCM can reproduce the typical bolus movements, as the portion of the tracer, traveling with the wave-front of the membrane, was located inside the relaxing point. Furthermore, the tracer appeared in the form of pockets, especially at low viscosity media, located within the haustra during the wall motion. However, these pockets disappeared after the completion of the wave and its redistribution due to backflow. This phenomenon occurred less frequently in more viscous fluids.

'To and fro' motion occurred during and after the end of the wave. However, this was less extended as the viscosity increased. In less viscous medium, retrograde motion appeared between 4 – 6 s frames whereas antegrade occurred between 7 – 12 s frames (Fig. 5.17). In case of medium viscosity medium, the corresponding backward and forward motion took place between 8 – 10 s and 10 – 12 frames, respectively (Fig. 5.18). In the most viscous medium, retrograde motion appeared between 7 – 11 s frames but less significant antegrade in 11 – 12 s frames.

In all PET experiments, a significant amount of the tracer remained at the beginning of the tube (i.e. within the caecum and close to terminal ileum), something which has also been observed in the *in vivo* scintigraphy studies (Dinning et al., 2008, Cook et al., 2000). This is probably because the propulsion of the fluids might not be strong at the beginning of the human proximal colon contraction, as the propagating wave is not yet fully developed.

It should be noted that these observations might differ significantly if PET images captured using different fluid volume, though, with the same motility pattern. Nevertheless, the behaviour of the colon wall depends on the mechanical and chemical stimulus and the disease state as described in Chapter 2. Thus, propulsion and mixing of the contents should carefully be assessed when changing only the volume but keeping the same motility pattern. However, this approach might be far from the reality of what occurs in the proximal colon. For instance, increased motility index of the proximal colon has been reported in the presence of elevated amounts of short chain fatty acids upon fermentation (Kamm et al., 1992) or after meal ingestion (Reddy et al., 1991). Taking also into account that the fluid volumes range 10 – 125 mL (Sutton, 2009), the same motility pattern of various occlusion degrees (i.e. decrease of the tube diameter) could probably occur in the presence of different fluid volumes due to a strong chemical (e.g. fatty acids) or neurogenic (e.g. meal) stimulus. Thus, the current work can be further extended to examine the interplay between wall motion, external stimulus and fluid motion. However, this task is beyond the scope of this work, since advances in e.g. stimulus-response soft materials should be introduced.

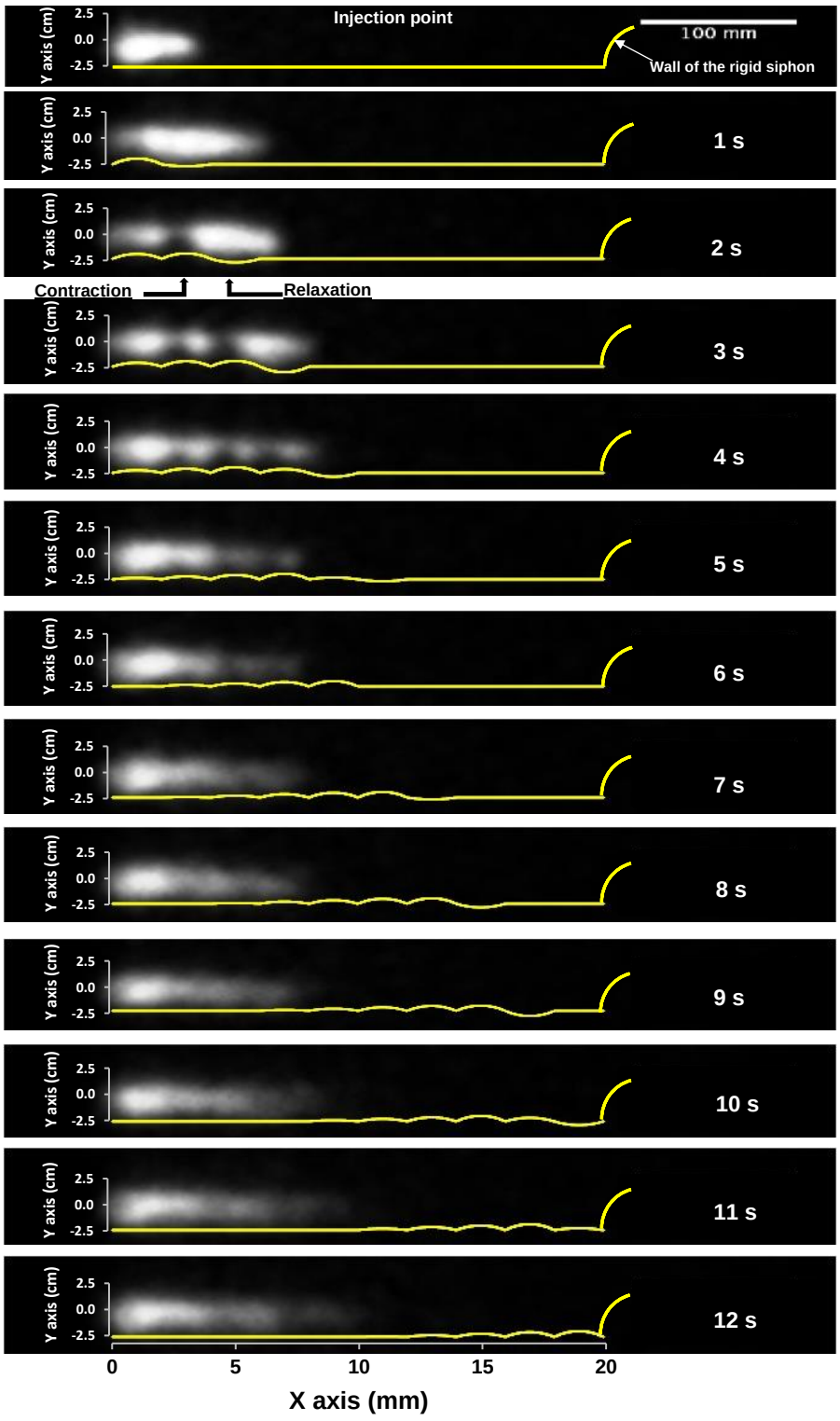

Figure 5.17. Time series of PET images (recording time 1s/f) and the corresponding membrane status obtained during an antegrade propagating wave using 0.25% NaCMC (w/w) as fluid. The occlusion degree was 73%; wave speed 0.02 m s^{-1}; DCM tube filled 50% with fluid.

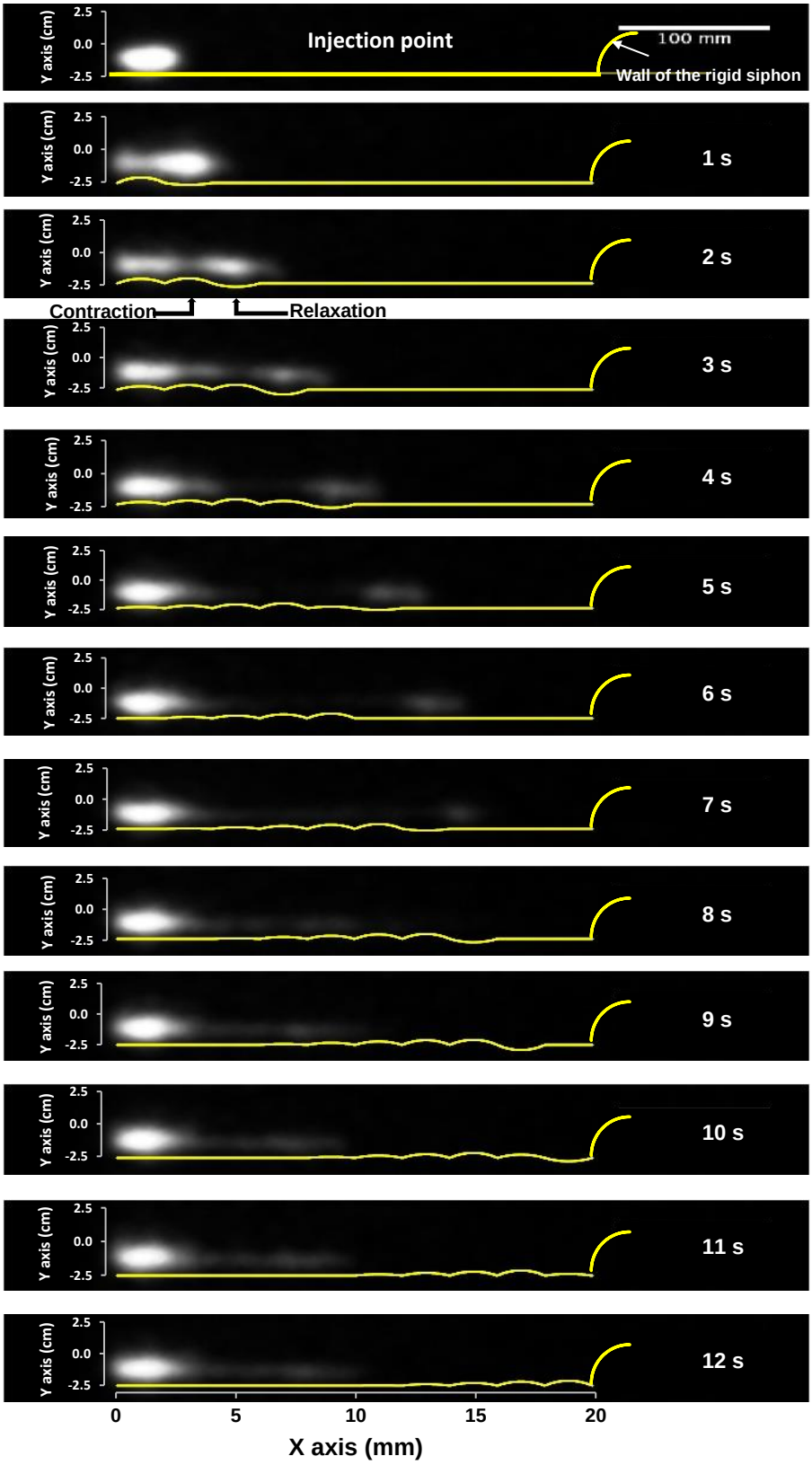

Figure 5.18. Time series of PET images (recording time 1s/f) and the corresponding membrane status obtained during an antegrade propagating wave using 0.50% NaCMC (w/w) as fluid. The occlusion degree was 73%; wave speed 0.02 m s^{-1}; DCM tube filled 50% with fluid.

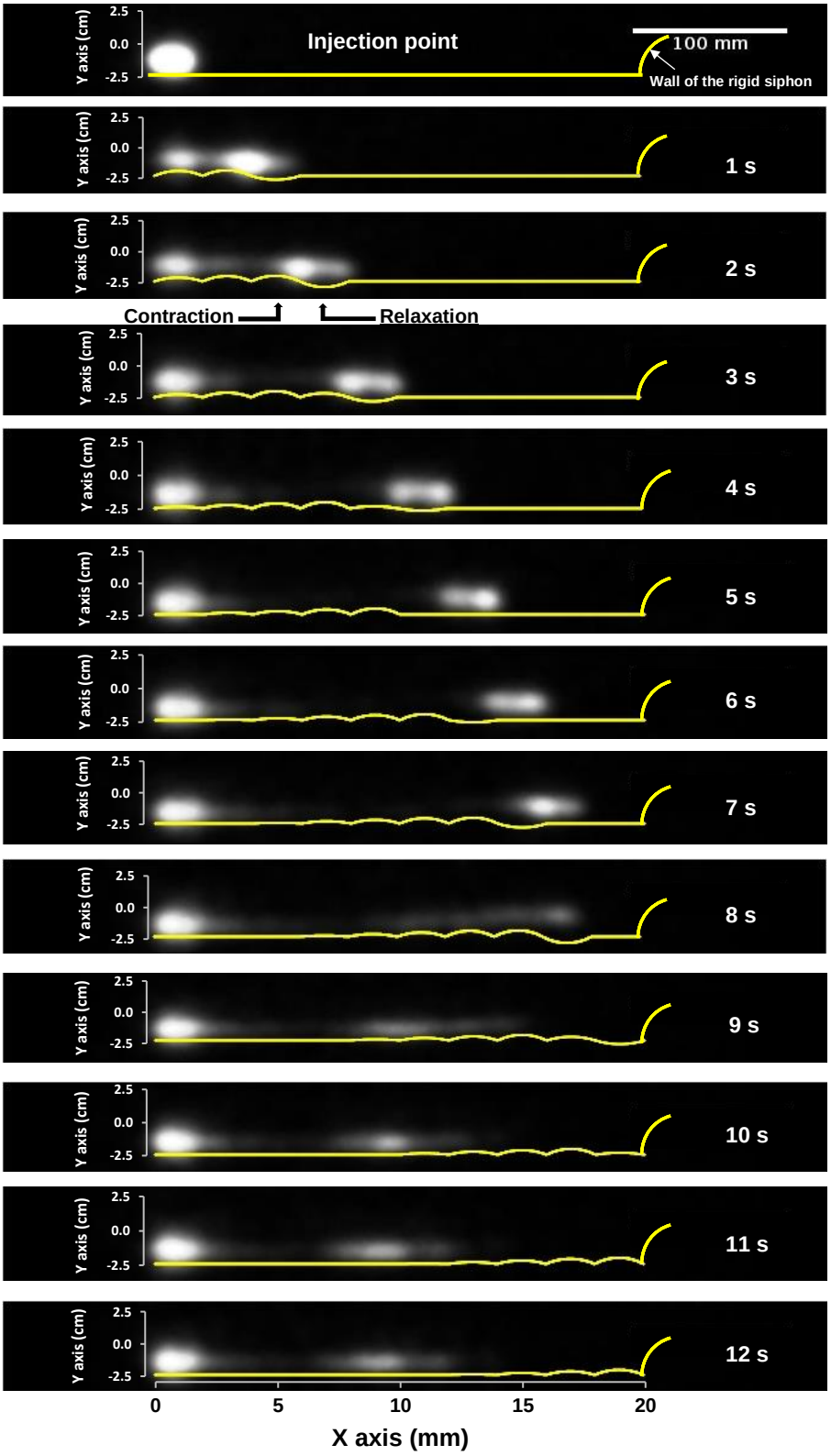

Figure 5.19. Time series of PET images (recording time 1s/f) and the corresponding membrane status obtained during an antegrade propagating wave using 0.75% NaCMC (w/w) as fluid. The occlusion degree was 73%; wave speed 0.02 m s^{-1}; DCM tube filled 50% with fluid.

The most important output of this experimental set up is that flow episodes can be associated with the wall motion; even for short distances as in the case of low viscosity media. However, this requires a higher recording frequency to be detectable. Furthermore, the occlusion degree was 73% and the DCM tube was filled 50% with fluids. Previously the manometry showed, under these conditions, a pressure amplitude of ≤2 mmHg. Based on the criteria used in the *in vivo* studies for what is considered a propagating sequence (PS) of low amplitude (i.e. 2 – 5 mmHg with velocity 0.002 – 0.02 m s^{-1}), the flow episodes in the present work should not be associated with the wall motion, since the pressure forces were ≤2 mmHg. This would underestimate how extensively the wall motion (i.e. pressure waves) is associated with the fluid flow. However, the researchers/clinicians rely mainly on the manometry to decide what is the lowest limit of the amplitude based on which a pressure wave will be considered as PS.

The propulsion of the fluids within the DCM under increasing viscosity and fixed motility pattern was also assessed by applying repeated CPPW; a delay of 10 s between the waves was applied to ensure stagnant fluid before the next CPPW. Since the CPPW lasted for 10 s, in this case the PET images captured after the end of the CPPW; this recording duration time was the same used in previous *in vivo* studies (Dinning et al., 2008). Thus, the distribution of the tracer is due to a motility event, occurred earlier to the captured image. The PET images showed that at low viscosity media (0.25% NaCMC w/w) the tracer was distributed throughout the DCM tube after nine antegrade CPPWs (Fig. 5.20). However, as the viscosity increased the distribution of the tracer was much less uniform (Fig. 5.21). Two spots with high tracer intensities were formed showing that plug flow occurred in high viscosity media. The final distribution of the tracer was affected by the 'to and fro' motion of the fluid. These movements are a combination of the forward propulsion of the fluid and the backflow after the wave has passed. The extension of the 'to and fro' depends on the viscosity of the fluid.

Several issues were raised with using prolonged recording time. The first is that the tracer could already be distributed in the colon before capturing the final image, which might cause difficulties in distinguishing clear movement of the tracer in a later motility event. Secondly,

several pressure waves which are not considered as motility events (i.e. <2 mmHg), may have taken place before a pressure wave of amplitude >2 mmHg occurred and thus, the tracer might have occupied a significant area of the colon before capturing an image. Third, high resolution manometry showed that there are motility events of duration <10 s (Dinning et al., 2014a), that means that capturing frames at 10 s, will miss flow episodes occurred earlier and associated with the wall motion.

In more viscous media a portion of the tracer might be located several centimetres from the injection point after the wave (Figure 5.22). Thus, if a pressure wave, which fulfils the criteria of being a PS, starts from the caecum, a portion of the tracer will already be several centimetres ahead. Therefore, it would be difficult to associate the flow episode with the origin of the pressure wave.

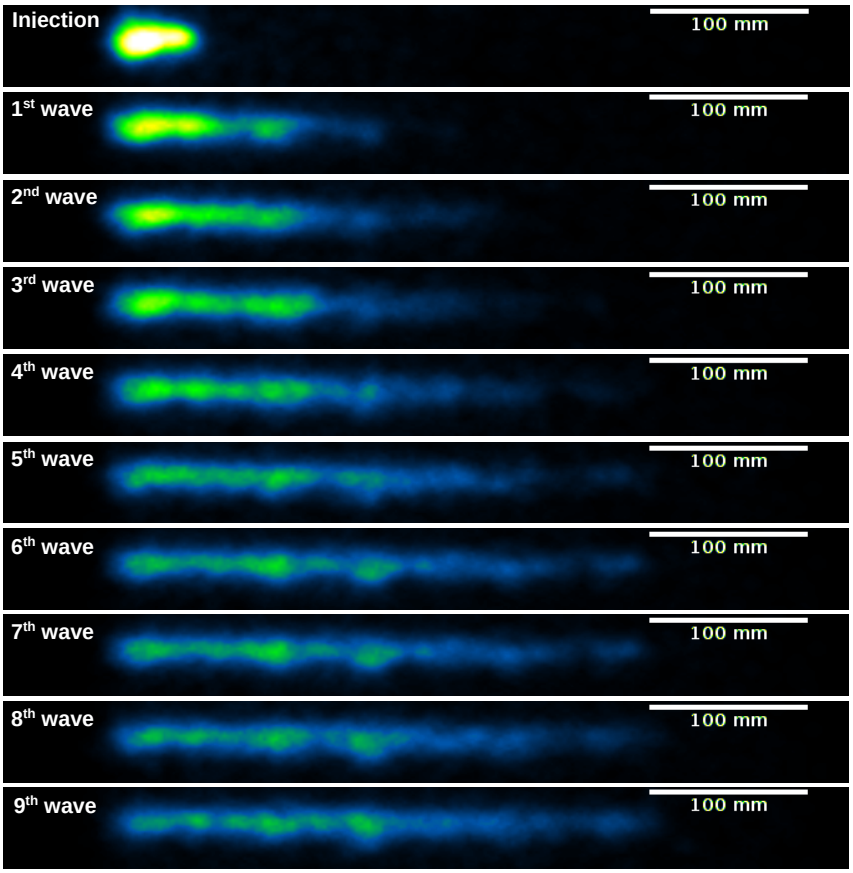

Figure 5.20. PET images of 0.25% NaCMC (w/w) after the completion of each antegrade cyclic propagating pressure wave (CPPW). The recording time is a frame per 10s. A time delay of 10 s was used before the next CPPW applied.

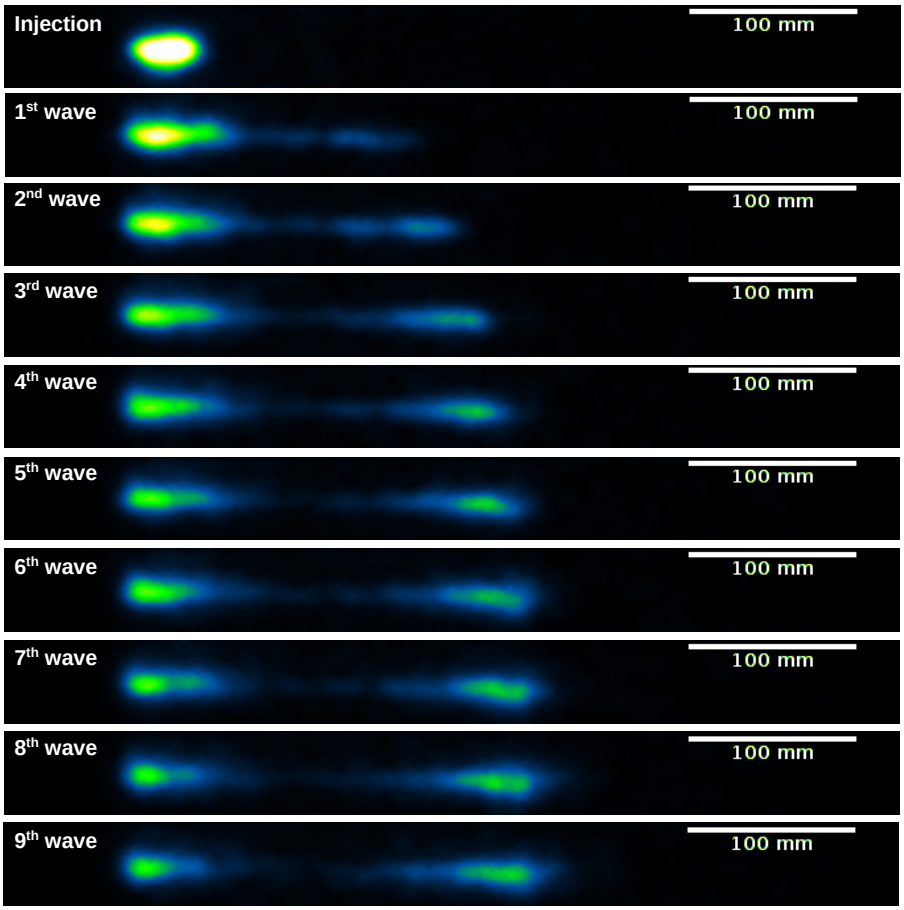

Figure 5.21. PET images of 0.50% NaCMC (w/w) after the completion of each antegrade cyclic propagating pressure wave (CPPW). The recording time is a frame per 10 s. A time delay of 10 s was used before the next CPPW applied.

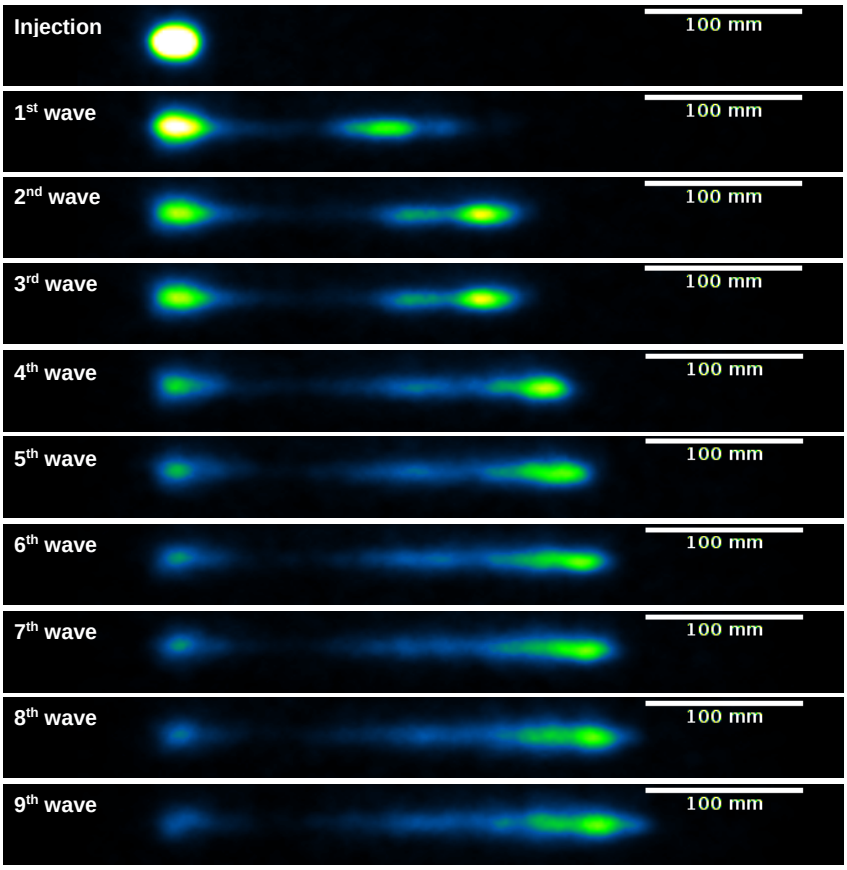

Figure 5.22. PET images of 0.75% NaCMC (w/w) after the completion of each antegrade cyclic propagating pressure wave (CPPW). The recording time is a frame pre 10 s. A time delay of 10 s was used before the next CPPW applied.

5.5 Conclusions

A novel biomechanical computer – controlled model of the human proximal colon was designed, developed, fabricated and used to simulate colon motility. The effect of wall motion, viscosity and volume of the fluids on the performance of the manometry was investigated whilst Positron Emission Tomography was used to visualize the fluid flow within the colon model under fixed conditions.

The results showed that the position of the catheter, the occlusion rate, the viscosity and the fluid volume affected the interpretation of the manometry. In particular, as the viscosity and the occlusion rate were increased the amplitude of the pressure also increased. Furthermore,

manometry failed to differentiate changes for lumen occlusion degrees of the membrane <80% and at low viscosities. In addition, the sensitivity of the manometry was dramatically decreased when the apparatus was half full. Thus, the criteria based on which a pressure wave should be associated with the movements of the contents, might have to be reconsidered. PET images revealed that pressure waves with amplitudes <2mmHg can be highly associated with flow episodes, distributing a significant amount of fluid (i.e. tracer) over long distances. In the half – full DCM unit, manometry can differentiate pressures caused by the viscous media and those caused by the physical contact of the membrane and the sensor; when the pressure sensor remains submerged in the fluid and the viscosity is sufficiently high.

This study yields valuable information about the interpretation of the manometry results with potential consequences on clinical management strategies, both diagnostic and therapeutic, in the human proximal colon. This information is also useful to develop *in vitro* methods to assess the performance of dosage forms targeted to the colon under more biorelevant conditions.

However, further investigation needs to be done with regards the velocities and the transit times of the fluids through the DCM tube under known wall motion and how the viscosity will affect these parameters. Limited work has been done *in vivo* using magnetic pill tracking system obtaining information with regards to the distance covered and the direction of the displacements of the pill as well as velocities during residence in the human colon (Hiroz et al., 2009, Hénin et al., 2016). Thus, in the following chapter Positron Emission Particle Tracking (PEPT) system is utilized to better understand the flow and the mixing process in human proximal colon using DCM.

Nomenclature

n	power law exponent
Re	Reynolds number
d_d	Particle diameter (m)
$\bar{u}$	Fluid velocity (m s^{-1})
d_h	Hydraulic diameter (m)
P_j	Probability of the individual velocity data points to be within the range of the velocities
U_x	Propulsive velocities in *x* axis
Δx	Particle displacements in x axis
ΔU	Increments

Greek symbols

τ	shear stress (Pa)
τ_γ	yield stress (Pa)
$\dot{\gamma}$	shear rate (s^{-1})
μ_A	Apparent viscosity (mPa s)
p	Density (kg m^{-3})
ρ_d	Particle density (kg m^{-3})

Abbreviations

DCM	Dynamic Colon Model
DGM	Dynamic Gastric model
GI	Gastrointestinal
NaCMC	Sodium carboxymethylcellulose
PEPT	Positron Emission Particle Tracking
PET	Positron Emission Tomography
PSs	Propagating Sequences
TIM-1	TNO (gastro-) Intestinal Models
TIM-2	TNO Colon simulator
TNO	Nederlandse Organisatie voor Toegepast
n.b	neutrally buoyant
CPDF	Cumulative Probability Distribution Function
L	Low viscosity fluid
M	Medium viscosity fluid
H	High viscosity fluid
CPPWs	Cyclic Propagating Pressure Waves
N.T	Net Transport
pp	polypropylene
ps	polystyrene

6 Understanding flow and mixing process in proximal human colon

Abstract

The tubular Dynamic Colon Model (DCM) was utilised to understand fluid motion and mixing in the proximal human colon. The tube was half-filled with fluids with different apparent viscosities and flow measurements were carried out using a radioactive tracer particle; alteration of the particle buoyancy was performed to gain understanding of previous experiments carried out *in vivo*, and to examine particle motion relative to the bulk fluid and the gas-liquid interface. The net forward propulsion of the particle increased with the fluid viscosity, attributed to both viscous damping of the backflow of the fluid by gravity once the wall motion had ceased coupled with much reduced particle relaxation time in the viscous media. The backflow caused retrograde movements of the particle which were not related to the wall motion. Shorter residence times and greater velocities were obtained for a floating particle on the gas-liquid interface, implying the presence of a surface wave moving faster than the bulk liquid.

These in vitro results give insight into in vivo observations, with potential implementation on improving the non-invasive techniques, used to monitor in vivo the colon motility. Furthermore, understanding the flow motion and the behaviour of the particles with different buoyancy, may also contribute to the proper design of drug formulations where fragments of the dosage form formed upon disintegration in the human proximal colon.

6.1 Introduction

The human colon is the last site in the GI tract for absorption of digestive residues and is a potential location for systemic and local delivery of drugs (Antonin et al., 1996). The complex motor activity of the colon wall (Karaus and Wienbeck, 1991) facilitates propulsion and mixing of the colonic contents (Dinning et al., 2014a). Various motions of the colon wall have been previously observed with high amplitude propagating sequences causing mass movement of the colonic contents (Bassotti et al., 1995), whereas low-amplitude propagating sequences comprised of slow waves in both antegrade (forward) and retrograde (backward) directions facilitate both propulsion and mixing (Dinning et al., 2014a).

Factors that contribute to the motion and transit of the fluids, include: (1) the short travel distance of the propagating sequences (PSs) (Dinning et al., 2014a), (2) the retrograde PSs (Dinning et al., 2008, Hiroz et al., 2009), (3) the reflux (i.e. backflow) of over half of the bolus movements and (4) the apparent viscosity (rheology) of the colonic luminal contents (Proano et al., 1990).

A magnet tracking system has been employed as an *in vivo* non – invasive technique which does not suffer from the technical limitations of manometry and scintigraphy (Hiroz et al., 2009). This magnetic tracer comprised of a silicone coated pill, containing a cylindrical magnet of 1.8 g cm^{-3} density and ≈0.8 g and its position was tracked as a means of determining displacements and velocities of the colonic contents. However, the use of such a heavy pill causes issues in terms of the long relaxation time of the particle, so it may not follow the fluid motion. This can be revealed from the fact that the much lighter radio markers previously used [7] travelled much further through the fluid compared with the magnetic pill. Thus, although it is challenging, it is important to choose the particle properties to enable the fluid motion to be tracked over a wide range of viscosity, particularly since dewatering process takes place in the human colon.

Given the above findings, an *in vitro* model that simulates the dynamic colon environment as well as the use of a proper tracking technique of the fluid flow under known conditions, offers

the capability to develop understanding of the relationships between these parameters and to what extent these affect the mixing process and propulsion of the fluids in the caecum – ascending region. This is also important from a pharmaceutical development perspective, since valuable information can be obtained on optimising drug delivery to the colon.

Physiologically representative engineering intestinal models need to be able to reproduce the widely accepted law of the intestine (Bayliss and Starling, 1899), which states that the colonic fluids move in the digestive tract due to the combined ascending excitatory (muscle contraction) coupled with the forward descending inhibition (muscle relaxation) (Sinnott et al., 2012). Although the most advanced models currently available such as the TNO TIM-1 (Minekus, 2015), TIM-2 (Venema, 2015) and IFR Dynamic Gastric model (DGM) (Thuenemann et al., 2015), aim to simulate the GI environment under well controlled conditions and have advanced dissolution science, yet they are not considered to be the final solution to the problem (McAllister, 2010). Some of the major drawbacks of TIM-2 are the complexity of the technique and lengthy equipment setup time resulting in a limited amount of data which can be obtained in a reasonable time period. Furthermore, the TIM-2 is not physiologically representative, with a different length, volume and mixing process when compared with the human colon (Blanquet et al., 2001a).

This chapter describes the first application of a computer – controlled biomechanical *in vitro* colon model to enable analysis of the mixing process in the proximal colon via analysis of the fluid motion in 3-D. The model mimics the colonic physical environment in terms of the anatomy of smooth muscle (Langer and Takács, 2004) and the propagating motor patterns monitored in the proximal colon (Dinning et al., 2014a). Thus, this study aims to determine how the hydrodynamics will be affected by the interplay between predetermined conditions (i.e. wall motion, viscosity, volume of fluids) in the partially filled artificial proximal colon. Positron Emission Particle Tracking (PEPT) developed at the University of Birmingham UK (Broadbent et al., 1993), was used to determine the displacement of a radioactive tracer particle inserted into the DCM tube and then subjected to a predetermined wall motility pattern;

altering the buoyancy (and thus relaxation time) of the particle enables the motion of the particle relative to the fluid to be examined, to some extent this mimics *in vivo* particle tracking experiments. Furthermore, this study aims to provide information about the physical conditions that colon-specific drug delivery systems will face during their passage through the proximal colon.

6.2 Materials and Methods

6.2.1 Materials

Sodium carboxymethylcellulose (NaCMC) of 700000 molecular weight and sodium chloride (NaCl) were purchased from Sigma (St., Louis, USA).

6.2.2 Fluids used in PEPT experiments

Fluid of 0.25% (low apparent viscosity, denoted L), 0.50% (medium apparent viscosity, denoted M) and 0.75% $NaCMC_{(700000)}$ (w/w) (high apparent viscosity, denoted H) were used to mimic the dewatering process which takes place in the human colon. The concentrations of NaCMC were chosen based on previous studies published to evaluate the effect of the viscosity on dissolution profile of drugs targeted human colon (Stamatopoulos et al., 2016a, Stamatopoulos et al., 2015, Stamatopoulos et al., 2016b). The flow rheology of the media was measured after the addition of the sodium chloride (3% w/w) to adjust the density of the media relative to particles used in Positron Emission Particle Tracking experiments. A Discovery Hybrid Rheometer (TA Instruments) coupled with a 40 mm diameter, 4° cone and plate geometry was used to perform the rheological measurements. The flow rheology was well described by Herschel – Bulkley model for a shear thinning fluid,

$$\tau = \tau_\gamma + K\dot{\gamma}^n \tag{6.1}$$

where τ is the shear stress, τ_γ is the yield stress, $\dot{\gamma}$ is the shear rate, K is the consistency index and n is the power law exponent (< 1). The parameter values obtained are presented in

6.2.3 Positron Emission Particle Tracking (PEPT) system

Positron Emission Particle Tracking (PEPT), developed at the University of Birmingham was used to assess fluid patterns within the DCM tube under the CPPWs. Details of the PEPT methodology can be found in previous publications (Broadbent et al., 1993, Simmons et al., 2012). The half-filled DCM tube was placed between the two detectors of the DAC Forte PET scanner (Fig. 6.1a – b) and the radioactive particle was introduced in the first segment.

The tracer used was an ion-exchange resin particle of diameter 250 – 300 μm doped with ^{18}F, provided by the School of Physics at the University of Birmingham. Two larger particles made from different materials were then used to enclose the tracer. The first was a spherical polystyrene particle (3 mm Ø). The tracer was enclosed by drilling a hole of 1 mm Ø in the plastic particle and sealing the tracer inside by reheating the polystyrene. The same procedure was also carried out using a polypropylene of 3 mm Ø. Due to the different densities of the plastic particles, the former would be expected to be neutrally buoyant (n.b) whereas the latter will float, and thus was expected to indicate motion at the liquid – air interface.

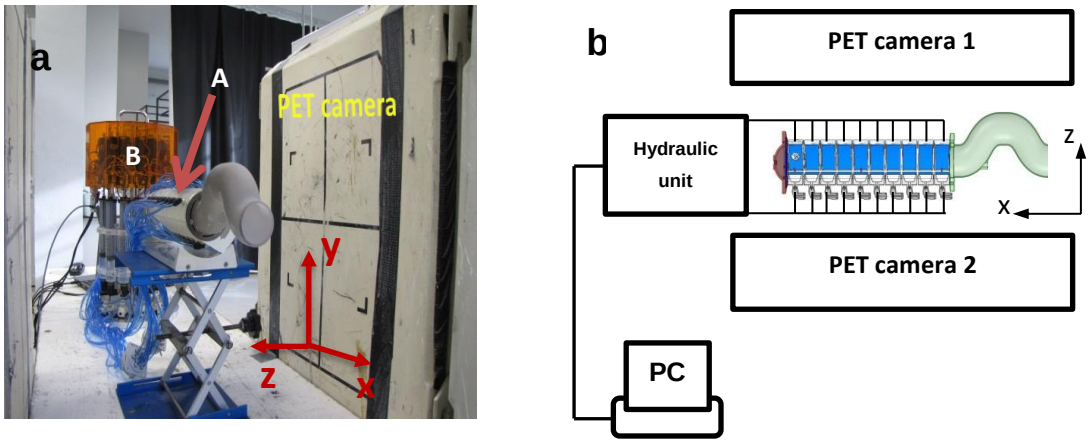

Figure 6.1. (a) DCM tube (A) in between PET cameras coupled with the hydraulic system (B); b) schematic representation of the DCM – PET configuration.

For both floating and n.b particles, the particle relaxation time, which is the time for the particle to respond to changes in the fluid motion, was determined using Eq. 6.2, giving the particle's response time to fluid flow.

$$t_o = \frac{\rho_d d_d^2}{18\mu_A} \tag{6.2}$$

where ρ_d is the particle density (kg m^{-3}), d_d is the particle diameter (m) and μ_A is the apparent viscosity (kg m^{-1} s^{-1}) of the fluid at $\dot{\gamma}$ = 10 s^{-1}. The value of Reynolds number, Re, for the flow in the partially filled DCM was determined using Eq. 6.3, the values in Table 6.1 show that the flow was laminar for all experiments (Re << 2000).

$$\mathrm{Re} = \frac{d_h \bar{u} \rho}{\mu_A} \tag{6.3}$$

where $\bar{u}$ is the flow velocity (m s^{-1}), d_h is the hydraulic diameter (m) and ρ is the fluid density (kg m^{-3}).

The data acquisition algorithm developed by the School of Physics (Leadbeater and Parker, 2009) provides the location of the particle in Cartesian co – coordinates at discrete time intervals. Repeated CPPWs were applied at a speed of 0.02 m s^{-1} with a 10 s time delay between them to ensure the fluid became static before the next CPPW occurred. Thus, one particle pass was considered as a complete travel of the tracer along the DCM tube. When the radioactive particle reached the very end of the tube, the tracer was collected and placed back inside the first segment. Then, a new series of CPPWs were applied. This procedure was repeated 30 times for each viscous media used.

6.2.4 PEPT data processing

The data were reconstructed to reflect the position of the radioactive tracer with respect to the DCM tube coordinates. Before starting the experiments, the tracer was positioned at the middle of the first segment, so that the *x*, *y* and *z* coordinates were obtained. In all experiments,

the particle was positioned approximately at the same starting point; i.e. x = 0 ± 0.002 m and y = 0 ± 0.003 m. However, in case of the neutrally buoyant particle, the zero position with regards the z axis was 5 ± 2 mm below the surface of the fluid. Subsequently, smoothing of the PEPT data was performed using the Savitzky-Golay smoothing/filter method (Savitzky and Golay, 1964) with 2nd order polynomial fitting, giving a low signal – to – noise ratio. Since both plastic particles had a characteristic dimension of 0.003 m, a minimum reasonable displacement along the tube (i.e. *x* axis) was considered to be 0.01 m. Thus, analysis of propulsive velocities in the DCM tube was performed using Eq. (6.4)

$$U_x = \frac{\Delta x}{\Delta t} \tag{6.4}$$

where Δx is for displacements ≥ 0.01 m.

Further statistical analysis of the velocities obtained as well as the residence times of the particle within each unit of the DCM tube was performed using the cumulative probability distribution function (CPDF) shown in Eq. 6.5 below.

$$CPDF_j = P_1 + P_2 \ldots + P_j \tag{6.5}$$

where (P_j) is the probability of the individual velocity data points to be within the range of the velocities. PEPT data the individual locations of the particle along the DCM tube (i.e. *x* axis) were split into 10 matrices reflecting the 10 units of the DCM. Thus, for example, the first matrix contains only the individual positions of the particle located within the width of the first unit $(i.e. 0 < x_i \leq 2cm)$ as well as the corresponding time points. Subsequently, the velocities were sorted out based on the positions of the particle found within the width of i^{th} unit and which had been used to calculate U_{x_i}. Thus, ten new matrices were obtained containing the velocities determined with in each unit. Then, the range of the velocity of the particle in each matrix is divided into equal increments, ΔU. The probability (P_j) of the individual velocity data points to be within the range of the velocities, was obtained by dividing the number of data

samples occurring in an increment by the total number of data samples. Therefore, the CPDF was calculated giving the probability that a velocity will be within the jth increment (Eq. 6.5).

In order to assess the mixing across the cross section area of the DCM tube, the distribution of the particle, as it moves through each unit, was visualized by condensing all the experimental data into a single 2D grid of $1x10^{-6}$ m^2 resolution. Then, counting of the passes of the particle from each cell of the grid was performed and presented in a data density plot.

6.2.5 Synchronization of PEPT data with DCM wall motion

The relationship between the wall motion and the movement of the radioactive particle was investigated. Synchronization of the PEPT data with the motility pattern of the flexible membrane of the DCM was performed by matching the sampling frequency of the PEPT system with the frame rate of the camera used to record the membrane motion. However, this was not a straight forward procedure since the acquisition frequency was not constant as it was dependent upon the radioactivity of the tracer and the probability of detection which varied with its spatial location (Guida et al., 2009).

The occlusion degree (73%) and rate (1.6 cm s^{-1}) as well as the time of the membrane to go back to the initial position (0.36 cm s^{-1}) were the same for all units. These values were obtained after capturing images of the cross section of a single unit of DCM during oscillations of the flexible membrane using a camera operating at a frame rate of 50 fps. A CPPW was produced by adding a time delay between the motions of each unit. Thus, knowing the position of the membrane of each unit every second, the acquisition frequency of the particle movements in its x coordinate was determined every second of the entire recording time. Giving a simple example, let's assume that at the first second the data points were 100 whereas in the next one the data points were 50. Thus, in the first case the total displacement of the membrane (i.e. 1.6 cm) was divided in 100 equal increments i.e. 0:0.016:1.6, whereas in the second case in 50 equal increments i.e. 0:0.032:1.6. Frames at different time points gave information about

the membrane status – motion and the corresponding behaviour of the particle; i.e. location as well as forward – backward movements. MATLAB R2015a (The MathWorks, Inc., Natick, MA) was used to perform image and data analysis.

6.2.6 Statistical analysis

Sigmaplot vs. 12.5 was used to perform statistical analysis of the PEPT data. Comparisons between multiple groups for non-normal and unequal size data were performed using Krustal – Wallis one way ANOVA on ranks. Differences were considered significant at $p < 0.05$.

6.3 Results

6.3.1 Velocity and residence time distribution within each unit of the DCM tube

Table 6.1 shows the relaxation times of the floating and neutrally buoyant (n.b) particle used in this study with respect to the relaxation times of the magnetic pill which was used to monitor *in vivo* colonic movements (Hiroz et al., 2009). The particle tracers used in this study had relaxation times an order of magnitude smaller than the magnetic pill. In particular, the floating particle had relaxation times of 0.059, 0.004 and 0.002 s whereas values for the n.b particle are 0.065, 0.005 and 0.003 s for L (8 mPa s), M (100 mPa s) and H (200 mPa s) fluids respectively. The magnetic pill had values of relaxation time of 0.4, 0.03, 0.015 s for L, M and H fluids respectively. The results showed that the particles used in this study, will more accurately describe the fluid flow for a wider range of viscosity than the magnetic pill. The pill used by Hiroz et al., (2009) might be expected to somewhat follow the flow only when the viscosity of the colonic fluids is sufficiently high.

Table 6.1. Rheological properties of the fluids used in PEPT experiments as well as relaxation times and range of the residence times of the floating and neutrally buoyant particle along the Dynamic Colon Model tube obtained in different viscous media.

									Residence times (s)	
Fluid	%NaCMC (w/w)	μ_A (m Pa s)	k (Pa s^{-n})	n	Re	t_o (s)			Floating particle	Neutrally buoyant particle
L	0.25	8	0.04	0.9	80	0.059^{+}	0.065^{++}	0.378^{+++}	$25^{a} – 125^{b}$	$50^{a} – 300^{b}$
M	0.50	106	0.20	0.7	5.6	0.004^{+}	0.005^{++}	0.028^{+++}	$50^{a} – 125^{b}$	$150^{a} – 300^{b}$
H	0.75	200	0.83	0.6	0.9	0.002^{+}	0.003^{++}	0.015^{+++}	$100^{a} – 125^{b}$	$175^{a} – 300^{b}$

[a] The low values correspond to the residence times observed in the 1st unit of DCM tube; [b] The high values correspond to the residence times obtained in the last unit of the tube; $^{+}t_o$: particle relaxation times (s) of floating particle; $^{++}t_o$: particle relaxation times (s) of neutrally buoyant particle; $^{+++}t_o$: particle relaxation times (s) of magnetic pill used in Hiroz et al., (2009).

Figure 6.2 shows the cumulative probability distribution function for the particle velocities and the residence times for both the floating and neutrally buoyant particles tracked within each unit respectively. High probabilities for positive velocities were obtained for both particles and for all the viscous media, demonstrating net forward propulsion of the fluids under antegrade CPPWs. However, as the viscosity increased, significant variations were noticed between the units (i.e. elements as indicated in the legend in Fig. 6.2). For example, unlike the low viscous media, L, in the medium, M and high, H apparent viscosity media, high variation was observed in CPDF values for velocities within the range 0 – 0.02 m s^{-1}; based on the data obtained for the floating particle (Fig. 6.2a1). Examining closely the data for the 6th – 10th units, the probability of velocities close to zero decreases below 60% but is significantly larger for velocities > 0.02 m s^{-1}. This implies a non-uniform distribution of the velocities on the surface of the fluid and along the tube. In addition, high velocities were observed mainly within the region of the DCM where the wave has grown sufficiently; i.e. after the 5th unit. In contrast, lower variation was observed in the probabilities for the neutrally buoyant (n.b) particle for the M and H media (Fig. 6.2a2). In particular, the probability for the floating particle to reach velocities of e.g. 0.02 m s^{-1} magnitude, varied between 57% – 100% and 60% – 96% for the M and H media, respectively. On the other hand, the corresponding probabilities for the n.b particle were found to be 85% – 95% and 85% – 98%. Thus, it is likely for the n.b particle to experience similar velocities in the most viscous media, H, regardless to its location along the tube. This implies a more uniform distribution of the velocities in the bulk fluid compared to the surface.

With regards to the residence times, significant differences were observed between the floating and the n.b particle. In particular, in fluid L, for a residence time of 150 s, a probability above 95% was observed for the floating particle independent of its location along the tube whereas the corresponding residence time for the n.b particle was found to be twice this value (i.e. 300 s). In fluid M the transit time for the floating particle was 125 s and the corresponding value for the n.b tracer was 250 s. In the case of fluid H the residence times for the floating and n.b particle were found to be 250 s and 300 s, respectively. Moreover, for fluids L and M higher variation of the probability distribution functions was observed between the units for residence times < 100 s (Fig. 6.2b1) compared to the n.b particle (Fig. 6.2b2). In contrast, for fluid H, similar residence times were obtained (i.e. 300 s) for probabilities >95% for both particles.

The overall result observed was that a wider range of residence times was obtained for the n.b particle compared to floating one for probabilities >80%, regardless of the media. In addition, the extreme limits of those ranges were higher for the n.b particle compared to the floating particle. These differences might be due to slightly lower relaxation times of floating particle, i.e. faster response to fluid flow and hence lower variation in residence times after each CPPW applied. In addition, the relocation of the n.b particle (i.e. either close to wall or close to the surface of the fluid) after every contraction of each unit could also be causing variation in the residence times, since the path of the n.b particle depends greatly upon its starting position.

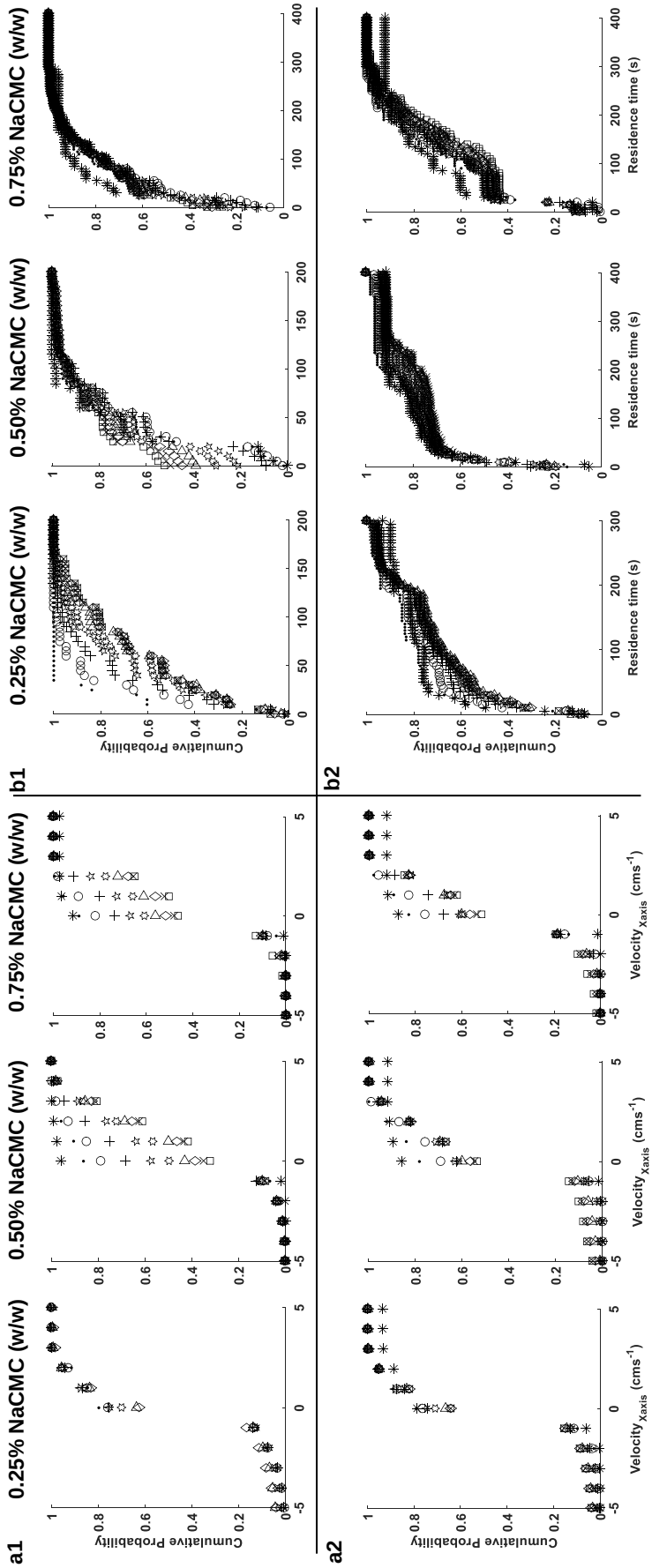

Figure 6.2. Cumulative probability – velocity per element for floating (a1) and neutrally buoyant (a2) particle and cumulative probability – velocity per element for floating (b1) and neutrally buoyant (b2) particle.

6.3.2 Assessing mixing in DCM model

Figure 6.3 shows the data density plots of the axial displacements of the floating and n.b particle in each of the media. In media L, the motion of the floating particle was limited around the centre of the DCM tube. This means that the particle follows the small changes in the level of the wave height during the wall motion without significant oscillations in the *y* and *z* directions. However, considering the wider area covered by the n.b particle, it seems that the mixing in the bulk fluid was more intensive.

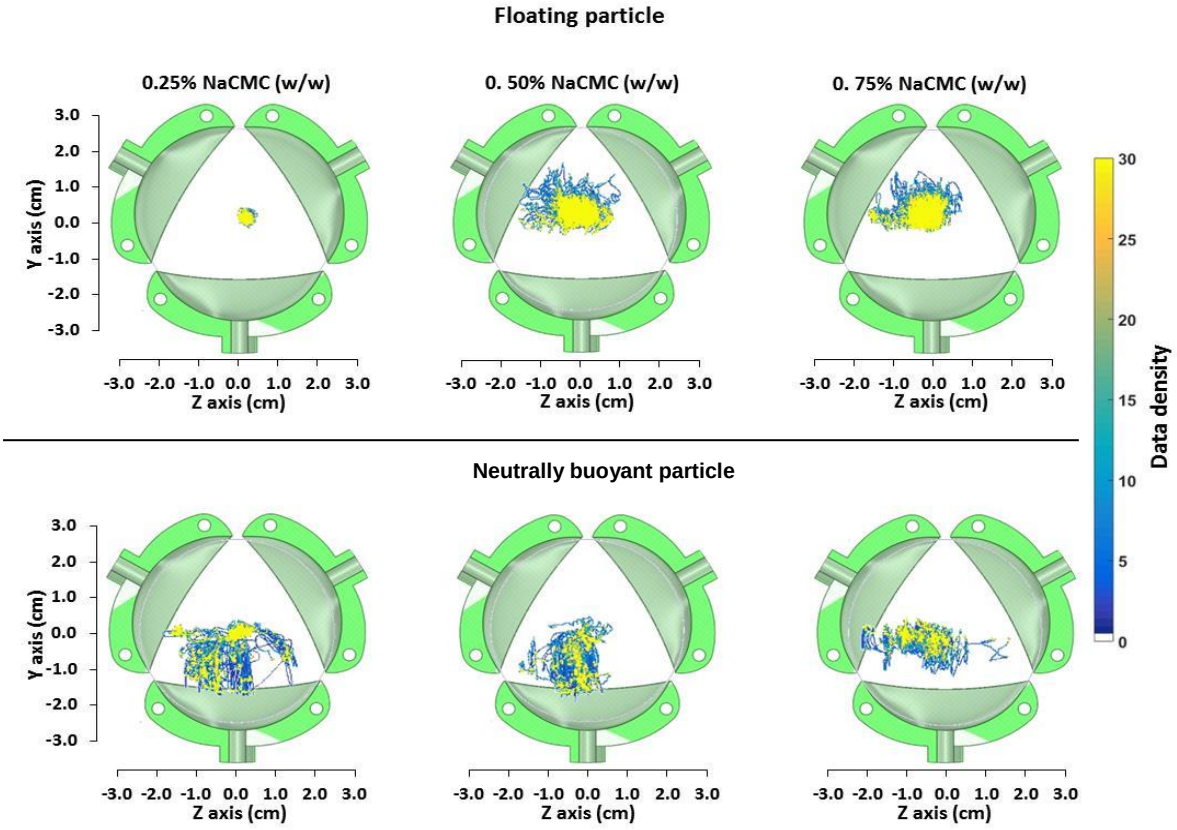

Figure 6.3. Data density of the axial displacements of floating and neutrally buoyant particle across the cross section of the Dynamic Colon model tube, in different viscous media.

However, increasing the apparent viscosity by using fluids M and H led to a significant change in the behaviour of the floating particle, with large oscillations observed. Indeed, in fluid L the movements of the floating particle around the centre of the tube were ±0.005 m in both axes whereas in fluid M and fluid H the oscillations were approximately ±0.01 m in the y direction and ±0.015 m in the z direction for both. It seems that for low viscosities the fluid is more prone to a sloshing motion whereas for high viscosities this motion is damped and the fluid moves in a plug – like manner (plug flow). This could explain why the values of the wave height for the M and H media were closer to the maximum displacement (0.012 m) of the membrane during the contraction.

In case of the n.b particle, the apparent viscosity seemed to affect the efficiency of the mixing of the bulk fluid, since a relatively smaller area was occupied by the tracer in the M and H media compared to fluid L. Unlike fluids L and M, the particle movements in fluid H were mainly close to the surface of the fluid and along the *z* axis whereas in the other two viscous media the tracer had almost reached the bottom of the haustrum. However, it must be noted that the behaviour of the n.b particle depends also on its location along the *y* and *z* axes after each propagating wave. Thus, if the n.b particle is located e.g. 0.005 – 0.01 m below the surface of the fluid and after a single or several waves it has been relocated closer to the surface, then it will follow different path compared to the circumstance in which the particle remains at its original depth. Indeed, the data for the n.b particle showed that a significant reallocation of the tracer occurred after the contraction of the first unit (Figure 6.4). However, in case of fluids L and M, the n.b particle remained sufficiently submerged in the fluid compared to fluid H.

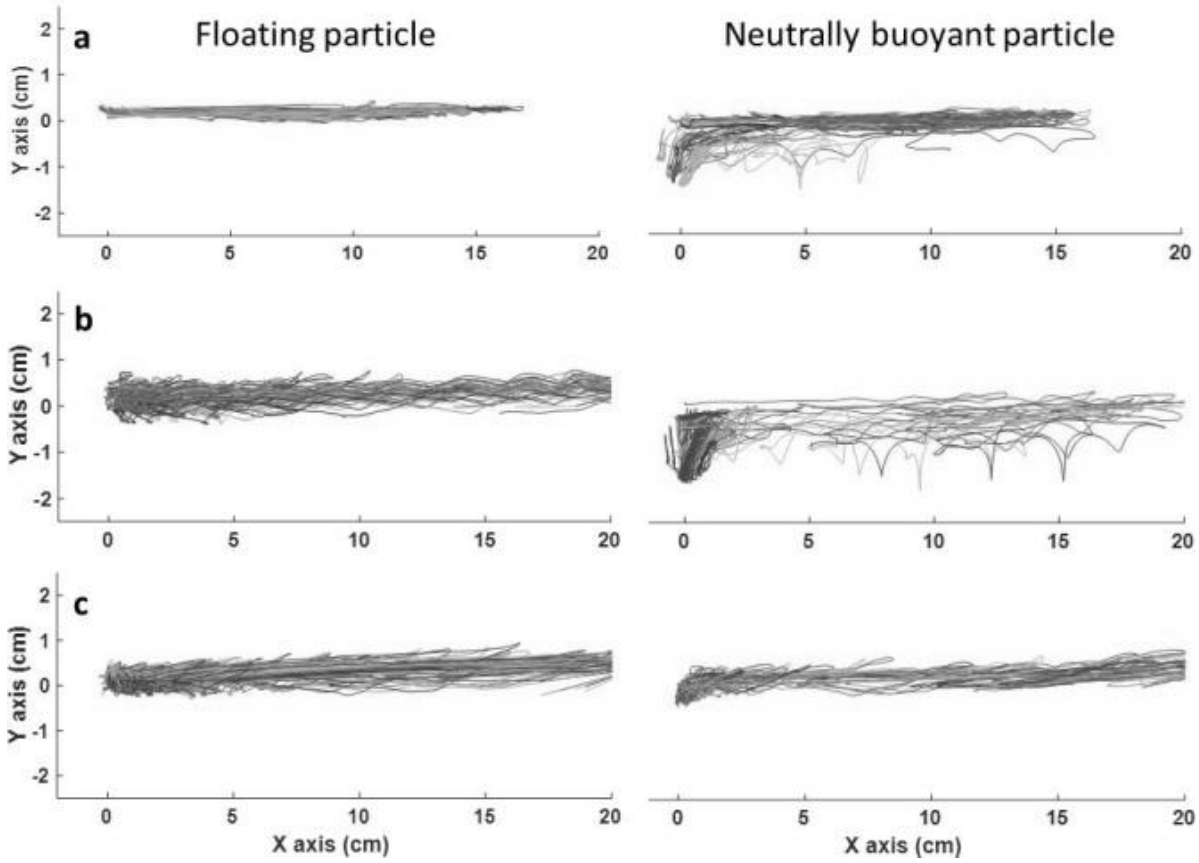

Figure 6.4. Plots of *y* and *x* axes of the floating and neutrally buoyant particle for all the individual passes of the tracer along the DCM tube.

6.3.3 Analysis of distances covered at different velocities

Previous *in vivo* analysis of the movements of the fluids of the colon using magnetic pill (Hiroz et al., 2009) revealed a large spectrum of distances covered at different velocities, however, their distribution was identical in both forward and backward directions. In this study, similar results were obtained. However, a direct comparison with the *in vivo* data is not straightforward since the particles in this study have relaxation times which are an order of magnitude smaller than those used in (Hiroz et al., 2009). In addition, the wall motion as well as the viscosity, the volume and the density of the fluid were predetermined and fixed in the experiments presented in this work in contrast to the dynamically changing *in vivo* colonic environment.

Figure 6.5 shows the distance covered by the tracer particles at different velocities, in both retrograde (negative velocity) and antegrade (positive velocity) directions. In fluid L for both floating and n.b particles a strong backflow is observed with similar magnitude to the forward motion; the distances covered at different velocities were within the same range 0.01 – 0.095 m. This was also revealed from the high negative velocities observed for both particles, reaching values ≈0.04 m s^{-1}. With regards to fluid M, the range of the distances for the floating particle covered in retrograde direction were within the range of 0.01 – 0.08 m for velocities between 0.002 – 0.015 m s^{-1} whereas the distances covered in antegrade direction were in the range of 0.01 – 0.18 m for velocities between 0.001 – 0.02 m s^{-1}. However, the n.b particle experienced a backflow similar to that observed for fluid L. In the case of fluid H, results showed the least backflow of the fluid with retrograde velocities of 0.002 – 0.01 m s^{-1} for the floating particle and 0.002 – 0.017 m s^{-1} for the n.b particle. The range of the antegrade displacements were between 0.01 – 0.19 m and 0.01 – 0.17 m for the floating and n.b particle, respectively. In addition, most retrograde displacements were < 0.05 cm for the floating and n.b particle, respectively. The maximum velocity for the antegrade displacements was analogous to the wave speed (0.02 m s^{-1}) with the only exception to be the data obtained in fluid H for the floating particle where the velocities were slightly higher than the wave speed (0.023 m s^{-1}).

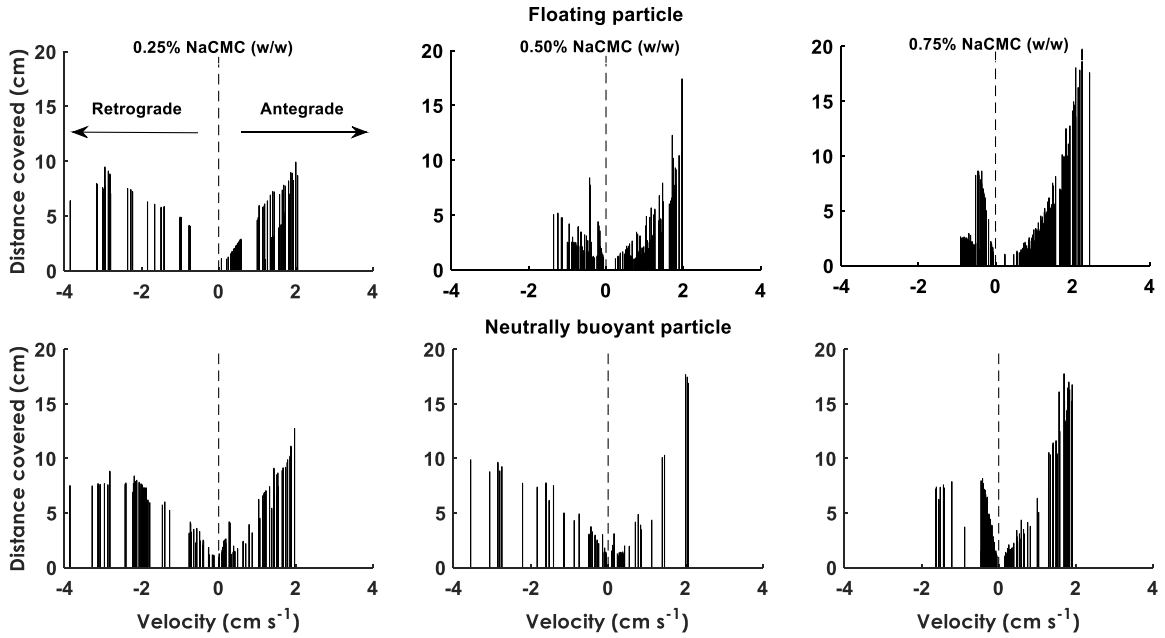

Figure 6.5. Analysis of distances covered at different velocities based on tracking data of the floating and neutrally buoyant particle obtained in different viscous media. Negative and positive velocities indicate the retrograde and antegrade motion of the particle, respectively.

6.3.4 Relationships between particle movements and wall motion

As already mentioned, previous *in vivo* studies have demonstrated contradictory correlation between the propagating pressure waves driven by the wall movement and the net movement of the colonic contents (Cook et al., 2000), despite improvements in the analytical techniques over time (Dinning et al., 2008). Thus, it is important to understand the relationship between the wall motion and movements of the contents. Hiroz et al. 2009 used magnetic pill tracking system to examine displacements of the colonic contents in healthy subjects; although, the authors did not compare the tracking data with manometry or scintigraphy. An alternative technique was implemented here in order to evaluate relationships between the wall motion of the flexible membrane of the DCM tube and the corresponding movements of a radioactive tracer. Thus, PEPT experiments were conducted in different apparent viscosities of NaCMC solutions.

Figures 6.6, 6.7 and 6.8 show the tracking data of the displacements of the floating and the n.b particle along the DCM tube (i.e. *x* axis) after every CPPW. In particular, every peak corresponds to a complete CPPW and each line to a single passing of the tracer before be positioned at the beginning of the DCM tube and new measured started. The tracking data showed that in some cases there was a 'to and fro' motion of the tracer for several CPPWs, before the particle moves gradually close to the very end of the tube whereas in other cases the particle needed just one and/or two CPPWs to cover the entire length of the DCM tube.

The number of the CPPWs needed in order the particle to cover the entire length of the DCM tube was estimated for all viscosities and for both particles (Figure 6.9). Statistical analysis showed that there was significant difference between the floating and the n.b particle in H fluid ($p<0.05$) but not in L and M fluids. In this case, it seems that in high viscosity fluid the effectiveness of the propulsion differed between the two particles with more CPPWs needed for the n.b particle. This is probably due to high variability (i.e. large standard deviation bars, Figure 6.9) of the data obtained for the number of CPPWs in L fluid resulting in no statistically significant difference between the two particles. This variation is most likely linked to the variability of the data with regards to the distance covered per wave in antegrade and retrograde direction (Figure 6.10).

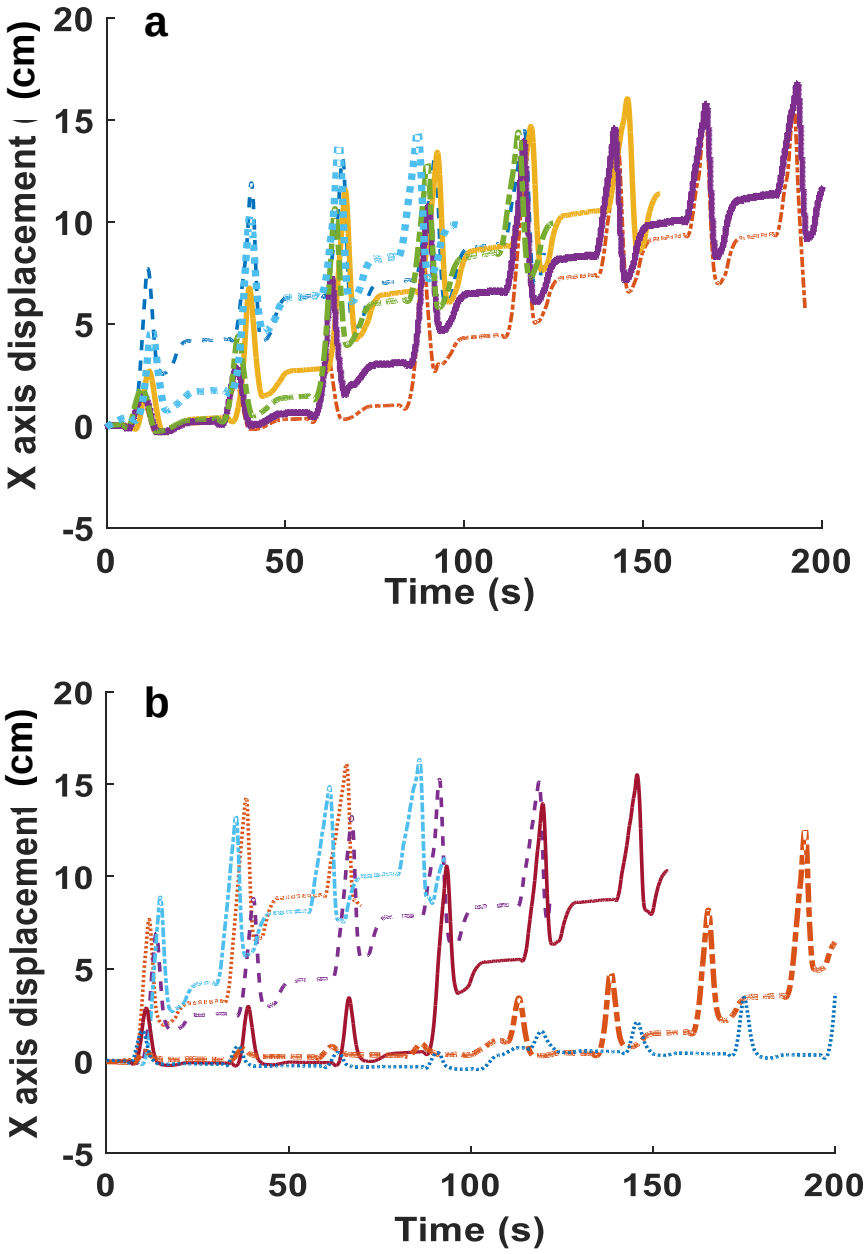

Figure 6.6. Plot of individual passes of the (a) floating particle and (b) neutrally buoyant particle along the DCM tube (*x* axis) in 0.25% NaCMC (w/w); every line represents one pass whereas each peak represents the motion of the particle in antegrade or retrograde direction after a single antegrade propagating wave (CPPW). The plateau between the peaks is the time delay of 10 s before the next CPPW applied.

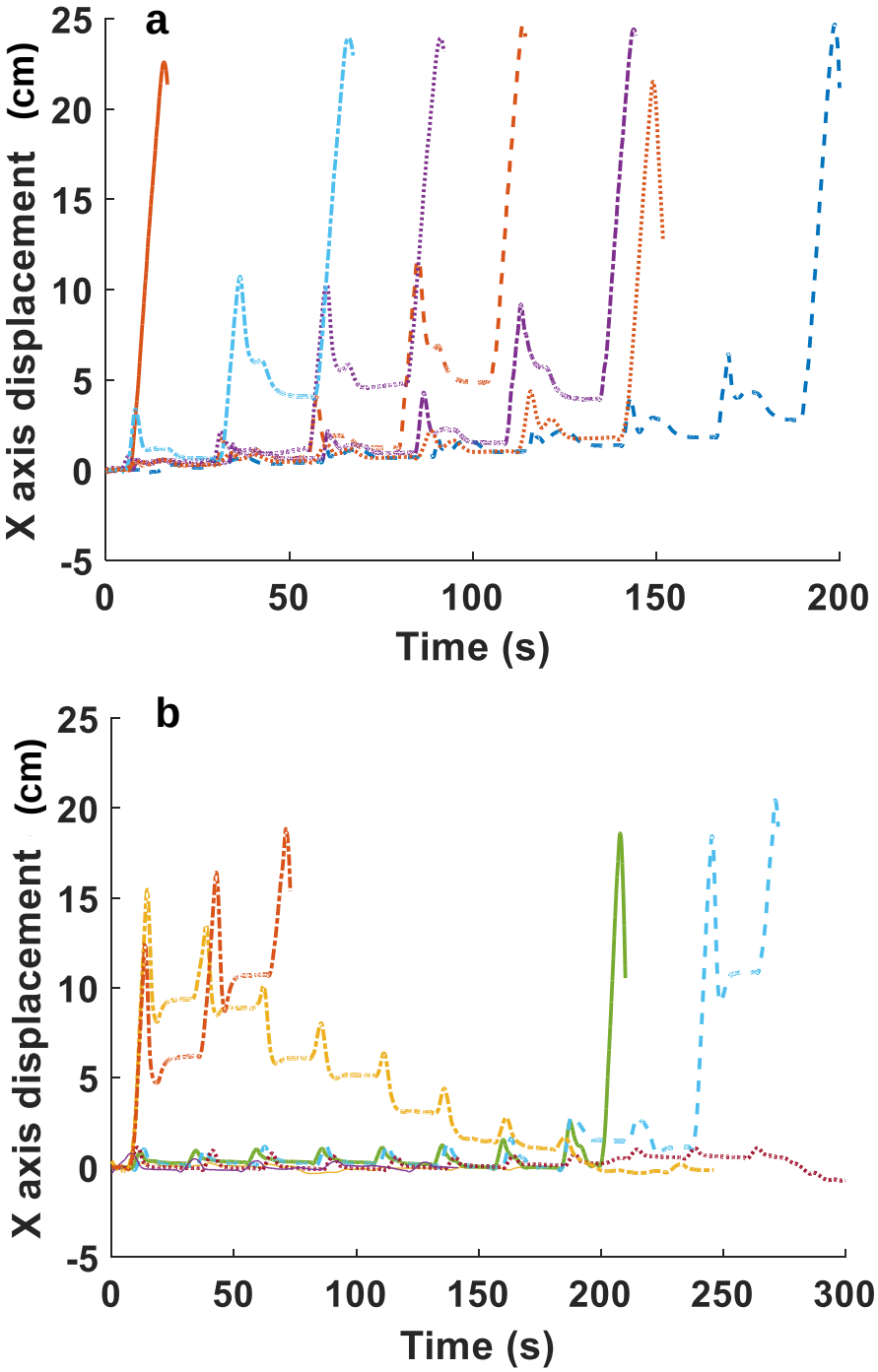

Figure 6.7. Plot of individual passes of the (a) floating particle and (b) neutrally buoyant particle along the DCM tube (*x* axis) in 0.50% NaCMC (w/w); every line represents one pass whereas each peak represents the motion of the particle in antegrade or retrograde direction after a single antegrade propagating wave (CPPW). The plateau between the peaks is the time delay of 10 s before the next CPPW applied.

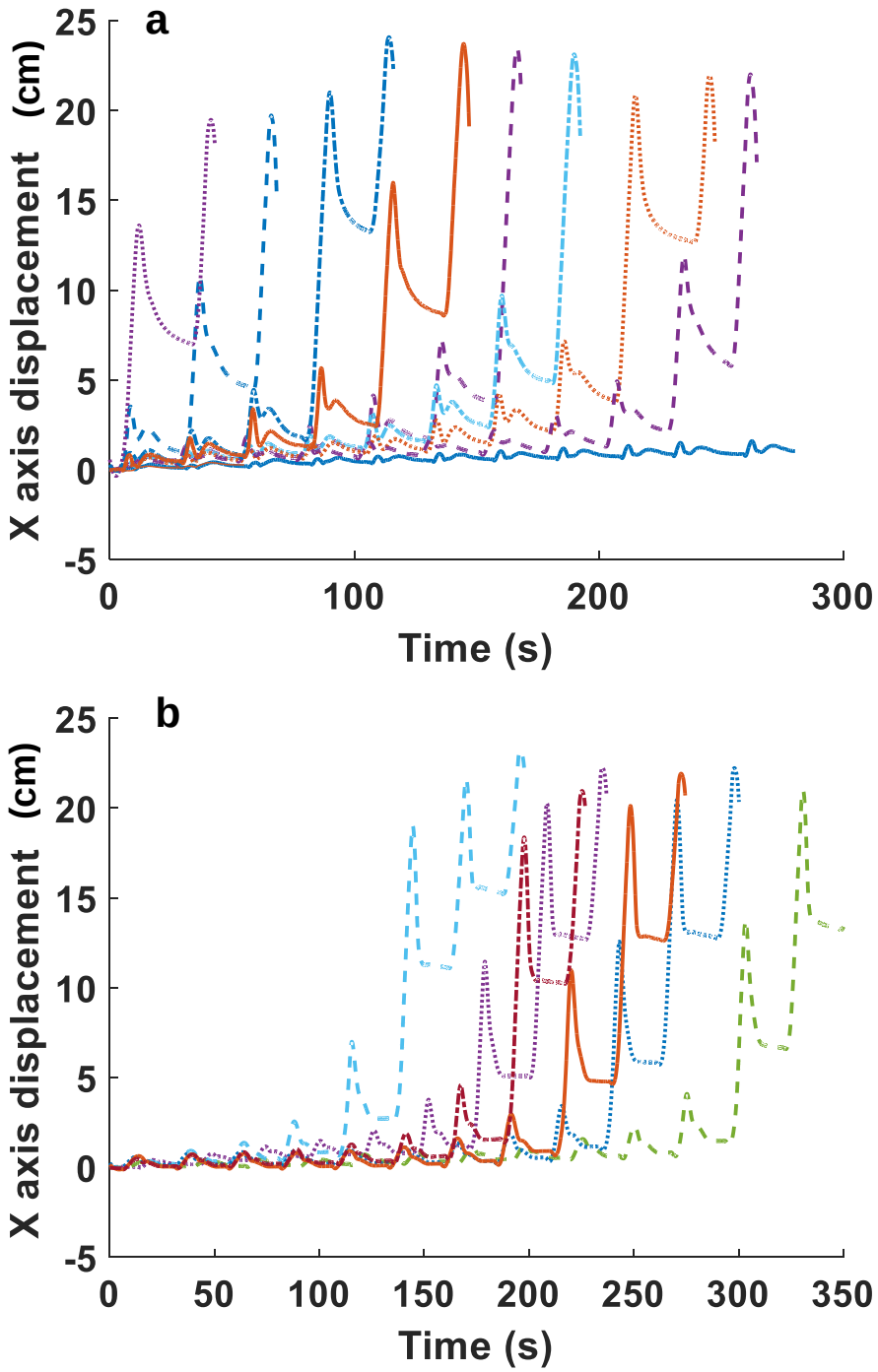

Figure 6.8. Plot of individual passes of the (a) floating particle and (b) neutrally buoyant particle along the DCM tube (*x* axis) in 0.75% NaCMC (w/w); every line represents one pass whereas each peak represents the motion of the particle in antegrade or retrograde direction after a single antegrade propagating wave (CPPW). The plateau between the peaks is the time delay of 10 s before the next CPPW applied.

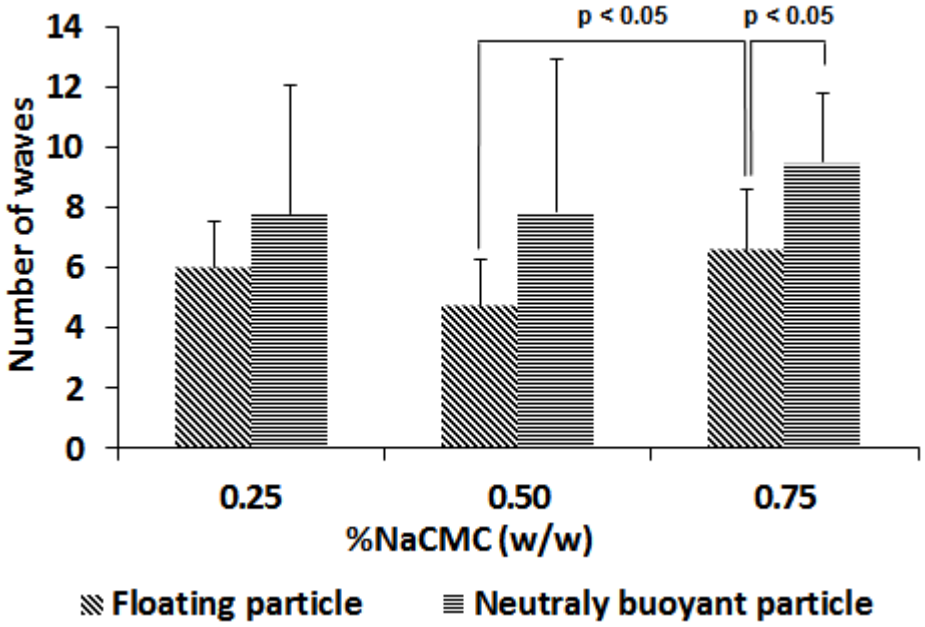

Figure 6.9. Mean values of the number of propagating waves needed for the particle to reach the very end of the tube; pp (polypropylene – floating particle); ps (polystyrene – neutrally buoyant particle); n=number of samples

Figure 6.10 shows the boxplots of the distance covered per wave for each particle and for each viscous media. The net transport (N.T) was within the range of 0.05 – 0.2 m, almost independent of the rheology of the fluid, but with slightly higher values in fluids M and H. However, there was a statistically significant difference between floating particle (0.053 m ±0.074) and n.b particle (0.026 m ±0.054) with regards to the net transport in M fluid. In general, the floating particle showed higher N.T per wave in all fluids compared to n.b particle. In particular, the average N.T values were 0.014 m ±0.019 and 0.049 m ±0.061 for L and H fluid, respectively, whereas the corresponding values for the n.b particle were 0.012 m ±0.023 and 0.037 m ±0.039.

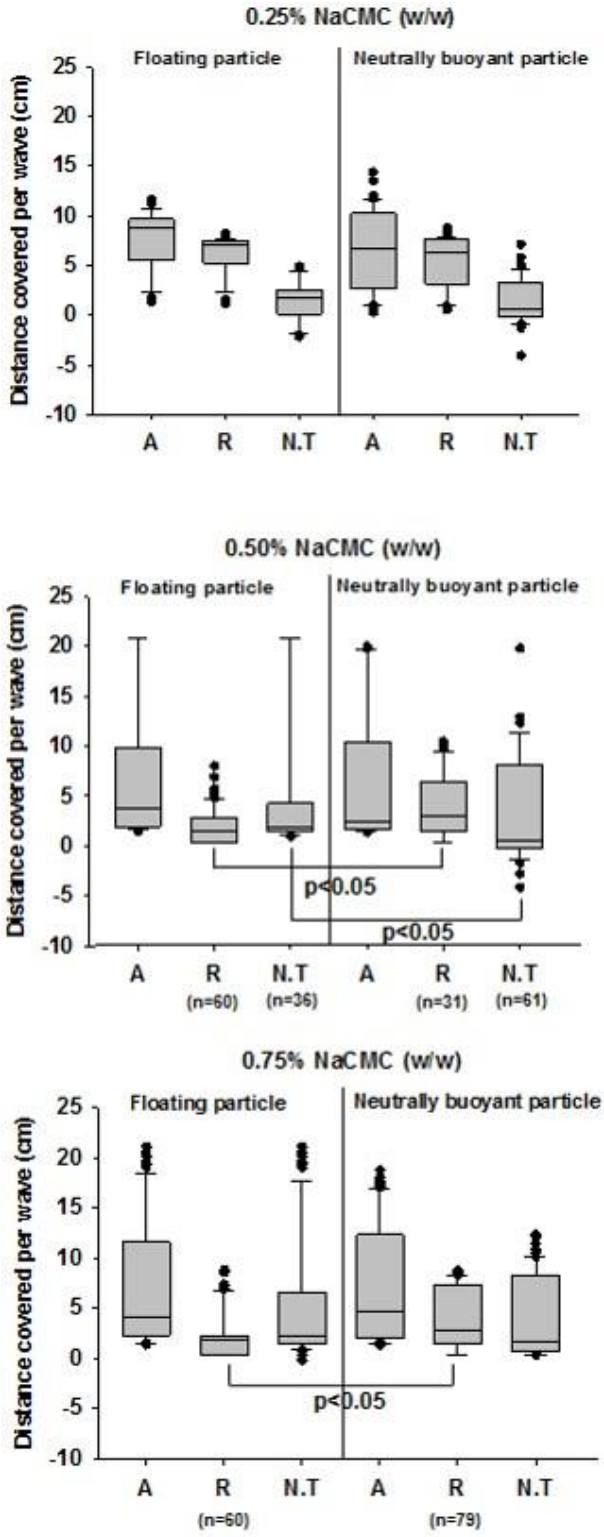

Figure 6.10. Box plots of distance covered per peristaltic wave in different viscous media (0.25%, 0.50% and 0.75% NaCMC(w/w); (A) anterograde motion, (R) retrograde motion and (N.T) net transport of the particle.

In case of L fluid, there was no statistically significant differences between the two particles with regards to the distance covered in antegrade and retrograde direction as well as in N.T per wave. This might explain why there was no also significant difference between the particles in the average number of CPPWs applied to cover the entire length of the DCM tube (Fig. 6.9). However, a no clear association could be found for the other two fluids. In M fluid, there was statistically significant difference ($p< 0.05$) between the particles with regards to the distance covered in retrograde direction as well as in N.T but not with the average number of CPPWs. In case of H fluid, statistically significant difference was found between the particles only with regards to the distance covered in retrograde direction but not in N.T. However, there was significant difference in the number of CPPWs applied. This unclear correlation might be related to the big variation in the data with regards the antegrade distance covered per wave, especially in M and H fluid, resulting in big variation on the number of CPPWs per pass. Indeed, the boxplots showed that the antegrade displacement of the floating particle varied 2 – 12 cm, 2 – 21 cm and 3 – 20 cm in L, M and H fluid, respectively. This means, as mentioned above, that in some cases the particle will need several CPPWs to reach the end of the tube and in some other case just one. This uncertainty of the results might be linked to the relationships between the motion of the membrane and the corresponding location of the particle. Thus, during the contraction/relaxation of the membrane, if the particle is located before, within or after the contraction point, it is possible to affect the effectiveness of the transit of the particles.

Figures 6.11 and 6.12 show the series of frames indicating the status of the membrane and the direction of its movement for each unit as well as the extension of the propagating wave with the corresponding location of the n.b particle. The red bars refer to the stage of the membrane between the neutral position (indicated with capital letter N) and the contraction (indicated with capital letter C) whereas green bars refer to the stage of the membrane between the neutral and the relaxed position (indicated with capital letter R). The arrows indicate the direction of the motion of the membrane; i.e. either towards the relaxation point or

back to neutral position. These frames represent three different cases where different distances covered per CPPW. These examples illustrate how the extension of the propagating wave and the corresponding location of the particle can be not strongly related.

In the first case (Figure 6.11a), the particle moves forward in the first two frames following the front of the antegrade propagating wave. However, in the third frame, the particle is seen to return to its initial position while the wave travels towards the very end of the tube. In the last frame, a small forward displacement of the particle was observed after the completion of the wave. Thus, the net transport in this case was ≈ 0.01 m whilst the wave travelled a distance of 0.2 m. In the second case (Figure 6.11b), the particle followed the wave for a longer distance, covering the 62% of the total DCM tube length before moving back, covering a distance of 0.075 m in the retrograde direction and ending up in the second unit. A small net forward displacement of 0.057 m, greater than that for the first case, occurred after the wave reached the end of the tube. In the third case (Figure 6.11c) the particle travels with the wave for 0.065 m before moving in retrograde direction, with a net transport of 0.02 m.

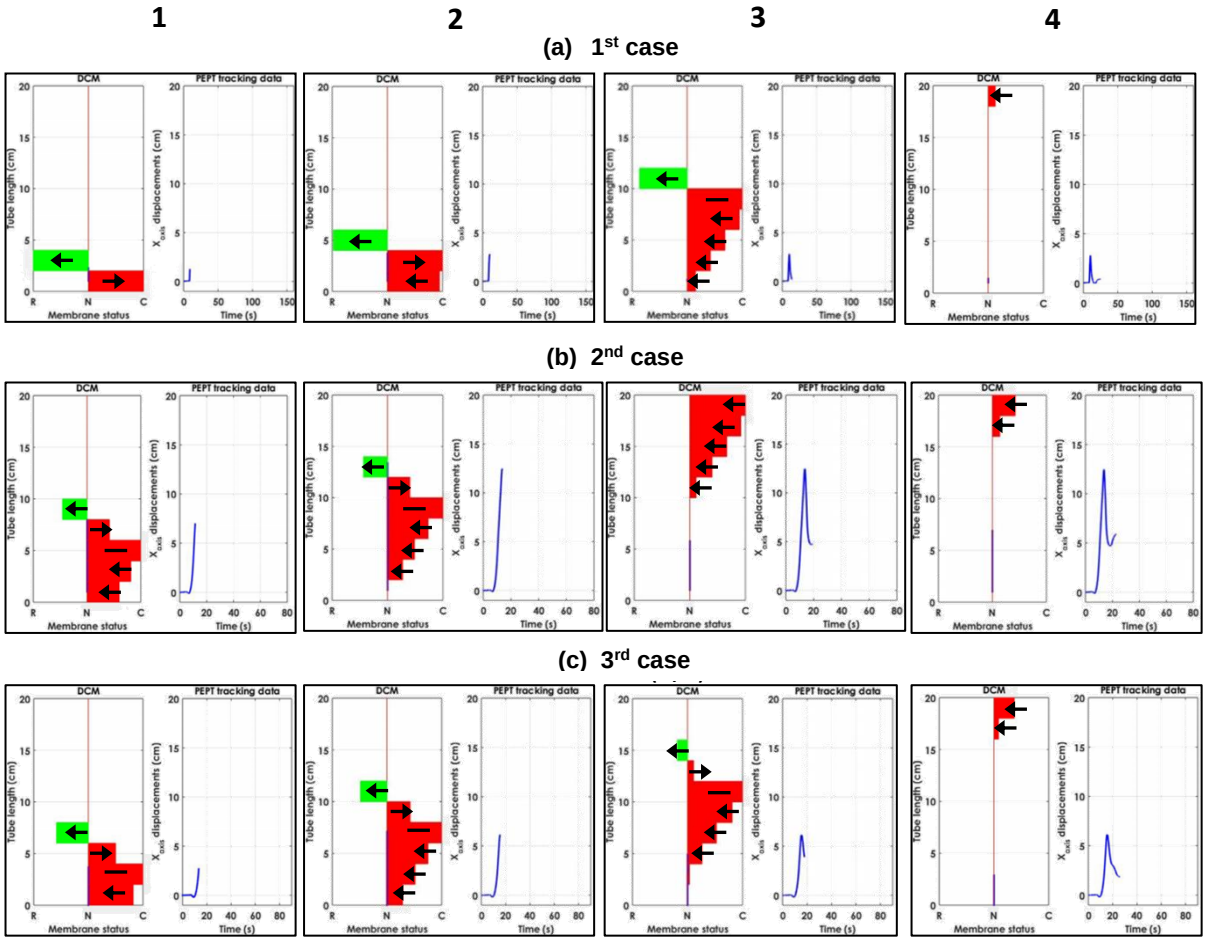

Figure 6.11. Series of four frames of a single antegrade wave, showing the relationship between the wall motions of the DCM tube and the movements of the radioactive tracer in L media. Membrane travels both from the neutral position (N) towards the contraction (C) or relaxation (R) position and vice versa as indicated by the arrows. The solid line represents the steady period of 1 s of the membrane before travel back to the neutral position.

Figure 6.12 shows the frames for the second CPPW which was applied 10 s after the first. For the first case (Figure 6.12a), the particle covered a longer distance with a net forward transport of 2.5 cm. For the second case (Figure 6.12b), the particle was located after the third unit of the DCM and it was always 2 – 3 cm ahead of the wave front. Thus, the particle covered a distance of 10 cm before moving backwards resulting in a net forward transport of 3 cm. With regards to the third case (Figure 6.12c), the n.b particle travelled almost the entire length

of the tube before it moved backwards due to the backflow. In this case the net transport was 0.09 m. There was no antegrade displacement of the particle after the accomplishment of the CPPW, as indicated in the fourth frame, although, it was observed in the other two cases. This short forward displacement of the particle occurred always after the completion of the CPPW and may imply that there was a “to and fro” fluid motion across the entire length of the tube. This motion moves firstly in retrograde direction along the entire length of the DCM tube and then again in the antegrade direction causing a small forward displacement to the particle. However, this “to and fro” motion was weaker in the fluid H; refer to Figure 6.8 and compare with L (Figure 6.6) and M fluid (Figure 6.7).

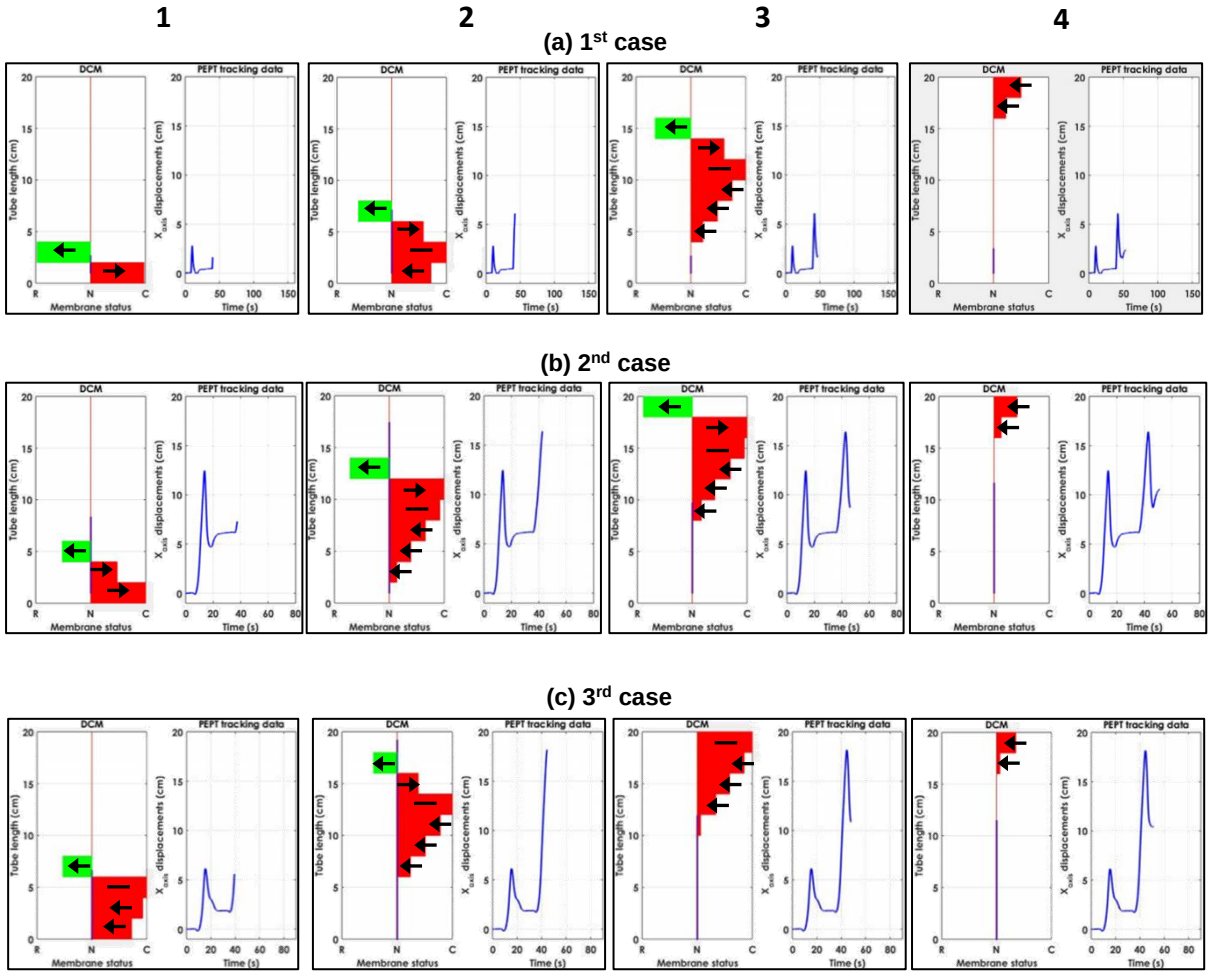

Figure 6.12. Series of four frames of the second antegrade wave applied after 10 s from the first wave. Relationship is presented between the wall motions of the DCM tube and the movements of the radioactive tracer in different viscous media. Membrane can travel both from the neutral position (N) towards the contraction (C) or relaxation (R) position and vice versa as indicated by the arrows. The solid line represents the steady period of for 1 s of the membrane before travel back to the neutral position.

6.4 Discussion

A novel biomechanical engineering model of the human proximal colon was used to assess the mixing under antegrade CPPWs by tracking the displacements of a radioactive tracer in three dimensions. Relationships between the particle movements and the wall motion of the DCM tube were also examined. The advantage of using an *in vitr*o model is that parameters such as motility pattern, viscosity, volume of fluids and properties of the tracking particles can be predetermined and controlled during the experiment. This allows assessment of the interplay between these parameters and how they affect the mixing and propulsion of the fluids in proximal colon. However, this is not possible in *in vivo* studies due to lack of control and constant change in the colonic environment. For example, the rheological properties of the colonic fluids will change in terms of viscosity as a function of time since the dewatering process occurs at the rate of 2.7 ± 0.3 mL min^{-1} (Palma et al., 1981). Moreover, as the results showed, the viscosity might affect the propulsion of the fluids causing variability on the movements of the particles. However, the effect of the viscosity should be assessed in relation to the location of the particle linked to the wall motion. This means that, even if the particle is front of the contraction point, it likely that the particle will follow the CPPW for short distances in low viscosity fluid, as indicated in most cases of the individual passes (Figure 6.6) and which can be related to the first case in Figures 6.11a and 6.12a. In contrast, if the viscosity of the fluid is high and the particle has the desired position with respect to the contraction point, it is likely to follow the CPPW for much longer distances as indicated in several cases for M (Figure 6.7) and H fluid (Figure 6.8). However, this is not the case for the n.b particle for L and M fluids where a mixture of different patterns appeared even in case where the particle was ahead to the first units of the DCM tube after the CPPW had ended. Another parameter which complicates the relationships between particle displacements and wall motion, is the relocation of the particle along the vertical axis (Y axis) of the DCM tube, i.e. displacement close to the wall or close to the surface of the fluid, the flow field will be different; see the individual passes of the two particles as presented in Figure 6.4 and Figure 6.5 in which the

path that the particles followed is not the same for each run even when the particle was placed more or less at the same location at the beginning of each run.

The motion of the wall was well controlled and with fixed viscosity of the fluid, hence, the pressure force profile for each repeated CPPW was constant. However, as the series of PEPT experiments showed, the location and the properties of the particle used to track the propulsion of the fluids made the interpretation of the fluid flow more complicated. This demonstrates why correlation of pressure waves monitored with manometry *in vivo* and colonic movements is not an easy task. However, more passes of each particle for all the fluids are needed to fully describe the flow field. However, in this first analysis valuable information was obtained of what might cause variations in the tracking data from *in vivo* studies; since the passes per subject (only one per subject) and the total number of subjects (n=20) used are limited in *in vivo* studies (Hiroz et al., 2009).

However, the above observations might explain several phenomena which occur within the human proximal colon. As the wave ends before the end of the DCM tube (i.e. the rigid siphon), leading to backflow, the same occurrences could be observed in the *in vivo* proximal colon since the majority of the propagating waves are of short extension (Dinning et al., 2008, Bampton et al., 2000) (i.e. before the hepatic flexure). This could also explain why in the *in vivo* studies, over the half of the identified flow episodes occurred in the absence of the pressure waves. Thus, apart from the low sensitivity of manometry which occurs when the gut's diameter exceeds 0.056 m (Von Der Ohe et al., 1994), the gravity causes flow which is not correlated with the wall motion, which may also explain the reduced association between flow and pressure waves in proximal colon.

Different results were obtained when different particles were used to monitor fluid flow. In particular, it seemed that the residence times of the n.b particle were much higher compared to those of the floating particle. Thus, for example, transit times recorded *in vivo*, could vary significantly not only due to differences among the volunteers but also due to the different behaviour of the particles used to monitor the colonic movements, for example, in the case of

the magnetic pill tracking system (Hiroz et al., 2009). This is also important to understand possible changes in the residence times of particles, agglomerates and intact tablets (or tablet fragments/particles) of different dosage forms which are designed to reach the colon.

Assuming the particles are following the fluid motion, enables an Eulerian analysis of the mixing across the cross section of the DCM tube to be carried out. This showed that the mixing is more intensive if the n.b particle is used as a reference, although it gets less efficient as the viscosity is increased (refer to Figure 6.5). Thus, increasing the apparent viscosity might promote to some extent the propulsion of the fluids but does not promote mixing in the radial direction. However, it must be noted that the efficiency of the mixing should be carefully assessed since the location of the particle along the y axis is critical in defining which path the particle will follow and hence more passes of the particle need to be obtained in order to map the entire flow field in the DCM tube. Thus, if the n.b particle is relocated close to the surface of the fluid after the contraction of the first unit without having the time to be efficiently re-submerged, then it will remain close to the surface and it will mainly move along the *z* axis; this is mainly the case for the most viscous media (fluid H). This could be also the case for dosage forms where the lighter agglomerates – particles, formed from the partial disintegration of the formulation, will reach a different level in the DCM tube.

It should note that information about how particles with bioadhesive properties would interact with the DCM wall, as in the human colon, cannot be obtained in this stage. Hence characterization of the mixing of this type of particles could probably give a wider spectrum with regards to behaviour of these particle under colon wall motion. However, this a very challenging task since the turnover of the mucus layer would probably affect also the motion of the particles close to the surface and possibly their redistribution in the bulk fluid. This task would be interesting to be investigated but it's beyond the scope of this work.

The velocities experienced by the particles during the wall motion of the DCM tube never exceed 0.022 m s^{-1} for antegrade displacements, which are relatively close to values reported in *in vivo* studies i.e. 0.017 m s^{-1} (Hiroz et al., 2009). However, velocities as high as 0.04 m s^{-}

[1] were observed for the retrograde displacements of the particles. These values are higher than those observed using the magnetic pill *in vivo* and are most probably due to the shorter particle relaxation times in this study.

The relaxation times showed that for fluid L both particles would need more time to respond to flow compared to much shorter times in M and H fluid, respectively. However, floating and n.b particle will follow the fluid motion in all fluids with higher accuracy in M and H media. The higher particle relaxation time and the stronger backflow in L fluid might explain why there was not good correlation between the wall motion and the particle displacements as well as why no significant differences were observed between the range of the velocities in both retrograde and antegrade direction for both particles. This might also be the reason why there were no significant variations in the probabilities of the velocities that the particles would experience between the units of the DCM tube. These observations are very important in order to correctly assess the propulsion of the contents in the human colon and especially in the proximal region. In particular, the magnetic pill used in (Hiroz et al., 2009) will fail to accurately describe the movements of the contents unless the viscosity of the fluids would be sufficiently high. Therefore, the hypothesis that the magnetic pill follows the luminal contents accurately should be applied with caution.

6.5 Conclusions

In the present study, the novel biorelevant model of the proximal colon was used to examine how the flow and the mixing of the colonic fluids will be affected by the interplay between wall motion, viscosity and the properties of the particle used to monitor fluid movements. The proposed *in vitro* model allowed understanding the relationships between the wall motion and the propulsion of fluids which are affected by the viscosity, the location of the particle and the strong backflow caused by the gravity effect after the wave has passed. Different results can be obtained in terms of velocities and residence times by changing the particle used as

reference for analysing the fluid motion. In general, high velocities and longer retrograde displacements were observed for the floating particle which is also controlled by the viscosity of the fluids. These differences also reflected how accurately the particle describes the fluid motion, since small relaxation times were obtained for different viscous media. In addition, it seems that the viscosity promotes the propulsion of fluids; provided that the particle has the desired location with respect to the contraction point.

Furthermore, flow episodes can occur which are not related to the wall motion. A large variation in the data for the total number of the propagating waves needed for the particle to reach the very end of the tube was obtained demonstrating that the short extent waves, the viscosity, the position of the particle and the reflux of the fluids strongly influence the transit of the contents.

The *in vitro* observations might help to explain *in vivo* phenomena, using the proposed Dynamic Colon Model for assessing different parameters which are difficult if not impossible to be determined or controlled during *in vivo* experiments. In addition, this work could be potentially extended to examine different motility patterns which reflect a disease state of the colon such as diarrhoea and constipation. Furthermore, different fluid volumes should also be examined reflecting the fasted and fed state in the colon.

Abbreviations

DCM	Dynamic Colon Model
GI	Gastrointestinal
HCl	Hydrochloric acid
NaCMC	Sodium carboxymethylcellulose
PET	Positron Emission Tomography
PSs	Propagating Sequences
S	Sampling Point
TIM-2	TNO Colon simulator
TNO	Nederlandse Organisatie voor Toegepast
USP	United States Pharmacopeia

7 Dissolution profile of theophylline modified release tablets, using a biorelevant Dynamic Colon Model (DCM)[3]

Abstract

The human proximal colon has been considered a favourable site to deliver drugs for local and systemic treatments. However, modified dosage forms face a complex and dynamically changing colonic environment. Therefore, it has been realized that in addition to the use of biorelevant media, the hydrodynamics also need to be reproduced to create a powerful *in vitro* dissolution model to enable *in vivo* performance of the dosage forms to be predicted.

The novel biorelevant Dynamic Colon Model (DCM) has been developed which provides a realistic environment in terms of the architecture of the smooth muscle, the physical pressures and the motility patterns occurring in the proximal human colon.

The dissolution profile and the distribution of the highly soluble drug, theophylline, was assessed by collecting samples at different locations along the DCM tube. Differences in the release rates of the drug were observed which were affected by the sampling point location, the viscosity of the fluid and the mixing within the DCM tube. Images of the overall convective motion of the fluid inside the DCM tube obtained using Positron Emission Tomography enabled relation of the distribution of the tracer to likely areas of high and low concentrations of the theophylline drug.

This information provides improved understanding of how phenomena such as supersaturation and precipitation of the drug during the passage of the dosage form through the proximal colon.

[3] Stamatopoulos, K., Batchelor, H. & Simmons, M. J. H. 2016. European Journal of Pharmaceutics and Biopharmaceutics, 108, 9-17.

7.1 Introduction

The environment of the human colon is considered favourable for systemic and local delivery of drugs (Antonin et al., 1996, Tozaki et al., 1997). The neutral pH, the reduced digestive enzymatic activity and the much longer transit times compared to the upper gastrointestinal (GI) tract (Sinha and Kumria, 2003), makes the colon an attractive site for drug delivery.

Predictive dissolution methods can contribute to a reduction in or refinement of *in vivo* studies during the design, development and evaluation of drug delivery systems. Thus, the establishment of an *in vivo*-*in vitro* correlation is of great importance. Temperature, pH, ionic strength, buffer capacity, present of surfactants and or digestive enzymes, greatly influence the release of the drug from modified-release dosage forms (Garbacz et al., 2008). However, it has been realised that both physicochemical characteristics of the gastrointestinal fluids as well as hydrodynamics need to be reproduced in order to make a powerful *in vitro* model to predict *in vivo* performance (Garbacz et al., 2008, Garbacz and Klein, 2012, Fotaki et al., 2009a). Existing compendial dissolution methods oversimplify the complex and dynamic environment of the human colon (Spratt et al., 2005). Thus, apart from the application of the biorelevant media in the dissolution methods (Schellekens et al., 2007, Jantratid et al., 2009, Klein, 2010, Jantratid et al., 2008, Wagner et al., 2012), attempts have been made to improve the bio-relevance of the hydrodynamic and mechanical conditions in dissolution methods (Klančar et al., 2013, Abrahamsson et al., 2005, Thuenemann et al., 2015, Garbacz et al., 2008, Blanquet et al., 2004).

Advances in manometry (Dinning et al., 2014a) and in non-invasive monitoring systems (Hiroz et al., 2009, Rao et al., 2009) have provided insights on colon motility and transit times; demonstrating the complex and dynamic environment that a modified dosage form is exposed to during its passage through the lower GI tract. Five types of propagating motor patterns have been identified by use of high – resolution fibre – optic manometry (Dinning et al., 2014a). Four of them (cyclic motor, short single, long single and occasional retrograde motor pattern) are related to low – amplitude propagating sequences (range of average values: 2 – 10 mmHg)

and form the majority of the motility events (Dinning et al., 2014a). The remaining pattern forms high – amplitude propagating sequences (PSs) (>116 mmHg) (Dinning et al., 2014a). The low – amplitude PSs were as likely to be associated with colonic movements as high - amplitude PSs (Dinning et al., 2008). However, the low – amplitude PSs seem to be related mainly to the mixing of fluids (segmentation) (Gabrio Bassotti, 1999) whereas high – amplitude PSs cause mass movements (peristalsis) of the colonic fluids (Bharucha, 2012). However, the pressure signal of the catheter is affected by the viscosity of the colonic fluids (Arkwright et al., 2013). Arkwright et al, (Arkwright et al., 2013) showed that the predetermined amplitude of the applied pressure on a flexible wall was not the same as the pressure measured by the catheter placed inside the elastic tube filled with viscous lumen. Thus, *in vitro* models should take this into consideration. Otherwise, it is likely that the applied pressures in the lumen by the flexible tube, like in case of the large intestine simulator TIM-2 (Venema, 2015), will not accurately reflect the physical amplitudes.

In vivo studies of the human colon have shown that other factors, in addition to the PSs, affect the propulsion and the mixing of the colonic fluids (Dinning et al., 2008). The travel distance of the PSs, the viscosity (Proano et al., 1990) and the reflux of 50% of the bolus, slow the propulsion of the fluids (Dinning et al., 2008). Thus, the mixing of the colonic fluids is served with the combination of these parameters causing ‘to and fro’ motion of the contents.

Apart from the use of biorelevant media, the proper simulation of the hydrodynamics in proximal colon should be performed via the reproduction of the architecture of the colon. Moreover, the volume and the spread of the fluids will also affect the dissolution and the distribution of the drug along the proximal colon. The distribution of the drug could be also considered as a parameter which might determine the fraction of the absorptive surface area of the colon wall on which the drug will be exposed. Thus, it is also critical to understand how colon motility influences not only the dissolution profile but also the distribution of the drug within the proximal colon.

The aim of this study was to use the developed computer – controlled Dynamic Colon Model (DCM), in order to understand the colonic behaviour of an extended release oral dosage form exposed to a more realistic colonic environment. The model was designed to reproduce the anatomy and propagating motor patterns within the human proximal colon. A solid phase catheter was used to monitor the pressure forces generated by the wall motion within the DCM and Positron Emission Tomography (PET) was used to visualize the overall convection of fluids. The dissolution behaviour of an extended release dosage form (theophylline) was assessed in different viscous media within the DCM; the different media represented the dewatering process which takes place in the human colon.

7.2 Materials and methods

7.2.1 Materials

Sodium carboxymethylcellulose (NaCMC) of 90000 and 700000 molecular weight was purchased from Sigma (St., Louis, USA). Theophylline anhydrous and potato starch were bought from Acros Organics (Loughborough, UK). Sodium hydroxide, hydrochloric acid (1M) and potassium hydrogen (KH_2PO_4)- and dihydrogen phosphate (K_2HPO_4) were purchased from Sigma (St., Louis, USA). The radioactive solution of radionuclide ^{18}F, used in PET experiments, was provided from the School of Physics and Astronomy of the University of Birmingham, UK.

7.2.2 Dissolution experiments

The dissolution profile of the theophylline released from the NaCMC(90000) based tablet was assessed in different viscous media and under a fixed motion of DCM flexible wall which was engineered to mimic the main motility pattern observed in human proximal colon. The tablet was directly introduced into the prefilled DCM tube; assuming that the dosage form reached the human colon intact. This approach is not far from the reality since studies have shown that colon-specific coated formulations reach the lower GI tract intact (Amidon et al., 2015b).

The preparation of the tablets was performed as described in section 2.9.3.

The dissolution experiments were set up based on two assumptions: (i) the DCM tube was placed horizontally in accordance to the normal reclining position of patients during manometric, scintigraphy and MRI procedures; (ii) it is assumed that the DCM operates in the fed state in which more propagating sequences of pressure waves are taking place in proximal colon (Dinning et al., 2014a). The DCM tube was filled to 50% full which corresponds to 100 mL of NaCMC $_{(700000)}$ using solutions with different concentrations (0.25 and 0.50%, w/w). This volume was chosen in order to compare the results with the published data obtained from the mini volume USP 2 (Stamatopoulos et al., 2015). In addition, 100 mL is close to the overall volume that a dosage form is likely to be exposed to during its passage through the human colon (McConnell et al., 2008).

The frequency of the pressure events during the dissolution test was set up to represent values within the human colon previously reported in the literature (Dinning et al., 2008). Thus, the total duration time of the dissolution experiments was selected to be 560 min and every 5 min an CPPW was applied. Samples were collected from three different locations: at the beginning (S1), in the middle (S2) and at the end (S3) of the DCM tube (Figure 7.1) in order to evaluate the distribution of the released drug. The samples were collected at predetermined time intervals (5, 10, 30, 60, 120, 240, 360, 480 and 560 min). Subsequently, all the samples were passed through a 0.4 μm PTFE filter (Stamatopoulos et al., 2015) prior to the quantitative analysis of theophylline which was performed using UV analysis according to Stamatopoulos et al. (Stamatopoulos et al., 2015). The temperature during the dissolution experiments was maintained at 37 ^{o}C using a 300W infrared ceramic lamp. The volume of the medium removed at each time point was replaced with fresh media.

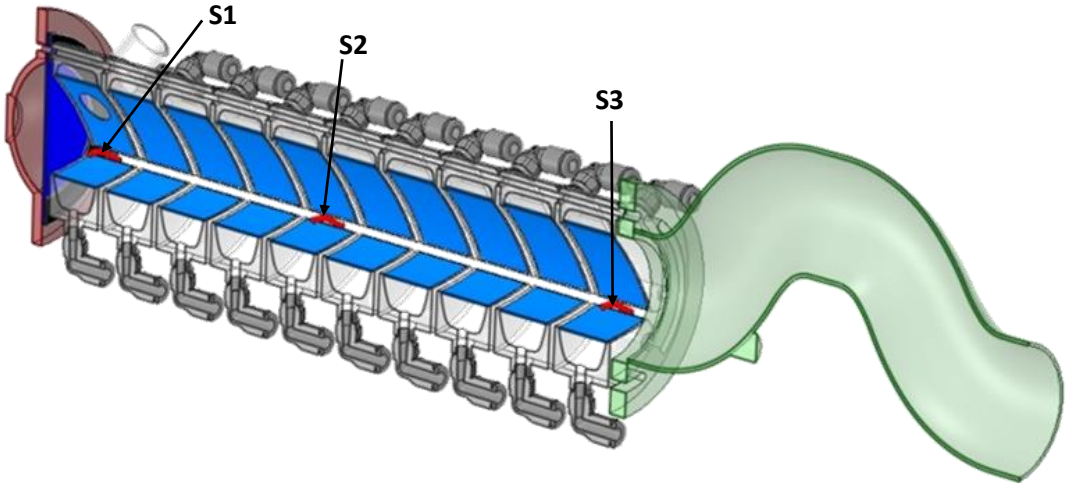

Figure 7.1. 3D model of DCM tube using ANSYS Spaceclaim 2015; S1, S2 and S3 represent the location of the sampling points along the DCM tube.

7.2.3 Positron Emission Tomography (PET) experiments

The PET experiments were conducted according to §5.3.4. Ten antegrade waves, with 10 s time delay between them, were applied. As in scintigraphy studies, each PET image shows the distribution of the radioactive solution along the length of the DCM tube. The PET data was used to correlate to the dissolution data of the theophylline tablets.

7.3 Results and discussion

7.3.1 Release profile of theophylline in different viscous media

Figure 7.2 shows the dissolution profile of the theophylline in viscous media which was obtained from the three different sampling points, located at the beginning, at the middle and at the end of the DCM tube. The results for the 0.25% $NaCMC_{(700000)}$ (w/w) solution (Figure 7.2a), show that there was an unequal distribution of the released drug along the length of the tube, resulting in a different release rate. The highest release rate, and hence the highest concentration, was observed at the beginning of the DCM tube, where the tablet was initially

located, followed by the second sampling point and finally by the third one located at the end of the tube, as expected. The dissolution profile of the theophylline in 0.50% NaCMC (w/w) (Figure 7.2b) followed the same order as in 0.25% NaCMC (w/w) in terms of the release rate according to the sampling point. The results showed relatively similar release rate of the drug in S1 for the 0.50% NaCMC (w/w) to that one in 0.25% NaCMC (w/w) for the same sampling point, but very slow for the other two sampling points (i.e. S2, S3). In particular, at the following sampling time points, i.e. 2, 6 and 8 h, the released drug (%) in 0.25% NaCMC (w/w) was within the range of 3.7% – 30.7%, 15% – 76.6% and 34.8% – 85.5% respectively, whereas in 0.5% NaCMC was 0.2% – 29.5%, 0.5% – 82.4% and 3% – 76.7%. The lower values in all above ranges correspond to S3 and the high ones to S1. These results demonstrated several key features. Firstly, the fluctuations in the drug concentrations and hence of the dissolution profile, most likely reflect the ineffective transport of the drug along the tube, resulting in the formation of areas with high accumulation of the drug; especially at the beginning of the DCM tube, at which the tablet had been introduced. Furthermore, the distribution of the drug in 0.50% NaCMC (w/w) solution was less efficient compared to 0.25% NaCMC (w/w), as anticipated. In the case of 0.50% NaCMC (w/w), most of the drug was accumulated mainly at the beginning of the tube giving release rates close to those obtained in 0.25% NaCMC (w/w). However, this doesn't mean a faster hydration of the tablet and hence a faster release of the drug in more viscous media (Stamatopoulos et al., 2015). It means that beside the slower release rate of the drug, the inadequate transport in 0.50 NaCMC (w/w) solution leads to high accumulation of the drug molecules in a small area, which may be of value in the local treatment of the ascending colon. In contrast, the distribution of the drug in 0.25% NaCMC (w/w) seems to be more effective.

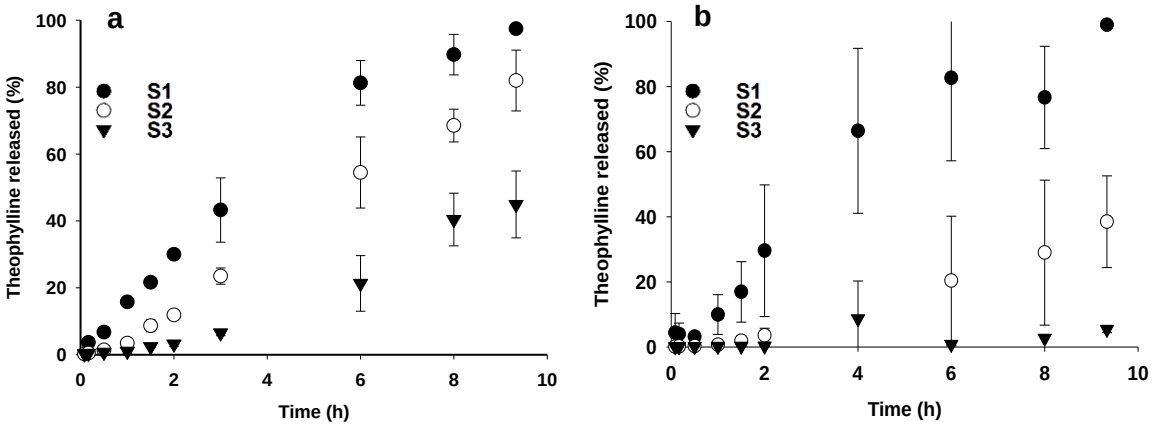

Figure 7.2. Dissolution curves of theophylline obtained from three different sampling points along the length of the DCM tube (◆ S1; ■ S2; ▲ S3). The dissolution experiments were performed in (a) 0.25% and (b) 0.50% NaCMC$_{(700000)}$ (w/w) solutions adjusted at pH 7.4 using phosphate buffer; Temperature was 37 ºC; Standard deviation bars for the dissolution profile theophylline (n=6).

Second, higher variability was observed in the dissolution data obtained with using 0.50% NaCMC (w/w). It was noticed, by plotting separately the dissolution data of two single different runs, that the dissolution curves of S1 and S2, and to a much lesser extent of S3, showed completely different profiles (Figure 7.3) compared to the dissolution curves of S1 & S2 obtained in the less viscous solution (0.25% NaCMC (w/w)). It seems that as well as the non-homogeneous distribution of the drug along the DCM tube, the location and the erosion of the tablet due to wall motion might affect the release rate of the drug.

b

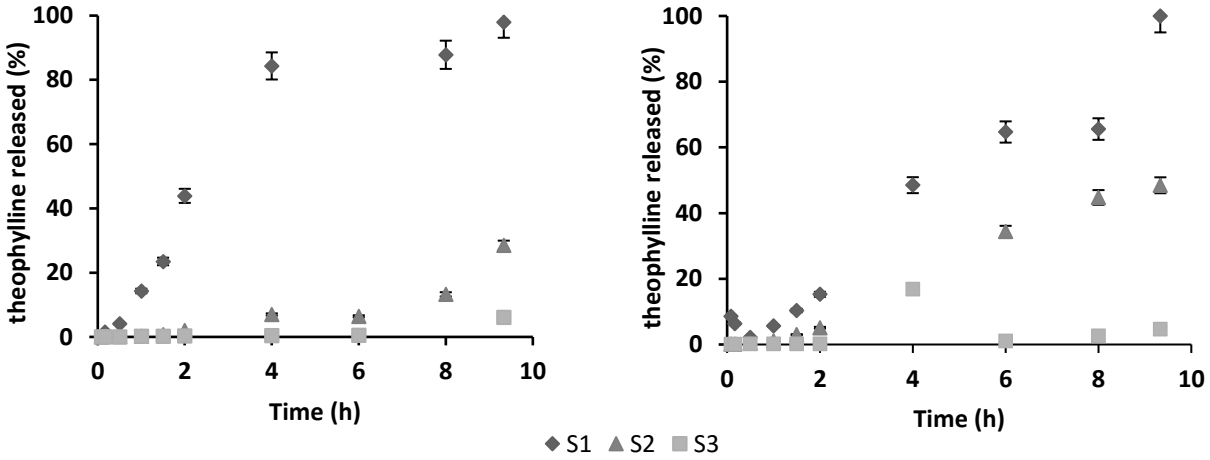

Figure 7.3. Dissolution profile of theophylline of two different runs in 0.50% NaCMC (w/w) adjusted at pH 7.4 using phosphate buffer; The dissolution curves were obtained from three different sampling points along the length of the DCM tube (◆ S1; ▲ S2; ■ S3). Temperature was 37 ^{o}C; Error bars for the dissolution profile of theophylline (n=3).

Indeed, images from the interior of the DCM tube (Figure 7.4A) showed fragments of the dosage form which were found to be located either in the cavity of the membrane (Figure 7.4B) or on the connection point, the so-called semilunar folds, between the two segments. It seems that if the tablet is located within the cavity of the membrane then the disintegration could be intensive, since the membrane will squeeze and break the dosage form. These observations in combination with the poor distribution of the released drug could explain the differences observed in dissolution profiles and consequently the irregular absorption profiles observed from extended release tablets (Garbacz et al., 2008).

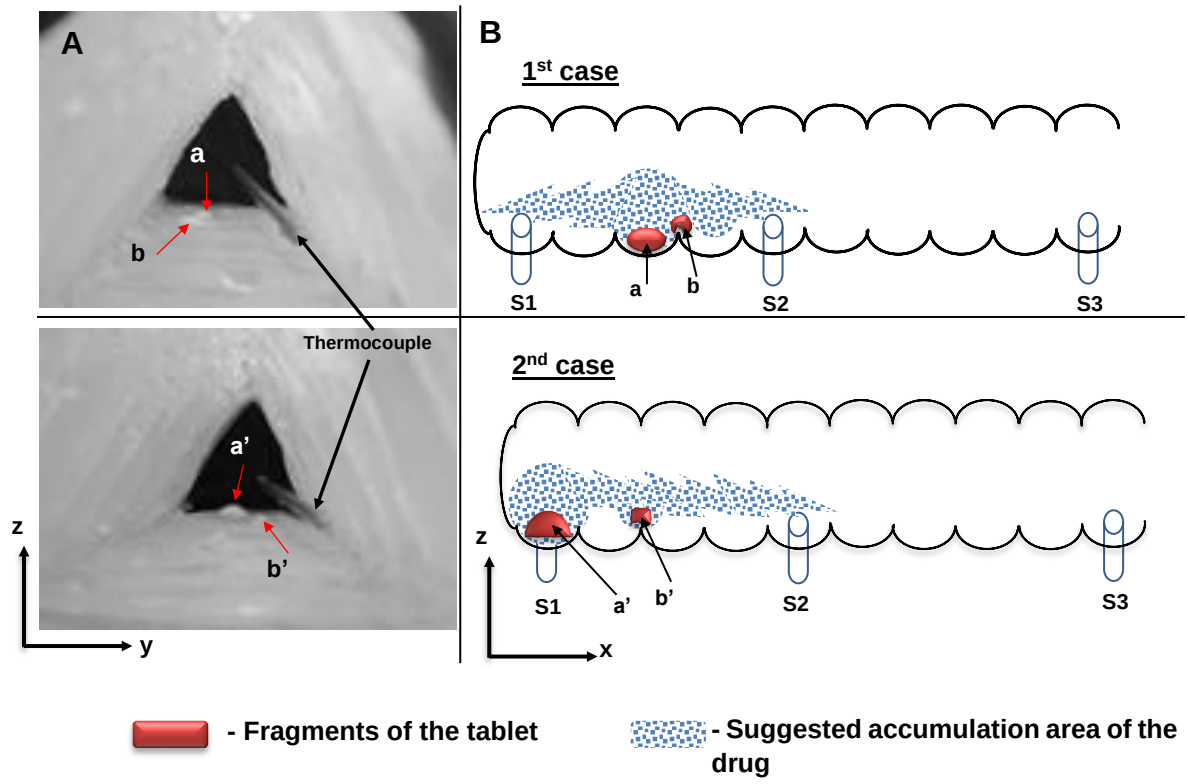

Figure 7.4. (A) Images of the cross section of the DCM tube and (B) schematic illustration of the in vitro model along the x axis, showing the position of the partially disintegrated tablet in two separated runs of the dissolution experiments. Arrows in (A) showing the fragments of the tablet.

Moreover, observations of the final solution of 0.25% NaCMC (w/w) (Figure 7.5) collected after the end of the dissolution experiments, showed that the dosage form had been disintegrated in small agglomerates. In this experiment the tablet was directly placed in the colon model without being exposed to gastric and subsequently to intestinal fluids as normally happens for the oral administrated dosage forms. In addition, there was partial disintegration of the tablet in the mini volume USP 2 dissolution apparatus. However, in this experiment, mechanical stress applied on the tablet due to membrane oscillation, leading to complete disintegration of the tablet. Thus, the current model can be utilised to profile localised delivery profiles for colonic specific delivery systems. However, since the passive or active transport is

not reproduced, the current model is limited for giving information about the systemic delivery profiles.

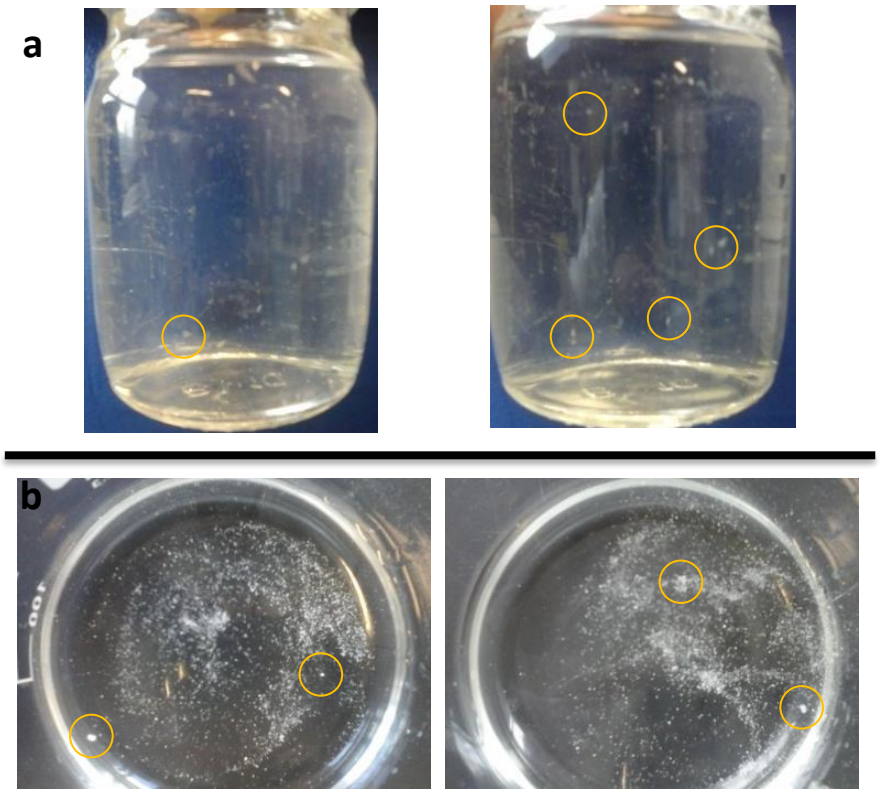

Figure 7.5. Images of the final solutions of the two different viscous media (a) 0.25% and (b) 0.50% NaCMC(700000) (w/w) after the end of two separate runs of the dissolution experiments. Big agglomerates of the disintegrated tablet found in the final solution of 0.50% NaCMC(700000) (w/w) indicated inside the circles.

7.3.2 Visual identification of propagating wall motion of DCM tube using Positron Emission Tomography (PET)

In order to better understand the fluctuations in the concentration of the drug along the tube caused by the wall motion of DCM, PET experiments were performed. This was possible by recording the intensity of the radioactive tracer injected at the beginning of the tube, during

repeating CPPWs waves with 10 s time delay. This time delay was allowed to represent sequential waves whilst condensing the overall time of the experiment to manage the lifespan of the radioactive marker. A 10 s delay provided sufficient time for the fluid to become static between waves.

PET images of the 0.25% w/w NaCMC solution (Figure 7.6) showed a gradual distribution of the radioactive tracer along the DCM, with only a small amount of tracer detected at the very end of the tube even after 10 waves (Figure 7.6d). Higher intensities were observed in the areas at which S1 and S2 are located. In addition, although, the tracer intensity around points S1 and S2 seem to be approximately of the same magnitude after 10 waves (with a slight lower intensity at S1), the corresponding dissolution curves showed greater differences. Nevertheless, it has to be acknowledged that the PET is an accelerated mimic of the dissolution test, since a CPPW was occurring every 10 s, compared with a CPPW wave every 5 min in the dissolution experiments. In addition, the drug is gradually released from the tablet resulting in a continuously “injection” in the solution making the dissolution experiment a repeating cycle of the PET experiment. Practically this means that a high concentration of the drug will always be observed at the beginning of the DCM tube, representing the injection point in PET experiments (Figure 7.6a), and after several CPPWs the drug will gradually distribute along the tube as shown in Figure 7.6b, Figure 7.6c and Figure 7.6d.

The PET images represent an approximation of the distribution of the drug giving information about the zones of high and low concentrations. In particular, only a small portion of the tracer reached the very end of the tube; where the S3 is located (Figure 7.6d). This explains why low release rates (e.g. 45% @ 9 h) were obtained in the dissolution profiles at point S3 in 0.25% NaCMC (w/w). In addition, radioactive tracer was mainly accumulated around point S2 whereas a slight decrease was observed at S1 (Figure 7.6d). The same pattern was observed in dissolution test in which the release rate was increasing and was getting closer to that of S1 as the end of the experiment was reached.

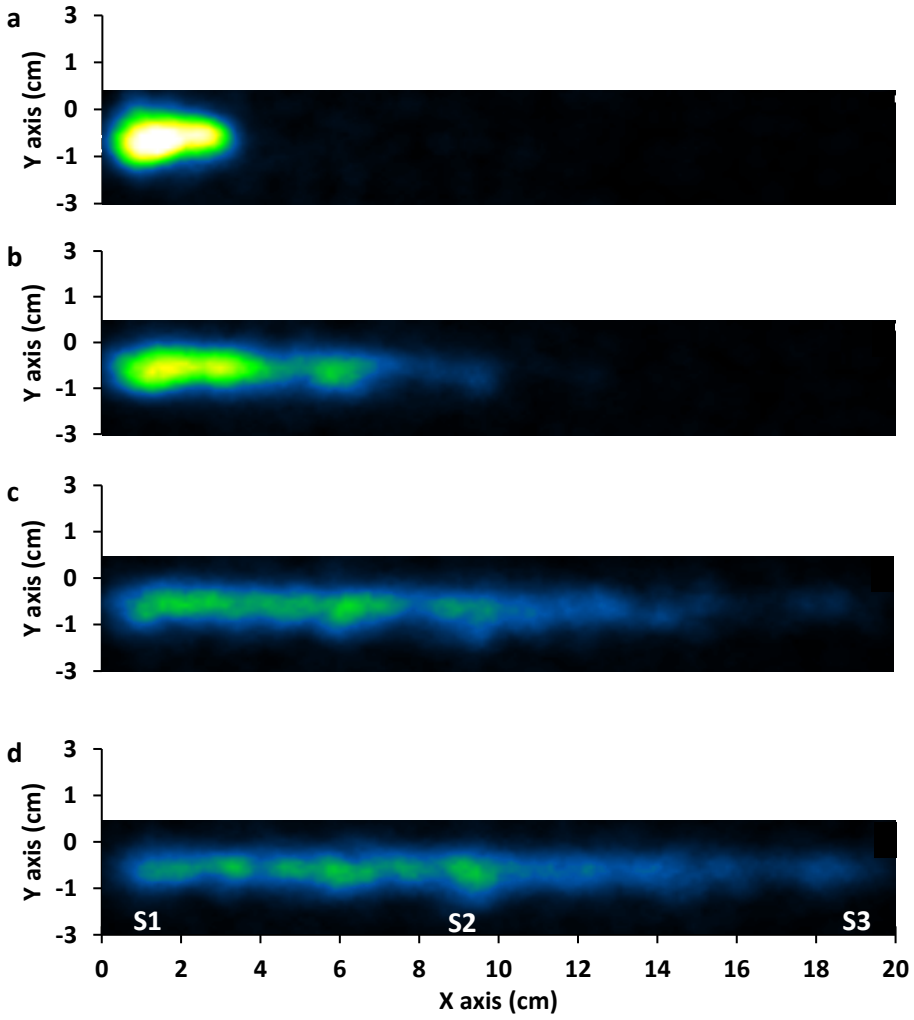

Figure 7.6. PET images of (a) injection, (b) 1st wave, (c) 5th wave and (d) 10th wave using 0.25% NaCMC (w/w).

Further increase in viscosity leads to a different profile of the distribution of the radioactive tracer. With 0.50% NaCMC (w/w) (Figure 7.7) a significant amount of the tracer remained at the beginning of the tube whereas another considerable amount appeared between the points S2 and S3 after 5 (Figure 7.7c) and 10 (Figure 7.7d) CPPWs. However, close to S2 a slight increase on the intensity of the radiolabelled solution was observed due to the backward tailing of the radioactive tracer caused by the backflow formed as the CPPWs wave reached the very end of the tube. In addition, no tracer reached the very end of the tube explaining why very

low release rates, almost zero percent, were found in 0.50% NaCMC (w/w) based on the dissolution data obtained from samples collected in S3 location.

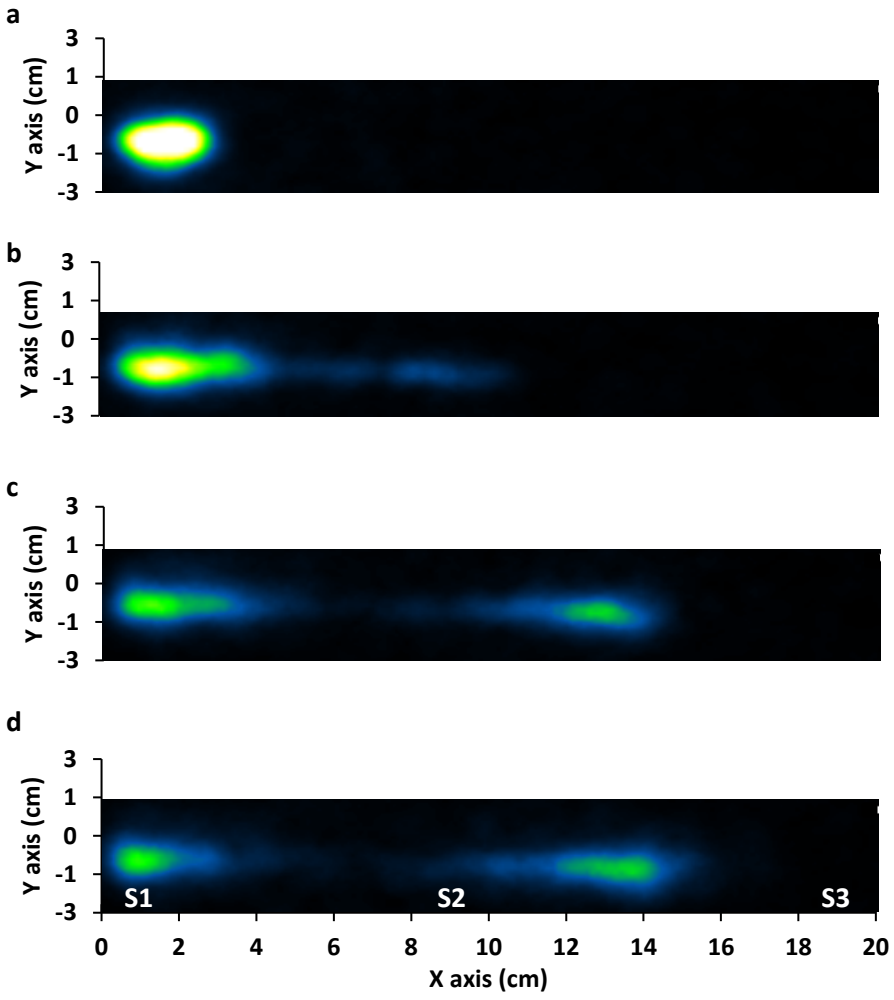

Figure 7.7. PET images of (a) injection, (b) 1st wave, (c) 5th wave and (d) 10th wave using 0.50% NaCMC (w/w).

Furthermore, due to the DCM wall motion and the partial disintegration of the tablet, fragments of the dosage form were found several centimetres from the first segment of the model (Figure 7.4A). Assuming that the drug will be mainly accumulated around the fragments, areas of high drug concentrations (Figure 7.4B) might be differently distributed along the DCM tube with respect to the spots of high intensities of the tracer; as indicated in PET images of 0.50% NaCMC (w/w) (Figure 7.7). In particular, PET experiments showed one spot close to

the injection point and another one several centimetres further from the S2 (Figure 7.7d). However, elongation of the first spot was observed towards the direction of the wave whereas lengthening of the second spot was appeared mainly in the opposite direction due to the backflow which is stronger as getting closer to the very end of the tube. Thus, tracers of the radioactive solution were detected close to S2. Thus, this 'to and fro' fluid motion will also affect the distribution of the drug. Hence, if the tablet or fragments are located between S1 and S2, it is likely that "elongation" of the high drug accumulation area might be occurred in both directions (Figure 7.4B; 1st case). As a further consequence the release rates of the drug obtained from S1 and S2 will be approximately similar (Figure 7.6b). In contrast, when the tablet remains in the first segment and only a small fragment is located a few centimetres further, the distribution of the drug might be looked like as in the 2nd case (Figure 7.4B; 2nd case) and the corresponding release rates as showed in Figure 7.6a.

Although PET images do not actually show the entire distribution of the drug, valuable information can be obtained about the high and low accumulation zones of the drug in viscous media. However, the protocol of the PET experiments is not far from what is applied *in vivo* during scintigraphy studies, since a watery solution is injected in human colon without knowing the actual viscosity of the colonic fluids which is presumably higher than that of the radioactive solution.

7.3.3 Comparison of the DCM with the compendial mini volume USP 2 dissolution apparatus

Table 7.1 presents the release rates of theophylline in different viscous media as published by Stamatopoulos et al., (Stamatopoulos et al., 2015). The release rates obtained from DCM showed higher variability between the sampling points compared to the mini volume USP 2; this is a result of the more realistic geometry and motility within the DCM. However, this means that the comparison of the two dissolution apparatus is not straightforward due to their different configurations. In DCM tube the medium fills 50% of the tube whereas the flow is induced by the wall motion as well as by the reflux of the fluid. In addition, in DCM there is a discontinuous

wall motion in comparison to the continuous impeller rotation in USP 2. Furthermore, in USP 2 the tablet is normally placed within the stagnant zone below the shaft in which low velocities (Stamatopoulos et al., 2015) and low shear rates (Bai et al., 2011) have been reported and which are not changing as the agitation speed is increased (Bai et al., 2011). In contrast the dosage form faces a dynamic environment in the DCM tube in which disintegration takes place due to the oscillation of the flexible wall. Moreover, by reproducing the architecture of the smooth muscle and the dimensions of the proximal colon, DCM provides information about the distribution of the drug, with respect to the available surface area of the colonic wall; however, this needs further investigation since with PET only the ^{18}F ions were tracked and not the drug molecules. Moreover, mimicking the variability in the distribution of the drug could be useful to evaluate the variability in humans. This is not possible with the compendial dissolution methods (e.g. USP 1 – 4 dissolution apparatus) or with their improvements, e.g. stress test apparatus (Garbacz et al., 2008) or with the most advanced multi-compartmental computer controlled large intestine simulator (TIM-2, TNO) since the volume, dimensions and the geometry are not relevant to the physical organ (Blanquet et al., 2001a). However, the dissolution profile of the current formulation used in this work, was tested only in one volume and using a fixed motility pattern. The current work should be extended to understand how the formulation and the distribution of the drug will be affected under different motility patterns reflecting different colonic conditions (e.g. normal, disease, fasted or fed state). This information might help to understand under which conditions the formulation needs to be tested using DCM and where a simple compendial dissolution methods is sufficient to described the *in vivo* performance of the formulation.

Table 7.1. Comparison of the release rates of the theophylline obtained from Dynamic Colon Model (DCM) with the published data obtained from mini volume USP2

	%NaCMC (w/w)			
	0.25%		0.50%	
Time (h)	DCM[a]	mini USP2[b]	DCM[a]	mini USP2[b]
2	3.7 – 30.7	10.0 – 15.0	0.2 – 29.5	10.0 – 12.0
6	15.0 – 76.6	30.0 – 40.0	0.5 – 82.4	30.0 – 50.0
8	34.8 – 85.5	45.0 – 58.0	3.0 – 76.7	40.0 – 55.0

[a] The low limit of the ranges corresponds to the third sampling point (S3) and the high one to the first sampling point (S1); [b] The low values correspond to the SP1 (close to the surface of the medium) and the high to the SP2 (close to the tip) (Stamatopoulos et al., 2015).

7.4 Conclusions

Dissolution experiments of theophylline released from $NaCMC_{(90000)}$ based tablets were performed in different viscous media and under fixed wall motion profile similar to the main colon motility pattern recorded *in vivo* in healthy humans (Dinning et al., 2014a). Thus, the disintegration of the tablet and the release of the drug took place under biorelevant conditions. However, the exact history of the pressures applied on the tablet during the repeated wave pressures needs to be investigated by tracking the position of the tablet. This will allow evaluating if the tablet was phasing pressures within the range measured in the centre of the contracting point (Figure 5.11, 73% occlusion) or lower which probably take place between the pockets.

The distribution of the drug was determined by collecting samples from different locations along the DCM tube and performing Positron Emission Tomography (PET). The results showed areas of high and low accumulation of the drug. Thus, using the proposed *in vitro* model it is possible to assess the behaviour not only of the dosage form but also how the drug will be distributed along the human colon; assuming that the more the surface area that the drug would be exposed the higher the possibility of being absorbed by the GI tract or the more available for local therapy. In addition, this information, might allow understanding how of

phenomena like supersaturation and precipitation of the drug during the passage of the dosage form through the proximal colon.

8 Conclusions & Future Work

8.1 Final Conclusions

The study presented here was concerned with understanding the impact of the hydrodynamics in the human proximal colon, in particular relating the motility of the colon wall and the viscosity of the fluids to the performance of MR dosage forms, mixing processes and underlying fluid hydrodynamics. The overall aim was to understand the environment in which targeted dosage forms are exposed during their passage through the human colon.

It has been realized that physicochemical properties of the fluids as well as the hydrodynamics within the GI tract should be both reproduced to adequately evaluate *in vitro* performance of drug delivery systems. The current compendial dissolution methods oversimplify the GI tract whereas the advanced *in vitro* models (e.g. TIM-2) are not completely biorelevant.

Nevertheless, USP 2 is still used in pharmaceutical industry during the design, development and evaluation of the dosage forms. Numerous studies have analysed the hydrodynamics in 1L USP 2 dissolution apparatus, showing the poor mixing performance and reproducibility of dissolution testing data. Recently mini volume USP 2 has gained popularity due to the reduced mass of material required, analytical methodology and discriminatory power of conventional apparatus. However, hydrodynamics are still needed to be analysed since they don't reflect those of the 1L USP 2. In addition, mini volume UPS 2 is the closest to the volume of fluids presented in the human proximal colon and therefore it can be partially compared with the *in vitro* model of the human colon developed in this project.

The experiments presented in Chapter 3 investigated the impact of the viscosity on the dissolution profile of theophylline (a high water soluble drug) released from a hydrophilic matrix. To understand how the viscosity as well as sampling point can affect the release rates of the drug, images of a fluorescence dye released from the same hydrophilic matrix were captured with using PLIF technique. The current dye (i.e. Rhodamine 6G) matched the

dissolution profile of the drug, allowing a more systematic assessment of the distribution of the drug, mainly around the sampling points. Thus, the current optical technique might allow to predefine factors such as viscosity, impeller rotation speed, sampling point which will affect the consistency of the dissolution method and hence the release profile of the drugs with using fluorescence dye release data.

The results showed a time delay for the released dye-drug to reach the upper zone of the dissolution apparatus leading to different release rates when different sampling points are used for generating the dissolution profile of the targeted drug. In addition, as the viscosity was increasing the dye was manly accumulated at the bottom of the mini vessel whereas the hydration and the disintegration of the tablet were slower in most viscous fluids.

The proof – of – concept that the dye matches the dissolution profile of the drug allowed a more systematic evaluation of the mixing performance of the mini volume USP 2. Thus, in Chapter 4 the areal distribution method and the individual striations method were combined to provide an improved and more detailed measure of the mixing performance according to the level of mixedness, Gi. This is advantageous to determine which region within the USP 2 mini vessel shows the highest mixing level; something very important in terms of choice of sampling point. The results showed that the highest mixedness level was mainly located above the blade and close to the wall, i.e. the region where intensive mixing takes place; therefore, the recommendation is that the sample tube (cannula) should be placed in this region.

In Chapter 5 the development of the biorelevant *in vitro* model of the human proximal colon is presented. The proposed model reproduces the main features of the human colon anatomy. The design was based on clinical data and fieldwork in the operation theatres of the Heartland Hospital of Birmingham.

The effect of wall motion, viscosity and volume of the fluids on the performance of the manometry was investigated whilst Positron Emission Tomography was used to visualize the fluid flow within the colon model under fixed conditions.

The results showed that the position of the catheter, the occlusion rate, the viscosity and the fluid volume affected the interpretation of the manometry. As the viscosity and the occlusion rate were increased the amplitude of the pressure was also increased. Furthermore, manometry failed to differentiate changes for occlusion degrees of the membrane <80% and at low viscosities. In addition, the sensitivity of the manometry was dramatically decreased when the apparatus was half full. Thus, the criteria based on which a pressure wave should be associated with the movements of the contents, might have to be reconsidered. PET images revealed that pressure waves with amplitudes <2mmHg can be highly associated with fluid flow.

Further investigation on the mixing and fluid flow under predetermined condition was presented in Chapter 6. Positron Emission Particle Tracking (PEPT) system was used as an alternative to magnetic pill tracking system, used to analyse *in vivo* the motility events in human colon. In this chapter, how the interpretation of the flow and the mixing of the colonic fluids will be affected by the interplay between wall motion, viscosity and the properties of the particle used to monitor colonic movements, was examined. Different results can be obtained in terms of velocities and residence times by changing the particle used as reference for analysing the fluid motion. In general, high velocities and longer retrograde displacements were observed for the floating particle which is also controlled by the viscosity of the fluids. These differences also reflected how accurately the particle describes the fluid motion, since small relaxation times were obtained for different viscous media.

Finally, in Chapter 7 the dissolution profile of theophylline released form a hydrophilic matrix was obtained using the Dynamic Colon Model (DCM). The dissolution profile and the distribution of theophylline, was assessed by collecting samples at different locations along the DCM tube. Differences in the release rates of the drug were observed which were affected by the sampling point location, the viscosity of the fluid and the mixing within the DCM tube. Images of the overall convective motion of the fluid inside the DCM tube obtained using Positron Emission Tomography enabled relation of the distribution of the tracer to likely areas

of high and low concentrations of the theophylline drug. In overall, the distribution of the drug was interplay of dissolution, mixing and spread of the dosage forms along the DCM tube. Furthermore, the release rates obtained from DCM showed higher variability between the sampling points compared to the mini volume USP 2 (refer to Table 7.1); this is a result of the more realistic geometry and motility within the DCM. However, the comparison of the dissolution apparatus is not straightforward due to different configuration. The DCM tube was half-filled whereas the flow is induced by the wall motion as well as by the reflux of the fluid. In addition, in DCM there is a discontinuous wall motion in comparison to the continuous impeller rotation in USP 2. Furthermore, in USP 2 the tablet is normally placed within the stagnant zone below the shaft in which low velocities (Stamatopoulos et al., 2015) and low shear rates (Bai et al., 2011) have been reported and which are not changing as the agitation speed is increased (Bai et al., 2011). In contrast the dosage form faces a dynamic environment in the DCM tube in which disintegration takes place due to the oscillation of the flexible wall.

The present study demonstrated that the Dynamic Colon Model provided a more realistic colonic environment to understand phenomena which are difficult to be assessed *in vivo*.

Using the proposed *in vitro* model, it is possible to assess the behaviour not only of the dosage form but also how the drug will be distributed along the human colon; assuming that the more the surface area that the drug would be exposed the higher the possibility of being absorbed by the GI tract or the more available for local therapy.

8.2 *Future work*

The primary development of the proposed Dynamic Colon Model could be further improved by (i) optimising the wall motion of the flexible membrane, (ii) developing stimuli-response artificial colon wall to mechanical and/or chemical external signals (i.e. myogenic and/or neurogenic stimuli of the smooth muscle), (iii) reproduce the dewatering process in human proximal colon incorporating hydrogels into the wall surface and (iv) extended analysis of the fluid flow inside the DCM tube.

Optimisation of the wall motion of the flexible membrane

The reproduction of the smooth motion of the colon wall needs further improvement. In the current model the two edges (i.e. semilunar folds) of the haustrum are fixed and they don't contract. Thus, part of the transit is missed since there is a gap between two haustra without wall motion. This problem could only partially be solved by keeping the previous haustrum at the contraction stage for enough time until the next one is being completely contracted. The acrylic body used in this version of the DCM could be replaced by changing the design of the mould and compartmentalizing the haustrum in smaller sections. Thus, the semilunar fold will also contract providing a smoother wall motion. This will provide a more accurate reproduction of the motility patterns and the fluid flow in the human colon. For instance, during mixing and propulsion of fluids there is a front peak at the contraction point which is moving continuously at the direction of the wave causing vortexing of the fluid within the ahead relaxing region (Figure 8.1). This is not possible with the current design.

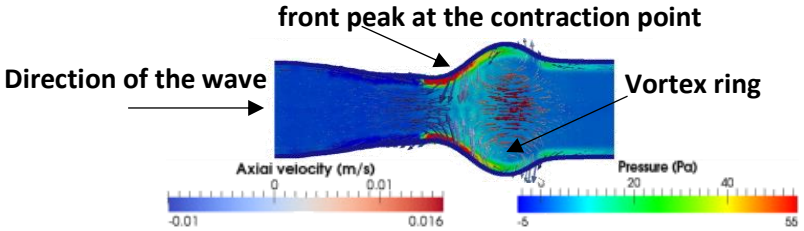

Figure 8.1.Velocity and pressure gradients within the contraction/relaxation region (reproduced from Sinnot et al. 2012 with permission)

Development of a stimuli-response artificial colon wall

In the current *in vitro* model the motility of the flexible wall was adjusted to the pressure amplitudes measured *in vivo*. However, the results showed that the manometry failed to differentiate changes in the occlusion degrees. Thus, different motility patterns might give similar profile of the pressures. Thus, an alternative strategy should be followed in order to reproduce the motility, based on the response of the viscoelastic smooth muscle to chemical

and mechanical stimuli. Therefore, the occlusion degrees and the occlusion rates should be based on the strength of the stimulus and the corresponding mechanical tolerance (e.g. stiffness) of the elastic material to that stimulus.

Reproduce the dewatering process in human proximal colon

Previous *in vivo* studies have shown that the absorption rate of the water from the colon wall is 2 – 3 mL/min (Palma et al., 1981) using PEG – 4000 as a non-absorbable marker. This information can be used to develop a flexible membrane which can match the dewatering rate of the colon with following the principle of the dialysis membranes. Thus, stretchable hydrogels combined with silicone (Zhang et al., 2014, Cha et al., 2013) could be a potential solution. This would enable better demonstration of the uptake/absorption of drugs at the colonic wall surface, providing an opportunity to better investigate how drugs and nutrients are absorbed and the influence of dosage form design on their delivery. However, it has to point out that with the current approach only the passive and not the active transport of the drugs will be reproduced. Nevertheless, the results can be combined with assessing the permeability of the released drug using cell lines.

Extending analysis of the fluid flow inside the DCM tube

In the current work the fluid flow inside the DCM tube was analysed under one motility pattern. However, relationships between wall motion, fluid volume, and fluid flow need further investigation with performing experiments under different motility patterns. Moreover, the passes of the trace particle through the DCM tube should be increased with improving the PEPT technique. Normally, in static mixers the passes to ensure full mapping of the fluid flow are close to 500. However, in this case there is a closed loop of constant flow rate whereas in the DCM tube the tracer needed to be replaced manually at the beginning for each run. Thus, a reasonable number of passes assuring adequate characterization of the fluid flow in DCM tube should be chosen for this purpose. In addition, improved design of the radioactive tracers

will help to use particles which follow the fluid flow more accurately (i.e. small relaxation times) for a wider range of viscosities. In addition, further work required to examine other types of dosage forms and the volume of the fluids by regulating the flow rate of the inlet medium, mimicking the ileum emptying process. Moreover, the colonic fluids are an inhomogeneous mixture of small particles dispersed in a viscous liquid. There is limited *in vivo* data on the particle size and particle size distribution of the solid fraction of the colonic fluids (Reppas et al., 2015). The results provided by Reppas et al. (2015) will be used to formulate biorelevant solution which contains a solid fraction of known particle sizes and particle size distribution. These particle sizes will also be used as reference to design tracers for analysing and visualize the fluid motion in DCM model with using PET/PEPT.

Another important issue which needs to be examined is the effect of gases produced upon fermentation on the interpretation of the manometry. The lumen is only infrequently open to atmospheric pressure during flatus or belching, and is not normally able to freely vent gas.

Comparison of *in vitro* dissolution data obtained from DCM with other dissolution apparatuses such as USP 1, 3, 4 and TNO TIM-2 as well as *in vivo* data. This is important because the compendial dissolution apparatuses are still used during the development of a formulation. In addition, the wall motility and the generated shear forces may not be the parameters that affect the drug release mechanism, like in case of the osmotic pressure delivery systems. However, on the other hand the composition of the media might affect the performance of the dosage form (e.g. present of solubilizers or emulsifiers) like in case of formulations contain low water soluble drugs. Thus, in practice might different *in vitro* models be used focusing on single or multiple aspects affecting the *in vivo* performance of the dosage form. Hence, in which case as well as at which stage of the development of the formulation the DCM should be used, it should be examined with respect to the existing *in vitro* models and the targeted product.

Utilization of PLIF method to analysis drug release from dosage forms

Further work should be done on utilizing the current PLIF method (refer to Chapter 3) for drugs of a range of solubilities; provided that the most appropriate dye has been selected. This is of great importance especially for poorly water soluble drugs, where the low amounts dissolved in viscous media could lead to even higher variance in the dissolution data generated with the conventional sampling technique.

9 References

ABRAHAMSSON, B., PAL, A., SJOBERG, M., CARLSSON, M., LAURELL, E. & BRASSEUR, J. G. 2005. A novel in vitro and numerical analysis of shear-induced drug release from extended-release tablets in the fed stomach. *Pharm Res,* 22**,** 1215-26.

AGUIRRE, M., JONKERS, D. M., TROOST, F. J., ROESELERS, G. & VENEMA, K. 2014. In vitro characterization of the impact of different substrates on metabolite production, energy extraction and composition of gut microbiota from lean and obese subjects. *PLoS One,* 9**,** e113864.

AHMAD, M. Z., AKHTER, S., AHMAD, I., SINGH, A., ANWAR, M., SHAMIM, M. & AHMAD, F. J. 2012. In vitro and in vivo evaluation of Assam Bora rice starch-based bioadhesive microsphere as a drug carrier for colon targeting. *Expert Opin Drug Deliv,* 9**,** 141-9.

ALBERINI, F., SIMMONS, M. J. H., INGRAM, A. & STITT, E. H. 2014a. Assessment of different methods of analysis to characterise the mixing of shear-thinning fluids in a Kenics KM static mixer using PLIF. *Chemical Engineering Science,* 112**,** 152-169.

ALBERINI, F., SIMMONS, M. J. H., INGRAM, A. & STITT, E. H. 2014b. Use of an areal distribution of mixing intensity to describe blending of non-newtonian fluids in a kenics KM static mixer using PLIF. *AIChE Journal,* 60**,** 332-342.

ALVAREZ-FUENTES, J., FERNANDEZ-AREVALO, M., GONZALEZ-RODRIGUEZ, M. L., CIRRI, M. & MURA, P. 2004. Development of enteric-coated timed-release matrix tablets for colon targeting. *J Drug Target,* 12**,** 607-12.

AMIDON, S., BROWN, J. E. & DAVE, V. S. 2015a. Colon-Targeted Oral Drug Delivery Systems: Design Trends and Approaches. *AAPS PharmSciTech,* 16**,** 731-741.

AMIDON, S., BROWN, J. E. & DAVE, V. S. 2015b. Colon-targeted oral drug delivery systems: design trends and approaches. *AAPS PharmSciTech,* 16**,** 731-41.

ANTONIN, K. H., RAK, R., BIECK, P. R., PREISS, R., SCHENKER, U., HASTEWELL, J., FOX, R. & MACKAY, M. 1996. The absorption of human calcitonin from the transverse colon of man. *International Journal of Pharmaceutics,* 130**,** 33-39.

ARKWRIGHT, J. W., DICKSON, A., MAUNDER, S. A., BLENMAN, N. G., LIM, J., O'GRADY, G., ARCHER, R., COSTA, M., SPENCER, N. J., BROOKES, S., PULLAN, A. & DINNING, P. G. 2013. The effect of luminal content and rate of occlusion on the interpretation of colonic manometry. *Neurogastroenterol Motil,* 25**,** 10.

ASGHAR, L. F. & CHANDRAN, S. 2006. Multiparticulate formulation approach to colon specific drug delivery: current perspectives. *J Pharm Pharm Sci,* 9**,** 327-38.

BAI, G., ARMENANTE, P. M., PLANK, R. V., GENTZLER, M., FORD, K. & HARMON, P. 2007. Hydrodynamic Investigation of USP Dissolution Test Apparatus II. *Journal of Pharmaceutical Sciences,* 96**,** 2327-2349.

BAI, G., WANG, Y. & ARMENANTE, P. M. 2011. Velocity profiles and shear strain rate variability in the USP Dissolution Testing Apparatus 2 at different impeller agitation speeds. *Int J Pharm,* 403**,** 1-14.

BAMPTON, P. A. & DINNING, P. G. 2013. High resolution colonic manometry--what have we learnt?--A review of the literature 2012. *Curr Gastroenterol Rep,* 15**,** 013-0328.

BAMPTON, P. A., DINNING, P. G., KENNEDY, M. L., LUBOWSKI, D. Z. & COOK, I. J. 2001. Prolonged multi-point recording of colonic manometry in the unprepared human colon: providing insight into potentially relevant pressure wave parameters. *Am J Gastroenterol,* 96**,** 1838-48.

BAMPTON, P. A., DINNING, P. G., KENNEDY, M. L., LUBOWSKI, D. Z., DECARLE, D. & COOK, I. J. 2000. Spatial and temporal organization of pressure patterns throughout the unprepared colon during spontaneous defecation. *Am J Gastroenterol,* 95**,** 1027-35.

BASSOTTI, G., ANTONELLI, E., VILLANACCI, V., BALDONI, M. & DORE, M. P. 2014. Colonic motility in ulcerative colitis. *United European Gastroenterology Journal,* 2**,** 457-462.

BASSOTTI, G., BUCANEVE, G., PELLI, M. A. & MORELLI, A. 1990. Contractile Frequency Patterns of the Human Colon. *Neurogastroenterology & Motility,* 2**,** 73-78.

BASSOTTI, G., CROWELL, M. D. & WHITEHEAD, W. E. 1993. Contractile activity of the human colon: lessons from 24 hour studies. *Gut,* 34**,** 129-133.

BASSOTTI, G., DE ROBERTO, G., CHISTOLINI, F., SIETCHIPING-NZEPA, F., MORELLI, O. & MORELLI, A. 2004. Twenty-four-hour manometric study of colonic propulsive activity in patients with diarrhea due to inflammatory (ulcerative colitis) and non-inflammatory (irritable bowel syndrome) conditions. *Int J Colorectal Dis,* 19**,** 493-7.

BASSOTTI, G. & GABURRI, M. 1988. Manometric investigation of high-amplitude propagated contractile activity of the human colon. *American Journal of Physiology - Gastrointestinal and Liver Physiology,* 255**,** G660-G664.

BASSOTTI, G., GERMANI, U. & MORELLI, A. 1995. Human colonic motility: physiological aspects. *Int J Colorectal Dis,* 10**,** 173-80.

BASSOTTI, G., IMBIMBO, B. P., BETTI, C., DOZZINI, G. & MORELLI, A. 1992. Impaired colonic motor response to eating in patients with slow-transit constipation. *Am J Gastroenterol,* 87**,** 504-8.

BAXTER, J. L., KUKURA, J. & MUZZIO, F. J. 2005a. Hydrodynamics-induced variability in the USP apparatus II dissolution test. *Int J Pharm,* 292**,** 17-28.

BAXTER, J. L., KUKURA, J. & MUZZIO, F. J. 2005b. Shear-induced variability in the United States pharmacopeia apparatus 2: Modifications to the existing system. *The AAPS Journal,* 7**,** E857-E864.

BAYLISS, W. M. & STARLING, E. H. 1899. The movements and innervation of the small intestine. *The Journal of Physiology,* 24**,** 99-143.

BAZZOCCHI, G., ELLIS, J., VILLANUEVA-MEYER, J., REDDY, S. N., MENA, I. & SNAPE, W. J., JR. 1991. Effect of eating on colonic motility and transit in patients with functional diarrhea. Simultaneous scintigraphic and manometric evaluations. *Gastroenterology,* 101**,** 1298-306.

BHARUCHA, A. E. 2012. HIGH AMPLITUDE PROPAGATED CONTRACTIONS. *Neurogastroenterology and motility : the official journal of the European Gastrointestinal Motility Society,* 24**,** 977-982.

BLANQUET, S., MAROL-BONNIN, S., BEYSSAC, E., POMPON, D., RENAUD, M. & ALRIC, M. 2001a. The 'biodrug' concept: an innovative approach to therapy. *Trends Biotechnol,* 19**,** 393-400.

BLANQUET, S., MAROL-BONNIN, S., BEYSSAC, E., POMPON, D., RENAUD, M. & ALRIC, M. 2001b. The ‘biodrug’ concept: an innovative approach to therapy. *Trends in Biotechnology,* 19**,** 393-400.

BLANQUET, S., ZEIJDNER, E., BEYSSAC, E., MEUNIER, J. P., DENIS, S., HAVENAAR, R. & ALRIC, M. 2004. A dynamic artificial gastrointestinal system for studying the behavior of orally administered drug dosage forms under various physiological conditions. *Pharm Res,* 21**,** 585-91.

BOCANEGRA, L. M., MORRIS, G. J., JUREWICZ, J. T. & MAUGER, J. W. 1990. Fluid and Particle Laser Doppler Velocity Measurements and Mass Transfer Predictions for the Usp Paddle Method Dissolution Apparatus. *Drug Development and Industrial Pharmacy,* 16**,** 1441-1464.

BROADBENT, C. J., BRIDGWATER, J., PARKER, D. J., KENINGLEY, S. T. & KNIGHT, P. 1993. A phenomenological study of a batch mixer using a positron camera. *Powder Technology,* 76**,** 317-329.

BROUWERS, J., ANNEVELD, B., GOUDAPPEL, G.-J., DUCHATEAU, G., ANNAERT, P., AUGUSTIJNS, P. & ZEIJDNER, E. 2011. Food-dependent disintegration of immediate release fosamprenavir tablets: In vitro evaluation using magnetic resonance imaging and a dynamic gastrointestinal system. *European Journal of Pharmaceutics and Biopharmaceutics,* 77**,** 313-319.

BRUCHHAUSEN, M., GUILLARD, F. & LEMOINE, F. 2005. Instantaneous measurement of two-dimensional temperature distributions by means of two-color planar laser induced fluorescence (PLIF). *Experiments in Fluids,* 38**,** 123-131.

BRUN, R., MICHALEK, W., SURJANHATA, B. C., PARKMAN, H. P., SEMLER, J. R. & KUO, B. 2012. Comparative analysis of phase III migrating motor complexes in stomach and small bowel using wireless motility capsule and antroduodenal manometry. *Neurogastroenterol Motil,* 24**,** 332-e165.

BURISCH, J., JESS, T., MARTINATO, M. & LAKATOS, P. L. 2013. The burden of inflammatory bowel disease in Europe. *Journal of Crohn's and Colitis,* 7**,** 322-337.

BUSCIGLIO, A., GRISAFI, F., SCARGIALI, F. & BRUCATO, A. 2014. Mixing dynamics in uncovered unbaffled stirred tanks. *Chemical Engineering Journal,* 254**,** 210-219.

CARINO, S. R., SPERRY, D. C. & HAWLEY, M. 2006. Relative bioavailability estimation of carbamazepine crystal forms using an artificial stomach-duodenum model. *Journal of Pharmaceutical Sciences,* 95**,** 116-125.

CASTELA-PAPIN, N., CAI, S., VATIER, J., KELLER, F., SOULEAU, C. H. & FARINOTTI, R. 1999. Drug interactions with diosmectite: a study using the artificial stomach–duodenum model. *International Journal of Pharmaceutics,* 182**,** 111-119.

CHA, C., ANTONIADOU, E., LEE, M., JEONG, J. H., AHMED, W. W., SAIF, T. A., BOPPART, S. A. & KONG, H. 2013. Tailoring hydrogel adhesion to polydimethylsiloxane substrates using polysaccharide glue. *Angew Chem Int Ed Engl,* 52**,** 6949-52.

CHENG, D., FENG, X., CHENG, J., YANG, C. & MAO, Z.-S. 2015. Experimental study on the dispersed phase macro-mixing in an immiscible liquid–liquid stirred reactor. *Chemical Engineering Science,* 126**,** 196-203.

CHOURASIA, M. K. & JAIN, S. K. 2003. Pharmaceutical approaches to colon targeted drug delivery systems. *J Pharm Pharm Sci,* 6**,** 33-66.

CONLY, J. M., STEIN, K., WOROBETZ, L. & RUTLEDGE-HARDING, S. 1994. The contribution of vitamin K2 (menaquinones) produced by the intestinal microflora to human nutritional requirements for vitamin K. *Am J Gastroenterol,* 89**,** 915-23.

CONNINGTON, K., KANG, Q., VISWANATHAN, H., ABDEL-FATTAH, A. & CHEN, S. 2009. Peristaltic particle transport using the lattice Boltzmann method. *Physics of Fluids,* 21**,** 053301.

CONTI, S., MAGGI, L., SEGALE, L., OCHOA MACHISTE, E., CONTE, U., GRENIER, P. & VERGNAULT, G. 2007a. Matrices containing NaCMC and HPMC: 1. Dissolution performance characterization. *International Journal of Pharmaceutics,* 333**,** 136-142.

CONTI, S., MAGGI, L., SEGALE, L., OCHOA MACHISTE, E., CONTE, U., GRENIER, P. & VERGNAULT, G. 2007b. Matrices containing NaCMC and HPMC: 2. Swelling and release mechanism study. *International Journal of Pharmaceutics,* 333**,** 143-151.

CONVENTION, U. S. P. 2009. *USP 32 NF 27: United States Pharmacopeia [and] National Formulary*, United States Pharmacopeial Convention.

COOK, I. J., FURUKAWA, Y., PANAGOPOULOS, V., COLLINS, P. J. & DENT, J. 2000. Relationships between spatial patterns of colonic pressure and individual movements of content. *Am J Physiol Gastrointest Liver Physiol,* 278**,** G329-41.

CORSETTI, M., PAGLIARO, G., DEMEDTS, I., DELOOSE, E., GEVERS, A., SCHEERENS, C., ROMMEL, N. & TACK, J. 2016. Pan-Colonic Pressurizations Associated With Relaxation of the Anal Sphincter in Health and Disease: A New Colonic Motor Pattern Identified Using High-Resolution Manometry. *Am J Gastroenterol*.

COSTA, M., DODDS, K. N., WIKLENDT, L., SPENCER, N. J., BROOKES, S. J. & DINNING, P. G. 2013a. Neurogenic and myogenic motor activity in the colon of the guinea pig, mouse, rabbit, and rat. *Am J Physiol Gastrointest Liver Physiol,* 305**,** G749-59.

COSTA, M., WIKLENDT, L., ARKWRIGHT, J. W., SPENCER, N. J., OMARI, T., BROOKES, S. J. & DINNING, P. G. 2013b. An experimental method to identify neurogenic and myogenic active mechanical states of intestinal motility. *Front Syst Neurosci,* 7.

COSTA, M., WIKLENDT, L., ARKWRIGHT, J. W., SPENCER, N. J., OMARI, T., BROOKES, S. J. H. & DINNING, P. G. 2013c. An experimental method to identify neurogenic and myogenic active mechanical states of intestinal motility. *Frontiers in Systems Neuroscience,* 7**,** 7.

COSTA, M., WIKLENDT, L., SIMPSON, P., SPENCER, N. J., BROOKES, S. J. & DINNING, P. G. 2015. Neuromechanical factors involved in the formation and propulsion of fecal pellets in the guinea-pig colon. *Neurogastroenterol Motil,* 27**,** 1466-77.

COSTA, P. & LOBO, J. M. S. 2001. Influence of Dissolution Medium Agitation on Release Profiles of Sustained-Release Tablets. *Drug Development and Industrial Pharmacy,* 27**,** 811-817.

COX, D. C., FURMAN, W. B., THORNTON, L. K., MOORE, T. W. & JEFFERSON, E. H. 1983. Systematic error associated with apparatus 2 of the USP dissolution test III: limitations of calibrators and the USP suitability test. *J Pharm Sci,* 72**,** 910-3.

COX, D. C., WELLS, C. E., FURMAN, W. B., SAVAGE, T. S. & KING, A. C. 1982. Systematic error associated with apparatus 2 of the USP dissolution test II: Effects of deviations in vessel curvature from that of a sphere. *J Pharm Sci,* 71**,** 395-9.

CREMA, A., FRIGO, G. M. & LECCHINI, S. 1970. A pharmacological analysis of the peristaltic reflex in the isolated colon of the guinea-pig or cat. *Br J Pharmacol,* 39**,** 334-45.

CUMMINGS, J. H., BINGHAM, S. A., HEATON, K. W. & EASTWOOD, M. A. 1992. Fecal weight, colon cancer risk, and dietary intake of nonstarch polysaccharides (dietary fiber). *Gastroenterology,* 103**,** 1783-9.

D'ANTONA, G., HENNIG, G. W., COSTA, M., HUMPHREYS, C. M. & BROOKES, S. J. 2001. Analysis of motor patterns in the isolated guinea-pig large intestine by spatio-temporal maps. *Neurogastroenterol Motil,* 13**,** 483-92.

D'ARCY, D. M., CORRIGAN, O. I. & HEALY, A. M. 2005. Hydrodynamic simulation (computational fluid dynamics) of asymmetrically positioned tablets in the paddle dissolution apparatus: impact on dissolution rate and variability. *J Pharm Pharmacol,* 57**,** 1243-50.

DANCKWERTS, P. V. 1952. The definition and measurement of some characteristics of mixtures. *Applied Scientific Research, Section A,* 3**,** 279-296.

DAS, S., DESHMUKH, R. & JHA, A. K. 2010. Role of natural polymers in the development of multiparticulate systems for colon drug targeting. *Systematic Reviews in Pharmacy,* 1**,** 79-85.

DAVIDSON, J. B., O'GRADY, G., ARKWRIGHT, J. W., ZARATE, N., SCOTT, S. M., PULLAN, A. J. & DINNING, P. J. 2011. Anatomical registration and three-dimensional visualization of low and high-resolution pan-colonic manometry recordings. *Neurogastroenterol Motil,* 23**,** 387-90, e171.

DEITEREN, A., CAMILLERI, M., BHARUCHA, A. E., BURTON, D., MCKINZIE, S., RAO, A. & ZINSMEISTER, A. R. 2010. PERFORMANCE CHARACTERISTICS OF SCINTIGRAPHIC COLON TRANSIT MEASUREMENT IN HEALTH AND IRRITABLE BOWEL SYNDROME AND RELATIONSHIP TO BOWEL FUNCTIONS. *Neurogastroenterology and motility : the official journal of the European Gastrointestinal Motility Society,* 22**,** 415-e95.

DEY, N. S., MAJUMDAR, S. & RAO, M. E. B. 2008. Multiparticulate Drug Delivery Systems for Controlled Release. *Tropical Journal of Pharmaceutical Research,* 7**,** 1067-1075.

DIAKIDOU, A., VERTZONI, M., GOUMAS, K., SODERLIND, E., ABRAHAMSSON, B., DRESSMAN, J. & REPPAS, C. 2009. Characterization of the contents of ascending colon to which drugs are exposed after oral administration to healthy adults. *Pharm Res,* 26**,** 2141-51.

DICKINSON, P. A., ABU RMAILEH, R., ASHWORTH, L., BARKER, R. A., BURKE, W. M., PATTERSON, C. M., STAINFORTH, N. & YASIN, M. 2012. An Investigation into the Utility of a Multi-compartmental, Dynamic, System of the Upper Gastrointestinal Tract to Support Formulation Development and Establish Bioequivalence of Poorly Soluble Drugs. *The AAPS Journal,* 14**,** 196-205.

DINNING, P. G., ARKWRIGHT, J. W., COSTA, M., WIKLENDT, L., HENNIG, G., BROOKES, S. J. H. & SPENCER, N. J. 2011. Temporal relationships between wall motion, intraluminal pressure, and flow in the isolated rabbit small intestine. *American Journal of Physiology - Gastrointestinal and Liver Physiology,* 300**,** G577-G585.

DINNING, P. G., BAMPTON, P. A., ANDRE, J., KENNEDY, M. L., LUBOWSKI, D. Z., KING, D. W. & COOK, I. J. 2004. Abnormal predefecatory colonic motor patterns define constipation in obstructed defecation. *Gastroenterology,* 127**,** 49-56.

DINNING, P. G., BAMPTON, P. A., KENNEDY, M. L., KAJIMOTO, T., LUBOWSKI, D. Z., DE CARLE, D. J. & COOK, I. J. 1999. Basal pressure patterns and reflexive motor responses in the human ileocolonic junction. *American Journal of Physiology - Gastrointestinal and Liver Physiology,* 276**,** G331-G340.

DINNING, P. G., COSTA, M., BROOKES, S. J. & SPENCER, N. J. 2012. Neurogenic and myogenic motor patterns of rabbit proximal, mid, and distal colon. *Am J Physiol Gastrointest Liver Physiol,* 303**,** G83-92.

DINNING, P. G. & DI LORENZO, C. 2011. Colonic dysmotility in constipation. *Best Pract Res Clin Gastroenterol,* 25**,** 89-101.

DINNING, P. G., SZCZESNIAK, M. M. & COOK, I. J. 2008. Proximal colonic propagating pressure waves sequences and their relationship with movements of content in the proximal human colon. *Neurogastroenterol Motil,* 20**,** 512-20.

DINNING, P. G., WIKLENDT, L., GIBBINS, I., PATTON, V., BAMPTON, P., LUBOWSKI, D. Z., COOK, I. J. & ARKWRIGHT, J. W. 2013. Low-resolution colonic manometry leads to a gross misinterpretation of the frequency and polarity of propagating sequences: Initial results from fiber-optic high-resolution manometry studies. *Neurogastroenterol Motil,* 25**,** e640-9.

DINNING, P. G., WIKLENDT, L., MASLEN, L., GIBBINS, I., PATTON, V., ARKWRIGHT, J. W., LUBOWSKI, D. Z., O'GRADY, G., BAMPTON, P. A., BROOKES, S. J. & COSTA, M. 2014a. Quantification of in vivo colonic motor patterns in healthy humans before and after a meal revealed by high-resolution fiber-optic manometry. *Neurogastroenterol Motil,* 26**,** 1443-57.

DINNING, P. G., WIKLENDT, L., OMARI, T., ARKWRIGHT, J. W., SPENCER, N. J., BROOKES, S. J. H. & COSTA, M. 2014b. Neural mechanisms of peristalsis in the isolated rabbit distal colon: a neuromechanical loop hypothesis. *Frontiers in Neuroscience,* 8.

DINNING, P. G., ZARATE, N., HUNT, L. M., FUENTEALBA, S. E., MOHAMMED, S. D., SZCZESNIAK, M. M., LUBOWSKI, D. Z., PRESTON, S. L., FAIRCLOUGH, P. D., LUNNISS, P. J., SCOTT, S. M. & COOK, I. J. 2010. Pancolonic spatiotemporal mapping reveals regional deficiencies in, and disorganization of colonic propagating pressure waves in severe constipation. *Neurogastroenterol Motil,* 22**,** e340-9.

EDSMAN, K. & HAGERSTROM, H. 2005. Pharmaceutical applications of mucoadhesion for the non-oral routes. *J Pharm Pharmacol,* 57**,** 3-22.

EDWARDS, M. F., BAKER, M. R. & GODFREY, J. C. 1992. Chapter 8 - Mixing of liquids in stirred tanks. *In:* HARNBY, N., EDWARDS, M. F. & NIENOW, A. W. (eds.) *Mixing in the Process Industries (Second Edition).* Oxford: Butterworth-Heinemann.

ERIK, S. 2010. Physiological Factors Affecting Drug Release and Absorption in the Gastrointestinal Tract. *Oral Drug Absorption.* CRC Press.

FALLINGBORG, J., CHRISTENSEN, L., JACOBSEN, B. & RASMUSSEN, S. 1993. Very low intraluminal colonic pH in patients with active ulcerative colitis. *Digestive Diseases and Sciences,* 38**,** 1989-1993.

FARMER, A. D., SCOTT, S. M. & HOBSON, A. R. 2013. Gastrointestinal motility revisited: The wireless motility capsule. *United European Gastroenterology Journal,* 1**,** 413-421.

FLOREY, H. 1955. Mucin and the protection of the body. *Proc R Soc Lond B Biol Sci,* 143**,** 147-58.

FOTAKI, N., AIVALIOTIS, A., BUTLER, J., DRESSMAN, J., FISCHBACH, M., HEMPENSTALL, J., KLEIN, S. & REPPAS, C. 2009a. A comparative study of different release apparatus in generating in vitro-in vivo correlations for extended release formulations. *Eur J Pharm Biopharm,* 73**,** 115-20.

FOTAKI, N., AIVALIOTIS, A., BUTLER, J., DRESSMAN, J., FISCHBACH, M., HEMPENSTALL, J., KLEIN, S. & REPPAS, C. 2009b. A comparative study of different release apparatus in generating in vitro–in vivo correlations for extended release formulations. *European Journal of Pharmaceutics and Biopharmaceutics,* 73**,** 115-120.

FUKUI, E., MIYAMURA, N., UEMURA, K. & KOBAYASHI, M. 2000. Preparation of enteric coated timed-release press-coated tablets and evaluation of their function by in vitro and in vivo tests for colon targeting. *International Journal of Pharmaceutics,* 204**,** 7-15.

GABRIELE, A., NIENOW, A. W. & SIMMONS, M. J. H. 2009. Corrigendum to ‘‘Use of angle resolved PIV to estimate local specific energy dissipation rates for up- and down-pumping pitched blade agitators in a stirred tank” [Chem. Eng. Sci. 64 (2009) 126–143]. *Chemical Engineering Science,* 64**,** 4196.

GABRIO BASSOTTI, G. D. R., DANILO CASTELLANI, LUCA SEDIARI, ANTONIO MORELLI 2005. Normal aspects of colorectal motility and abnormalities in slow transit constipation. *World Journal of Gastroenterology,* 11**,** 2691-2696.

GABRIO BASSOTTI, G. I., SERAFINA FIORELLA, LUIS BUSTOS-FERNANDEZ, AND CLAUDIO R. BILDER 1999. Colonic Motility in Man: Features in Normal Subjects and in Patients With Chronic Idiopathic Constipation. *THE AMERICAN JOURNAL OF GASTROENTEROLOGY,* 97**,** 1760-1770.

GARBACZ, G., GOLKE, B., WEDEMEYER, R. S., AXELL, M., SODERLIND, E., ABRAHAMSSON, B. & WEITSCHIES, W. 2009. Comparison of dissolution profiles obtained from nifedipine extended release once a day products using different dissolution test apparatuses. *Eur J Pharm Sci,* 38**,** 147-55.

GARBACZ, G. & KLEIN, S. 2012. Dissolution testing of oral modified-release dosage forms. *J Pharm Pharmacol,* 64**,** 944-68.

GARBACZ, G., WEDEMEYER, R.-S., NAGEL, S., GIESSMANN, T., MÖNNIKES, H., WILSON, C. G., SIEGMUND, W. & WEITSCHIES, W. 2008. Irregular absorption profiles observed from diclofenac extended release tablets can be predicted using a dissolution test apparatus that mimics in vivo physical stresses. *European Journal of Pharmaceutics and Biopharmaceutics,* 70**,** 421-428.

GAZZANIGA, A., IAMARTINO, P., MAFFIONE, G. & SANGALLI, M. E. 1994. Oral delayed-release system for colonic specific delivery. *International Journal of Pharmaceutics,* 108**,** 77-83.

GRAY, V., KELLY, G., XIA, M., BUTLER, C., THOMAS, S. & MAYOCK, S. 2009. The Science of USP 1 and 2 Dissolution: Present Challenges and Future Relevance. *Pharmaceutical Research,* 26**,** 1289-1302.

GUIDA, A., FAN, X., PARKER, D. J., NIENOW, A. W. & BARIGOU, M. 2009. Positron emission particle tracking in a mechanically agitated solid–liquid suspension of coarse particles. *Chemical Engineering Research and Design,* 87**,** 421-429.

HAMMER, J., PRUCKMAYER, M., BERGMANN, H., KLETTER, K. & GANGL, A. 1997. The distal colon provides reserve storage capacity during colonic fluid overload. *Gut,* 41**,** 658-63.

HEBDEN, J. M., GILCHRIST, P. J., PERKINS, A. C., WILSON, C. G. & SPILLER, R. C. 1999. Stool water content and colonic drug absorption: contrasting effects of lactulose and codeine. *Pharm Res,* 16**,** 1254-9.

HÉNIN, E., BERGSTRAND, M., WEITSCHIES, W. & KARLSSON, M. O. 2016. Meta-analysis of Magnetic Marker Monitoring Data to Characterize the Movement of Single Unit Dosage Forms Though the Gastrointestinal Tract Under Fed and Fasting Conditions. *Pharmaceutical Research,* 33**,** 751-762.

HERBST, F., KAMM, M. A., MORRIS, G. P., BRITTON, K., WOLOSZKO, J. & NICHOLLS, R. J. 1997. Gastrointestinal transit and prolonged ambulatory colonic motility in health and faecal incontinence. *Gut,* 41**,** 381-9.

HIGUCHI, M., YOSHIHASHI, Y., TARADA, K. & SUGANO, K. 2014. Minimum rotation speed to prevent coning phenomena in compendium paddle dissolution apparatus. *European Journal of Pharmaceutical Sciences,* 65**,** 74-78.

HINTON, J. M., LENNARD-JONES, J. E. & YOUNG, A. C. 1969. A new method for studying gut transit times using radioopaque markers. *Gut,* 10**,** 842-847.

HIROZ, P., SCHLAGETER, V., GIVEL, J. C. & KUCERA, P. 2009. Colonic movements in healthy subjects as monitored by a Magnet Tracking System. *Neurogastroenterol Motil,* 21**,** 1365-2982.

HU, Y., LIU, Z., YANG, J., JIN, Y. & CHENG, Y. 2010. Study on the reactive mixing process in an unbaffled stirred tank using planar laser-induced fluorescence (PLIF) technique. *Chemical Engineering Science,* 65**,** 4511-4518.

JAIN, D., RATURI, R., JAIN, V., BANSAL, P. & SINGH, R. 2011. Recent technologies in pulsatile drug delivery systems. *Biomatter,* 1**,** 57-65.

JANTRATID, E., DE MAIO, V., RONDA, E., MATTAVELLI, V., VERTZONI, M. & DRESSMAN, J. B. 2009. Application of biorelevant dissolution tests to the prediction of in vivo performance of

diclofenac sodium from an oral modified-release pellet dosage form. *Eur J Pharm Sci,* 37**,** 434-41.

JANTRATID, E., JANSSEN, N., CHOKSHI, H., TANG, K. & DRESSMAN, J. B. 2008. Designing biorelevant dissolution tests for lipid formulations: Case example – Lipid suspension of RZ-50. *European Journal of Pharmaceutics and Biopharmaceutics,* 69**,** 776-785.

JIMÉNEZ-CASTELLANOS, M. R., ZIA, H. & RHODES, C. T. 1993. Mucoadhesive Drug Delivery Systems. *Drug Development and Industrial Pharmacy,* 19**,** 143-194.

JOHNSON, I. T. & GEE, J. M. 1981. Effect of gel-forming gums on the intestinal unstirred layer and sugar transport in vitro. *Gut,* 22**,** 398-403.

JOUËT, P., SABATÉ, J. M., COFFIN, B., LÉMANN, M., JIAN, R. & FLOURIÉ, B. 2011. Fermentation of starch stimulates propagated contractions in the human colon. *Neurogastroenterology and Motility,* 23**,** 450.

KAMM, M. A., VAN DER SIJP, J. R. & LENNARD-JONES, J. E. 1992. Observations on the characteristics of stimulated defaecation in severe idiopathic constipation. *Int J Colorectal Dis,* 7**,** 197-201.

KANG, M. J., KHANAL, T., KIM, H. G., LEE, D. H., YEO, H. K., LEE, Y. S., AHN, Y. T., KIM, D. H., JEONG, H. G. & JEONG, T. C. 2012. Role of metabolism by human intestinal microflora in geniposide-induced toxicity in HepG2 cells. *Arch Pharm Res,* 35**,** 733-8.

KAPLAN, G. G. 2015. The global burden of IBD: from 2015 to 2025. *Nat Rev Gastroenterol Hepatol,* 12**,** 720-727.

KARAUS, M. & WIENBECK, M. 1991. Colonic motility in humans--a growing understanding. *Baillieres Clin Gastroenterol,* 5**,** 453-78.

KELVIN, F. M. & GARDINER, R. 1987. *Clinical Imaging of the Colon and Rectum*, Books on Demand.

KHAN, M. Z., STEDUL, H. P. & KURJAKOVIC, N. 2000. A pH-dependent colon-targeted oral drug delivery system using methacrylic acid copolymers. II. Manipulation of drug release using Eudragit L100 and Eudragit S100 combinations. *Drug Dev Ind Pharm,* 26**,** 549-54.

KHAN, M. Z. I., PREBEG, Ž. & KURJAKOVIĆ, N. 1999. A pH-dependent colon targeted oral drug delivery system using methacrylic acid copolymers: I. Manipulation of drug release using Eudragit® L100-55 and Eudragit® S100 combinations. *Journal of Controlled Release,* 58**,** 215-222.

KIM, E. R. & RHEE, P.-L. 2012. How to Interpret a Functional or Motility Test - Colon Transit Study. *Journal of Neurogastroenterology and Motility,* 18**,** 94-99.

KIM, H., LEE, Y., YOO, H., KIM, J., KONG, H., YOON, J. H., JUNG, Y. & KIM, Y. M. 2012. Synthesis and evaluation of sulfate conjugated metronidazole as a colon-specific prodrug of metronidazole. *J Drug Target,* 20**,** 255-63.

KLANCAR, U., MARKUN, B., BAUMGARTNER, S. & LEGEN, I. 2013. A novel beads-based dissolution method for the in vitro evaluation of extended release HPMC matrix tablets and the correlation with the in vivo data. *Aaps J,* 15**,** 267-77.

KLANČAR, U., MARKUN, B., BAUMGARTNER, S. & LEGEN, I. 2013. A Novel Beads-Based Dissolution Method for the In Vitro Evaluation of Extended Release HPMC Matrix Tablets and the Correlation with the In Vivo Data. *The AAPS Journal,* 15**,** 267-277.

KLEIN, S. 2010. The Use of Biorelevant Dissolution Media to Forecast the In Vivo Performance of a Drug. *The AAPS Journal,* 12**,** 397-406.

KLEIN, S. & SHAH, V. 2008a. A Standardized Mini Paddle Apparatus as an Alternative to the Standard Paddle. *AAPS PharmSciTech,* 9**,** 1179-1184.

KLEIN, S. & SHAH, V. P. 2008b. A Standardized Mini Paddle Apparatus as an Alternative to the Standard Paddle. *AAPS PharmSciTech,* 9**,** 1179-1184.

KONG, F. & SINGH, R. P. 2008. Disintegration of solid foods in human stomach. *J Food Sci,* 73**,** R67-80.

KORSMEYER, R. W., GURNY, R., DOELKER, E., BURI, P. & PEPPAS, N. A. 1983. Mechanisms of solute release from porous hydrophilic polymers. *International Journal of Pharmaceutics,* 15**,** 25-35.

KOSARAJU, S. L. 2005. Colon Targeted Delivery Systems: Review of Polysaccharides for Encapsulation and Delivery. *Critical Reviews in Food Science and Nutrition,* 45**,** 251-258.

KOSTEWICZ, E. S., ABRAHAMSSON, B., BREWSTER, M., BROUWERS, J., BUTLER, J., CARLERT, S., DICKINSON, P. A., DRESSMAN, J., HOLM, R., KLEIN, S., MANN, J., MCALLISTER, M., MINEKUS, M., MUENSTER, U., MULLERTZ, A., VERWEI, M., VERTZONI, M., WEITSCHIES, W. & AUGUSTIJNS, P. 2014. In vitro models for the prediction of in vivo performance of oral dosage forms. *Eur J Pharm Sci,* 57**,** 342-66.

KOULAOUZIDIS, A., IAKOVIDIS, D. K., KARARGYRIS, A. & RONDONOTTI, E. 2015. Wireless endoscopy in 2020: Will it still be a capsule? *World Journal of Gastroenterology : WJG,* 21**,** 5119-5130.

KOZIOLEK, M., SCHNEIDER, F., GRIMM, M., MODEB, C., SEEKAMP, A., ROUSTOM, T., SIEGMUND, W. & WEITSCHIES, W. 2015. Intragastric pH and pressure profiles after intake of the high-caloric, high-fat meal as used for food effect studies. *Journal of Controlled Release,* 220, Part A**,** 71-78.

KRÖGEL, I. & BODMEIER, R. 1998. Pulsatile Drug Release from an Insoluble Capsule Body Controlled by an Erodible Plug. *Pharmaceutical Research,* 15**,** 474-481.

KRUL, C., LUITEN-SCHUITE, A., BAAN, R., VERHAGEN, H., MOHN, G., FERON, V. & HAVENAAR, R. 2000. Application of a dynamic in vitro gastrointestinal tract model to study the availability of food mutagens, using heterocyclic aromatic amines as model compounds. *Food and Chemical Toxicology,* 38**,** 783-792.

KUKURA, J., ARRATIA, P. E., SZALAI, E. S. & MUZZIO, F. J. 2003a. Engineering tools for understanding the hydrodynamics of dissolution tests. *Drug Dev Ind Pharm,* 29**,** 231-9.

KUKURA, J., ARRATIA, P. E., SZALAI, E. S. & MUZZIO, F. J. 2003b. Engineering Tools for Understanding the Hydrodynamics of Dissolution Tests. *Drug Development and Industrial Pharmacy,* 29**,** 231-239.

KUKURA, J., BAXTER, J. L. & MUZZIO, F. J. 2004. Shear distribution and variability in the USP Apparatus 2 under turbulent conditions. *Int J Pharm,* 279**,** 9-17.

LAI, S. K., WANG, Y. Y., WIRTZ, D. & HANES, J. 2009. Micro- and macrorheology of mucus. *Adv Drug Deliv Rev,* 61**,** 86-100.

LANGER, P. & TAKÁCS, Á. 2004. Why are taeniae, haustra, and semilunar folds differentiated in the gastrointestinal tract of mammals, including man? *Journal of Morphology,* 259**,** 308-315.

LARSSON, M., MINEKUS, M. & HAVENAAR, R. 1997. Estimation of the Bioavailability of Iron and Phosphorus in Cereals using a Dynamic In Vitro Gastrointestinal Model. *Journal of the Science of Food and Agriculture,* 74**,** 99-106.

LAW, A. W.-K. & WANG, H. 2000. Measurement of mixing processes with combined digital particle image velocimetry and planar laser induced fluorescence. *Experimental Thermal and Fluid Science,* 22**,** 213-229.

LEADBEATER, T. W. & PARKER, D. J. 2009. A high speed PC-based data acquisition and control system for positron imaging. *Nuclear Instruments and Methods in Physics Research Section A: Accelerators, Spectrometers, Detectors and Associated Equipment,* 604**,** 355-358.

LEVY, G. & JUSKO, W. J. 1965. Effect of viscosity on drug absorption. *Journal of Pharmaceutical Sciences,* 54**,** 219-225.

LIU, Y.-A., CHUNG, Y.-C., PAN, S.-T., HOU, Y.-C., PENG, S.-J., PASRICHA, P. J. & TANG, S.-C. 2012. 3-D illustration of network orientations of interstitial cells of Cajal subgroups in human colon as revealed by deep-tissue imaging with optical clearing. *American Journal of Physiology - Gastrointestinal and Liver Physiology,* 302**,** G1099-G1110.

LONG, M. & CHEN, Y. 2009. Chapter 14 - Dissolution Testing of Solid Products. *Developing Solid Oral Dosage Forms.* San Diego: Academic Press.

MACFARLANE, G. T., GIBSON, G. R. & CUMMINGS, J. H. 1992. Comparison of fermentation reactions in different regions of the human colon. *J Appl Bacteriol,* 72**,** 57-64.

MADERUELO, C., ZARZUELO, A. & LANAO, J. M. 2011. Critical factors in the release of drugs from sustained release hydrophilic matrices. *Journal of Controlled Release,* 154**,** 2-19.

MAÑÉ, N., MARTÍNEZ-CUTILLAS, M., GALLEGO, D. & JIMENEZ, M. 2015. Enteric motor pattern generators involve both myogenic and neurogenic mechanisms in the human colon. *Frontiers in Physiology,* 6.

MANFRED R. VON DER OHE, M. C., LARRY K. KVOLS, AND GEORGE M. THOMFORDE 1993. Motor dysfunction of the small bowel and colon in patients with the carcinoid syndrome and diarrhea. *The new England journal of medicine,* 329**,** 1073-1078.

MAQBOOL, S., PARKMAN, H. P. & FRIEDENBERG, F. K. 2009. Wireless Capsule Motility: Comparison of the SmartPill® GI Monitoring System with Scintigraphy for Measuring Whole Gut Transit. *Digestive Diseases and Sciences,* 54**,** 2167-2174.

MARONI, A., ZEMA, L., LORETI, G., PALUGAN, L. & GAZZANIGA, A. 2013. Film coatings for oral pulsatile release. *International Journal of Pharmaceutics,* 457**,** 362-371.

MCALLISTER, M. 2010. Dynamic dissolution: a step closer to predictive dissolution testing? *Mol Pharm,* 7**,** 1374-87.

MCCONNELL, E. L., FADDA, H. M. & BASIT, A. W. 2008. Gut instincts: Explorations in intestinal physiology and drug delivery. *International Journal of Pharmaceutics,* 364**,** 213-226.

METZNER, A. B. & OTTO, R. E. 1957. Agitation of non-Newtonian fluids. *AIChE Journal,* 3**,** 3-10.

MIHAILOVA, O., LIM, V., MCCARTHY, M. J., MCCARTHY, K. L. & BAKALIS, S. 2015. Laminar mixing in a SMX static mixer evaluated by positron emission particle tracking (PEPT) and magnetic resonance imaging (MRI). *Chemical Engineering Science,* 137**,** 1014-1023.

MILLER, D. A., GAMBA, M., SAUER, D., PURVIS, T. P., CLEMENS, N. T. & WILLIAMS III, R. O. 2007. Evaluation of the USP dissolution test method A for enteric-coated articles by planar laser-induced fluorescence. *International Journal of Pharmaceutics,* 330**,** 61-72.

MINEKUS, M. 2015. The TNO Gastro-Intestinal Model (TIM). *In:* VERHOECKX, K., COTTER, P., LÓPEZ-EXPÓSITO, I., KLEIVELAND, C., LEA, T., MACKIE, A., REQUENA, T., SWIATECKA, D. & WICHERS, H. (eds.) *The Impact of Food Bioactives on Health: in vitro and ex vivo models.* Cham: Springer International Publishing.

MIRZA, T., JOSHI, Y., LIU, Q. J. & VIVILECCHIA, R. 2005. Evaluation of Dissolution Hydrodynamics in the USP, Peak™ and Flat-Bottom Vessels Using Different Solubility Drugs. *Dissolution Technologies*.

MITCHELL, K., FORD, J. L., ARMSTRONG, D. J., ELLIOTT, P. N. C., HOGAN, J. E. & ROSTRON, C. 1993. The influence of drugs on the properties of gels and swelling characteristics of matrices containing methylcellulose or hydroxypropylmethylcellulose. *International Journal of Pharmaceutics,* 100**,** 165-173.

MOLODECKY, N. A., SOON, I. S., RABI, D. M., GHALI, W. A., FERRIS, M., CHERNOFF, G., BENCHIMOL, E. I., PANACCIONE, R., GHOSH, S., BARKEMA, H. W. & KAPLAN, G. G. 2012. Increasing Incidence and Prevalence of the Inflammatory Bowel Diseases With Time, Based on Systematic Review. *Gastroenterology,* 142**,** 46-54.e42.

MORENO-OSSET, E., BAZZOCCHI, G., LO, S., TROMBLEY, B., RISTOW, E., REDDY, S. N., VILLANUEVA-MEYER, J., FAIN, J. W., JING, J., MENA, I. & ET AL. 1989. Association between postprandial changes in colonic intraluminal pressure and transit. *Gastroenterology,* 96**,** 1265-73.

MORONI, A. & GHEBRE-SELLASSIE, I. 1995. Application of Poly(oxyethylene) Homopolymers in Sustained Release Solid Formulations. *Drug Development and Industrial Pharmacy,* 21**,** 1411-1428.

MRSNY, R. J. 1992. The colon as a site for drug delivery. *Journal of Controlled Release,* 22**,** 15-34.

MUDIE, D. M., MURRAY, K., HOAD, C. L., PRITCHARD, S. E., GARNETT, M. C., AMIDON, G. L., GOWLAND, P. A., SPILLER, R. C., AMIDON, G. E. & MARCIANI, L. 2014. Quantification of Gastrointestinal Liquid Volumes and Distribution Following a 240 mL Dose of Water in the Fasted State. *Molecular Pharmaceutics,* 11**,** 3039-3047.

NARDUCCI, F., BASSOTTI, G., GABURRI, M. & MORELLI, A. 1987. Twenty four hour manometric recording of colonic motor activity in healthy man. *Gut,* 28**,** 17-25.

NUGENT, S., KUMAR, D., RAMPTON, D. & EVANS, D. 2001. Intestinal luminal pH in inflammatory bowel disease: possible determinants and implications for therapy with aminosalicylates and other drugs. *Gut,* 48**,** 571-577.

OCHOA, L., IGARTUA, M., HERNANDEZ, R. M., GASCON, A. R. & PEDRAZ, J. L. 2005. Preparation of sustained release hydrophilic matrices by melt granulation in a high-shear mixer. *J Pharm Pharm Sci,* 8**,** 132-40.

PALMA, R., VIDON, N. & BERNIER, J. J. 1981. Maximal capacity for fluid absorption in human bowel. *Dig Dis Sci,* 26**,** 929-34.

PARKER, D. J., ALLEN, D. A., BENTON, D. M., FOWLES, P., MCNEIL, P. A., TAN, M. & BEYNON, T. D. 1997. Developments in particle tracking using the Birmingham Positron Camera. *Nuclear Instruments and Methods in Physics Research Section A: Accelerators, Spectrometers, Detectors and Associated Equipment,* 392**,** 421-426.

PARKER, D. J. & FAN, X. 2008. Positron emission particle tracking—Application and labelling techniques. *Particuology,* 6**,** 16-23.

PARKER, D. J., FORSTER, R. N., FOWLES, P. & TAKHAR, P. S. 2002. Positron emission particle tracking using the new Birmingham positron camera. *Nuclear Instruments and Methods in Physics Research Section A: Accelerators, Spectrometers, Detectors and Associated Equipment,* 477**,** 540-545.

PAROJCIC, J., VASILJEVIC, D., IBRIC, S. & DJURIC, Z. 2008. Tablet disintegration and drug dissolution in viscous media: paracetamol IR tablets. *Int J Pharm,* 355**,** 93-9.

PEPPAS, N. A., THOMAS, J. B. & MCGINITY, J. 2009. Molecular Aspects of Mucoadhesive Carrier Development for Drug Delivery and Improved Absorption. *Journal of biomaterials science. Polymer edition,* 20**,** 1-20.

PHILIP, A. K. & PATHAK, K. 2006. Osmotic flow through asymmetric membrane: A means for controlled delivery of drugs with varying solubility. *AAPS PharmSciTech,* 7**,** E1-E11.

PHILIP, A. K. & PHILIP, B. 2010. Colon Targeted Drug Delivery Systems: A Review on Primary and Novel Approaches. *Oman Medical Journal,* 25**,** 79-87.

PIANKO-OPRYCH, P., NIENOW, A. W. & BARIGOU, M. 2009. Positron emission particle tracking (PEPT) compared to particle image velocimetry (PIV) for studying the flow generated by a pitched-blade turbine in single phase and multi-phase systems. *Chemical Engineering Science,* 64**,** 4955-4968.

PICON, L., LEMANN, M., FLOURIE, B., RAMBAUD, J. C., RAIN, J. D. & JIAN, R. 1992. Right and left colonic transit after eating assessed by a dual isotopic technique in healthy humans. *Gastroenterology,* 103**,** 80-5.

PRASAD, K., BADARINATH, A.V., ANILKUMAR, P., RAVISANKAR REDDY, B., NAVEEN, N., NIROSHA, M., & HYNDAVI, M. 2011. Colon targeted drug delivery systems: a review. *Journal of Global Trends in Pharmaceutical Sciences,* 2**,** 459-475.

PRASANTH, V. V., JAYAPRAKASH, R. & MATHEW, S. T. 2012. Colon Specific Drug Delivery Systems: A Review on Various Pharmaceutical Approaches. *Journal of Applied Pharmaceutical Science,* 2**,** 163-169.

PRITCHARD, S. E., MARCIANI, L., GARSED, K. C., HOAD, C. L., THONGBORISUTE, W., ROBERTS, E., GOWLAND, P. A. & SPILLER, R. C. 2014. Fasting and postprandial volumes of the undisturbed colon: normal values and changes in diarrhea-predominant irritable bowel syndrome measured using serial MRI. *Neurogastroenterol Motil,* 26**,** 124-30.

PROANO, M., CAMILLERI, M., PHILLIPS, S. F., BROWN, M. L. & THOMFORDE, G. M. 1990. Transit of solids through the human colon: regional quantification in the unprepared bowel. *Am J Physiol,* 258**,** G856-62.

QINGXI WANG, N. F., AND YUN MAO 2009. Biorelevant Dissolution: Methodology and Application in Drug Development. *Dissolution Technologies***,** 6-12.

QUIGLEY, E. M., BORODY, T. J., PHILLIPS, S. F., WIENBECK, M., TUCKER, R. L. & HADDAD, A. 1984. Motility of the terminal ileum and ileocecal sphincter in healthy humans. *Gastroenterology,* 87**,** 857-66.

QURESHI, S. A. & SHABNAM, J. 2001a. Cause of high variability in drug dissolution testing and its impact on setting tolerances. *European Journal of Pharmaceutical Sciences,* 12**,** 271-276.

QURESHI, S. A. & SHABNAM, J. 2001b. Cause of high variability in drug dissolution testing and its impact on setting tolerances. *Eur J Pharm Sci,* 12**,** 271-6.

RADWAN, A., AMIDON, G. L. & LANGGUTH, P. 2012. Mechanistic investigation of food effect on disintegration and dissolution of BCS class III compound solid formulations: the importance of viscosity. *Biopharm Drug Dispos,* 33**,** 403-16.

RANGACHARI, P. 1990. Six-Pack Balancing Act: A Conceptual Model for the Intestinal Lining. *Canadian Journal of Gastroenterology,* 4.

RAO, S. S., KUO, B., MCCALLUM, R. W., CHEY, W. D., DIBAISE, J. K., HASLER, W. L., KOCH, K. L., LACKNER, J. M., MILLER, C., SAAD, R., SEMLER, J. R., SITRIN, M. D., WILDING, G. E. & PARKMAN, H. P. 2009. Investigation of colonic and whole-gut transit with wireless motility capsule and radiopaque markers in constipation. *Clin Gastroenterol Hepatol,* 7**,** 537-44.

RAO, S. S., SADEGHI, P., BEATY, J. & KAVLOCK, R. 2004. Ambulatory 24-hour colonic manometry in slow-transit constipation. *Am J Gastroenterol,* 99**,** 2405-16.

RAO, S. S., SADEGHI, P., BEATY, J., KAVLOCK, R. & ACKERSON, K. 2001. Ambulatory 24-h colonic manometry in healthy humans. *Am J Physiol Gastrointest Liver Physiol,* 280**,** G629-39.

RAO, S. S. & WELCHER, K. 1996. Periodic rectal motor activity: the intrinsic colonic gatekeeper? *Am J Gastroenterol,* 91**,** 890-7.

REDDY, S. N., BAZZOCCHI, G., CHAN, S., AKASHI, K., VILLANUEVA-MEYER, J., YANNI, G., MENA, I. & SNAPE, W. J., JR. 1991. Colonic motility and transit in health and ulcerative colitis. *Gastroenterology,* 101**,** 1289-97.

REPPAS, C., FRIEDEL, H. D., BARKER, A. R., BUHSE, L. F., CECIL, T. L., KEITEL, S., KRAEMER, J., MORRIS, J. M., SHAH, V. P., STICKELMEYER, M. P., YOMOTA, C. & BROWN, C. K. 2014. Biorelevant in vitro performance testing of orally administered dosage forms-workshop report. *Pharm Res,* 31**,** 1867-76.

REPPAS, C., KARATZA, E., GOUMAS, C., MARKOPOULOS, C. & VERTZONI, M. 2015. Characterization of Contents of Distal Ileum and Cecum to Which Drugs/Drug Products are Exposed During Bioavailability/Bioequivalence Studies in Healthy Adults. *Pharmaceutical Research,* 32**,** 3338-3349.

ROOS, A. A., EDLUND, U., SJÖBERG, J., ALBERTSSON, A.-C. & STÅLBRAND, H. 2008. Protein Release from Galactoglucomannan Hydrogels: Influence of Substitutions and Enzymatic Hydrolysis by β-Mannanase. *Biomacromolecules,* 9**,** 2104-2110.

RUBINSTEIN, A. 1990. Microbially controlled drug delivery to the colon. *Biopharm Drug Dispos,* 11**,** 465-75.

SAAD, R. J. 2016. The Wireless Motility Capsule: a One-Stop Shop for the Evaluation of GI Motility Disorders. *Current Gastroenterology Reports,* 18**,** 14.

SAAD, R. J. & HASLER, W. L. 2011. A Technical Review and Clinical Assessment of the Wireless Motility Capsule. *Gastroenterology & Hepatology,* 7**,** 795-804.

SADAHIRO, S., OHMURA, T., YAMADA, Y., SAITO, T. & TAKI, Y. 1992. Analysis of length and surface area of each segment of the large intestine according to age, sex and physique. *Surg Radiol Anat,* 14**,** 251-7.

SANDERS, K. M., WARD, S. M. & KOH, S. D. 2014. Interstitial cells: regulators of smooth muscle function. *Physiol Rev,* 94**,** 859-907.

SANDLE, G. I. 1998. Salt and water absorption in the human colon: a modern appraisal. *Gut,* 43**,** 294-9.

SARNA, S. K. & SHI, X.-Z. 2006. CHAPTER 39 - Function and Regulation of Colonic Contractions in Health and Disease A2 - Johnson, Leonard R. *Physiology of the Gastrointestinal Tract (Fourth Edition).* Burlington: Academic Press.

SAVITZKY, A. & GOLAY, M. J. E. 1964. Smoothing and Differentiation of Data by Simplified Least Squares Procedures. *Analytical Chemistry,* 36**,** 1627-1639.

SCHELLEKENS, R. C., STUURMAN, F. E., VAN DER WEERT, F. H., KOSTERINK, J. G. & FRIJLINK, H. W. 2007. A novel dissolution method relevant to intestinal release behaviour and its application in the evaluation of modified release mesalazine products. *Eur J Pharm Sci,* 30**,** 15-20.

SCHILLER, C., FROHLICH, C. P., GIESSMANN, T., SIEGMUND, W., MONNIKES, H., HOSTEN, N. & WEITSCHIES, W. 2005. Intestinal fluid volumes and transit of dosage forms as assessed by magnetic resonance imaging. *Aliment Pharmacol Ther,* 22**,** 971-9.

SCHNEIDER, F., GRIMM, M., KOZIOLEK, M., MODEß, C., DOKTER, A., ROUSTOM, T., SIEGMUND, W. & WEITSCHIES, W. 2016. Resolving the physiological conditions in bioavailability and bioequivalence studies: Comparison of fasted and fed state. *European Journal of Pharmaceutics and Biopharmaceutics,* 108**,** 214-219.

SCOTT, S. M. 2003. Manometric techniques for the evaluation of colonic motor activity: current status. *Neurogastroenterol Motil,* 15**,** 483-513.

SHAIKH, R., RAJ SINGH, T. R., GARLAND, M. J., WOOLFSON, A. D. & DONNELLY, R. F. 2011. Mucoadhesive drug delivery systems. *Journal of Pharmacy and Bioallied Sciences,* 3**,** 89-100.

SIMMONS, M. J. H., ALBERINI, F., TSOLIGKAS, A. N., GARGIULI, J., PARKER, D. J., FRYER, P. J. & ROBINSON, S. 2012. Development of a hydrodynamic model for the UV-C treatment of turbid food fluids in a novel 'SurePure turbulator™' swirl-tube reactor. *Innovative Food Science & Emerging Technologies,* 14**,** 122-134.

SINDHU ABRAHAM, M. S. 2007. Development of modified pulsincap drug delivery system of metronidazole for drug targeting. *Indian Journal of Pharmaceutics Sciences,* 69**,** 24 - 27.

SINHA, V., SINGH, A., KUMAR, R. V., SINGH, S., KUMRIA, R. & BHINGE, J. 2007. Oral colon-specific drug delivery of protein and peptide drugs. *Crit Rev Ther Drug Carrier Syst,* 24**,** 63-92.

SINHA, V. R. & KUMRIA, R. 2001. Polysaccharides in colon-specific drug delivery. *International Journal of Pharmaceutics,* 224**,** 19-38.

SINHA, V. R. & KUMRIA, R. 2003. Microbially triggered drug delivery to the colon. *European Journal of Pharmaceutical Sciences,* 18**,** 3-18.

SINNOTT, M. D., CLEARY, P. W., ARKWRIGHT, J. W. & DINNING, P. G. 2012. Investigating the relationships between peristaltic contraction and fluid transport in the human colon using Smoothed Particle Hydrodynamics. *Comput Biol Med,* 42**,** 492-503.

SINNOTT, M. D., CLEARY, P. W., DINNING, P. G., ARKWRIGHT, J. W. & COSTA, M. 2015. Interpreting manometric signals for propulsion in the gut. *Computational Particle Mechanics,* 2**,** 273-282.

SOULIMAN, S., BEYSSAC, E., CARDOT, J. M., DENIS, S. & ALRIC, M. 2007. Investigation of the biopharmaceutical behavior of theophylline hydrophilic matrix tablets using USP methods and an artificial digestive system. *Drug Dev Ind Pharm,* 33**,** 475-83.

SOULIMAN, S., BLANQUET, S., BEYSSAC, E. & CARDOT, J.-M. 2006. A level A in vitro/in vivo correlation in fasted and fed states using different methods: Applied to solid immediate release oral dosage form. *European Journal of Pharmaceutical Sciences,* 27**,** 72-79.

SOUTHWELL, B. R., CLARKE, M. C. C., SUTCLIFFE, J. & HUTSON, J. M. 2009. Colonic transit studies: normal values for adults and children with comparison of radiological and scintigraphic methods. *Pediatric Surgery International,* 25**,** 559-572.

SPENCER, N. J., DINNING, P. G., BROOKES, S. J. & COSTA, M. 2016. Insights into the mechanisms underlying colonic motor patterns. *J Physiol,* 594**,** 4099-116.

SPENCER, N. J., KYLOH, M., WATTCHOW, D. A., THOMAS, A., SIA, T. C., BROOKES, S. J. & NICHOLAS, S. J. 2012. Characterization of motor patterns in isolated human colon: are there differences in patients with slow-transit constipation? *Am J Physiol Gastrointest Liver Physiol,* 302**,** 29.

SPRATT, P., NICOLELLA, C. & PYLE, D. L. 2005. An Engineering Model of the Human Colon. *Food and Bioproducts Processing,* 83**,** 147-157.

STAMATOPOULOS, K., ALBERINI, F., BATCHELOR, H. & SIMMONS, M. J. H. 2016a. Use of PLIF to assess the mixing performance of small volume USP 2 apparatus in shear thinning media. *Chemical Engineering Science,* 145**,** 1-9.

STAMATOPOULOS, K., BATCHELOR, H. K., ALBERINI, F., RAMSAY, J. & SIMMONS, M. J. 2015. Understanding the impact of media viscosity on dissolution of a highly water soluble drug within a USP 2 mini vessel dissolution apparatus using an optical planar induced fluorescence (PLIF) method. *Int J Pharm,* 495**,** 362-373.

STAMATOPOULOS, K., BATCHELOR, H. K. & SIMMONS, M. J. H. 2016b. Dissolution profile of theophylline modified release tablets, using a biorelevant Dynamic Colon Model (DCM). *European Journal of Pharmaceutics and Biopharmaceutics,* 108**,** 9-17.

STATHOPOULOS, E., SCHLAGETER, V., MEYRAT, B., RIBAUPIERRE, Y. & KUCERA, P. 2005. Magnetic pill tracking: a novel non-invasive tool for investigation of human digestive motility. *Neurogastroenterol Motil,* 17**,** 148-54.

SUTTON, S. C. 2009. Role of physiological intestinal water in oral absorption. *Aaps J,* 11**,** 277-85.

SZMULOWICZ, U. & HULL, T. 2011. Colonic Physiology. *In:* BECK, D. E., ROBERTS, P. L., SACLARIDES, T. J., SENAGORE, A. J., STAMOS, M. J. & WEXNER, S. D. (eds.) *The ASCRS Textbook of Colon and Rectal Surgery.* Springer New York.

TAKAYA, T., NIWA, K., MURAOKA, M., OGITA, I., NAGAI, N., YANO, R., KIMURA, G., YOSHIKAWA, Y., YOSHIKAWA, H. & TAKADA, K. 1998. Importance of dissolution process on systemic availability of drugs delivered by colon delivery system. *J Control Release,* 50**,** 111-22.

THUENEMANN, E. C., MANDALARI, G., RICH, G. T. & FAULKS, R. M. 2015. Dynamic Gastric Model (DGM). *In:* VERHOECKX, K., COTTER, P., LÓPEZ-EXPÓSITO, I., KLEIVELAND, C., LEA, T., MACKIE, A., REQUENA, T., SWIATECKA, D. & WICHERS, H. (eds.) *The Impact of Food Bioactives on Health: in vitro and ex vivo models.* Cham: Springer International Publishing.

TOZAKI, H., KOMOIKE, J., TADA, C., MARUYAMA, T., TERABE, A., SUZUKI, T., YAMAMOTO, A. & MURANISHI, S. 1997. Chitosan capsules for colon-specific drug delivery: improvement of insulin absorption from the rat colon. *J Pharm Sci,* 86**,** 1016-21.

TRAN, K., BRUN, R. & KUO, B. 2012. Evaluation of regional and whole gut motility using the wireless motility capsule: relevance in clinical practice. *Therapeutic Advances in Gastroenterology,* 5**,** 249-260.

VAN CRUYNINGEN, I., LOZANO, A. & HANSON, R. K. 1990. Quantitative imaging of concentration by planar laser-induced fluorescence. *Experiments in Fluids,* 10**,** 41-49.

VARUM, F. J., MCCONNELL, E. L., SOUSA, J. J., VEIGA, F. & BASIT, A. W. 2008. Mucoadhesion and the gastrointestinal tract. *Crit Rev Ther Drug Carrier Syst,* 25**,** 207-58.

VARUM, F. J., VEIGA, F., SOUSA, J. S. & BASIT, A. W. 2011. Mucoadhesive platforms for targeted delivery to the colon. *Int J Pharm,* 420**,** 11-9.

VENEMA, K. 2015. The TNO In Vitro Model of the Colon (TIM-2). *In:* VERHOECKX, K., COTTER, P., LÓPEZ-EXPÓSITO, I., KLEIVELAND, C., LEA, T., MACKIE, A., REQUENA, T., SWIATECKA, D. & WICHERS, H. (eds.) *The Impact of Food Bioactives on Health: in vitro and ex vivo models.* Cham: Springer International Publishing.

VERWEI, M., MINEKUS, M., ZEIJDNER, E., SCHILDERINK, R. & HAVENAAR, R. 2016. Evaluation of two dynamic in vitro models simulating fasted and fed state conditions in the upper gastrointestinal tract (TIM-1 and tiny-TIM) for investigating the bioaccessibility of pharmaceutical compounds from oral dosage forms. *International Journal of Pharmaceutics,* 498**,** 178-186.

VON DER OHE, M. R., HANSON, R. B. & CAMILLERI, M. 1994. Comparison of simultaneous recordings of human colonic contractions by manometry and a barostat. *Neurogastroenterology & Motility,* 6**,** 213-222.

WAGNER, C., JANTRATID, E., KESISOGLOU, F., VERTZONI, M., REPPAS, C. & B. DRESSMAN, J. 2012. Predicting the oral absorption of a poorly soluble, poorly permeable weak base using biorelevant dissolution and transfer model tests coupled with a physiologically based pharmacokinetic model. *European Journal of Pharmaceutics and Biopharmaceutics,* 82**,** 127-138.

WANG, B. & ARMENANTE, P. M. 2016. Experimental and computational determination of the hydrodynamics of mini vessel dissolution testing systems. *International Journal of Pharmaceutics,* 510**,** 336-349.

WANG, J. & FLANAGAN, D. R. 2009. Chapter 13 - Fundamentals of Dissolution A2 - Qiu, Yihong. *In:* CHEN, Y., ZHANG, G. G. Z., LIU, L. & PORTER, W. R. (eds.) *Developing Solid Oral Dosage Forms.* San Diego: Academic Press.

WASHINGTON, N., WASHINGTON, C. & WILSON, C. 2000. *Physiological Pharmaceutics: Barriers to Drug Absorption*, Taylor & Francis.

WILDE, L., BOCK, M., GLÖCKL, G., GARBACZ, G. & WEITSCHIES, W. 2014a. Development of a pressure-sensitive glyceryl tristearate capsule filled with a drug-containing hydrogel. *International Journal of Pharmaceutics,* 461**,** 296-300.

WILDE, L., BOCK, M., WOLF, M., GLOCKL, G., GARBACZ, G. & WEITSCHIES, W. 2014b. Development of pressure-sensitive dosage forms with a core liquefying at body temperature. *Eur J Pharm Biopharm,* 86**,** 507-13.

YANG, L. 2008. Biorelevant dissolution testing of colon-specific delivery systems activated by colonic microflora. *J Control Release,* 125**,** 77-86.

YANG, L., CHU, J. S. & FIX, J. A. 2002. Colon-specific drug delivery: new approaches and in vitro/in vivo evaluation. *International Journal of Pharmaceutics,* 235**,** 1-15.

YANG, L., JOHNSON, B. & FASSIHI, R. 1998. Determination of Continuous Changes in the Gel Layer Thickness of Poly(ethylene oxide) and HPMC Tablets Undergoing Hydration: A Texture Analysis Study. *Pharmaceutical Research,* 15**,** 1902-1906.

ZHANG, H., BIAN, C., JACKSON, J. K., KHADEMOLHOSSEINI, F., BURT, H. M. & CHIAO, M. 2014. Fabrication of robust hydrogel coatings on polydimethylsiloxane substrates using micropillar anchor structures with chemical surface modification. *ACS Appl Mater Interfaces,* 6**,** 9126-33.

ZHANG, M., HU, Y., WANG, W., SHAO, T. & CHENG, Y. 2013. Intensification of viscous fluid mixing in eccentric stirred tank systems. *Chemical Engineering and Processing: Process Intensification,* 66**,** 36-43.

ZULEGER, S., FASSIHI, R. & LIPPOLD, B. C. 2002. Polymer particle erosion controlling drug release. II. Swelling investigations to clarify the release mechanism. *International Journal of Pharmaceutics,* 247**,** 23-37.

ZULEGER, S. & LIPPOLD, B. C. 2001. Polymer particle erosion controlling drug release. I. Factors influencing drug release and characterization of the release mechanism. *International Journal of Pharmaceutics,* 217**,** 139-152.